The Role of Orphan Receptor GPR84 in Macrophage Biology and Inflammation

A thesis submitted for the degree of
Doctor of Philosophy

University of Oxford

Michaelmas Term 2023

Vincent Bond Luscombe

Somerville College
Sir William Dunn School of Pathology

ABSTRACT

GPR84 is a Class A orphan GPCR expressed primarily by innate immune cells. Despite significant advances in our understanding of GPR84 in the past 23 years the endogenous agonist(s) remain unknown. Current evidence suggests a primary role for this receptor in inflammation, though its pathophysiological role and the best strategy to exploit its activity therapeutically also remain unknown. This is true at both the physiological level, exemplified by disease models and clinical studies, but also at the molecular level, exemplified by a lack of understanding of downstream pathways and their relationship to cellular function. Surrogate agonists acting at this receptor have been shown to promote the mobilisation of inflammatory mediators, chemotaxis, and phagocytosis in a cell and context-dependent manner. However, the influence of agonist bias via the transducer proteins $G\alpha_i$ and β-arrestin-2 on these cellular responses are unclear. The development of chemical and biological tools to study the function of GPR84 are described herein, including two probes suitable for use *in vivo* and recombinant cell lines that phenocopy the response of macrophages. A detailed assessment of the signalling and kinetics of responses elicited by the agonists 6-OAU and DL-175 revealed that DL-175 exhibits a delayed impedance response, a delayed and suppressed activation of Akt, and an impaired ability to internalise the receptor. Finally, through the development of a screening set of chemically and biologically diverse agonists a relationship between agonist desensitisation potency and cAMP potency was found, but only a weak relationship between level of internalisation and level of bias. The lack of strong explanatory correlations between compounds in each assay highlights the potential to 'dial' receptor signalling in or out based on chemical structure. This work has furthered our molecular understanding of GPR84 signalling and supports research for the development of novel compounds with novel properties.

ACKNOWLEDGEMENTS

I would like to express my sincere gratitude to the many people behind this thesis, for supporting my experimental work, nurturing my curiosity, and inspiring me. As my thesis developed, my appreciation deepened. Yet, with such personal growth, I was led to wonder: was I writing the thesis, or was the thesis writing me? A valid question meant only as a humorous reflection, but for authorship purposes I would like to clarify that I did, in fact, write the thesis.

Special thanks to Prof. Greaves for your guidance, encouragement, wisdom, and humour. I am especially grateful for the academic freedom you gave me, and for always pushing me at the right times. Thank you Dr. Baena-López for your direction in the early phases of my research. To the wider Greaves Lab past and present, thank you for making it so fun; Laura, Conan, Ada, Lior, Annabell, Agata, Gareth, Lili, Josh II, Rowan, Kacper, and Prof. Sallenave. Thank you to Prof. Russell and the chemistry team, particularly Pinqi, for such an exciting and productive collaboration.

I would also like to acknowledge my graduate funding from the Sir William Dunn School of Pathology Studentship, Mary Somerville Clarendon Graduate Studentship, and Clarendon Fund, as well as research support from the EPA Trust, Guy Newton Research Fund, and CIU Trust, and travel support from Somerville's Hansell Fund and the British Pharmacology Society. It was a profound privilege to study at both the Dunn School and Somerville College, two pioneering institutions with storied histories and vibrant atmospheres. These hallowed walls indeed.

Finally, I extend my heartfelt appreciation to my friends and family for their enduring support during my DPhil. To my friends at the Oxford University Water Polo Club for the many memorable matches, varsities, and tours. To Vinnies. To the Kiwis turned Londoners Nathan, Sam, and Michael for hosting my fun escapes to the big city. To Halley Rose for your spirit and ginspiration. To my family and Aunty Maryanne and Uncle John for inspiring me. To Mum and Dad for your years of unconditional support, for always making the journey to visit me abroad, for always putting my work first, and for always believing in me, I will always be grateful.

ABBREVIATIONS

3-OH-C10, 3-hydroxy capric acid; **3-OH-C12**, 3-hydroxylauric acid; **ATP**, Adenosine triphosphate; **AUC**, Area under curve; **BMDM**, Bone-marrow-derived macrophage; **BNCI**, Baseline normalised cell index; **bp**, Base pair; **BRET**, Bioluminescence resonance energy transfer ; **BSA**, Bovine serum albumin; **C10**, Capric acid; **C11**, Undecanoic acid; **C12**, Lauric acid; **cAMP**, Cyclic adenosine monophosphate; **cDNA**, Complementary DNA; **CDS**, Coding sequence; **CEI**, Cell electical impedance; **CMV**, Cytomegalovirus; **CNS**, central nervous system ; **CRC**, Concentration-response curves; **CRISPR**, Clustered regularly interspaced short palindromic repeats; **Cryo-EM**, Cryogenic electron microscopy ; **DNA**, Deoxyribonucleic acid; **ECL**, Extracellular loop; **EST**, Expressed sequence tag; **FFA**, Free fatty acid; **FFAR**, Free fatty acid receptor; **FSK**, Forskolin; **G-CSF**, Granulocyte colony-stimulating factor; **GM-CSF**, Granulocyte-macrophage colony-stimulating factor; **GPCR**, G-protein-coupled receptor; **GRK**, G protein-coupled receptor kinase; **HBA**, Hydrogen bond acceptor; **HBD**, Hydrogen bond donor; **HDL**, High-density lipoprotein; **ICL**, Intracellular Loop; **IPF**, Idiopathic pulmonary fibrosis; **KO**, Knockout; **LCFA**, Long-chain fatty acid; **LDH**, Lactate dehydrogenase ; **LDL**, Low-density lipoprotein; **LPS**, Lipopolysaccharide; **MCFA**, Medium-chain fatty acid; **M-CSF**, Macrophage colony-stimulating factor ; **MCT**, Medium-chain triglyceride ; **MLM**, Mouse liver microsome; **mRNA**, Messenger RNA; **NAFLD**, Non-alcoholic fatty liver disease ; **NAM**, Negative allosteric modulator; **NCBI**, National Center for Biotechnology Information; **NET**, Neutrophil extracellular trap; **NIH**, National Institutes of Health; **NT**, N-terminus; **ORF**, Open reading frame; **PCR**, Polymerase chain reaction; **PET**, Positron emission tomography; **PK**, Pharmacokinetic; **PMA**, Phorbol 12-myristate 13-acetate; **PTX**, Pertussis toxin; **RLU**, Relative luminescence unit; **RNA**, Riboxynucleic acid; **ROS**, Reactive oxygen species; **RTCA**, Real-time cell analysis; **RT-PCR**, Reverse transcription polymerase chain reaction; **SAR**, Structure-activity relationship; **SCFA**, Short-chain fatty acid; **SDS-PAGE**, Sodium dodecyl sulfate–polyacrylamide gel electrophoresis; **SNP**, single nucleotide polymorphism; **TG**, Triglyceride; **TM**, Transmembrane.

CONTENTS

LIST OF FIGURES

LIST OF TABLES

Chapter One.

INTRODUCTION

1.1. Orphan Receptor GPR84

1.1.1. Identification and Cloning

In 2001 two separate groups were able to identify a novel G-protein coupled receptor (GPCR) encoded by *GPR84*, previously known as *EX33*. Wittenberger et al. (2001) employed a search of the NCBI expressed sequence tag (EST) database of cDNA sequences using 189 diverse GPCR protein query sequences as bait. After filtering out hits identical to known GPCRs, non-significant hits, orthologues from various species, and olfactory GPCRs, and when focussing on mammalian ESTs, 14 candidates were chosen for cloning. *GPR84* was identified from human leukemic B cells by 10 different bait GPCR sequences. This was a 1,191 base pair (bp) open reading frame (ORF) localised to chromosome 12q13.13 and contained a coding sequence uninterrupted by introns which codes for a 396 amino acid protein. The mouse GPR84 orthologue was also identified and cloned as a 396 amino acid protein with 85% identity to the human protein. Interestingly, no related GPCRs could be found in order to assign human or murine GPR84 to an appropriate subfamily (Wittenberger et al., 2001).

Yousefi et al. (2001) identified GPR84 using a distinct strategy whereby degenerate primers were used in reverse transcription polymerase chain reactions (RT-PCRs) to study potentially novel chemokine receptor family members in human neutrophils. Here, RNA was extracted from primary human peripheral blood neutrophils which were either unstimulated or stimulated for 5 h with granulocyte-macrophage colony-stimulating factor (GM-CSF), or stimulated by co-culture with pre-stimulated human primary bronchial epithelial cells. The degenerate primers were designed against conserved amino acid sequences found in intracellular loop (ICL) 2 and transmembrane (TM) 7 of known human chemokine receptors and had been previously used successfully by another group to identify CCR6 as the receptor for CCL20 (Power et al., 1997, Yousefi et al., 2001). PCR products

were cloned and amplification products from colonies were compared by insert size and restriction site analysis, revealing 20 distinct genes present in both stimulated and unstimulated neutrophils. *EX33*, or *GPR84* was the only novel GPCR among other already known chemokine receptors which were identified, although again, *EX33* had no significant similarity to known GPCRs, chemotactic or otherwise (Yousefi et al., 2001). The protein GPR84 is referred to for all species, while nucleic acids encoding this protein will henceforth be referred to as *GPR84* for humans and *Gpr84* for other species.

The Genome Reference Consortium Human Build 38 patch release 14 (GRCh38.p14, GenBank accession GCA_000001405.29), released February 2022 with NCBI RefSeq annotations from March 2023 (GCF_000001405.40-RS_2023_03), still supports the initial findings from the characterisation of *GPR84* in 2001. The *GPR84* gene, localised to chromosome 12q13.13, contains a non-coding exon 1 containing an upstream in-frame stop codon, a 533 bp intron, and a second exon with the ORF start codon in a Kozak consensus sequence, as well as a poly(A) signal 193 bp downstream of the stop codon (O'Leary et al., 2016, Wittenberger et al., 2001, Yousefi et al., 2001). Human *GPR84* mRNA (RefSeq NM_020370.3) contains a 1,191 bp coding sequence (CDS) which translates into a 396 amino acid protein (Figure 1).

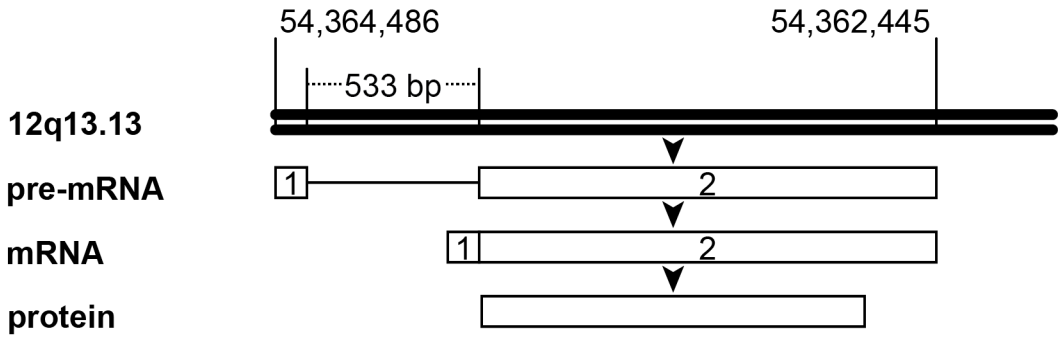

Figure 1: Gene structure and protein biosynthesis of GPR84. GPR84 is localised to chromosome 12q13.13 and contains two exons separated by a single 533 bp intron, beginning at base pair 54,364,486. The CDS of GPR84 is located on exon 2, where the 1,191 bp span codes for the 396 amino acid protein sequence of GPR84. (Gene ID: 53831, Location NC_000012.12, NCBI Reference Sequence NM_020370.3).

In the original 'GRAFs' classification system which defined subgroups of over 800 GPCRs into Glutamate, Rhodopsin, Adhesion, Frizzled/Taste2, and Secretin families, GPR84 and 23 others could not be classified in the other groupings due to their high dissimilarity to other known receptors (Fredriksson et al., 2003). However, it has since been classified as a Rhodopsin family member and Class A receptor. GPR84 is not phylogenetically related to the free fatty acid receptors (FFARs) (Ichimura et al., 2009), but relationships have been drawn to GPR50 and the melatonin MT_1 and MT_2 receptors (Vassilatis et al., 2003).

1.1.2. Evolution

Joost and Methner (2002), in the year following the identification of GPR84, aligned the protein sequences of 84 non-olfactory and non-gustatory human orphan GPCRs alongside 196 human GPCRs with known ligands in a study aimed at defining a more complete phylogenetic relationship between these receptors to facilitate ligand recognition. The resulting phylogenetic tree resulted in 19 subgroups for 241 Family A GPCRs, rooted to the human Family B receptor GPRC5B, one tree for 23 Family B GPCRs, and one tree for 14 Family C GPCRs, both rooted to Family A 5-HT_{1A} receptor. This study utilised BLASTP to align protein sequences, excluded the highly variable N- and C- terminal regions, and then used neighbour-joining to construct a phylogenetic tree within which GPR84 clustered with the biogenic amine receptors for acetylcholine, adenosine, and histamine. While the analysis of ligands for each receptor were inferenced from other known receptors, GPR84 was seen to belong to a highly heterogeneous group, including a number of other distantly related orphan receptors, where GPR84 existed in a subgroup with just one other receptor, GPR88 (Joost and Methner, 2002), which remains an orphan in 2023 (Alexander et al., 2021). Notably, GPR84 did not cluster with the chemokine receptors, peptide receptors, or nucleotide and lipid receptors in the other Family A groupings (Joost and Methner, 2002).

Noting that there are no paralogues of GPR84 in the human genome, Schulze et al. (2022) analysed the DNA sequences of over 200 vertebrate species in order to identify orthologues following speciation events. Orthologues of GPR84 were identified in cartilaginous fishes, which exhibited sequence identities of 30-40% to both human and zebrafish GPR84, as well as sea lampreys

which exhibited sequence identities of 41% to human and 40% to zebrafish GPR84. As no orthologue could be identified in lancelets, and cartilaginous fishes and sea lampreys diverged from bony vertebrates 450 and 550 million years ago respectively, it dates the evolutionary age of GPR84 to over 550 million years (Schulze et al., 2022). Interestingly, GPR84 was found to be absent in birds, and likely lost selective pressure in bats where it now exists only as a pseudogene (Schulze et al., 2022).

GPR84 orthologues have been well annotated in vertebrates but less so in invertebrates. Orthologous genes to human GPR84 have been predicted in NCBI for 389 vertebrate species and predicted to 645 similar genes in bilateria (Maglott et al., 2005), and predicted in the marine water flea (*Diaphanosoma celebensis*), water flea (*Daphnia magna*), and common fruit fly (*Drosophila melanogaster*) (Kim et al., 2021). In preliminary research we identified putative orthologous genes in the common fruit fly (*Drosophila melanogaster*), *Moody* and *Tre1*, as well as in the nematode worm (*Caenorhabditis elegans*), *Npr-8*. While these GPCRs are relatively dissimilar to hGPR84 (21-27% identity by BLAST) they each have compelling functions. NPR-8 is a host-defence GPCR in worms (Sellegounder et al., 2019), Moody is expressed in glial cells and maintains the integrity of the blood-brain barrier in the adult fly (Bainton et al., 2005), and Tre1 is involved in the transepithelial migration of germ cells in a manner compared to that of chemokine-directed leukocyte migration (Kunwar et al., 2003).

Studies in lower order species have cloned and functionally characterised GPR84 orthologues in Minzhu pigs (*Sus scrofa*) (Wang et al., 2014), mice (*Mus musculus*) (Yousefi et al., 2001), Chinese giant salamander (*Andrias davidianus*) (Yu et al., 2022), African clawed frog (*Xenopus laevis*) (Perry et al., 2010), zebrafish (*Danio rerio*) (Huang et al., 2014), grass carp (*Ctenopharyngodon Idella*) (Li et al., 2023b), common carp (*Cyprinus carpio*) (Yao et al., 2023), and other studies have identified and characterised an orthologue in rainbow trout (*Oncorhynchus mykiss*) (Calo et al., 2023, Velasco et al., 2021). These studies in lower vertebrates highlight the wide range of research interest in GPR84 and the potential use of model species for *in vivo* research on the role of GPR84 throughout evolution.

In primates a study was undertaken to identify genetic features underlying their body size and lifespan. *GPR84* was found as one of 276 genes whose rate of evolution positively correlated with lifespan (Tejada-Martinez et al., 2022). Other inflammation and immunity-related genes alongside *GPR84* were *HIVEP3*, and *MARCO*, and were hypothesised to contribute to disease protection in primates (Tejada-Martinez et al., 2022). In humans, a genetic study was carried out to identify differentially regulated genes between ancient populations of humans with differing diets and lifestyles by using machine models trained on gene expression (Colbran et al., 2021). The authors hypothesised that immune and metabolic traits were under strong selective pressure between populations which had transitioned from hunter-gatherer, pastoralist, and agricultural lifestyles. Indeed, the gene ontology analysis revealed enriched annotation terms around immunity and metabolism. Interestingly, *GPR84* in the adrenal gland was predicted to be among the most differentially regulated genes between three lifestyle groups of ancient humans; with negative regulation in agricultural populations compared to an increasing predicted regulation in pastoral and hunter-gatherer populations. Shifts between these lifestyles of ancient humans involved changes in population density, interaction with the environment, and substantial dietary shifts, and likely resulted in selective pressures based on pathogen exposures too (Colbran et al., 2021). This raises more interesting questions about the role of adrenal GPR84 throughout human evolution. Macrophages have been identified in both the adrenal medulla and cortex (González-Hernández et al., 1994, Hume et al., 1984) and are likely the major cell type expressing *GPR84*, though their precise function in immunity, homeostasis, or endocrine signalling is not understood.

An analysis of 33 naturally occurring single nucleotide polymorphisms (SNPs) in human GPR84 revealed that 22 resulted in a loss of membrane expression, where most of these also affected residues that were highly evolutionarily conserved (Schulze et al., 2022). Loss-of-function SNPs, causing either loss of membrane expression or loss of potency to capric acid, exhibited a higher than expected allele frequency in Indonesian and some Northeast Asian populations, suggesting a possible beneficial role in these mutations that improve host survival. No variants of GPR84 are yet linked to disease or pathogenesis including 275 known SNPs affecting the GPR84 CDS (Schulze et al., 2022).

If GPR84 responds to bacterial metabolites which are indicative of overall bacterial load, and GPR84 assists recruited immune cells in clearing this load, then a positive selection for a non-functional minor allele in Asian populations would suggest some benefit in tolerating higher bacterial loads. One possibility is that the enhanced inflammation mediated by GPR84 is inappropriate and instead damaging in these populations. Another possibility is that the differing diets in these populations may have required tolerance to, for example, beneficial bacteria, as suggested by Peters et al. (2020) for the intake of fermented foods.

1.1.3. Expression

1.1.3.1. *Immune Cell Expression*

GPR84 is expressed predominantly on immune cells, where mRNA transcripts have been detected and quantified in bone marrow, lungs, neutrophils and eosinophils, monocytes and macrophages, and microglia, as well as at lower levels in splenic B and T cells (Bouchard et al., 2007, Groot-Kormelink et al., 2012, Hohenhaus et al., 2013, Lattin et al., 2008, Venkataraman and Kuo, 2005, Wang et al., 2006, Yousefi et al., 2001).

In a micro-array analysis of 91 murine cell types and tissues *Gpr84* expression was found to be restricted to macrophages and granulocytes (Lattin et al., 2008). In particular, *Gpr84* was found to be restricted to bone-marrow-derived macrophages (BMDMs) and microglia in the unstimulated state, and enriched in BMDMs as compared to thioglycollate-elicited peritoneal macrophages and RAW264.7 macrophages, (Lattin et al., 2008). In humans, *GPR84* was seen to be slightly more highly expressed by phorbol 12-myristate 13-acetate (PMA) differentiated macrophage surrogate cell lines THP-1 and U937 than alveolar macrophages, monocyte-derived macrophages, and PMA-treated promyelocytic HL60 leukemia cells (Groot-Kormelink et al., 2012). These differing expression levels between macrophages may reflect differing roles of GPR84 between the diverse set of macrophage populations.

Immune cells exhibit a low basal level of expression of *GPR84* which can be transcriptionally upregulated by inflammatory stimuli. Lipopolysaccharide (LPS) for example can upregulate *Gpr84* in murine BMDMs to over three hundred fold over basal (Recio et al., 2018). This

inducible regulation of transcription also occurs to varying degrees at other cell types and tissues, and poses a challenge in attributing tissue expression to native cells versus infiltrating immune cells. Despite this, strong evidence for a role of GPR84 in immune cells is provided by the predominant regulation of *GPR84* expression by inflammatory mediators (Luscombe et al., 2020). Firstly, in monocultures of defined cell type and growth conditions the molecular inducers causing upregulation of *GPR84* are largely inflammation-associated (Table I). Secondly, disease states and disease models in both humans and mice identify differences in *GPR84* expression in inflammatory contexts (Table II). In mice, 1 mg/kg *i.p.* injection of LPS causes significant upregulation of *Gpr84* in adipose tissue, bone marrow, brain, lung, kidney, and intestines (Recio et al., 2018).

While most experiments quantify expression by mRNA transcript the only direct quantitative evidence to date that these lead to increases in GPR84 protein levels was a study in THP-1 monocytes. In this experiment, LPS-treatment of THP-1 cells resulted in a 10-fold increase in *GPR84* mRNA and a concomitant 3.5-fold increase in protein, as determined by the specific binding of the radiolabelled antagonist [^{3}H]G9543 to THP-1 membranes (Mancini et al., 2019). The transcription factors STAT3 and C/EBPβ activation have been shown to promote GPR84 expression in myeloid derived suppressor cells when stimulated with GM-CSF and granulocyte colony-stimulating factor (G-CSF) (Qin et al., 2023), highlighting a potentially common mechanism of upregulation in myeloid cells and warrants further investigation. Rho kinases may also be upstream of GPR84 expression, as the inhibitor ripasudil was able to attenuate LPS-induced *Gpr84* expression in BV-2 cells as well as in optic nerve crush induced expression in retinal microglia (Sato et al., 2023). Additionally, TNFα and IL-1 blocking antibodies are able to reduce LPS-mediated increases in *Gpr84* expression in BV-2 cells to below baseline levels, indicating a major role for these cytokines in regulating expression, which is done via a dexamethasone insensitive pathway (Bouchard et al., 2007).

Table I: Molecular inducers causing upregulation of GPR84 mRNA in cells

Molecular Inducer	Cell Type/Cell Line Origin	Species	References
Capsaicin	oesophagus	human	(Abdel-Aziz et al., 2016)
CpG-ODN	astrocytes	mouse	(Madeddu et al., 2015)
	microglia	mouse	(Madeddu et al., 2015)
ET-1	lung fibroblasts	human	(Nguyen et al., 2020)
G-CSF	MDSCs	mouse	(Qin et al., 2023)
GM-CSF	MDSCs	mouse	(Qin et al., 2023)
IL-1	microglia	mouse	(Bouchard et al., 2007)
IL-1β	adipocytes	human	(Muredda et al., 2018)
	chondrocytes	human, mouse	(Wang et al., 2021)
IL-33	adipocytes	human	(Zaibi et al., 2018)
LPS	adipocytes	human, mouse	(Nagasaki et al., 2012)
	alveolar macrophage	mouse	(Yin et al., 2020)
	liver	zebrafish	(Huang et al., 2014)
	macrophages	human, mouse	(Bouchard et al., 2007, Gagnon et al., 2018, Hohenhaus et al., 2013, Lattin et al., 2008, Puengel et al., 2020, Recio et al., 2018, Wang et al., 2006)
	microglia	mouse	(Bouchard et al., 2007, Sato et al., 2023, Recio et al., 2018)
	monocytes	human	(Bouchard et al., 2007, Mancini et al., 2019, Müller et al., 2017, Wang et al., 2006)
	neutrophils	human, mouse	(Puengel et al., 2020, Wang et al., 2023b)
	podocytes	human	(Gagnon et al., 2018)
LTA	PBMCs	human	(Kang et al., 2012)
oxLDL	macrophages	human	(Recio et al., 2018)
Pam3Cysk	macrophages	mouse	(Recio et al., 2018)
R837	astrocytes	mouse	(Madeddu et al., 2015)
	microglia	mouse	(Madeddu et al., 2015)
TGF-β	lung fibroblasts	human	(Nguyen et al., 2020)
	dermal fibroblasts	human	(Gagnon et al., 2018)
	podocytes	human	(Gagnon et al., 2018)
TNFα	microglia	mouse	(Bouchard et al., 2007)
	adipocytes	human, mouse	(Muredda et al., 2018, Nagasaki et al., 2012)
Zymosan	macrophages	mouse	(Recio et al., 2018)

CpG-ODN, CpG oligodeoxynucleotides; ET-1, Endothelin 1; IFN-α, Interferon α; IL-1, Interleukin-1; IL-1β, Interleukin 1β; IL-33, Interleukin 33; LPS, Lipopolysaccharide; LTA, Lipoteichoic acid; MDSC; Myeloid-derived suppressor cells, oxLDL, oxidised LDL; PBMC, Peripheral blood mononuclear cells; TGF-β, Transforming Growth Factor β; TNFα, Tumor necrosis factor α.

Table II: Disease models associated with an upregulation of GPR84 mRNA in tissues

Disease Model	Cell Type/Tissue	Species	References
Acute Lung Injury	BALF	mouse	(Wang et al., 2023b, Yin et al., 2020)
	lung tissue	mouse	(Yin et al., 2020)
	parenchymal cells	mouse	(Yin et al., 2020)
Amyloidosis	microglia	mouse	(Audoy-Rémus et al., 2015)
Cuprizone demyelination	microglia	mouse	(Bédard et al., 2007)
Diabetes	bone marrow	mouse	(Recio et al., 2018)
	brain	mouse	(Recio et al., 2018)
	kidney	mouse	(Recio et al., 2018)
	brain	mouse	(Recio et al., 2018)
Endotoxemia	brain	mouse	(Bouchard et al., 2007, Recio et al., 2018, Kalita et al., 2023)
	adipose tissue	mouse	(Recio et al., 2018)
	blood	mouse	(Bouchard et al., 2007)
	bone marrow monocytes	mouse	(Recio et al., 2018)
	intestine	mouse	(Recio et al., 2018)
	kidney	mouse	(Recio et al., 2018)
	lung	mouse	(Recio et al., 2018)
	microglia	mouse	(Bouchard et al., 2007)
Experimental autoimmune encephalomyelitis	brain	mouse	(Bouchard et al., 2007)
Heart failure	lung	rat	(Nguyen et al., 2020)
NAFLD	liver	human, mouse	(Puengel et al., 2020)
Nephropathy	kidney	mouse	(Gagnon et al., 2018)
Neuropathic pain	sciatic nerve	rat, mouse	(Nicol et al., 2015, Yosten et al., 2020)
Non-small Cell Lung Cancer	blood	human	(Qin et al., 2023)
Obesity	aorta	mouse	(Recio et al., 2018)
	colon	mouse	(Peiris et al., 2018)
	epididymal fat	mouse	(Nagasaki et al., 2012)
	quadriceps muscle	mouse	(Montgomery et al., 2019)
Oesophageal Squamous Cell Cancer	blood	human	(Qin et al., 2023)
Oesophagitis	blood	rat	(Abdel-Aziz et al., 2016)
	oesophageal epithelia	rat	(Abdel-Aziz et al., 2016)
	oesophagus	human	(Abdel-Aziz et al., 2016)
Optic nerve crush	retinal microglia	mouse	(Sato et al., 2023)

Orthotopic Oesophageal Carcinoma	MDSCs	mouse	(Qin et al., 2023)
Roux-en-Y gastric bypass surgery	colon	mouse	(Peiris et al., 2018)
Traumatic brain injury	brain	mouse	(Israelsson et al., 2008)
Ulcerative colitis	blood	human	(Planell et al., 2017)
	colonic macrophages	human	(Zhang et al., 2022)
	colon	mouse	(Zhang et al., 2022)
	peripheral blood leukocytes	mouse	(Zhang et al., 2022)
Viral encephalitis	brain	mouse	(Madeddu et al., 2015)

BALF; Bronchoalveolar lavage fluid, NAFLD, Non-alcoholic fatty liver disease, MDSC; Myeloid-derived suppressor cells.

1.1.3.2. *Gastrointestinal and Oral Cavity Expression*

The gastrointestinal tract constitutes a large surface area interacting with the outside world, and is therefore an important immune interface, with many innate immune cells residing in the lamina propria. However, there are still only limited reports of GPR84 expression in the gastrointestinal tract. In the original characterisation of GPR84, Yousefi et al. (2001) detected expression in the human colon but did note that granulocytes could have been responsible for this observation. In a large profiling study of 26 mouse tissues, *Gpr84* was not detected in the colon or intestine by RT-PCR (Vassilatis et al., 2003).

More recently, *Gpr84* mRNA was found at low levels only in the colon of obese mice or mice that had undergone gastric bypass surgery (Peiris et al., 2018). Some expression was seen in the gastrointestinal tract of mice, with highest expression in the ileum, while in humans the highest expression was seen in the antrum (Symonds et al., 2015). More broad expression profiling of mouse tissues shows low levels of expression in the stomach and ghrelin secreting cells, and no expression in the colon and intestine (Engelstoft et al., 2013, Vassilatis et al., 2003). There also appears to be limited expression in enteroendocrine cells, key chemosensing cells with abundant expression of the FFAR subtypes 1-4. Expression has been detected in the corpus mucosa of suckling mouse pups and in rats (Goebel et al., 2011, Widmayer et al., 2017). The higher expression of receptor during the

suckling phase, and subsequent loss of receptor expression in the post-weaning phase of rat pups has been proposed as being an adaptive change to the dietary composition which transitions away from high fat milks to protein and carbohydrate rich solid foods (Widmayer et al., 2017). As calorific load has been shown to have an impact on *Gpr84* expression in colonic tissue it has been suggested that GPR84 could be a target for modulating appetite (Aktar et al., 2023). In the dextran sulphate sodium-induced colitis model in mice, low levels of *Gpr84* were detected in intestinal lamina propria cells, but not intestinal epithelial cells (Zhang et al., 2022). This study elucidated how GPR84 regulates changes in the intestinal macrophage pool, and highlighted expression on inflammatory macrophages in the lamina propria as well as colonic mucosa following treatment (Zhang et al., 2022).

In humans, patients with ulcerative colitis have increased *GPR84* in the blood compared with controls or patients in remission (Planell et al., 2017) as well as in colonic macrophages (Zhang et al., 2022). In the digestive tract, *GPR84* has been detected in the oesophagus of patients with oesophagitis, and further upstream in the oral cavity it has been detected on human and mouse taste buds (Abdel-Aziz et al., 2016, Costanzo et al., 2019, Liu et al., 2021, Liu et al., 2018). More recently, immunohistochemical studies have identified GPR84 on human enteroendocrine L and enterochromaffin cells in the human proximal colon mucosa (Peiris et al., 2022). The co-localisation of GPR84 with the gut signalling molecule 5-HT and the long-chain fatty acid receptor FFA4 on enteroendocrine cells could suggest a role for GPR84 in endocrine function (Aktar et al., 2023). These studies would benefit from antibody specificity tests, either by Western blot against the tissue lysate to demonstrate reactivity against a protein of approximately the expected size, or against *Gpr84*$^{-/-}$ knockout (KO) tissue to test for a lack of staining. We have previously shown a lack of specificity in commercially available GPR84 antibodies by Western blot, which sometimes appear to bind to a protein of the approximate expected monomeric receptor size (Luscombe et al., 2020, Recio et al., 2018), which calls into question the reliability of GPR84 antibodies for co-localisation studies.

1.1.3.3. *Liver Expression*

Non-alcoholic fatty liver disease (NAFLD) is associated with an upregulation of *GPR84* in the livers of humans and mice and its upregulation was correlated with both inflammatory markers and histological examination of fibrosis severity (Puengel et al., 2020). However, hepatocyte expression was low and undetectable on hepatic stellate cells, cells which are largely responsible for the progression of fibrosis. This indicates that the antifibrotic effects of targeting GPR84 is instead more likely related to its expression on infiltrating myeloid cells. In particular, antagonism of GPR84 reduced the percentage of infiltrating monocyte-derived macrophages into the liver during acute and chronic inflammation whereas the number of tissue resident Kupffer cells remained unchanged (Puengel et al., 2020).

By using a radiolabelled agonist structurally resembling 6-OAU to perform saturation binding experiments Köse et al. (2020) observed specific binding of [^{3}H]PSB-1584 to rat, mouse, and calf liver tissues, as well as in the HepG2 human hepatocarcinoma cell line, but not in the MCA-RH7777 rat hepatoma cell line. This radiolabelling study was one of few to date to quantify protein as opposed to mRNA. Notably, all tissues examined had lower specific binding than CHO-β-arrestin-hGPR84 (DiscoverX) cells, a commonly used commercially available cell line. The rat and mouse liver tissues as well as HepG2 cell lines also exhibited 6-13-fold lower K_D values of [^{3}H]PSB-1584 binding compared to CHO-β-arrestin-hGPR84 (DiscoverX). While the liver membrane preparations can include either tissue-resident or infiltrating immune cells, expression on the human hepatocarcinoma cell line indicates some expression outside of myeloid cells. Human liver expression was untested in these studies.

Taken together, tissue and cellular expression data show a relatively low level of *GPR84* expression in the liver in un-inflamed conditions, and larger tissue profiling studies have not shown expression in the liver (Vassilatis et al., 2003). Under the inflammatory conditions of NAFLD liver expression of *GPR84* then increases, largely due to the activation or infiltration of immune cells. It is therefore likely that hepatic *GPR84* expression may be a general phenomenon of liver injury,

stress, or inflammatory state, and warrants testing in other disease states, especially those in communicable diseases such as hepatitis infection.

1.1.3.4. *Adipose Tissue Expression*

Adipose tissue is a key site of free fatty acid (FFA) release in to the blood (Karpe et al., 2011), and may therefore be a site of interest for the interaction of medium-chain fatty acids (MCFAs) with GPR84. Nagasaki et al. (2012) found that mice fed a high fat diet had higher *Gpr84* expression in epididymal fat pads than normal diet mice. The inflammatory condition and infiltration of macrophages was also observable with increases in TNFα, MCP-1, and the macrophage marker F4/80. Expression in murine 3T3-L1 adipocyte cells was relatively low and 20-fold lower than that in unstimulated murine RAW264.7 macrophage-like cells. In no-contact co-culture experiments of these two cell types, 3T3-L1 adipocytes upregulated both *Gpr84* and *Mcp-1* in the presence of RAW264.7 macrophage-like cells. Furthermore, both TNFα and LPS were shown to induce *Gpr84* expression in 3T3-L1 adipocytes in a dose-dependent manner and up to 200- and 60-fold respectively, as well as to a lesser degree, 5- to 15-fold, in human adipose tissue-derived stromal cell adipocytes. The authors therefore propose a scheme in which activated macrophages, themselves expressing GPR84, infiltrate adipose tissue and cause lesser degrees of GPR84 expression on adipocytes via secretion of TNFα (Nagasaki et al., 2012). Following this, Trayhurn and Denyer (2012) found that macrophage-conditioned medium could also induce GPR84 expression in human adipocytes. This was later found to involve the key cytokines TNFα, IL-1β, and IL-33, which all cause acute upregulation of *GPR84* in human adipocytes (Muredda et al., 2018, Zaibi et al., 2018). More recently, GPR84 protein expression has been shown to be upregulated in the adipose tissue of LPS-treated mice by an increase in specific binding of a GPR84 positron emission tomography (PET) radiotracer, consistent with known inflammatory processes following LPS challenge (Kalita et al., 2023). These findings support the idea that inflammatory macrophages can induce expression in adipose tissue by identifying three inflammatory cytokines which cause *GPR84* upregulation, all of which would serve to enhance inflammation in the adipose tissue. Mouse models utilising

macrophage depletion would be useful tools to explore the role of GPR84 in the link between adiposity and inflammation further.

1.1.3.5. *Lung Expression*

Expression of *GPR84* on human alveolar macrophages has been documented (Groot-Kormelink et al., 2012). In unstimulated samples, low expression levels are seen in the lung tissue of mice (Vassilatis et al., 2003), however, following an *i.p.* injection of LPS these levels can increase 200-300 fold (Recio et al., 2018). Evidence from other disease models heavily implicates the recruitment of immune cells for this increase in expression. In mouse models of idiopathic pulmonary fibrosis (IPF), *Gpr84* was upregulated in inflammatory infiltrates using both a bleomycin and radiation model of IPF, but was only upregulated in bronchial epithelial cells in the bleomycin model (Saniere et al., 2019). As with the recruitment of immune cells in the gastrointestinal tract, a similar phenomenon may occur in the lungs of patients with IPF, where both infiltrating macrophages and bronchial epithelial cells express *GPR84* (Saniere et al., 2019). Intratracheal injection of LPS utilised as a mouse model of acute lung injury also upregulates *Gpr84* expression in the bronchoalveolar lavage fluid, lung tissue, and parenchymal lung cells (Wang et al., 2023b, Yin et al., 2020). Resident alveolar macrophages are involved in the early response to infection and recruitment of further immune cells and, alongside neutrophils, express *Gpr84* following induction of acute lung injury (Wang et al., 2023b, Yin et al., 2020). Expression of *Gpr84* in the lungs of rats was also upregulated following myocardial infarction, and expression in cultured human lung fibroblasts could be induced by both TGF-β and ET-1 (Nguyen et al., 2020). Taken together, these observations support a major role for immune cell recruitment and activation in the lung tissue expression of GPR84 while more limited expression is still seen on parenchymal cell types.

1.1.3.6. *Heart and Skeletal Muscle Expression*

The heart and skeletal muscle are two key sites of fatty acid uptake and oxidation, driven by mitochondria in order to sustain the contractile functions of these organs (Zhang et al., 2010). However, most untargeted transcriptomics approaches do not identify *GPR84* mRNA in the heart or skeletal muscle. *GPR84* transcripts were undetected by RT-PCR in human or mouse heart tissue

(Moore-Morris et al., 2009, Wang et al., 2006), supporting the finding of low protein expression in mouse heart by radiolabelling studies (Köse et al., 2020). In skeletal muscle, Montgomery et al. (2019) highlighted that *Gpr84* is present across more mouse tissue types, including skeletal muscle, when normalised to total RNA rather than *Gapdh*. Western blots indicated receptor was present in bone marrow, skeletal muscle, adipose tissue, and at low levels in the heart. Antibody specificity was tested by overexpression and knockdown of *Gpr84* in mouse tibialis anterior muscle using gene electrotransfer, showing increases and decreases in band intensity by Western blot respectively.

1.1.3.7. *Central Nervous System Expression*

GPR84 is selectively expressed by microglia in the central nervous system (CNS) (Bouchard et al., 2007, Gamo et al., 2008). It is expressed by the murine cell microglial BV-2 and neuroblastoma N18 cell lines (Atwood et al., 2011). In mice, high expression was seen in microglia and not in various other brain tissue samples such as the cerebral cortex, cerebellum, or spinal cord (Lattin et al., 2008). Furthermore, the induction of microglial GPR84 in the CNS occurs in response to inflammatory stimuli such as LPS-induced endotoxemia, experimental autoimmune encephalomyelitis, β-amyloid-induced toxicity, partial sciatic nerve ligation, hypoglossal axotomy, and cuprizone-induced demyelination (Audoy-Rémus et al., 2015, Bouchard et al., 2007, Gamo et al., 2008, Nicol et al., 2015), strongly suggesting that GPR84 plays a role in neuroinflammation. In pediatric cerebella, WNT pathway medulloblastomas show a decrease in *GPR84* expression, suggesting some baseline level of expression in pediatric cerebella (Whittier et al., 2013). Protein level expression has been demonstrated using radiolabelling studies which show specific binding in rat brain cortex and striatum (Köse et al., 2020), as well as using a PET tracer showing specific binding in the brains of LPS treated mice compared to saline controls (Kalita et al., 2023). The similarities between microglia and macrophages in upregulating GPR84 following an inflammatory stimulus hints at a conserved role of the receptor in the CNS and periphery. The fact that they reside in different and tightly controlled milieu is a question for how the potential physiological agonist or agonists might encounter both microglia and macrophages.

1.1.4. GPR84 Function

1.1.4.1. *A Brief History of GPR84 Discovery*

In 2001 GPR84, also known as EX33, was first identified and cloned independently by two groups from human neutrophils and human leukemic B cells (Wittenberger et al., 2001, Yousefi et al., 2001) (Figure 2).

In 2005 the first *Gpr84*$^{-/-}$ knockout mice were generated, exhibiting normal T- and B-lymphocyte proliferation, but an enhanced IL-4 production when T-cells were stimulated with anti-CD3 antibodies, indicating some role for Gpr84 in regulating IL-4 expression in activated T-cells (Venkataraman and Kuo, 2005).

In 2006 it was discovered that the natural products capric acid (henceforth sometimes referred to as C10) and 3,3'-diindolylmethane (DIM) are able to activate GPR84. MCFAs specifically of carbon chain lengths 9-14 activated GPR84, although the surrogate agonist DIM was found to be more potent than capric acid and the other chain lengths (Wang et al., 2006).

In 2013 the synthetic agonist 6-n-octylaminouracil (6-OAU) was discovered following a high-throughput screen (Suzuki et al., 2013). As a potent agonist with selectivity against FFA1 and 69 receptors, channels, and transporters, 6-OAU would become a standard agonist in the field. Additionally, Suzuki et al. (2013) demonstrated that MCFAs hydroxylated at the 2- or 3- position could activate GPR84 as well as or better than their nonhydroxylated forms.

In 2015 it was shown that *Gpr84* was upregulated in the spinal cord and sciatic nerve of mice following partial nerve ligation (Nicol et al., 2015). In this murine model of traumatic nerve injury, *Gpr84*$^{-/-}$ mice did not develop mechanical or thermal hypersensitivity, linking inflammatory GPR84 activation to nociceptive signalling via expression on peripheral macrophages (Nicol et al., 2015). GPR84 was also shown to be expressed in microglia and upregulated in a mouse model of Alzheimer's Disease, where it exerts a beneficial effect by promoting microgliosis and dendritic homeostasis and preventing further cognitive decline (Audoy-Rémus et al., 2015). Additionally, the

antagonist GLPG1205 failed to meet efficacy endpoints in a phase II clinical trial for ulcerative colitis (NCT02337608) (Vermeire et al., 2017).

In 2016 the potent lipid-mimetic agonists ZQ-16 (2-hexylsulfanyl-6-hydroxy-3H-pyrimidin-4-one) and LY237 (4-hydroxy-6-nonyl-1H-pyridin-2-one), the most potent agonist of the time, were described (Liu et al., 2016, Zhang et al., 2016).

In 2017 the GPR84 antagonist PBI-4050 (2-(3-pentylphenyl)acetic acid) failed to meet efficacy endpoints in the treatment of idiopathic pulmonary fibrosis **(**NCT02538536) (Khalil et al., 2019).

In 2018 the natural product embelin (2,5-dihydroxy-3-undecylcyclohexa-2,5-diene-1,4-dione) was discovered as a potent GPR84 agonist (Gaidarov et al., 2018). GPR84 activation drives human neutrophil chemotaxis and primes amplification of the oxidative burst, and in macrophage foam cells were shown to be involved in the process of reverse cholesterol transport (Gaidarov et al., 2018). The GPR84 agonist 6-OAU was also shown to augment macrophage inflammatory responses and enhance phagocytosis (Recio et al., 2018). Activation of GPR84 was also shown to trigger ROS release from TNFα or Latrunculin-A primed neutrophils (Sundqvist et al., 2018).

In 2019 the novel G-protein biased agonist DL-175 (3-(2-((4-chloronaphthalen-1-yl)oxy)ethyl)pyridine 1-oxide) was discovered following optimisation of a hit from a ligand-based virtual screen (Lucy et al., 2019). Dietary supplementation with lauric acid (C12, dodecanoic acid), perilla oil, and DIM together in colonic release capsules, a mixture targeting both GPR84 and FFAR4, was found to reduce energy intake in obese adults (NCT04292236) (Peiris et al., 2022).

In 2020 the GPR84 antagonist GLPG1205 (9-(2-cyclopropylethynyl)-2-[[(2S)-1,4-dioxan-2-yl]methoxy]-6,7-dihydropyrimido[6,1-a]isoquinolin-4-one) failed to meet primary endpoint outcomes for the treatment of IPF (NCT03725852) (Strambu et al., 2023).

In 2020 a radiolabelled analogue of 6-OAU was developed, [^{3}H]PSB-1584 (6-(hexylamino)-1H-pyrimidine-2,4-dione), which was used to measure the binding affinities of other agonists,

including DIM, which was shown to allosterically increase the specific binding of [^{3}H]PSB-1584 (Köse et al., 2020).

In 2022 key residues in the ICL3 of GPR84 were shown to undergo G-protein-coupled receptor kinase (GRK) 2/3-mediated phosphorylation in an agonist-dependent manner, revealing a step in the mechanism underlying the β-arrestin bias of DL-175 (Marsango et al., 2022).

In 2023 the structure of Gα_i-coupled hGPR84 was solved by cryogenic electron microscopy (cryo-EM) in complex with three agonists by two separate groups, Liu et al. (2023) having co-crystallised 3-OH-C12 (3-hydroxylauric acid) and LY237, and Zhang et al. (2023) with 6-OAU. All three structures show an orthosteric site completely occluded from the extracellular milieu, buried in the receptor and 'capped' by the N-terminal domain and extracellular loop (ECL) 2 (Liu et al., 2023, Zhang et al., 2023).

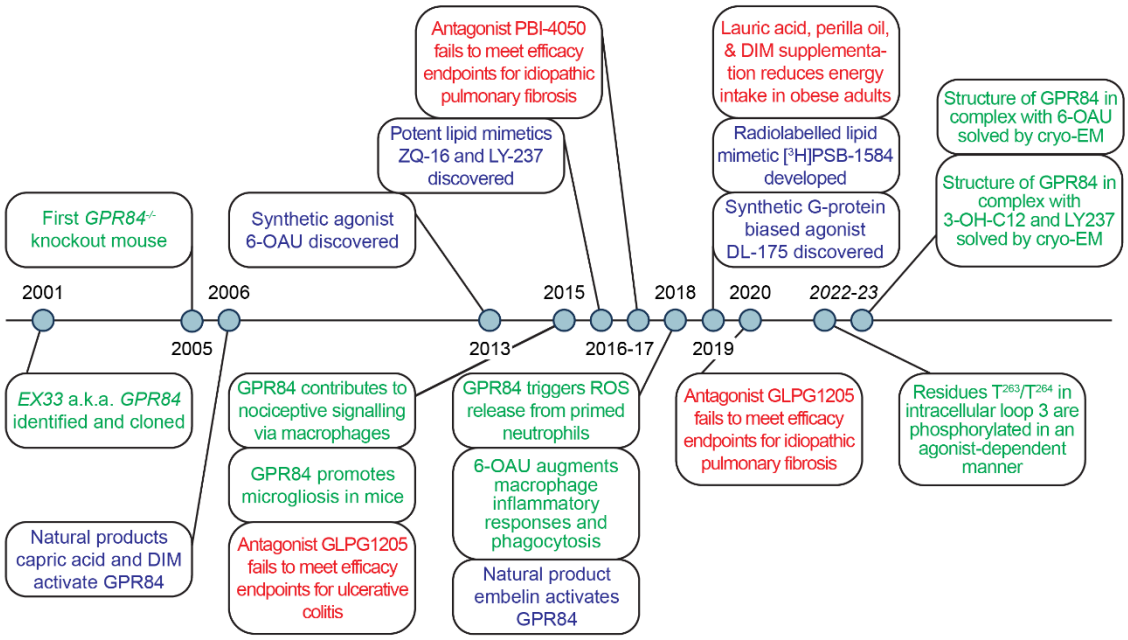

Figure 2: Timeline of GPR84 chemical discovery, biology, and clinical trials. Developments in chemical discovery (*blue*), GPR84 biology (*green*), and the clinical trials of antagonists (*red*) are shown by year. Reproduced with permission from Luscombe et al. (2023b). ROS, reactive oxygen species.

1.1.4.2. *Database Searches for Annotations on GPR84 Function*

In a review of the unexplored therapeutic opportunities in the human genome, Oprea et al. (2018) developed a 'Target Development Level' ranking system for druggable proteins for automatic searching and annotation. These categories reflect the research and development by protein; advanced targets with at least one clinically approved drug are in the T_{clin} (clinic) category, well developed targets such as those under clinical trials or possessing chemicals with high binding affinity are in the T_{chem} (chemistry) category, moderately investigated targets with disease relevance, GO annotations, or a threshold of commercial antibodies are in the T_{bio} (biology) category, and remaining proteins are left in the T_{dark} (dark genome) category. In this scheme, GPR84 fell into the T_{bio} (biology) category as of 2018. A total of 20,120 proteins were investigated, of which 11,086 were in the T_{bio} category. Of the 406 non-olfactory GPCRs, 145 (36%) were in the T_{bio} category. An investigation into the datasets considered for GPR84 show that it was relatively poorly ranked by PubMed publication scoring and GeneRIF annotations (ranked near ~10,000 / 20,120 proteins), moderately ranked for NIH research dollars (ranked ~6,000-8,000 / 20,120), but unusually well ranked for antibody count (ranked 3,345 / 20,120) and evidence-based intervention patent count (ranked 615 / 20,120) (Oprea et al., 2018).

Since 2018, the Pharos database has elevated GPR84 to the T_{chem} category, possessing 373 active ligands of which some are below an activity of < 30 nM, 12 GeneRIFs, 283 antibodies, and having met a threshold of publications (Sheils et al., 2020). In the Harmonizome, a database that collates and references gene and protein information from other '-omics' databases, GPR84 has 2,088 functional associations with existing datasets, primarily associations between expression in various tissue states (Rouillard et al., 2016). In contrast to these databases which focus on human health, the recently released Unknome database considers protein 'knownness' based on GO annotations from humans and 11 model organisms when organised according to the PANTHER classification of protein family groups (Rocha et al., 2023). Using modifiable criteria on the weighting of GO annotations, a protein's 'knownness' can be distilled into a single number, ranging from 0 to over 100. Human GPR84, and indeed its orthologues, have a very low level of

'knownness', all scoring 1.5 or below when using the default weightings. In fact, the entire PANTHER protein family containing GPR84 scores a standard 'knownness' of just 12.2. This score is based on the top-scoring and most 'known' protein in the family, which is that of the rat urotensin-2 receptor. Alternatively, the best characterised human protein in this family is the human Galanin type 2 receptor which scores a 'knownness' of 10.8 (Rocha et al., 2023). This review of published drug target databases highlights not only the scarcity of information regarding the function of GPR84 in other species, but also the function of the entire evolutionarily related GPCR family described by PANTHER (PTHR24230) (Thomas et al., 2022).

1.1.5. GPR84 Structure

There are four recently determined publicly available protein structures of GPR84, not including the AlphaFold model. Two publications reported the cryo-EM structure determinations of modified human GPR84 bound to the heterotrimeric G-protein subunits and a stabilising antibody in complex with the ligands LY237, 3-OH-C12, 6-OAU, as well as a modelled unliganded state (Liu et al., 2023, Zhang et al., 2023). Both structures utilised wild-type human GPR84 modified only at the N-terminus (NT) and C-terminus with tags to facilitate thermal stability, epitope recognition, protein expression, and association with the G-protein. Overall, the protein structure of GPR84 is similar to known lipid-sensing GPCRs (Liu et al., 2023). Most strikingly, the NT and ECL2 together form a 'roof-like' structure over the receptor transmembrane core, partitioning the orthosteric pocket from the extracellular milieu (Liu et al., 2023, Zhang et al., 2023) (Figure 3 A, B). This is reminiscent of the NT 'cap' which packs between ECL1 and ECL2 and folds over the top of the $S1P_1$ receptor, the first lipid-sensing GPCR to be crystallised (Hanson et al., 2012). However, the relatively long ECL2 of GPR84 forms a β-sheet and protrudes further in towards the receptor core as compared to other lipid receptors such as FFA_1, $S1P_1$, LPA_1, and CB_2, further restricting the size of the orthosteric pocket, and potentially explaining the medium-chain length specificity of GPR84 (Liu et al., 2023, Zhang et al., 2023). To reinforce this 'roof' a unique disulphide bridge pattern exists; a conserved TM3-ECL2 disulphide bond in known lipid structures, as well as a non-conserved NT-ECL2 disulphide bond (Liu et al., 2023, Zhang et al., 2023).

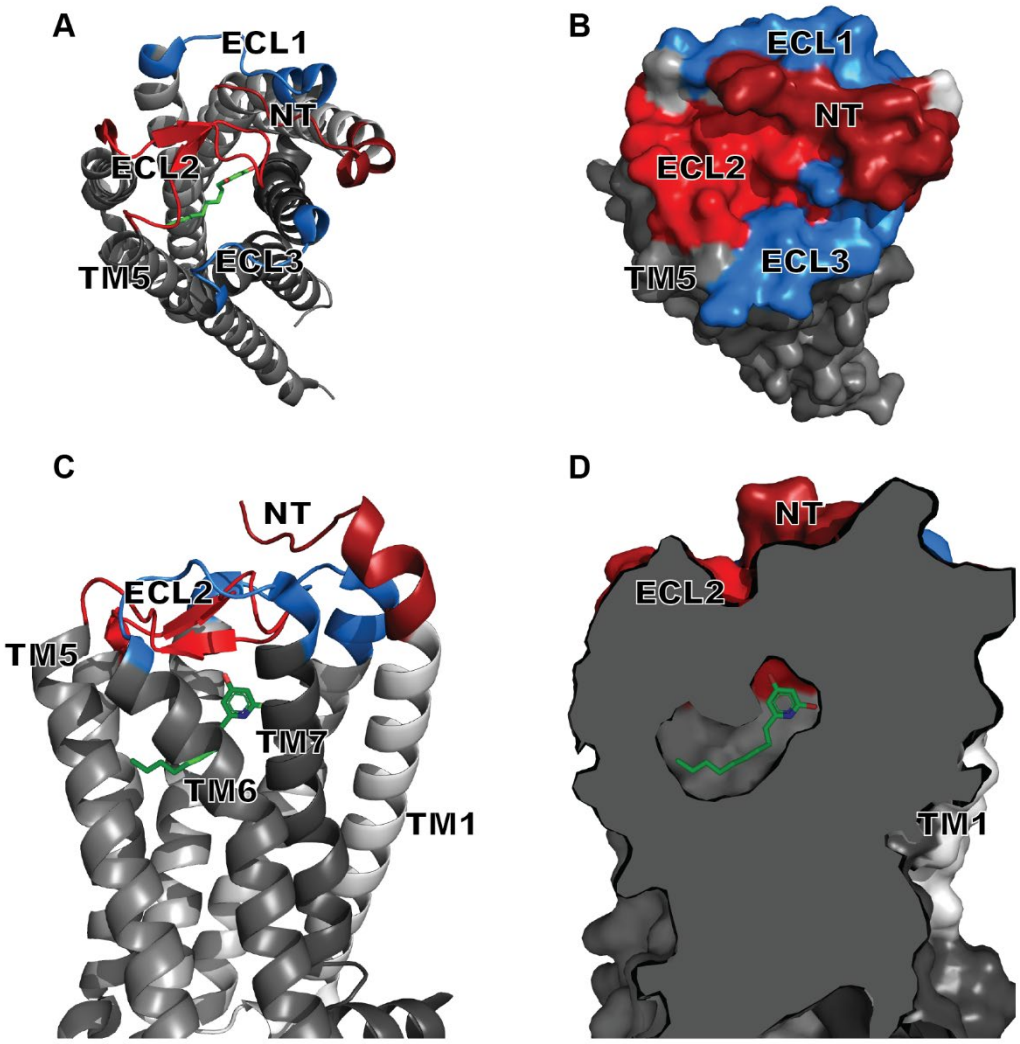

Figure 3: Structure and binding pocket of GPR84 bound with LY237. Human GPR84 Cryo-EM structure with transmembrane regions shown in grey, ECL1 and ECL3 in blue, ECL2 shown in red, the N-terminal cap shown in dark red, and LY237 in green sticks. $G\alpha_i$, $G\beta\gamma$, and antibody fragments hidden for clarity. Cartoon (A) and surface map (B) of the 'cap' on top of GPR84 created by ECL2 and the N-terminus. Full receptor cartoon (C) and a clipped plane surface map (D) of the orthosteric site occupied by LY237. Figure generated using PyMOL v2.5 (Schrödinger, LLC) adapted from and using the cyro-EM structure determined by Liu et al. (2023) (PDB ID: 8J19). ECL, extracellular loop; NT, N-terminus; TM, transmembrane.

The orthosteric site of GPR84 is completely buried inside the transmembrane bundle and inaccessible to the extracellular surface (Liu et al., 2023, Zhang et al., 2023) (Figure 3 C, D). The structures of $S1P_1$ and CB_1 revealed putative lipid entry portals from the bilayer with openings between TM1 and TM7 (Hanson et al., 2012, Shao et al., 2016). No such lipid entry channels were found in GPR84. The binding pose of 6-OAU shows its uracil acid head group facing the

extracellular surface with the hydrophobic chain buried inside the transmembrane bundle, which was similar to those of LTB_4, S1P, LPA, and PGE_2 in their respective receptors which do have openings to the extracellular environment (Zhang et al., 2023). Curiously, in an attempt to solve the structure of an unliganded GPR84, Liu et al. (2023) found a shape of EM density in the orthosteric pocket fitting MCFAs of 10-12 carbons long. Then, when adding 3-OH-C12 during the sample preparation process the complex was solved and binding pose of this MCFA found to resemble LY237, both bearing nonane tails which face a cleft between TM3 and TM5 (Liu et al., 2023). Using molecular dynamics simulations Liu et al. (2023) proposed a model whereby LY237 enters through an opening between ECL2 and TM7, made accessible by a spontaneous movement upwards of ECL2 during simulations.

The importance of ECL2 has been demonstrated through studies identifying $R172^{ECL2}$ as a binding partner for MCFAs (Mahmud et al., 2017). Furthermore, in a protein sequence analysis between human and 214 vertebrate GPR84 orthologues there were a number of residues that were 100% conserved, largely spatially distributed into the helical core from TM2 and TM3, and in ECL2 (Schulze et al., 2022). Without the NT-ECL2 disulphide bond or H352 in TM7 it is likely that GPR84 fails to fold correctly (Zhang et al., 2023), and additionally, many naturally occurring SNPs at GPR84 were found to affect surface receptor expression, particularly residues at the intracellular interface and a region between TM2-TM3-TM4 (Schulze et al., 2022). These highlight the potential for disease relevant mutations which confer altered receptor folding and trafficking.

1.2. Dietary Capric Acid as the Putative Endogenous Agonist of GPR84

1.2.1. Low Potency of Capric Acid

Wang et al. (2006) first demonstrated that GPR84 responds to MCFAs *in vitro* by testing saturated FFAs with carbon chain lengths from 1 to 22 in both cAMP and [^{35}S]GTPγS assays. These experiments revealed that FFAs with chain lengths 9 to 14 could activate the receptor, with the most potent of these being capric acid with a 10-carbon long chain. Given its relatively low EC_{50} of 4.5 μM in the cAMP assay it remained unclear if this was the true physiological agonist. However, it was an attractive addition to the emerging model that dietary fatty acids can be sensed by GPCRs,

and indeed exert many of their beneficial effects via these receptors. De-orphanisation of the FFARs occurred in the three years prior, with long-chain fatty acids having been shown to activate FFA1 (GPR40) and FFA4 (GPR120), and short chain fatty acids having been shown to activate FFA2 (GPR43) and FFA3 (GPR41) (Hirasawa et al., 2005, Stoddart et al., 2008) at concentrations below that found in plasma (Dranse et al., 2013).

There is no *a priori* potency needed for a ligand that is required for it to exert biologically meaningful effects. Capric acid, the most potent saturated MCFA, has a cAMP EC_{50} of 7.42 μM, a β-arrestin-2 EC_{50} of 6.08 μM, and a K_i of 1.78 μM at hGPR84, demonstrating both the low affinity and potency of capric acid (Köse et al., 2020). The low potency of capric acid is also evident in at least 17 GPR84 orthologues covering most of the mammalian orders (Schulze et al., 2022). While many GPCRs do sense their cognate ligands at nanomolar potency values, there are still examples of some which do not. The lipid-sensing cannabinoid receptor agonists are relatively low affinity but high efficacy ligands (Howlett, 2002). In the brain, the group III metabotropic glutamate receptor subfamily have nanomolar affinities for glutamate, with the exception of $mGlu_7$, which has a high micromolar affinity for glutamate and has instead been proposed to function as an 'emergency brake' on high glutamate levels, acting presynaptically to inhibit further glutamate release and prevent excitotoxicity (Fisher et al., 2018). Likewise, the recently de-orphanised HCA_2 receptor has a 700 μM affinity for its ligand, β-hydroxybutyrate, a ketone body that can achieve these high concentrations during fasting and ketogenesis (Offermanns and Schwaninger, 2015). Activation of HCA_2 on adipocytes then acts to inhibit lipolysis, activating a negative feedback loop that has been proposed to regulate energy release during starvation. HCA_2 also responds to chemicals in nature, including nicotinic acid which has an EC_{50} of 1 μM and exerts anti-inflammatory effects on macrophages such as an inhibition of NF-κB (Offermanns and Schwaninger, 2015). This raises the question of whether GPR84 could be a highly situational receptor, serving as a negative feedback loop or 'handbrake' in contexts of elevated capric acid or MCFAs.

More micromolar affinities of lipid-sensing GPCRs can be seen with the putative family members of GPR84, the FFARs. Short chain fatty acids such as acetate, propionate, and butyrate are

produced by anaerobic bacterial fermentation of carbohydrtates in the intestine, and can be found in the blood at high micromolar levels (Dranse et al., 2013, Le Poul et al., 2003). These short chain fatty acids can activate FFA2 and FFA3 in the low micromolar range (Le Poul et al., 2003). Long and medium chain fatty acids are typically derived from the diet, or are biosynthesised by key FFA handling organs such as adipose tissue or the liver (Dranse et al., 2013). Long chain fatty acids can activate FFA1 and FFA4 in the low micromolar range (Briscoe et al., 2003, Hirasawa et al., 2005, Itoh et al., 2003), and importantly, are also found in the serum at high micromolar concentrations (Dranse et al., 2013). Ranges of the agonist potency compared to the physiological levels of the endogenous agonists were reviewed by Dranse et al. (2013), and summarised as follows; FFA1 and FFA4 respond to long-chain fatty acids (LCFAs) with EC_{50} values in the ranges 1 - 30 μM which can be found in serum at between 200 – 500 μM, and FFA2 and FFA3 respond to short-chain fatty acids (SCFAs) with EC_{50} values between 0.1 – 1.0 mM which can be found in the gut at between 70 – 100 mM, or serum between 50 – 200 μM.

While the relatively high EC_{50} values of the FFARs were initially a challenge to pharmacologists, the more complete physiological characterisation of their role *in vivo* has led to their de-orphanisation (Smith, 2012). The tissue expression of the FFARs is appropriate for their role in the postprandial sensing of dietary FFAs and it has been demonstrated that their cognate ligands can reach circulating concentrations of over 100 × EC_{50} (Dranse et al., 2013, Smith, 2012). The same level evidence does not exist for GPR84 and capric acid. Circulating levels of capric acid only approach mid-micromolar levels in patients with genetic deficiencies of fatty acid oxidation, or in subjects directly receiving purified medium-chain triglyceride (MCT) supplementation, and at best, approach 36 × cAMP EC_{50} when subjects take two 20 mL doses of pure tricaprin oil, the capric acid triglyeride.

1.2.2. Circulating Concentrations of Capric Acid

Plasma concentrations of capric acid fluctuate markedly according to an individual's fasting state, intake of MCTs, and metabolic genotype. The largest study to date identified the average fed-state concentration of capric acid in the blood of 106 healthy Japanese volunteers was 0.3 μM

(Shrestha et al., 2015). This may elevate to ranges between 1.8 µM to 18 µM after an overnight fast as indicated in other studies (Costa et al., 1998, Courchesne-Loyer et al., 2017, Crotti et al., 2016, Lagerstedt et al., 2001, Lotti et al., 2017). Dietary intervention studies using special MCT formulations may also dramatically increase plasma levels of capric acid; two studies involving 10 and 8 participants each saw increases in plasma capric acid increase from 9.3 µM to 139.4 µM and from undetectable levels to 267 µM respectively (Courchesne-Loyer et al., 2017, St-Pierre et al., 2019). This is also the case in infants and children, which have been studied due to the MCT content of milks and infant formulas. Capric acid concentrations in preterm infants reached 41.60 µM and 83.99 µM with MCT supplementation, and 156.7 µM and 174 µM in children with intractable epilepsy (Carnielli et al., 1996, Haidukewych et al., 1982, Rodriguez et al., 2003, Sills et al., 1986). Metabolic deficiencies in fatty acid oxidation pathways can also result in elevated plasma capric acid concentrations. Five children with long-chain 3-hydroxyacyl CoA dehydrogenase mutations had plasma capric acid concentrations ranging from 2.5 µM – 11 µM, compared to the control average of 1.8 µM (Costa et al., 1998). Multiple acyl-CoA dehydrogenase deficiency was a genotype associated with the highest plasma capric acid levels at 71 µM in a neonatal subject (Costa et al., 1998) as well as at 30.8 µM in a child (Kimura et al., 2002). Medium-chain acyl-CoA dehydrogenase deficiency is also associated with elevated plasma capric acid, with subjects ranging from 2 – 228 µM (Onkenhout et al., 1995). These findings demonstrate that it is possible to reach micromolar concentrations of capric acid in the blood, but that is only observed with genetic deficiencies in fatty acid oxidation, or supplementation with pure MCTs, and is therefore unlikely to occur on a typical diet. There is still a need for studies to identify local concentrations of non-esterified capric acid in different tissues in the body, especially those at immune interfaces or with resident immune cells expressing GPR84, such as the CNS, intestinal tract, or adipose tissue.

1.2.3. Low Selectivity of Capric Acid

Capric acid has also been reported to activate other GPCRs, indicating a lack of specificity for GPR84. It has a reported EC_{50} of 3.16 µM at FFA4, 25.1 µM at FFA1 (Christiansen et al., 2015) and a micromolar EC_{50} at the lipid-sensing immune receptor CB_2 (Luscombe et al., 2020).

Undecanoic acid (C11) activates FFA1 with a lower EC_{50} than GPR84, and lauric acid activates FFA4 with a lower EC_{50} than GPR84 (Christiansen et al., 2015), highlighting the agonists from chain lengths 10, 11, and 12 lack selectivity for GPR84. It is known that FFA1 shares ligand overlap with both FFA4 and PPARγ, and that SCFAs share affinity for FFA2 and FFA3 (Smith, 2012, Ulven and Christiansen, 2015), so it is not without precedent that fatty acid sensing GPCRs have some overlap, especially when considering the only primary electrostatic binding groups are in the carboxylic acid head group.

One would expect the tissue distribution or expression profiles to offer some discrimination between ligand selectivity. FFA4 in particular is highly expressed by macrophages, although in contrast to GPR84, it exerts anti-inflammatory effects (Ulven and Christiansen, 2015). Likewise, 3-hydroxy capric acid (3-OH-C10) activates both HCA_3 and GPR84, and both receptors are expressed on monocytes, macrophages, and neutrophils (Peters et al., 2022). Curiously, HCA_3 is largely associated with anti-inflammatory effects, and the basis for why these G_i-coupled receptors might be co-expressed and share at least one agonist, despite exerting seemingly opposite functions, is a current area of research (Peters et al., 2022). Due to their low potency at GPR84 capric acid and MCFAs are often used at concentrations of or above 100 μM. In cell systems expressing multiple receptors that respond to MCFAs this presents a major issue with regards to mechanism. This is especially true if these receptors, such as FFA4 or HCA_3 exert anti-inflammatory effects and are likely to oppose the function of GPR84. Specific and potent fatty acid mimetics exist with which to probe GPR84, including 6-OAU and LY237, both of which are known to occupy the orthosteric binding pocket.

1.2.4. Low Efficacy of Capric Acid

Capric acid and MCFAs have also been shown to have low efficacy in more physiological assays. In a label-free cell impedance assay measuring cell shape change and morphology, 6-OAU and C5a cause specific and sharp positive responses in LPS treated BMDMs (Recio et al., 2018). In contrast, undecanoic acid, capric acid, and lauric acid at 10 μM caused weak responses with no specific peak, therefore resembling a baseline or vehicle response more so than 6-OAU or C5a (Recio

et al., 2018). In the initial characterisation of MCFAs RAW264.7 cells were exposed to 1 mM of undecanoic acid, capric acid, or lauric acid for 21 h, revealing an increase in IL-12 p40 production (Wang et al., 2006). However, this was not observed at 0.25 mM for capric acid or undecanoic acid, highlighting the low potency and lack of efficacy in this system at physiologically relevant concentrations of MCFAs. Similarly, capric acid was used at 500 μM for 22 h in experiments showing increased *Tnf* expression in human monocytes and THP-1 cells (Müller et al., 2017). In LPS-stimulated peripheral blood mononuclear cells, capric acid caused an increase in IL-6 and TNFα production, and decrease in IL-10 production, but only at 200 μM and not at 20 μM or 2 μM (Sam et al., 2021). THP-1 M1 macrophages stimulated with capric acid at 100 μM did result in enhanced reactive oxygen species (ROS) production, and notably this appeared to be independent of HCA_3 and specific to GPR84, although agonist was still applied for 24 h (Peters et al., 2022). In this study 100 μM capric acid was only approximately 50% efficacious in the cAMP assay on THP-1 M1 macrophages compared to 1 μM 6-OAU, which curiously did not result in enhanced ROS production (Peters et al., 2022). In TNFα-primed human neutrophils capric acid and undecanoic acid were used at 500 μM to achieve NADPH-oxidase activation comparable to 1 μM ZQ-16 (Sundqvist et al., 2018).

Consistently, the most prominent effects of GPR84 activation are of inflammatory function. So, in addition to the secretion of inflammatory mediators, capric acid has also been investigated in migration and phagocytosis experiments. When used at 1, 10 or 100 μM capric acid was shown not to induce migration of human primary neutrophils (Mikkelsen et al., 2022). In phagocytosis experiments capric acid exhibited a similar efficacy as 6-OAU and ZQ-16, but only at 100 μM, which was 1,000 and 10,000 × higher than that of 6-OAU and ZQ-16 (Kamber et al., 2021). These effects were absent in GPR84 KO macrophages, and did not replicate with acetic acid or palmitic acid, providing evidence for the specificity of this response (Kamber et al., 2021). However, taken together these results highlight the routine use of capric acid at concentrations above 100 μM with varying efficacy in the secretion of inflammatory cytokines, generation of reactive oxygen species, migration, and phagocytosis. What is clear is that, given its low potency, at concentrations below

100 μM capric acid would be expected to have limited or no efficacy in most of these inflammatory functions.

1.2.5. Fatty Acid Absorption & Distribution

Dietary fats are almost always esterified in triglycerides (TGs), and are first hydrolysed into FFAs by lipases in the oral cavity or in the stomach or intestine prior to absorption by enterocytes. Here, they are re-esterified into TGs and incorporated into chylomicrons and secreted into systemic circulation via the lymph (Hodson and Fielding, 2010). MCFAs, even when esterified, enter circulation directly via the portal vein and are rapidly taken up and oxidised by the liver (Mu and Høy, 2004, Wallace, 2019). Once in the liver, fatty acid synthetases responsible for re-esterification of fatty acids into TGs are also more selective for FFAs of 14 carbons or more, resulting in a lower abundance of MCFAs in TG fractions (Papamandjaris et al., 1998). Only small percentages of MCFAs circulate in chylomicrons, even with large dietary supplementation of MCTs (Swift et al., 1990). MCTs are more rapidly absorbed and enter circulation faster than LCFAs. LCFAs circulate the bloodstream in lipoproteins and can congeal on artery walls, influencing cardiometabolic risk. Due to their altered route of absorption, MCFAs are less likely to contribute to arterial fatty acid deposits (Wallace, 2019). MCFAs are also absorbed in the colon, which is the site of SCFA generation via bacterial fermentation, although absorption of MCFAs do not involve bacteria (Mu and Høy, 2004). If absorption of dietary MCFAs were sensed by GPR84, then one would expect high levels of expression in the enterocytes, liver, or colon. However, only a few reports exist describing relatively low levels of GPR84 expression in these tissues or cell types.

As would be expected from nutrient sensors, the de-orphanised FFARs are expressed in the gastrointestinal tract. All four FFAR subtypes are highly expressed by enteroendocrine L cells where they cause the release of gut hormones such as GLP-1 and Peptide YY (Kimura et al., 2020, Lu et al., 2018, Moodaley et al., 2017). FFA1 is also found in the brain, on monocytes, and in β-cells in pancreatic-islets (Briscoe et al., 2003, Itoh and Hinuma, 2005). FFA4 is expressed by intestinal K cells, gastric A and D cells, pancreatic islets, adipose tissue, lungs, taste buds, and macrophages (Moodaley et al., 2017, Suckow and Briscoe, 2017). FFA3 can also be found in the sympathetic

nervous system (Hara et al., 2014). FFA2 is expressed in adipocytes, and also in neutrophils and eosinophils (Hara et al., 2014). Notably, and in contrast to GPR84, FFA2 and FFA4 appear to have anti-inflammatory activity (Hara et al., 2014). The FFAR expression patterns as a whole, while varied, support their involvement in nutrient sensing and energy homeostasis (Hara et al., 2014).

Genetic evidence does not support a role for GPR84 in sensing dietary fatty acids and regulating appetite or energy storage. Recently, Du Toit et al. (2018) used genetic techniques to test if GPR84 was involved in sensing dietary MCFAs by feeding WT and KO mice with a diet rich in LCFA, MCFA, or control diet. The genetic deletion of GPR84 did not alter the increases in body mass or glucose tolerance observed with either high-fat diet (Du Toit et al., 2018). Similarly, no GPR84 KO effect was observed in the body weight or fat mass increases of mice fed a MCFA-rich diet (Montgomery et al., 2019). These results are contrasted by experiments on FFARs in mice. FFA3 KO mice have an increased body fat content (Bellahcene et al., 2013), as do FFA4 KO mice on high-fat diets (Ichimura et al., 2012, Oh et al., 2010). FFA2 and FFA3 double KO mice on high-fat diets have improved glucose tolerance (Tang et al., 2015). A full agonist of FFA1 has been shown to decrease food intake and body weight in rats (Ueno et al., 2019). Additionally, a genetic polymorphism in FFA4 that inhibits signalling has been associated with obesity risk in European populations (Ichimura et al., 2012).

Circulating immune cells could encounter the rapidly absorbed MCFAs in the bloodstream, although it is clear that plasma capric acid concentrations rarely approach the concentrations required to activate GPR84. One way dietary TGs could theoretically reach a high concentration and interact with innate immune cells would be in lymph nodes. Macrophages express lipoprotein lipases required to hydrolyse TGs for uptake (Ostlund-Lindqvist et al., 1983). However, under normal conditions these lipases are inhibited by Angptl4, including in the lymph nodes, thereby preventing inappropriate engorgement of lipids by activated macrophages (Lichtenstein et al., 2010).

1.2.6. Fatty Acid Metabolites

Energy demands of the body are supported by mitochondrial fatty acid β-oxidation, which occurs in key metabolising organs including the liver, heart, and skeletal muscle (Zhang et al., 2010).

To enter a cell, TGs are first hydrolysed by lipases and then FFAs enter the cell using fatty acid transport proteins, where they are rapidly turned into acyl-CoAs (Houten and Wanders, 2010). LCFA acyl-CoAs use the carnitine shuttle system to enter mitochondria, while MCFAs can instead enter mitochondria directly (Papamandjaris et al., 1998). Myocytes and hepatocytes generate ATP from FFAs in the mitochondria via β-oxidation and the Krebs cycle pathway in a process whereby two carbon atoms from the fatty acid are released as acetyl-CoA per cycle (Houten and Wanders, 2010, Ritchie et al., 2017, Zhang et al., 2010). Medium chain acyl-CoA dehydrogenase (MCAD) is then responsible for the metabolism of MCFA acyl-CoA species found inside the mitochondrial matrix, which may also be the result of shortened LCFAs following multiple cycles of β-oxidation (Houten and Wanders, 2010). Due to their rapid absorption and metabolism, MCT supplementation has been proposed to help undernourished patients, manage obesity, or manage patients with LCFA oxidation disorders (Labarthe et al., 2008) and have also been investigated for possible benefits in exercise performance, though most studies do not see an improvement (Chapman-Lopez and Koh, 2022). However, incompletely oxidised lipid species are present in conditions of excess circulating fatty acids, such as diabetes and obesity (Ritchie et al., 2017, Zhang et al., 2010), and may be relevant to potential interactions with GPR84.

Oxidised lipids in lipoproteins are another potential source of circulating modified MCFAs. Despite their rapid uptake and oxidation, dietary MCFAs can still influence the circulating lipoprotein pool. A meta-analysis revealed that MCFA-rich diets can increase high-density lipoprotein (HDL) and apolipoprotein A1 levels in humans compared to LCFA-rich diets, with no effect on TG, low-density lipoprotein LDL, and total cholesterol (Panth et al., 2018). As oxLDL has been shown to induce the expression of *GPR84* in human monocyte-derived macrophages (Recio et al., 2018), it is conceivable that GPR84 could play a role in atherogenesis. Oxidation products of LDL include oxidised fatty acids, and these are a recognised inflammatory trigger in atherosclerosis and may be encountered by macrophages during plaque progression.

MCFAs are oxidised more rapidly than LCFAs (DeLany et al., 2000), and one possibility is that GPR84 actually ‘senses’ the metabolites of MCFAs and not the fatty acids themselves. This was

first explored by Suzuki et al. (2013) when testing 2- and 3-hydroxylated MCFAs. These performed as well as or better than their non-hydroxylated counterparts in GPR84 assays (Suzuki et al., 2013). Studies have shown 3-hydroxy capric binds to GPR84 and can elicit cAMP responses, phosphorylate ERK, and recruit β-arrestin-2 (Köse et al., 2020, Peters et al., 2020). Due to their increased potency, some hydroxylated MCFAs are now being adopted alongside, or replacing saturated MCFAs and capric acid in experimental work. However, the potential origins and tissue distribution of these species remains uncharacterised. Effects on GPR84 may also be enantioselective, and testing these and comparing them to which enantiomers exist in nature and in the body may reveal clues into the function of GPR84.

Different biological processes result in different enantiomers of 2- and 3-hydroxy MCFAs, opening the possibility that through evolutionary selection GPR84 might exhibit selectivity for some form over another. Mammalian fatty acid 2-hydroxylase is an enzyme expressed in the brain, epidermis, and adipose tissue, and generates enantiopure (*R*)-2-hydroxy fatty acids (Guo et al., 2012). These 2-hydroxy fatty acids can undergo α-oxidation, which removes one carbon and the hydroxyl group, allowing the fatty acid to enter the β-oxidation pathway (Mori et al., 2023). Hydroxylation at the 3-position is carried out by hydratases during mitochondrial β-oxidation, generating transient (*S*)-3-hydroxyacyl-CoA intermediate species which are then catalysed by medium-/short-chain mitochondrial L-3 hydroxyacyl CoA dehydrogenases into 3-ketoacyl-CoA species (Jones and Bennett, 2011, Schulz et al., 2011). However, under normal physiological conditions 3-hydroxy capric acid still exists below 1 μM in human plasma, and may elevate to only 3 μM with MCT supplementation (Jones and Bennett, 2011). Small amounts of 2- and 3-hydroxy MCFAs are also present in dairy foods, where typical consumption might reach milligram quantities per day (Jenske and Vetter, 2009). Milks, cheeses, and avocado contain pure (*R*)-3-hydroxycapric acid and predominantly (*R*)-2-hydroxy capric acid (Jenske and Vetter, 2008). In foods the (*R*) configuration of 2- and 3-hydroxy MCFAs is far more prevalent and it is also assumed that the presence of (*S*)-2-hydroxy MCFAs in foods are actually of bacterial origin (Eckhardt, 2023, Jenske and Vetter, 2008). Microbial 3-hydroxy MCFAs are predominantly in the (*R*) configuration too,

while 2-hydroxy MCFAs are predominantly in the (*S*) configuration (Jenske and Vetter, 2008, Rietschel, 1976). Diet related 2- or 3-hydroxylated MCFAs are therefore expected to be in the (*R*) configuration, with microbial sources being of (*R*)-3-hydroxy MCFAs or (*S*)-2-hydroxy MCFAs (Table III).

Table III: Overview of different sources of 2- and 3-hydroxy MCFAs

Oxidised MCFA	Configuration	Can be derived from	References
3-hydroxy MCFA	(*R*)	Dietary milks, cheeses, avocado; predominant enantiomer.	(Jenske and Vetter, 2008)
		Microbes, predominant enantiomer	(Jenske and Vetter, 2008, Rietschel, 1976)
	(*S*)	Hydratases during mitochondrial β-oxidation, enantiopure product but rapidly epimerised to racemic mixture	(Jin et al., 1992)
2-hydroxy MCFA	(*R*)	Mammalian fatty acid 2-hydroxylase, enantiopure product.	(Guo et al., 2012)
		Dietary milks, cheeses, avocado; predominant enantiomer.	(Jenske and Vetter, 2008)
		Wool wax, enantiopure	(Guo et al., 2012)
	(*S*)	Components of bacterial LPS, predominant enantiomer	(Jenske and Vetter, 2008)

1.2.7. Overlap of Medium-Chain Fatty Acids with GPR84 Expression

Nutrient sensing and inflammatory pathways are inextricably linked to both diet and sleep cycles. If GPR84 were a sensor for dietary MCFAs, then one outstanding question is when this might take place given the low basal expression of GPR84 in unstimulated conditions. Presumably the upregulation of GPR84 is of physiological significance, and data has shown this upregulation takes many hours. Peak expression in BMDMs occurs closer to 6 – 8 h, and subsides by 16 – 24 h (Lattin et al., 2008, Recio et al., 2018). In adipocytes, TNFα, IL-1β, and IL-33 all induce expression by 3h or 4 h but subside by 24 h (Muredda et al., 2018, Zaibi et al., 2018). If GPR84 is a low affinity sensor for dietary fatty acids then an induction signal would need to occur some hours before a meal. Unless the metabolic role is unrelated to meal times, and is for example, a coincidence detector of inflammatory conditions and dietary intake of MCFAs, such as a global upregulation in diabetes or

obesity. However, what is clear, is that unlike the FFARs, GPR84 expression under normal conditions has a low spatiotemporal overlap with the absorption and handling of dietary fatty acids (Figure 4).

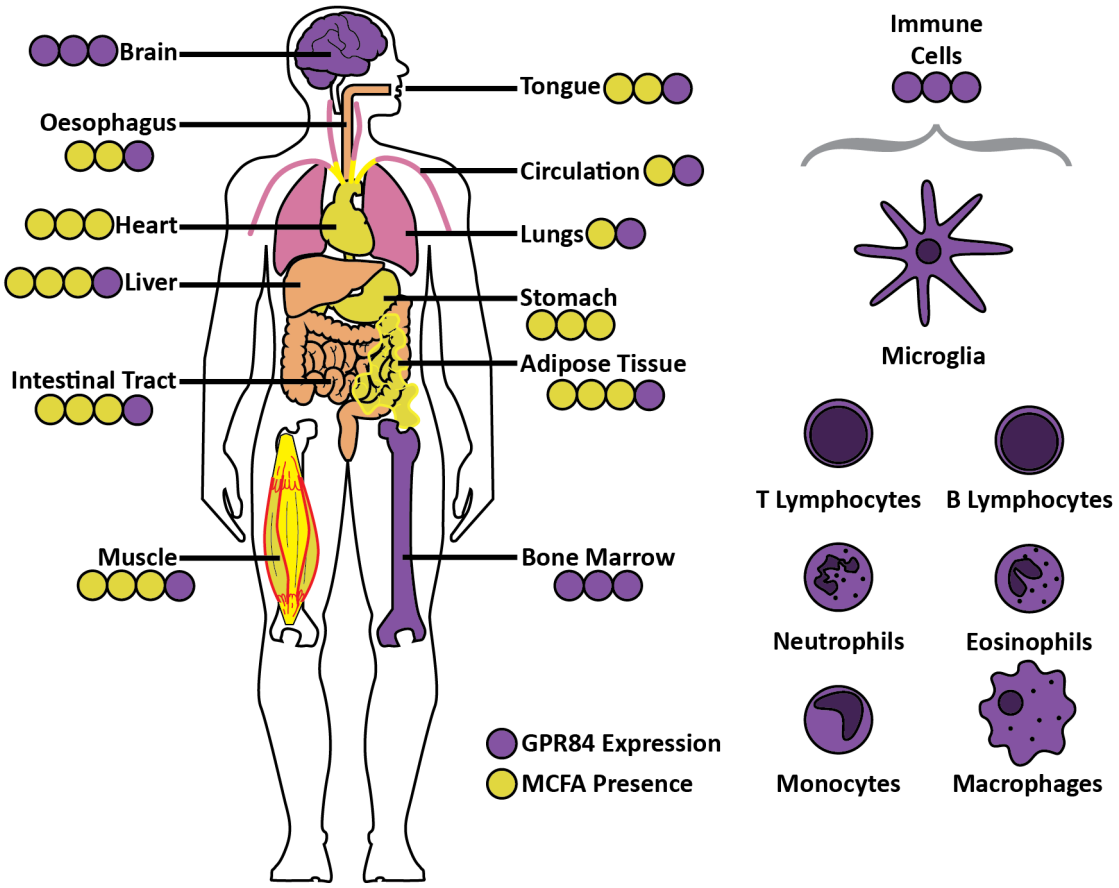

Figure 4: Overlap of GPR84 Expression with MCFAs. GPR84 receptor expression (*purple*) has limited spatiotemporal overlap with the absorption, handling, and use of dietary TGs and FFAs (*yellow*). An aggregate representation of the relative levels of expression and presence are indicated with coloured circles. MCFA dietary intake leads to processing in the gastrointestinal tract before rapid absorption via the portal vein to the liver. Most dietary and circulating MCFAs are TGs, with the highest hydrolytic activity to generate FFAs occurring in these key FFA-handling organs: the liver, heart, muscle, and adipose tissue. GPR84 expression is notably higher in bone marrow and the brain than at these key FFA-handling organs. GPR84 mRNA is primarily expressed by immune cells throughout the body. Reproduced with permission from Luscombe et al. (2020).

GPR84 may be expressed under chronic low-grade inflammatory conditions such as in diabetes and obesity. GPR84 expression is increased in the epididymal fat pads of mice on a high fat diet (Nagasaki et al., 2012). Expression is also upregulated in the brain, bone marrow, and kidneys of nonobese diabetic mice, and in the aortae of ApoE$^{-/-}$ high-fat diet mice (Recio et al., 2018). GPR84 expression is also upregulated in the liver of patients with NAFLD (Puengel et al., 2020).

Furthermore, mice on high-fat diets have higher plasma and faecal endotoxin levels as well as increased macrophage infiltration into adipose tissue (Kim et al., 2012). This is the site of TG hydrolysis and FFA uptake into adipocytes, and macrophages are known to express some of these lipases. Perhaps this is a potential site of MCFA-GPR84 signalling. Chronic, non-communicable diseases such as diabetes, atherosclerosis, and NAFLD may therefore upregulate GPR84 expression globally, where it can then serve some metabolic function under pathophysiological conditions.

1.2.8. Conclusions

Taken together, my review of the literature regarding the expression of GPR84 and absorption and distribution of MCFAs suggests that it is highly unlikely that GPR84 is a nutrient sensor for saturated dietary MCFAs. Capric acid has a low affinity and low potency for GPR84, a low efficacy in primary cells with regards to inflammatory function, and low selectivity for GPR84. Circulating concentrations of capric acid do not routinely reach levels required to activate GPR84, and no evidence yet suggests what local concentrations might achieve in specific tissues, such as in adipose tissue or in acute bacterial infection. GPR84 expression is both inducible and largely restricted to immune cells, and is spatiotemporally distinct from the absorption and metabolism of dietary MCFAs. Despite the rapid absorption and metabolism of MCFAs, one would still expect an expression profile more akin to that of the FFARs throughout the gastrointestinal tract and in metabolic organs. Still, other potential sources of closely related MCFAs exist, including hydroxylated species in bacterial cell wall components, oxidised lipids in lipoproteins, or metabolite dysregulation in fatty acid oxidation disorders. Unfortunately, the compositions, concentrations, and chiral configurations of these fatty acids in the body remain poorly characterised and warrant further research. Furthermore, for the reasons outlined, capric acid is also poor tool compound for probing the biology of GPR84 and there is a need for more selective, potent, and efficacious MCFAs or lipid mimetic tools.

1.3. Small Molecule Ligands of GPR84

1.3.1. GPR84 Agonists

1.3.1.1. *Chemical Discovery*

GPCRs are pleiotropic signalling proteins that, when liganded by so-called 'first messengers', adopt a particular conformation which favours interactions with intracellular transducer proteins which then exert further effects intracellularly. Agonists can stabilise receptor states that favour one or more of these downstream transducer proteins, such as the G-proteins themselves, GRKs, and β-arrestins (Smith et al., 2018). Such an agonist is referred to as 'biased', and will preferentially signal through the pathways mediated by these transducer proteins, such as the cAMP or IP_3 and DAG 'second messenger' pathways in the case of G-protein biased agonists, or through the β-arrestin signalling pathway in the case of β-arrestin biased agonists (Smith et al., 2018). As the number of signalling effectors and pathways increase downstream, it is possible to imagine how influential biased signalling can be at the cellular level. This signalling bias arises from the structure and properties of an agonist. However, biased signalling may also occur in systems with different levels of transducer proteins, or in situations where a receptor is poorly coupled to these proteins, and is differentiated as a 'system bias' rather than agonist bias.

Following the identification and cloning of GPR84, agonists were discovered under the broad categories of MCFAs, lipid mimetics, natural products, and synthetic agonists. With these tools now available to probe receptor activity, functional assays began to uncover signalling bias at GPR84. This began with the exploration of structure-activity relationships (SAR) around the natural product DIM with regard to the G-protein and β-arrestin pathways (Pillaiyar et al., 2017). DIM had previously been shown to bind allosterically compared to MCFAs (Nikaido et al., 2015). Most of the compounds in this series were biased towards the G-protein pathway, exemplified by PSB-16671 (di(5,7-difluoro-1H-indole-3-yl)methane) (Figure 5). Only a few compounds were found to have more limited levels of bias towards the β-arrestin pathway (Pillaiyar et al., 2017). These DIM derivatives are also known to act allosterically (Mahmud et al., 2017). Then further SAR around the lipid-mimetic 6-OAU and its derivatives were explored (Pillaiyar et al., 2018). This work highlighted

the variability, or tunability, of cAMP versus β-arrestin signalling, as unbiased compounds such as PSB-1584 were seen in the same series as PSB-16434, which had a 79-fold pathway selectivity towards cAMP (Pillaiyar et al., 2018). Additionally, a cyclopropane-containing MCFA isolated from the marine bacterium *Labrenzia* sp. 011 has been shown to recruit β-arrestin without affecting cAMP production in GPR84 stable cell lines, demonstrating bias towards β-arrestin from natural product MCFAs (Amiri Moghaddam et al., 2018). Finally, the G-protein biased *in vitro* tool compound DL-175 was discovered following a ligand-based virtual screen on a pharmacophore model based on 6-OAU-like compounds (Lucy et al., 2019) and is now available from commercial suppliers and been used to differentiate pathway bias in macrophages and neutrophils (Fredriksson et al., 2022, Lucy et al., 2019, Mårtensson et al., 2021).

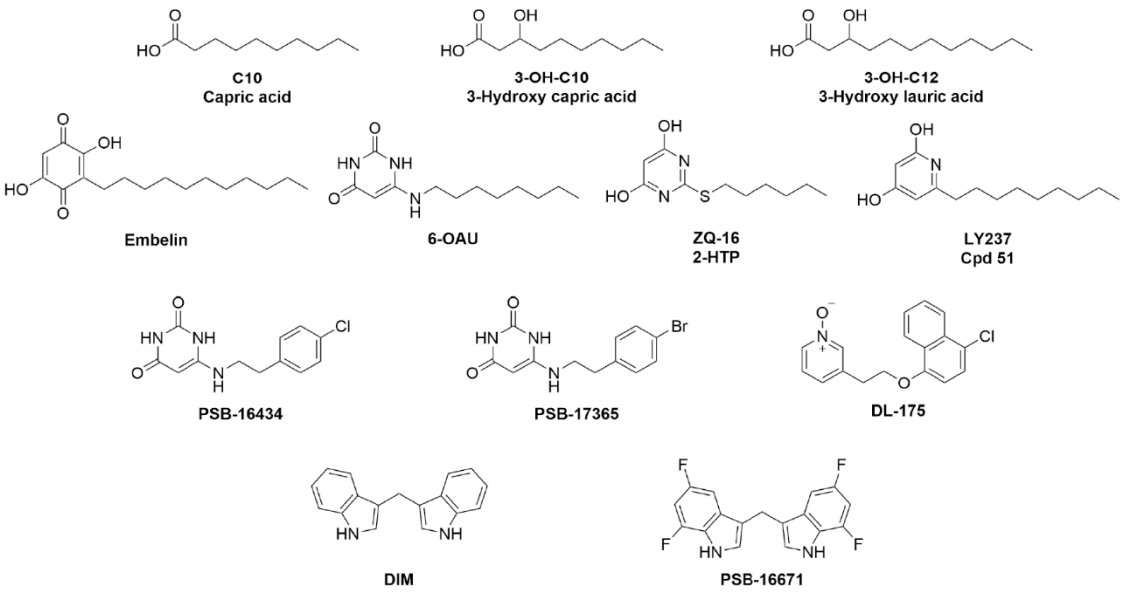

Figure 5: Representative structures of GPR84 agonists. The chemical structures of MCFAs (C10, *rac*-3-OH-C10, *rac*-3-OH-C12), lipid mimetics (Embelin, 6-OAU, ZQ-16, LY237), synthetic agonists (PSB-16434, PSB-17365, and DL-175), and diindolylmethane derivatives (DIM, PSB-16671) are shown. Reproduced with permission from (Luscombe et al., 2023b).

1.3.1.2. *Biased Agonists*

The currently described range of GPR84 agonists point to a marked system bias of this receptor in favour of G_i-mediated pathways over the β-arrestin pathway (Figure 6). We and others have observed trends that favour the G-protein pathway within the chemical series of the orthosteric agonists 6-OAU (Pillaiyar et al., 2018), DL-175, and some MCFAs (Lucy et al., 2019, Mikkelsen et

al., 2022, Peters et al., 2020). We analysed all literature reports of agonists used on GPR84 cell lines or cell types possessing both a G-protein pathway potency value (cAMP or GTPγS) as well as a β-arrestin pathway potency value. Commonly used tool compounds from GPR84 chemical classes, either as being potent agonists or of significant physiological interest, were plotted in colour. For clarity, compounds from chemical series describing the discovery of potent GPR84 agonists, e.g. 6-OAU derivatives, were plotted in grey. This analysis revealed a system bias towards the G-protein pathway when pooling experimental pEC_{50} values from separate experiments. As the potency values for these assays would be expected to be dependent on receptor expression, and additionally that the β-arrestin pathway bias would be expected to be dependent on the arrestin isoform, we have included a reference table of these details (Table IV). Only pEC_{50} values using β-arrestin-2 were found in the literature. GPR84 has also been shown to also recruit β-arrestin-1 upon stimulation with ZQ-16 (Marsango et al., 2022).

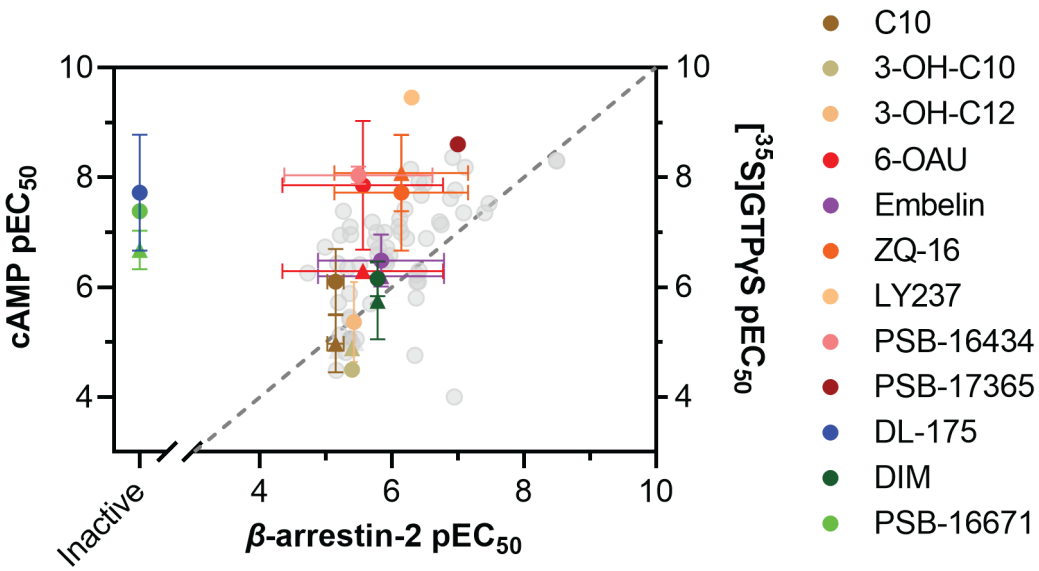

Figure 6: Human GPR84 exhibits a system bias towards the G-protein pathway. Correlation of previously reported pEC_{50} values determined in either cAMP (●) or [^{35}S]GTPγS (▲) assays with given pEC_{50} values from β-arrestin-2 recruitment assays. Previously reported ligands with numerically defined potencies against hGPR84 were analysed and pooled as replicates. Representative compounds from each class are shown in colour. A further 10 MCFA analogues, 2 lipid mimetic analogues, 10 diindolylmethane derivatives, and 35 6-OAU derivatives are shown in grey for clarity (See Table IV). A majority of GPR84 agonists fall above parity (dashed line) which indicates a higher potency in cAMP or [^{35}S]GTPγS assays than in the β-arrestin assay. Points represent mean ± SD if n ≥ 2, *n* = 1-6. Adapted from (Luscombe et al., 2023b).

Table IV: Cell Lines used in the characterisation of human GPR84 signalling bias

Agonist	Assay	Cell Line	Reference
C10	cAMP	CHO-hGPR84 (DiscoverX)	(Lucy et al., 2019, Recio et al., 2018, Luscombe et al., 2023a)
	cAMP	CHO-HA-hGPR84 #7F12 (high expression); CHO-HA-hGPR84 #3E11 (low expression)	(Luscombe et al., 2023a)
	cAMP	CHO-GPR84 (transient transfection)	(Wang et al., 2006)
	cAMP, β-arrestin	CHO-β-arrestin-2-hGPR84 (DiscoverX PathHunter)	(Pillaiyar et al., 2018, Pillaiyar et al., 2017, Southern et al., 2013)
	cAMP, GTPɣS	Flp-In T-REx HEK293-FLAG-hGPR84-eYFP	(Mahmud et al., 2017)
	GTPɣS	CHO-GPR84 (transient transfection)	(Wang et al., 2006)
C11	cAMP, β-arrestin	CHO-β-arrestin-2-hGPR84 (DiscoverX PathHunter)	(Köse et al., 2020)
	cAMP	CHO-GPR84 (transient transfection)	(Wang et al., 2006)
	GTPɣS	Sf9-hGPR84-bovine-$G\alpha_i$	(Suzuki et al., 2013)
C12	cAMP, β-arrestin	CHO-β-arrestin-2-hGPR84 (DiscoverX PathHunter)	(Köse et al., 2020)
	cAMP	CHO-GPR84 (transient transfection)	(Wang et al., 2006)
	GTPɣS	Sf9-hGPR84-bovine-$G\alpha_i$	(Suzuki et al., 2013)
C13	cAMP, β-arrestin	CHO-β-arrestin-2-hGPR84 (DiscoverX PathHunter)	(Köse et al., 2020)
	cAMP	CHO-GPR84 (transient transfection)	(Wang et al., 2006)
C14	cAMP, β-arrestin	CHO-β-arrestin-2-hGPR84 (DiscoverX PathHunter)	(Köse et al., 2020)
	cAMP	CHO-GPR84 (transient transfection)	(Wang et al., 2006)
	GTPɣS	Sf9-hGPR84-bovine-$G\alpha_i$	(Suzuki et al., 2013)
(*R,S*)-2-OH-C10	cAMP	HEK293-hGPR84	(Zhang et al., 2016)
	GTPɣS	Sf9-hGPR84-bovine-$G\alpha_i$	(Suzuki et al., 2013)
(*R,S*)-2-OH-C12	GTPɣS	Sf9-hGPR84-bovine-$G\alpha_i$	(Suzuki et al., 2013)

(*R,S*)-2-OH-C14	cAMP, β-arrestin	CHO-β-arrestin-2-hGPR84 (DiscoverX PathHunter)	(Köse et al., 2020)
(*R,S*)-3-OH-C10	cAMP, β-arrestin	CHO-β-arrestin-2-hGPR84 (DiscoverX PathHunter)	(Köse et al., 2020)
	GTPɣS	Sf9-hGPR84-bovine-$G\alpha_i$	(Suzuki et al., 2013)
(*R,S*)-3-OH-C12	cAMP, β-arrestin	CHO-β-arrestin-2-hGPR84 (DiscoverX PathHunter)	(Köse et al., 2020)
	cAMP	HEK293-hGPR84	(Zhang et al., 2016)
	β-arrestin	CHO-β-arrestin-2-hGPR84 (DiscoverX PathHunter)	(Pillaiyar et al., 2018)
	GTPɣS	Sf9-hGPR84-bovine-$G\alpha_i$	(Suzuki et al., 2013)
(*R,S*)-3-OH-C14	cAMP, β-arrestin	CHO-β-arrestin-2-hGPR84 (DiscoverX PathHunter	(Köse et al., 2020)
(*R*)-3-OH-C14	cAMP, β-arrestin	CHO-β-arrestin-2-hGPR84 (DiscoverX PathHunter	(Köse et al., 2020)
2-((1*S*,2*S*)-2-hexylcyclopropyl)acetic acid	cAMP, β-arrestin	CHO-β-arrestin-2-hGPR84 (DiscoverX PathHunter)	(Amiri Moghaddam et al., 2018)
6-OAU	cAMP, β-arrestin	CHO-β-arrestin-2-hGPR84 (DiscoverX PathHunter)	(Lucy et al., 2019, Pillaiyar et al., 2018)
	cAMP	CHO-hGPR84 (DiscoverX)	(Lucy et al., 2019, Luscombe et al., 2023a, Recio et al., 2018)
	cAMP	CHO-HA-hGPR84 #7F12 (high expression); CHO-HA-hGPR84 #3E11 (low expression)	(Luscombe et al., 2023a)
	cAMP	HEK293-hGPR84	(Zhang et al., 2016, Liu et al., 2016)
	β-arrestin	HEK293 Eluc-β-arrestin-2 + GPR84-Eluc (transient co-transfection)	(Zhang et al., 2016)
	GTPɣS	Sf9-hGPR84-bovine-$G\alpha_i$	(Suzuki et al., 2013)
6-OAU derivatives (35 compounds)	cAMP, β-arrestin	CHO-β-arrestin-2-hGPR84 (DiscoverX PathHunter)	(Lucy et al., 2019, Luscombe et al., 2023a)
DIM	cAMP, β-arrestin	CHO-β-arrestin-2-hGPR84 (DiscoverX PathHunter)	(Luscombe et al., 2023a)
	cAMP	CHO-GPR84 (transient transfection)	(Mårtensson et al., 2021)

	cAMP	HEK293-hGPR84	(Lucy et al., 2019)
	cAMP, GTPγS	Flp-In T-REx HEK293-FLAG-hGPR84-eYFP	(Mårtensson et al., 2021)
	GTPγS	Flp-In T-REx HEK293-FLAG-hGPR84-eYFP	(Köse et al., 2020, Pillaiyar et al., 2018)
	GTPγS	CHO-GPR84 cells	(Pillaiyar et al., 2018, Lucy et al., 2019, Pillaiyar et al., 2017)
DIM derivatives (10 compounds)	cAMP, β-arrestin	CHO-β-arrestin-2-hGPR84 (DiscoverX PathHunter)	(Gaidarov et al., 2018)
DL-175	cAMP	CHO-hGPR84 (DiscoverX)	(Mahmud et al., 2017)
	cAMP	CHO-HA-hGPR84 #7F12 (high expression); CHO-HA-hGPR84 #3E11 (low expression)	(Mahmud et al., 2017)
	cAMP	HEK293-hGPR84	(Gaidarov et al., 2018)
	β-arrestin	CHO-β-arrestin-2-hGPR84 (DiscoverX PathHunter)	(Pillaiyar et al., 2018, Lucy et al., 2019)
	β-arrestin	HEK293 SmBit-β-arrestin-2 + GPR84-LgBit (transient co-transfection)	(Liu et al., 2016, Mårtensson et al., 2021)
Embelin	cAMP, β-arrestin	CHO-β-arrestin-2-hGPR84 (DiscoverX PathHunter)	(Zhang et al., 2016)
	cAMP	HEK293-hGPR84	(Mårtensson et al., 2021)
	cAMP	Flp-In T-REx HEK293-FLAG-hGPR84-eYFP	(Mahmud et al., 2017)
	GTPγS	Flp-In T-REx HEK293-FLAG-hGPR84-eYFP	(Mancini et al., 2019)
Embelin derivative (C8)	cAMP	HEK293-hGPR84	(Liu et al., 2016)
LY237	cAMP	HEK293-hGPR84	(Lucy et al., 2019)
	β-arrestin	CHO-β-arrestin-2-hGPR84 (DiscoverX PathHunter)	(Pillaiyar et al., 2018, Lucy et al., 2019)
PSB-1584	cAMP, β-arrestin	CHO-β-arrestin-2-hGPR84 (DiscoverX PathHunter	(Lucy et al., 2019)
PSB-16434	cAMP, β-arrestin	CHO-β-arrestin-2-hGPR84 (DiscoverX PathHunter)	(Pillaiyar et al., 2018)
	cAMP	CHO-hGPR84 (DiscoverX)	(Pillaiyar et al., 2017)
PSB-17365	cAMP, β-arrestin	CHO-β-arrestin-2-hGPR84 (DiscoverX PathHunter)	(Wang et al., 2006)

PSB-16671	cAMP, β-arrestin	CHO-β-arrestin-2-hGPR84 (DiscoverX PathHunter)	(Zhang et al., 2016)
	GTPγS	Flp-In T-REx HEK293-hGPR84-Gαi2; THP-1 with LPS treatment; THP-1 no LPS treatment	(Mahmud et al., 2017)
ZQ-16	cAMP, β-arrestin	CHO-β-arrestin-2-hGPR84 (DiscoverX PathHunter)	(Mancini et al., 2019)
	cAMP	HEK293-hGPR84	(Wang et al., 2006)
	β-arrestin	HEK293 Eluc-β-arrestin-2 + GPR84-Eluc (transient co-transfection)	(Pillaiyar et al., 2017)
	β-arrestin	HEK293 SmBit-β-arrestin-2 + GPR84-LgBit (transient co-transfection)	(Mancini et al., 2019)
	cAMP, GTPγS	Flp-In T-REx HEK293-FLAG-hGPR84-eYFP	(Pillaiyar et al., 2018)
	GTPγS	Flp-In T-REx HEK293-hGPR84-Gαi2; THP-1 with LPS treatment; THP-1 no LPS treatment	(Pillaiyar et al., 2017)

2-OH-C14, 2-hydroxy myristic acid; 3-OH-C14, 3-hydroxy myristic acid. Representative compounds shown in colour in Figure 6 are highlighted in Bold. Reproduced with permission from (Luscombe et al., 2023b).

In contrast, compounds with bias towards the β-arrestin pathway are more commonly seen within the DIM class of allosteric agonists, although these are also micromolar potency and low affinity compounds (Pillaiyar et al., 2017, Köse et al., 2020). The absence of a physiological agonist with which to set as a reference ligand when determining bias factors remains a challenge to medicinal chemistry projects, though the evidence to date indicates that GPR84 is inherently poorly coupled to the β-arrestin pathway. With few exceptions, GPR84 agonists with sub-micromolar cAMP potencies are also biased towards cAMP (Figure 6). Furthermore, activity in the β-arrestin pathway is also highly variable, as analogues within the major ligand classes of MCFAs, 6-OAU derivatives, and DIM derivatives have been shown to have greater correlation between binding and cAMP potency than between binding and β-arrestin potency (Köse et al., 2020). Nonetheless, multiple distinct methods have shown that GPR84 can indeed couple to β-arrestins and it remains an

important pathway to investigate. This system bias is another mechanism by which cellular contexts dictate the resulting signals and physiological responses and have been observed in other inflammatory GPCR pairings such as CXCR4 and the arrestin-coupled ACKR3, CCR2 and the arrestin-coupled D6R, and the $C5a_1$ receptor and the arrestin-coupled $C5a_2$ receptor (Pandey et al., 2021, Yen et al., 2022). Indeed, it has been suggested that this system bias is a physiological property of GPR84 in a way that potentially discriminates between nutritive metabolites and structurally related metabolites of pathogenic origin, but also differentiates this receptor from similar immune-cell expressed G_i-coupled receptors such as HCA_3 (Peters et al., 2020).

As β-arrestins are part of the canonical desensitisation and internalisation pathways of GPCRs, an inherent system bias away from this pathway has broad implications for receptor regulation and drug design. The lack of efficacy of DL-175 in the GPR84-β-arrestin pathway has been demonstrated using tagged receptor and arrestin systems by chemiluminescent enzyme fragment complementation (Lucy et al., 2019, Mårtensson et al., 2021) and bioluminescence resonance energy transfer (BRET) (Marsango et al., 2022), as well as by measuring arrestin translocation to the membrane in enhanced bystander BRET assays (Fredriksson et al., 2022). It is now also known that two key threonine residues in ICL3 are phosphorylated by GRK2/3 following agonist stimulation with ZQ-16, but not DL-175 (Marsango et al., 2022). Phosphorylation of the residues T263 and T264 allow for subsequent interactions with β-arrestin-1 and β-arrestin-2 (Marsango et al., 2022). This is consistent with the idea that bias is orchestrated by GRK proteins in response to certain agonist-induced receptor conformations, which then influence β-arrestin interactions and signalling, rather than directly favouring or disfavouring interactions with β-arrestin itself (Choi et al., 2018, Zidar et al., 2009).

1.3.1.3. *Effects of Agonists on Innate Immune Cells*

As GPR84 is expressed predominantly on innate immune cell types, particularly monocytes, macrophages, and neutrophils, I have conducted a detailed literature review of the effects of GPR84 agonists on immune cell function. The use of surrogate GPR84 agonists has uncovered a role for this receptor in the mobilisation of inflammatory mediators, chemotaxis, and phagocytosis (Table V).

The secretion of inflammatory cytokines and prostanoids, as well as ROS production, neutrophil extracellular traps (NETs), and degranulation are regulated by GPR84 (Table V). Overall, the literature reports indicate that the activation of GPR84 results in an increase in the mobilisation of pro-inflammatory mediators or a decrease in anti-inflammatory mediators. The potent and specific agonist 6-OAU has been shown to increase the inflammatory cytokine TNFα in U937 macrophages, BMDMs, and THP-1 macrophages (Peters et al., 2022, Recio et al., 2018, Suzuki et al., 2013). In neutrophils, ROS production has been shown to increase upon stimulation with embelin, ZQ-16, LY237, DL-175, and 6-OAU (Gaidarov et al., 2018, Mårtensson et al., 2021, Sundqvist et al., 2018, Wang et al., 2023b). These observations alongside others of cytokine and chemokine expression and secretion indicate that GPR84 activation results in an increased secretion or mobilisation of pro-inflammatory mediators.

In only two cases were GPR84 agonists seen to decrease the secretion of inflammatory mediators. Firstly, in RAW264.7 macrophages infected with *Brucella abortus* treatment with 6-OAU was found to decrease CCL2 secretion (Reyes et al., 2021), which was in contrast to a previous study showing 6-OAU treatment increased CCL2 secretion in murine BMDMs (Recio et al., 2018). Secondly, a decrease in *Tnf* expression was observed by Ohue-Kitano et al. (2023) with 6-OAU treatment of palmitate-stimulated RAW264.7 cells, again in contrast to a previous study showing 6-OAU increased TNFα secretion in U937 macrophages (Suzuki et al., 2013). One possible explanation for these discrepancies are the stimulation and differentiation paradigms, as the pro-inflammatory effects were observed in M-CSF differentiated and LPS-stimulated BMDMs in the case of CCL2 secretion, and PMA-differentiated and LPS-stimulated U937 macrophages in the case of TNFα secretion (Recio et al., 2018, Suzuki et al., 2013). The decrease in CCL2 secretion was observed in RAW264.7 macrophages in a live-infection model utilising an immune-evasive bacterial pathogen, *Brucella abortus*, which is known to replicate in phagocytes. These bacteria are known to exhibit a non-canonical expression of virulence factors, and RAW264.7 macrophages with wild-type *Brucella abortus* have altered gene expression patterns over time which represent a modulated host immune response in response to the intracellular survival mechanisms of the pathogen (Jung et al.,

2018). Specifically, RAW264.7 macrophages infected with *Brucella abortus* have an upregulated *Gpr84* expression at 1 h, 6 h, and 12 h post-infection, and upregulated *Ccl2* at 1 h, 6 h, 12 h, and 24 h post-infection (Cha et al., 2013, Jung et al., 2018). The experiments by Reyes et al. (2021) used a 30 minute infection time and maintained 6-OAU for a 4 h pre-incubation and 48 h post-incubation. The mechanism behind the differential effects of 6-OAU stimulated changes in CCL2 secretion between LPS-stimulated BMDMs and live-infected RAW264.7 macrophages remains unclear, as does that of TNFα production in palmitate-stimulated RAW264.7 cells and LPS-stimulated U937 macrophages, and warrants further investigation into the potential context-dependent responses of GPR84.

GPR84 agonists have been demonstrated to act as chemoattractants, promoting chemotaxis, migration, and motility (Table V). For example, both 6-OAU and embelin have been shown to induce chemotaxis in primary human and murine neutrophils, as well as primary human and murine monocytes (Table V). However, results with macrophages are less clear. The agonist 6-OAU could act as a chemoattractant for PMA-differentiated U937 macrophages as measured by both real-time chemotaxis and Boyden chamber systems (Lucy et al., 2019, Suzuki et al., 2013), but 6-OAU did not cause chemotaxis in primary murine macrophage colony-stimulating factor (M-CSF) differentiated LPS-stimualted BMDMs, also measuring in real-time chemotaxis system (Recio et al., 2018). When exposed to BMDMs in a scratch assay 6-OAU was found to augment C5a-mediated migration, further complicating the effects of GPR84 on chemotaxis and migration (Recio et al., 2018), although an augmentation of C5a-mediated chemotaxis by 6-OAU was not tested. There is a growing appreciation that the underlying mechanisms of macrophage migration differs from those of its monocytic precursors (Rumianek and Greaves, 2020), and that different populations of macrophages exhibit different migratory behaviour (Iqbal et al., 2013). Given the relative scarcity of reports on GPR84-mediated chemotaxis, cell-type differences in GPR84-mediated chemotaxis remain unclear. In addition to cell type differences, the assay technology used to test for chemotaxis is important. The Boyden chamber, Dunn chamber, and under agarose systems have limitations in terms of throughput, quantification methods, and a lack of time resolved data. Real-time cell analysis

(RTCA) systems, such as the RTCA-DP xCelligence instrument utilised in BMDM chemotaxis assays toward 6-OAU, can monitor chemotaxis with a kinetic, high-throughput and quantitative readout. Given the seemingly complex nature of GPR84-mediated migration and chemotaxis in macrophages, microfluidic systems would better provide insights into cellular decision-making and chemotaxis involving two or more chemoattractants on adherent cell types. Fluid-walled microfluidics have already shown promise and uncovered migratory behaviour in BMDMs responding to C5a (Deroy et al., 2022), and such a system could be used to test for GPR84 agonist-mediated augmentations of C5a-mediated chemotaxis by tracking individual or subpopulations of cells over time with the added possibility to recover these at the end of the assay to quantify gene expression changes that might influence migratory behaviour.

GPR84 agonists have been shown to promote bacterial adhesion and phagocytosis in macrophages and is a more recent development in the field (Table V). Unlike observations in chemotaxis, phagocytosis measurements are almost exclusively made in macrophages. The GPR84 agonist 6-OAU has been shown to enhance bacterial adhesion, phagocytic activity, and the number of phagocytic cells using murine primary BMDMs (Recio et al., 2018). Interestingly, both 6-OAU and the biased agonist DL-175 promote phagocytosis in U937 macrophages (Lucy et al., 2019). GPR84 was also identified in a CRISPR screen for regulators of cancer cell phagocytosis (Kamber et al., 2021). Specifically, GPR84 mediates an enhanced uptake of pHrodo-labelled Ramos cancer cells by antibody dependent cellular phagocytosis. Here, 6-OAU was shown to enhance the phagocytic index of Ramos lymphoma target cells by PMA-differentiated LPS-stimulated U937 macrophages and LPS-stimulated J774 macrophages (Kamber et al., 2021). Only one report showed small decreases in the adhesion and uptake of live bacteria when stimulating RAW264.7 macrophages with 6-OAU (Reyes et al., 2021). This live infection model utilising pathogenic and immune-evasive *Brucella* spp. and *Salmonella* spp. also observed a decreased secretion of the pro-inflammatory monocyte chemoattractant protein CCL2 and likely relates to an altered signalling context or non-canonical virulence factor expression, provided *Gpr84* was expressed in this RAW264.7 macrophage stimulation paradigm.

Table V: Effects of GPR84 agonists on innate immune cells

Category	Agonists	Cell Type	Observation	Reference
Secretion / Mobilisation of Inflammatory Mediators	C10, C11, C12, DIM	RAW264.7[a]	↑IL-12 p40	(Wang et al., 2006)
	6-OAU, 3-OH-C12	Human PMNs[a]	↑IL-8	(Suzuki et al., 2013)
	6-OAU, 3-OH-C12	U937 macrophages[a,b]	↑TNFα	(Suzuki et al., 2013)
	C11	RAW264.7[a]	↑*Il12p40* expression	(Huang et al., 2014)
	C10	Human primary monocytes and THP-1[a]	↑*Tnf* expression	(Müller et al., 2017)
	6-OAU	Murine BMDMs[a,c]	↑TNFα ↑IL-6 ↑CCL2	(Recio et al., 2018)
	Embelin	Primary Human Macrophages[d,e]	↑PGE_2	(Gaidarov et al., 2018)
	Embelin	Primary Human Macrophages[d,e,f]	↑Cholesterol Efflux	(Gaidarov et al., 2018)
	Embelin	Primary Human Neutrophils[g/h]	↑ROS	(Gaidarov et al., 2018)
	ZQ-16	Primary Human Neutrophils[i,j] and monocyte-derived macrophages[c]	↑ROS	(Sundqvist et al., 2018)
	ZQ-16	Primary Human Neutrophils[i]	↑degranulation	(Sundqvist et al., 2018)
	DIM	Murine MH-S macrophage[a]	↑*Il6, Il12b, Cxcl2* expression	(Yin et al., 2020)
	ZQ-16, cmpd51, DL-175	Primary Human Neutrophils	↑ROS	(Mårtensson et al., 2021)
	C10	PBMCs[a]	↑IL-6 ↑TNFα ↓IL-10	(Sam et al., 2021)
	C10	PBMCs[k]	↑IL-1β ↑IL-6 ↓IL-10	(Sam et al., 2021)
	C10	PBMCs[l]	↑IL-1β ↑IL-6 ↑TNFα ↓IL-10	(Sam et al., 2021)
	6-OAU	RAW264.7[m]	↓CCL2	(Reyes et al., 2021)
	6-OAU	RAW264.7[m]	Unchanged ROS	(Reyes et al., 2021)
	6-OAU	Murine BMDMs[a,n]	↑IL-1β	(Zhang et al., 2022)

	6-OAU, C10, 3HDec	THP1 macrophages[a,b,d]	↑TNFα	(Peters et al., 2022)
	C10, 3HDec	THP1 macrophages[a,b,d]	↑ROS	(Peters et al., 2022)
	6-OAU	THP1 macrophages[a,b,d]	unchanged ROS	(Peters et al., 2022)
	C10, 3HDec	Human PMNs	↑NETosis	(Peters et al., 2022)
	Embelin, C10	RAW264.7[o]	↓*Tnf* expression	(Ohue-Kitano et al., 2023)
	6-OAU	Murine primary neutrophils[a]	↑ROS	(Wang et al., 2023b)
	6-OAU	Murine primary neutrophils[i]	↑degranulation	(Wang et al., 2023b)
Migration & Chemotaxis	6-OAU	Human PMNs	↑chemotaxis	(Suzuki et al., 2013)
	6-OAU	U937 macrophages[b]	↑chemotaxis	(Suzuki et al., 2013)
	6-OAU	Mouse primary microglia	↑motility	(Wei et al., 2017)
	Embelin	Primary human neutrophils	↑chemotaxis	(Gaidarov et al., 2018)
	ZQ-16/2-HTP	Primary human neutrophils	↑chemotaxis	(Sundqvist et al., 2018)
	6-OAU	Murine BMDMs[a,c]	no chemotaxis	(Recio et al., 2018)
	6-OAU	Murine BMDMs[a,c]	↑migration[h]	(Recio et al., 2018)
	2-HTP, PSB-16671	Murine primary neutrophils	↑migration	(Mancini et al., 2019)
	6-OAU	U937 macrophages[a,b]	↑chemotaxis	(Lucy et al., 2019)
	DL-175	U937 macrophages[a,b]	no chemotaxis	(Lucy et al., 2019)
	6-OAU, DL-175	primary human monocytes	↑chemotaxis	(Lucy et al., 2019)
	Embelin	Murine primary monocytes and neutrophils	↑chemotaxis	(Puengel et al., 2020)
	Embelin	Human primary monocytes and neutrophils	↑ chemotaxis	(Puengel et al., 2020)
	6-OAU, 3-OH-C12	Murine primary neutrophils and monocytes	↑chemotaxis	(Chen et al., 2022)
	Embelin, 3HDec	Murine primary neutrophils	↑migration	(Mikkelsen et al., 2022)
	3HDec	Murine primary Monocytes, THP-1	no migration	(Mikkelsen et al., 2022)
	Embelin, 3HDec, 3-OH-C12,	Human primary neutrophils	↑migration	(Mikkelsen et al., 2022)

	C10, 2-OH-C10, C12	Human primary neutrophils	no migration	(Mikkelsen et al., 2022)
	Embelin	THP-1	↑migration	(Mikkelsen et al., 2022)
	6-OAU, 3-OH-C12	Murine primary neutrophils and monocytes	↑chemotaxis	(Li et al., 2023a)
	6-OAU	Murine primary neutrophils	↑chemotaxis	(Wang et al., 2023b)
Phagocytosis & bacterial adhesion	6-OAU	Murine primary BMDMs[a,c]	↑adhesion[p]	(Recio et al., 2018)
	6-OAU	Murine primary BMDMs[a,c]	↑phagocytosis[q]	(Recio et al., 2018)
	6-OAU	Murine primary BMDMs[a,c]	↑number of phagocytic cells[r]	(Recio et al., 2018)
	6-OAU, DL-175	U937 macrophages[a,b]	↑phagocytosis[r]	(Lucy et al., 2019)
	6-OAU, ZQ-16, C10	U937 macrophages[a,b]	↑phagocytosis[s]	(Kamber et al., 2021)
	6-OAU, ZQ-16, C10	J774 macrophages[a]	↑phagocytosis[s]	(Kamber et al., 2021)
	6-OAU, C12	RAW264.7	↓adhesion[m] ↓uptake[m]	(Reyes et al., 2021)
	6-OAU	RAW264.7	↓adhesion[t] ↓uptake[t]	(Reyes et al., 2021)
	3HDec, C10	Human PMNs	↑phagocytosis[q]	(Peters et al., 2022)
	6-OAU	Murine primary BMDMs[c]	↑phagocytosis[u]	(Zhang et al., 2023)

[a]LPS-stimulated, [b]PMA-differentiated, [c]L929 or M-CSF-differentiated, [d]IFNɣ-stimulated, [e]GM-CSF-differentiated, [f]oxLDL-stimulated, [g]fMLP-stimulated, [h]C5a-stimulated, [i]TNFα-primed, [j]*In vivo* transmigrated tissue neutrophils, [k]Pam-3-CysK-stimulated, [l]Heat killed *Candida albicans*-stimulated, [m]*Brucella abortus* 544, [n]Nigericin/ATP/Aluminium hydroxide or MSU-stimulated, [o]Palmitate-stimulated, [p]*E. coli* DH5α, [q]pHrodo-conjugated *E. coli* bioparticles, [r]Opsonized polystyrene beads, [s]pHrodo-conjugated Safe^{KO} Ramos Cas9 cells, [t]*Salmonella* Typhimurium. [u]luciferase-expressing Raji cells. Reproduced with permission from (Luscombe et al., 2023b).

1.3.1.4. *Effects of Biased Signalling on Innate Immune Cells*

Biased signalling resulting from natural agonists has been shown to underlie context-specific signalling in other inflammation associated GPCRs, best exemplified by the 20 chemokine receptors and their distinct responses to the 50 described chemokines (Eiger et al., 2021). Should there be multiple physiological agonists of GPR84, it is conceivable that signalling bias could play a role in how innate immune cells differentiate between them. For example, biased signalling could contribute

to differentiating between beneficial exogenous bacterial metabolites originating from fermented foods and those from potentially harmful pathogens (Peters et al., 2020).

The use of specific GPR84 agonists has undoubtedly proven highly useful in interrogating the physiological role of this receptor. While there is still ongoing debate over the endogenous agonist, particularly whether it is some form of MCFA, I believe it is still necessary to use potent surrogate agonists to support conclusions made with MCFAs which are low potency, are often used at concentrations above 100 μM, and consequently lack selectivity for GPR84. Furthermore, the discovery and characterisation of biased and allosteric agonists has opened new avenues to probe the biology of innate immune cells and should be widely adopted alongside the use of 'balanced' agonists such as 6-OAU. For example, Lucy et al. (2019) compared 6-OAU and DL-175 and found that only 6-OAU promotes chemotaxis in PMA-differentiated LPS-stimulated U937 macrophages, while both agonists promote chemotaxis in human monocytes. Similar comparisons were made by Mikkelsen et al. (2022), noting that 3-hydroxy capric acid promotes neutrophil but not monocyte migration, and that 2- or 3-hydroxylated MCFAs appear to promote migration while their non-hydroxy conterparts did not. DL-175 and 6-OAU therefore represent useful tools for use in GPR84 research as potent, commercially available, and more selective agonists with differences in bias level.

There is still a need to interrogate the effects of these agonists on physiological cells. Delineating the effects of GPR84 signalling bias at the cellular or tissue level readouts is a challenging task and requires systematic investigation. The variety of cell-types and stimulation paradigms completely obscures comparisons that could be made about agonist-specific results in the secretion of cytokines, chemotaxis, or phagocytosis. Studying the function of GPR84 in primary cells poses three challenges; first, the receptor requires transcriptional upregulation that subsides over time (e.g. LPS-stimulation upregulates *Gpr84* with a peak at 8 h in BMDMs), second, some responses require priming (e.g. TNFα-priming prior to GPR84-mediated ROS release in neutrophils), and thirdly, activation of GPR84 will sometimes only augment existing responses (e.g. 6-OAU only augments C5a-mediated migration of BMDMs, or fMLP- or C5a-mediated ROS

production in neutrophils). We therefore encourage researchers to attempt multiple stimulation paradigms when testing for agonist-mediated effects.

GPR84 has been shown to activate transducer proteins including $G_{i/o}$, $G_{12/13}$, G_{15}, GRK2/3, β-arrestin-1, and β-arrestin-2 (Gaidarov et al., 2018, Marsango et al., 2022, Peters et al., 2022, Wang et al., 2006) which couple to effector molecules including β-catenin, DOK3, NLRP3, and phospholipase C (Dietrich et al., 2014, Gao et al., 2020, Peters et al., 2022, Zhang et al., 2022), small GTPases such as ras/rho and dynamin (Peters et al., 2022), kinases PI3K, Akt, ERK1/2, JNK, and p38 (Gao et al., 2020, Meng et al., 2017, Park et al., 2018, Recio et al., 2018), and the transcription factors NF-κB and STAT3 (Recio et al., 2018, Yin et al., 2020). Further investigation into the effector proteins downstream of GPR84, aside from adenylyl cyclase and β-arrestins, may be important when assessing physiological efficacy. For example, the M_1 muscarinic receptor can differentially couple to phospholipases C and D, a pathway bias with physiological relevance to targeting M_1 in disease (Marlo et al., 2009, Moran et al., 2019). However, in the case of GPR84, the best evidence to the importance of bias is the suggestion that the G_i-based agonist DL-175 promotes equivalent levels of phagocytosis but not chemotaxis as 6-OAU (Lucy et al., 2019). It is possible the differential effects of 6-OAU and DL-175 are due to different receptor-effector coupling profiles. For example, it has recently been shown that GPR84 couples to $G\alpha_{15}$ which results in phospholipase C activity, ERK phosphorylation, and calcium signalling (Peters et al., 2022). Given that GPCRs can not only promiscuously couple to a number of G-proteins, but can also 'switch' in coupling preferences over a signalling time course (Cawston et al., 2013), the $G\alpha_i$ and $G\alpha_{15}$ pathways may be important pharmacological descriptors for GPR84-mediated effects in innate immune cells.

Improving our molecular understanding of GPR84 signalling and the effector pathways required for its function in immune cells could aid in the optimisation of drug candidates to block or promote relevant pathways. For example, it might be desirable to inhibit the pathological recruitment of immune cells and activation of the cytokine storm at a site of injury while maintaining, or even promoting phagocytosis. The potential of biased agonism to selectively activate some cellular functions could hold promise in the development of compounds with more desirable activity, but as

discussed earlier, there are major challenges to studying GPR84 in immune cells and barriers to comparing the results from studies on a like-for-like basis.

1.3.2. GPR84 Antagonists

Multiple clinical trials targeting GPR84 using antagonists or negative allosteric modulators (NAMs) have been performed with none able to show efficacy in disease states including ulcerative colitis, idiopathic pulmonary fibrosis, and non-alcoholic fatty liver disease (Table VI). Even though the physiological agonist remains elusive and the potential pathophysiological roles of GPR84 are not understood there is still interest in the strategy of blocking GPR84 activation.

Table VI: Clinical trial results and pipeline of compounds targeting GPR84.

Cmpd	Activity	Indication	Phase	Completed	Outcome	Reference	NCT Identifier
GLPG1205	Antagonist / NAM	Ulcerative Colitis	Ph IIa	2015	Fail (Efficacy)	(Vermeire et al., 2017)	NCT02337608
GLPG1205	Antagonist / NAM	Idiopathic Pulmonary Fibrosis	Ph IIa	2020	Fail (Efficacy)	(Strambu et al., 2023)	NCT03725852
PBI-4050	GPR84 antagonist/ GPR40 agonist	Idiopathic Pulmonary Fibrosis	Ph I / II	2017	Fail (Efficacy)	(Khalil et al., 2019)	NCT02538536
PBI-4050	GPR84 antagonist/ GPR40 agonist	Alström Syndrome	Ph II	2018	Not reported	n/a	NCT02739217
PBI-4547	GPR84 antagonist & GPR40/120 agonist	Non-alcoholic Fatty Liver Disease	Pre-clin / Ph I	2019	Fail (PK)	NCT04068259	NCT04068259
Lauric Acid, Perilla Oil, and DIM	GPR84 & FFAR4 agonists	Obesity	n/a	2019	Reduced energy intake	(Peiris et al., 2022)	NCT04292236
LMNL6511	GPR84 antagonist	fibrotic diseases	Pre-clin	n/a	n/a	n/a	n/a

1.4. Thesis Aims and Objectives

GPR84 is expressed predominantly in immune cell types and is highly upregulated by inflammatory stimuli. Once expressed, activation of GPR84 using surrogate agonists results in an enhancement of inflammatory processes in a cell-type dependent manner. The use of surrogate agonists has undoubtedly helped to shed light on the biology of GPR84, uncovering roles of this receptor in the secretion of inflammatory mediators, chemotaxis and migration, and phagocytosis.

Despite major advancements in our understanding of the biology of GPR84, it remains both an orphan receptor and undrugged. The failure to translate GPR84 antagonists into the clinic highlights that the efficacy of blocking GPR84 is still unknown. This is true at both the disease level, with unanswered questions including: what is the endogenous agonist being blocked? Where? And in which disease states is this dysregulated? But also at the molecular level: what signalling pathways are being blocked? When?

The best strategy to exploit GPR84 therapeutically therefore remains unknown. Specifically, the desirable molecular properties of a small molecule targeting GPR84 also remain undefined. It is possible that, in a given pathological state with relevance to GPR84, blocking all receptor function is not the optimal solution. Perhaps, by leveraging the extraordinary conformational particularity of GPCRs, it is possible to selectively block or promote certain downstream pathways, resulting in unique and textured efficacies that can be deployed in relevant pathophysiological contexts (Figure 7).

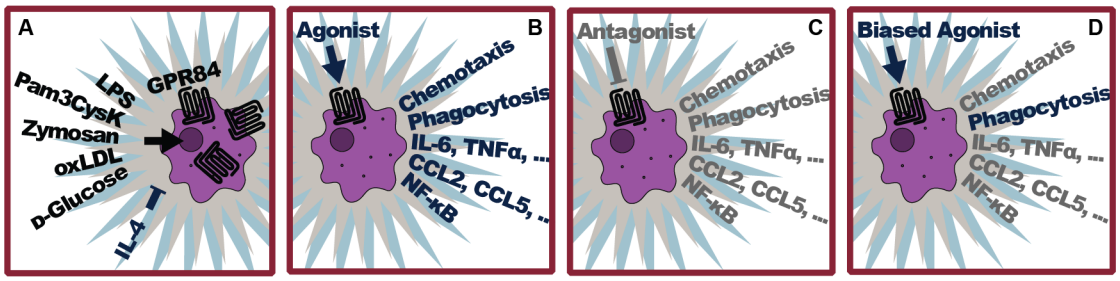

Figure 7: Targeting macrophage GPR84 using biased agonists. (A) GPR84 is upregulated by inflammatory stimuli. (B) Activation of GPR84 with agonists causes context-specific enhancements of pro-inflammatory responses. (C) Blocking GPR84 function using an antagonist will block all downstream pathways and functions. (D) Biased agonists can selectively activate some pathways of GPR84 and may result in selective activation of inflammatory processes.

Aim 1: To develop chemical and biological tools for studying GPR84 function *in vitro* and *in vivo*.

Aim 2: To investigate the receptor signalling differences underlying the differential responses of macrophages to GPR84 agonists 6-OAU and DL-175.

Aim 3: To assess the influence of G-protein biased signalling on receptor regulation by using structurally novel GPR84 agonists and characterise their functional effects on macrophages.

Chapter Two.

CHEMICAL AND BIOLOGICAL TOOL DEVELOPMENT

2.1. Introduction

2.1.1. Optimisation of the cAMP Assay for Screening

GPR84 is a $G\alpha_i$-coupled GPCR that mediates an inhibition of adenylyl cyclase, the enzyme family that converts ATP into the second messenger cAMP. Activation of GPR84 with an agonist therefore decreases intracellular cAMP production. This then triggers further effects downstream as cAMP is involved in regulating protein kinases. As cAMP is an important second messenger, cellular levels are tightly regulated, with degradation mediated by the cAMP phosphodiesterase enzymes. Numerous methods exist by which to study cAMP levels, including radiolabelling and chromatographic detection of [^{3}H]-cAMP production, antibody-based capture systems, reporter genes, and more elaborate single cell biosensors, with end-point detection ranging from radiometric, absorbent, fluorescent, or luminescent systems (Hill et al., 2010).

In my cAMP assays I chose to use the Eurofins DiscoverX HitHunter® cAMP Assay for Small Molecules as it has been previously used in this laboratory for the optimisation of DL-175. This is an end-point assay that involves cell lysis and detection of cellular cAMP by antibodies. The detection mixture contains a defined quantity of labelled cAMP. Cellular cAMP generated in the experiment competes with labelled cAMP for capture by an anti-cAMP antibody. If cellular cAMP levels are high, the labelled cAMP is displaced and complexes with an acceptor molecule. Specifically, the cAMP is labelled with a ProLabel enzyme-donor protein tag which complexes with an enzyme acceptor, known as enzyme fragment complementation, and results in functional β-galactosidase, which then hydrolyses a substrate into a luminescent product (Eglen, 2002). The result is a luminescent signal that is proportional to the amount of cellular cAMP produced following agonist treatment. As basal cAMP production is low, the adenylyl cyclase agonist forskolin (FSK) is used to stimulate cAMP production from which GPR84-mediated inhibition can then be measured.

As a natively G_i-coupled GPCR the cAMP assay was used in primary screening campaigns against hGPR84 using the CHO-hGPR84 (DiscoverX) cell line. Concentration-response curves (CRCs) can identify the EC_{50} of a given compound, and this potency value was used to drive SAR campaigns in the development efforts of chemical tools. The goal of this study was to optimise this assay for a more high-throughput readout by altering the assay reagents and plate format.

2.1.2. Hydroxylated MCFAs

MCFAs of carbon chain length 9-14 have been shown to activate GPR84, the most potent of which was found to be the 10-carbon capric acid, which exhibited an EC_{50} of 4.5 μM in a cAMP assay (Wang et al., 2006), and was then later demonstrated to exhibit a binding K_i of 1.78 μM against the radioligand [^{3}H]PSB-1584 (Köse et al., 2020). On a typical diet it is unlikely that plasma levels of capric acid reach micromolar levels, although levels can and do fluctuate markedly depending on an individual's fasting state. The high micromolar plasma concentrations of capric acid have only been observed following a supra-physiological intake of purified MCTs or in adults with fatty acid oxidation disorders (Luscombe et al., 2020). Earlier I have outlined some of the issues with capric acid interacting with GPR84 including its lack of selectivity, overlap with receptor expression, and unknown concentrations in certain tissues.

Hydroxylated forms of MCFAs are also active at GPR84, and was first explored by Suzuki et al. (2013) who demonstrated that 2- or 3-hydroxylated fatty acids often performed as well as or better than their alkyl counterparts. Kaspersen et al. (2017) found that 4- and 12-hydroxy lauric acid were active at GPR84, whereas lauric acid species hydroxylated at the 2-, 3-, or 5- through to 11-positions were not active. Hydroxylated MCFAs can be of exogenous or endogenous origin. Reports of chirally resolved hydroxylated MCFAs of enzymatic, food, or bacterial origins are scarce, but do indicate that dietary sources of 2- and 3-hydroxy MCFAs are in the (*R*) configuration, and bacterial sources are likely to be either (*R*)-3-hydroxy MCFAs or (*S*)-2-hydroxy MCFAs (Table III). As some mammalian enzymes generate enantiopure hydroxylated MCFAs, and dietary sources from milks and cheeses are predominantly of the (*R*) enantiomer, it raises the possibility that the receptor

selectivity profile may help to inform an evolutionary preference for hydroxylated MCFAs of mammalian, dietary, or bacterial origin.

We hypothesise that metabolites of MCFAs, including hydroxylated compounds, might be more physiologically relevant than MCFAs. By systematically interrogating 2- and 3-hydroxylated species synthesised in-house we show that not only are some of them more potent than their alkyl counterparts, but they also activate GPR84 with an altered chain length specificity.

2.1.3. Screening and Optimisation of DL-175

Prior to any available protein structures of GPR84, DL-175 was discovered using a ligand-based virtual screening methodology (Lucy et al., 2019). A literature set of 32 compounds bearing structural similarity to 6-OAU was used to generate a predictive QSAR model. A virtual library of 10,000 compounds was then screened against this model, and 45 hits taken forward into a cAMP assay in CHO-hGPR84 (DiscoverX) cells. The structurally novel hit 7 was inactive at β_2, CB_1, and untransfected CHO cell lines. Hit optimisation (Figure 8) led to the discovery of DL-175, the first potent and selective G-protein biased agonist at GPR84. DL-175 was found to have a similar cAMP potency as 6-OAU in the cAMP assay and was inactive on CHO background cells. At 3 μM it was selective against 14 human GPCRs using cAMP or Ca^{2+} flux assays, including the lipid receptors CB_1, CB_2, and FFARs 1-4, and was also selective in a gpcrMAX panel of 168 GPCRs measuring β-arrestin recruitment in both agonist and antagonist mode. DL-175 exhibits good solubility and stability in common buffers, and aggregation effects seen at high concentrations can be ameliorated with the addition of tween-80. However, in metabolic stability assays DL-175 was rapidly cleared in whole mouse hepatocytes ($t_{1/2}$ < 10 min). Therefore, while this agonist is a potent, selective, and chemically stable G-protein biased agonist, it is restricted to use *in vitro* (Lucy et al., 2019). In order to investigate GPR84 biology and the effects of biased agonists *in vivo*, and working with collaborators in the department of chemistry, we aimed to develop a metabolically stable analogue of DL-175.

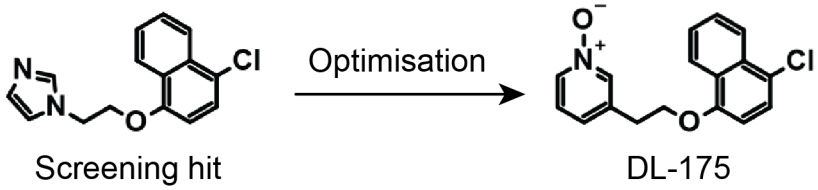

Figure 8: Chemical structure of DL-175. Chemical structures of screening hit 7 and the optimised tool compound DL-175 as described by Lucy et al. (2019).

2.1.4. Cell Line Development and Species Selectivity

GPR84 is still a receptor of unknown function in humans, but perhaps some answers lie in its role throughout evolution. If this receptor is important for host defence, then perhaps either by conserved function or by convergent evolution, GPR84 orthologues might respond to the same pathogen-derived ligands. GPR84 orthologues have been well annotated in vertebrates, with a majority of research focussing on mouse and human receptor, though some experimental work has been carried out in zebrafish models using putative GPR84 agonists. Generating cell lines expressing orthologues of GPR84 in the same cell background provides the potential of comparing species selectivity and function. Here, I focus on comparing the functional response of mouse compared to human GPR84 in order to inform existing programs using mice as preclinical models. I have also elected to clone zebrafish GPR84 due to its utility as an *in vivo* model, ease of genetic manipulation, and relative dissimilarity to human GPR84.

To determine the functional similarities between GPR84 orthologues, I aimed to generate several transgenic CHO cell lines for use as *in vitro* biological tools. Due to a lack of GPR84-specific antibodies (Luscombe et al., 2023a, Recio et al., 2018) an NT-fused HA-tag was included to facilitate antibody recognition and allow for further experiments on receptor localisation. The pcDNA3.1+ backbone was chosen as it confers mammalian cell resistance to the antibiotic G418, mimicking the widely used CHO-hGPR84 (DiscoverX) cell line. The broad strategy was to have DNA fragments synthesised commercially, and then insert these into pcDNA3.1+ by restriction enzyme cloning with sticky ends where they will be constitutively expressed under a CMV promoter (Figure 9).

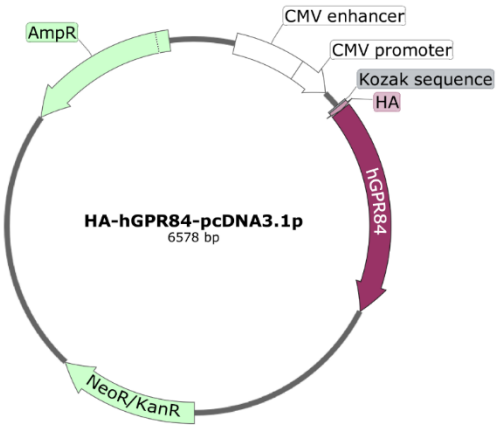

Figure 9: HA-GPR84 Expression vector map. Example Map of the HA-hGPR84 expression vector. The mouse and zebrafish GPR84 vectors use the same pcDNA3.1+ backbone.

2.1.5. Chapter Rationale and Experimental Aim

The aim of this chapter is to develop tools to study GPR84 by developing chemical probes, generating recombinant cell lines, and investigating the structure-activity relationships of agonists targeting GPR84.

2.2. Results

2.2.1. Optimisation of the cAMP Assay for Screening

I performed the cAMP as per the manufacturer's instructions as described previously by Lucy et al. (2019) in half-area 96-well plates (Greiner 675074) using AssayComplete Cell Culture Kit 107 (DiscoverX 92-3107G) in order to measure G_i-mediated inhibitions of adenylyl cyclase (Figure 10 A). Titrating unlabelled cAMP in the absence of any cell lysates shows a large and robust (~290,000 RLU) increase in luminescence (Figure 10 B). When cells are added and lysed, and the same detection methods are used, increases in cAMP production in CHO-hGPR84 (DiscoverX) cells are seen upon stimulation with increasing concentrations of forskolin. A constant EC_{80} concentration of forskolin (25 µM) was then applied to the cells during agonist stimulation with the GPR84 agonists 6-OAU and embelin, which cause concentration-dependent decreases in cAMP production (Figure 10 C). Importantly, these CRCs all fall within the linear range of cAMP detection as indicated by the concurrently run cAMP standard curve. One major advantage of this assay is the ability to interpolate actual cAMP concentrations from the standard curve. When the absolute concentration

of cAMP levels were back-calculated, the agonist potency values did not change compared to the relative luminescence unit (RLU) measurements (Figure 10 D).

I then adapted the assay format for 384-well plates and changed to a supplemented Ham's F12 media formulation. These changes were found to have no effect on assay performance (Figure 10 E). While optimising conditions, 0.01% (*w/v*) bovine serum albumin (BSA) from heat shock fractionation was found to slightly enhance the potency of some GPR84 agonists; DL-175, CS02, and 6-OAU, without affecting the standard curve and detection system (Table VII). Given that BSA functions as a carrier protein for fatty acids, I have included it in all subsequent cAMP experiments.

Table VII: Effect of including 0.1% BSA (*w/v*) on agonist potency in the cAMP assay.

Test Compound	hGPR84 cAMP EC_{50} (nM)*		Fold-difference (+BSA/-BSA)
	-BSA	+BSA	
cAMP standard	33.7	49.1	0.7
DL-175	43.8	12.6	3.5
CS02	1,920	547	3.5
6-OAU	6.86	3.28	2.1

*EC_{50} calculated from 12-point concentration response curves performed in triplicate, n = 1 - 3.

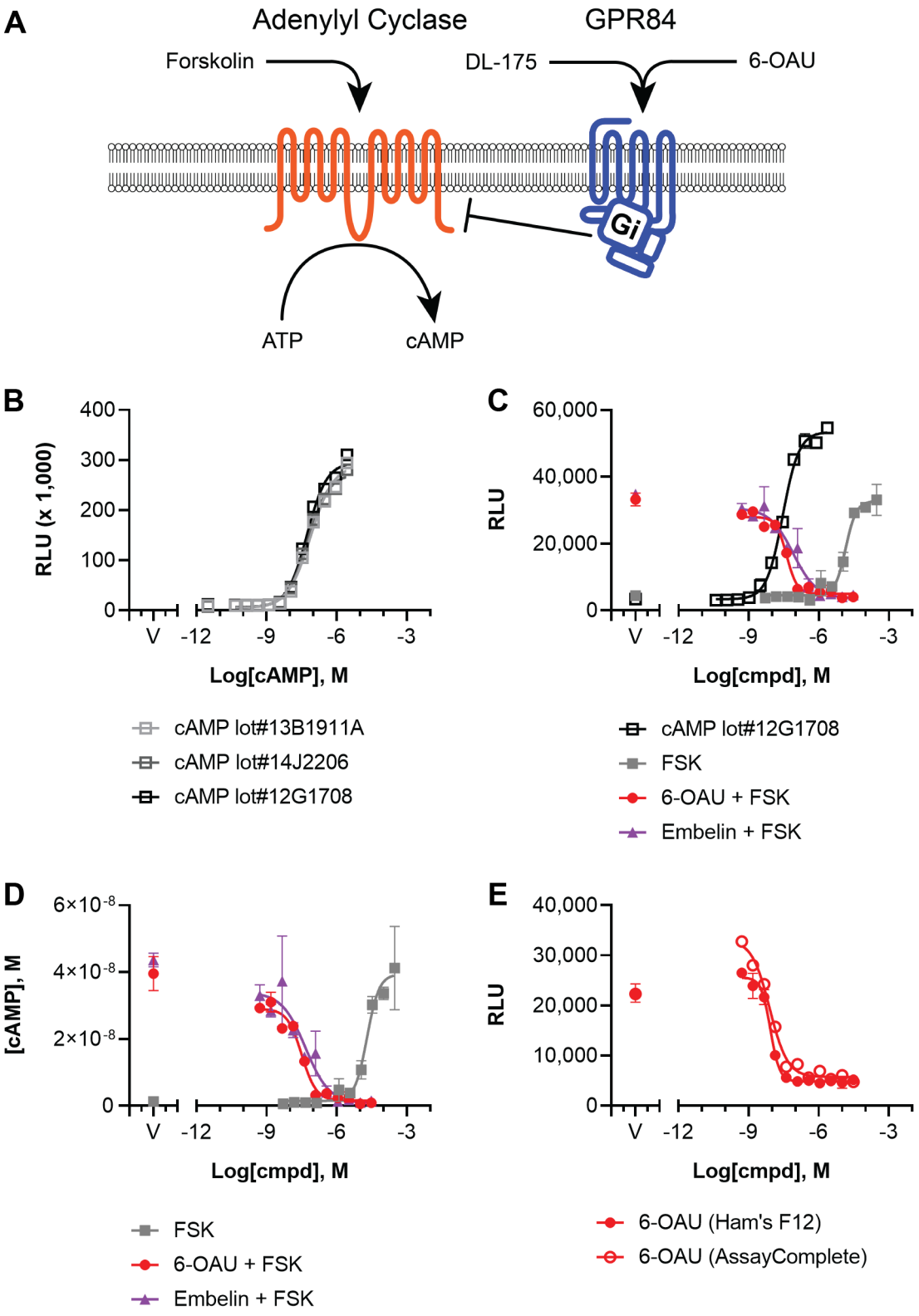

Figure 10: Optimisation of the cAMP assay. (A) Activation of $G\alpha_i$-coupled GPR84 causes a reduction in cAMP production. (B) The antibody-based cAMP detection system responds to titrated cAMP standards in the absence of cell lysates. (C) CHO-hGPR84 (DiscoverX) cells respond to forskolin and GPR84 agonists. (D) Back-calculating the absolute cAMP concentrations does not significantly alter the determined agonist potency (See Table VII). (E) Cells cultured in Ham's F12 supplemented media performed with similar cAMP responses to 6-OAU. Points represent mean ± SEM of triplicates, $n = 1$. FSK, forskolin; RLU, relative luminescence units; V, vehicle.

2.2.2. Hydroxylated MCFAs

MCFAs of chain lengths 9-14 and their 2- or 3-hydroxylated counterparts were purchased or synthesised in-house and tested for activity against hGPR84 in the cAMP assay (Figure 11 A). Plotting EC_{50} values against the MCFA carbon chain length reveals a chain-length specificity of receptor activity, with the most potent non-hydroxylated MCFA being capric acid of carbon length 10 (EC_{50} = 3.58 μM). The most potent 2-hydroxy MCFA was of carbon length 11 (EC_{50} = 0.70 μM), and the most potent 3-hydroxy MCFA was shared between lengths 11 (0.76 μM) and 12 (0.81μM) (Figure 11 B). Hydroxylation at either position was shown to increase the potency of all MCFAs of chain lengths 10-14.

The addition of a hydroxyl group generates a single chiral centre in the hydroxylated MCFAs, and the activity of these ligands at GPR84 is in some cases enantioselective (Figure 11 C). Enantiopure (*R*)-3-hydroxy capric acid (EC_{50} = 2.88 μM) was found to be more potent than (*S*)-3-hydroxy capric acid (EC_{50} = 16.2 μM), which had the largest disparity between isomers and consisted of a drop in potency for the (*S*) isomer compared to the racemic mixture. (*S*)-3-hydroxy lauric acid (EC_{50} = 501 nM) was more potent than (*R*)-3-hydroxy lauric acid (EC_{50} = 1.12 μM), and (*R*)-3-hydroxy myristic acid (EC_{50} = 3.09 μM) was more potent than (*S*)-3-hydroxy myristic acid (EC_{50} = 6.76 μM). In contrast, no differences were seen between the enantiomers of carbon chain lengths 9, 11, or 13. These results indicate some enantioselectivity between hydroxylated MCFAs of chain lengths 10, 12, and 14. Furthemore, the most potent MCFA tested to date was determined to be (*S*)-3-hydroxy lauric acid (EC_{50} = 0.50 μM). Taken together, multiple hydroxylated MCFA agonists were found to possess submicromolar potency at hGPR84, in rank order from most potent; (*S*)-3-hydroxy lauric acid > *rac*-2-hydroxy undecanoic acid > *rac*-3-hydroxy undecanoic acid > *rac*-3-hydroxy lauric acid.

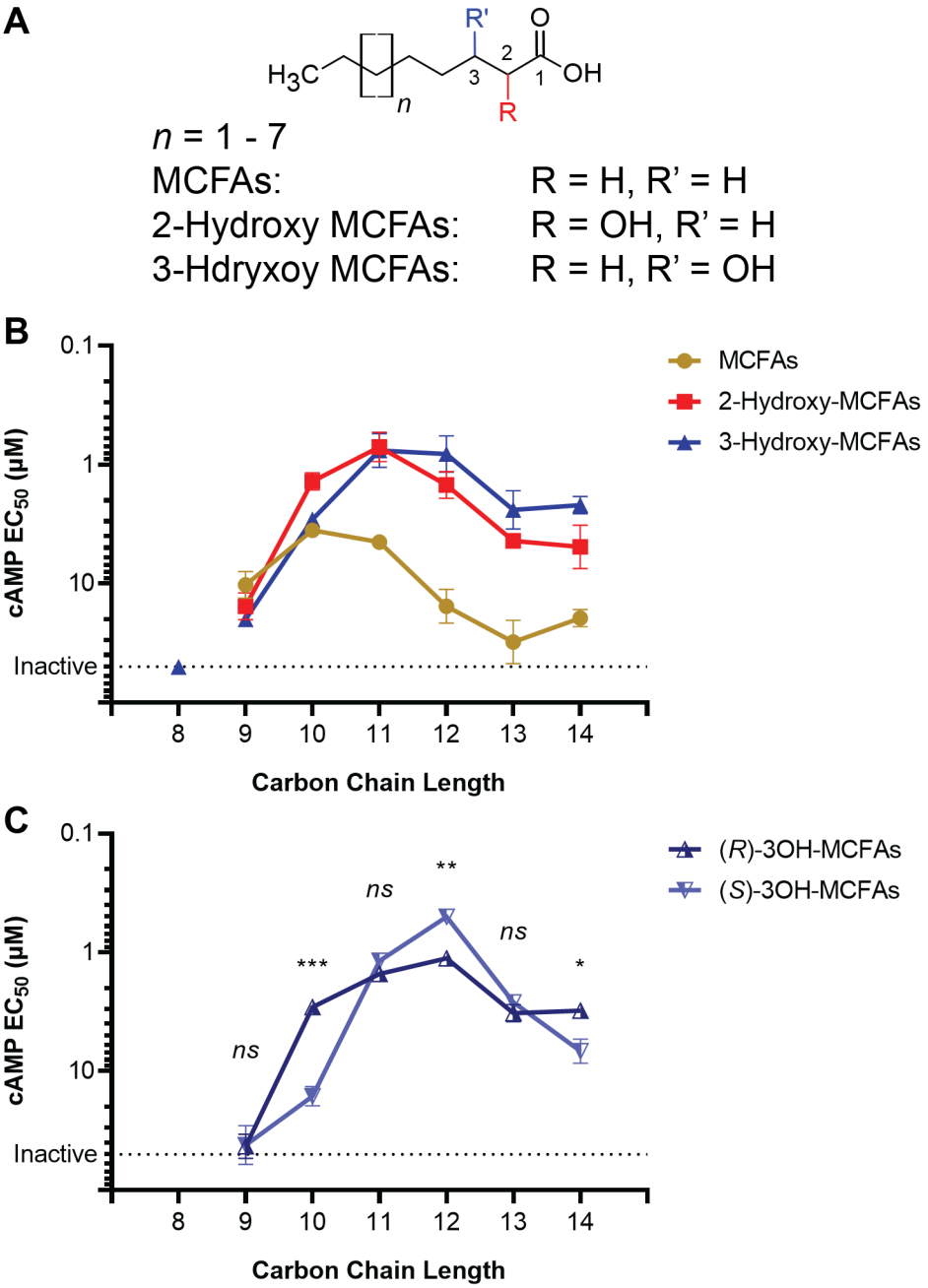

Figure 11: Hydroxylation of MCFAs can improve potency at GPR84. (A) Chemical structures of MCFAs synthesised for testing. EC_{50} values derived from concentration-response curves of test compounds for inhibition of forskolin-stimulated cAMP production in CHO-hGPR84 (DiscoverX) cells (B, C). Points represent mean ± SEM of 12-point curves performed in triplicate, n = 3-5. Significance between enantiomers shown by unpaired t-tests. MCFA, medium-chain fatty acid.

2.2.3. Screening and Optimisation of DL-175

Incubation of DL-175 with mouse hepatocytes and subsequent metabolite analysis using liquid chromatography-tandem mass spectrometry revealed three major metabolites involving monooxidation, dihydroxylation, and *O*-glucuronidation (Wang et al., 2023a). Based on this

information, our chemistry team hypothesised that the oxidation was predominantly occurring on the naphthalene ring. In order to test the SAR and metabolic liabilities of DL-175 more systematically, the compound was divided into three regions, the polar head group, the linker, and the hydrophobic tail (Figure 12) (Wang et al., 2023a).

Figure 12: Region breakdown of DL-175 for SAR. Chemical structure of DL-175 and the region breakdown for further SAR investigation as outlined by Wang et al. (2023a)

In this series over 60 compounds were synthesised and I tested their activity, with primary screening conducted against hGPR84 in the cAMP assay. In order to maximise reagent efficiency I changed from 12-point CRCs to 8-point CRCs, and altered the top concentration of test compound depending on the expected potencies, allowing me to test 14 compounds and the DL-175 CRC control per 384-well plate. SAR was driven by cAMP potency, and active compounds were prioritised for testing in β-arrestin-2 recruitment assays in order to confirm their signalling bias. As DL-175 had good selectivity against a variety of other GPCRs and the work herein involved structurally similar scaffolds, compounds were progressed to metabolic stability testing prior to selectivity assays.

The SAR around optimising DL-175 was found to be a balance between metabolic stability and potency. An initial investigation into the hydrophobic tail region revealed a loss of potency when the *para*-chloronapthyl group of DL-175 was replaced with a *para*-chlorophenyl group as in compound 19, but no improvement in stability when it was replaced with a tetralin group as in compound 16 (Table VIII). Further SAR of the hydrophobic tail was pursued with substituted arenes. Two compounds were progressed to metabolic studies, revealing once more a trade-off between potency and stability; with the more potent cyclopropyl containing compound 41 being quickly turned over, and the more stable 4-chloro-3-trifluoromethyl substituted compound 42 being less

Table VIII: Summary of the optimisation of metabolic stability of DL-175.

Compound	Structure	cAMP EC_{50} (nM) (pEC_{50} ± SEM) [Efficacy]	β-arrestin-2 EC_{50} (μM) [Efficacy]	MLM $t_{1/2}$ (min)
DL-175	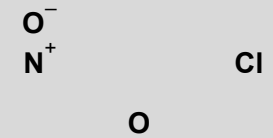	12.4 (7.91 ± 0.04) [99%]	>80 [13%]	13.8
16	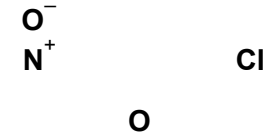	195 (6.71 ± 0.08) [98%]	>80 [7%]	4.8
19	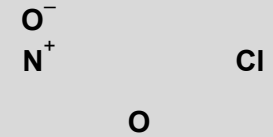	1360 (5.87 ± 0.10) [97%]	>80 [4%]	59.6
41	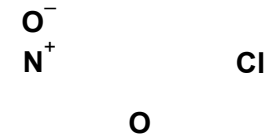	99.4 (7.00 ± 0.14) [99%]	>80 [-2%]	7.20
42	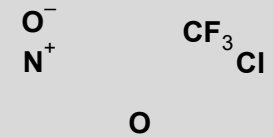	898 (6.05 ± 0.08) [102%]	>80 [0%]	49.9
60	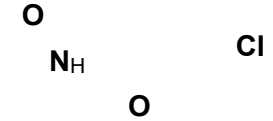	1470 (5.83 ± 0.02) [99%]	>80 [-1%]	11.7
68 AR-198 (OX04528)	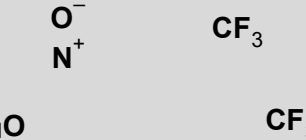	0.00598 (11.22 ± 0.16) [97%]	>80 [12%]	88.8
69 AR-211 (OX04529)	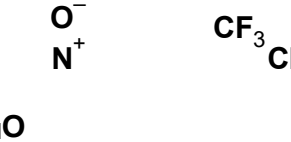	0.0185 (10.73 ± 0.18) [95%]	>80 [16%]	104.7

Data summarised and compound numbering from Wang et al. (2023a).

potent (Table VIII). Overall, 33 compounds were tested in the tail region and 5 were tested in mouse liver microsome (MLM) studies. The submicromolar potency of 42 was an improvement on 19, and approached the most potent hydroxylated MCFAs. However, further exploration of the head and linker regions still had the potential to improve potency and stability.

In the linker region, results from 14 compounds showed the optimal atom length was 3, and the ether of DL-175 could be replaced with an alkyl group with no change in potency (Wang et al., 2023a). Bioisosteres of the pyridine *N*-oxide were then explored in the polar head group region in order to eliminate this hypothesised metabolic hotspot. Results from 5 compounds quickly highlighted a low tolerance for *O*-methyl protected hydroxypyridines which lost activity at GPR84, but acceptable activity from pyridone substitutions (Wang et al., 2023a). However, the 6-pyridone substituted compound 60 was found to be metabolically unstable, indicating a liability in the pyridine moiety itself (Table VIII). Further work while maintaining the pyridine *N*-oxide with 7 novel compounds suggested some steric limitations in this region but importantly, that hydroxylation at the 3-position resulted in a 2000-fold increase in potency while still maintaining biased signalling and lack of activity in the β-arrestin-2 recruitment assay (Wang et al., 2023a).

With the discovery that potency could be dramatically improved while maintaining bias, and incorporating the findings from the other regions (Figure 13), two novel compounds with a 3-hydroxypyridine-*N*-oxide head group, 3 carbon linker, and disubstituted arene tail groups were generated for metabolic testing. AR-198 (68) and AR-211 (69) had cAMP potencies in the low picomolar range, no activity in the β-arrestin-2 recruitment assay, and were metabolically stable when tested in MLM assays (Table VIII). Comparison of AR-198 (68) and AR-211 (69) to the GPR84 agonists DL-175, 6-OAU, ZQ-16, and PSB-16434 in both cAMP and β-arrestin-2 recruitment assays demonstrates these newly developed compounds possess the highest degree of bias at GPR84 (Figure 14). These compounds were then progressed to selectivity assays, where they were found to be inactive in the cAMP assay against CHO-K1 parental cells, and inactive against FFA1, FFA4, and CB_2 in Ca^{2+} mobilisation assays (Figure 15 A - D). Furthermore, the compounds were found to be non-cytotoxic in the lactate dehydrogenase (LDH) release assay (Figure 15 E, F). Finally, AR-198 (68) and AR-211 (69) were progressed to *in vivo* pharmacokinetic (PK) studies. Following dosing of C57/BL6 mice at 10 mg/kg both compounds were found to quickly reach C_{max} in plasma and had appropriate half-lives of approximately 1 h (Table IX). Both compounds were found to circulate in plasma above their EC_{50} values for at least 4 hours, and were below the lower

limit of quantification by 24 hours, indicating good exposure and clearance in mice (Figure 16). Through systematic SAR on DL-175 we have therefore developed novel, highly potent, G-protein biased, and orally bioavailable tools suitable for *in vivo* mouse studies (Figure 17).

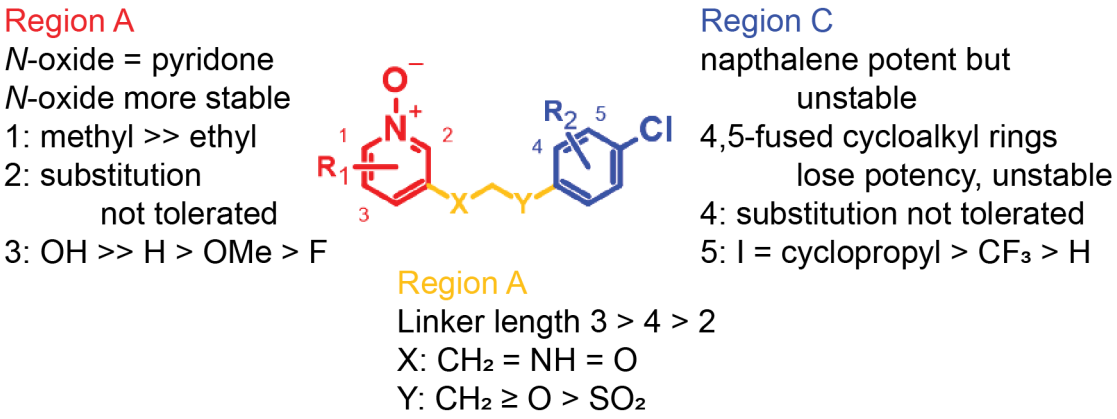

Figure 13: SAR summary of findings during the optimisation of DL-175. The SAR and metabolic studies are summarised by region as described by Wang et al. (2023a).

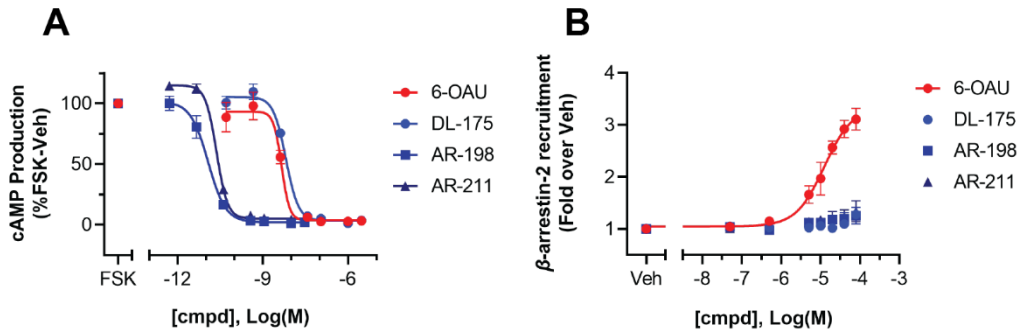

Figure 14: Biased signalling of the novel compounds AR-198 and AR-211. Representative cAMP inhibition and β-arrestin-2 recruitment assay demonstrating the enhanced potency and G-protein pathway bias of AR-198 and AR-211. (A) Inhibition of forskolin-stimulated cAMP production in CHO-hGPR84 (DiscoverX) cells. Data was normalised to forskolin-vehicle control (100%) and capric acid max control (0%). (B) Recruitment of β-arrestin-2 in CHO-β-arrestin-2-hGPR84 (DiscoverX) cells. Data was normalised and expressed as fold over vehicle responses. Points represent mean ± SEM, $n = 3$, experiments performed in triplicate. Adapted from Wang et al. (2023a). FSK, forskolin.

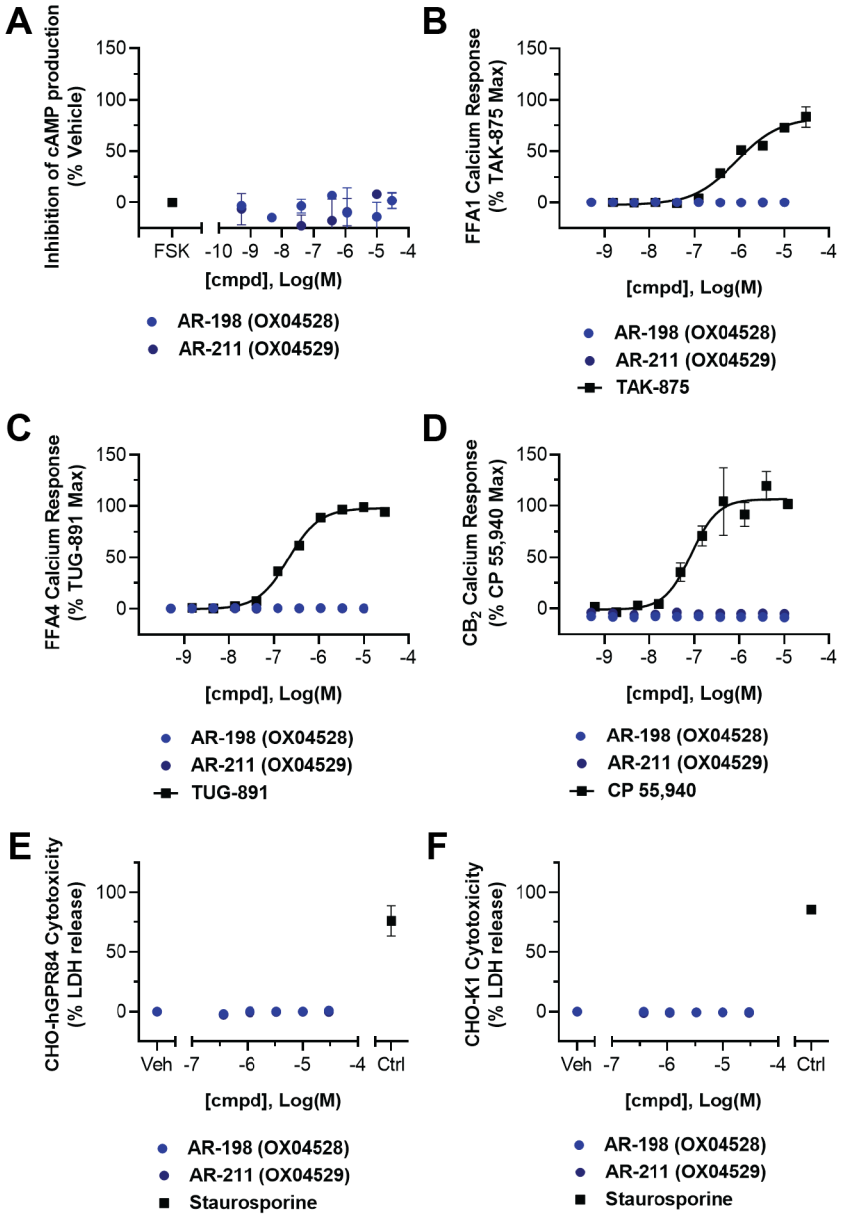

Figure 15: Selectivity and cytotoxicity of AR-198 and AR-211. (A) Inhibition of forskolin-stimulated cAMP production in CHO-K1 cells. Data was normalised to forskolin (0%) and vehicle / basal (100%) conditions. Points represent mean ± SEM, n = 3. Calcium responses of CHO cells overexpressing FFA1 (B), FFA4 (C), and CB2 (D), experiments performed by Wuxi AppTec Ltd (Shanghai, China). Points represent mean ± SD, n = 2. Cytotoxicity assays measuring LDH release following incubation of agonist or staurosporine (30 µM) in CHO-hGPR84 (DiscoverX) cells (E) and CHO-K1 parental cells (F). Data was normalised to vehicle (0%) and maximum LDH release by cell lysis (100%). Points represent mean ± SEM, n = 3. Adapted from Wang et al. (2023a). FSK, forskolin.

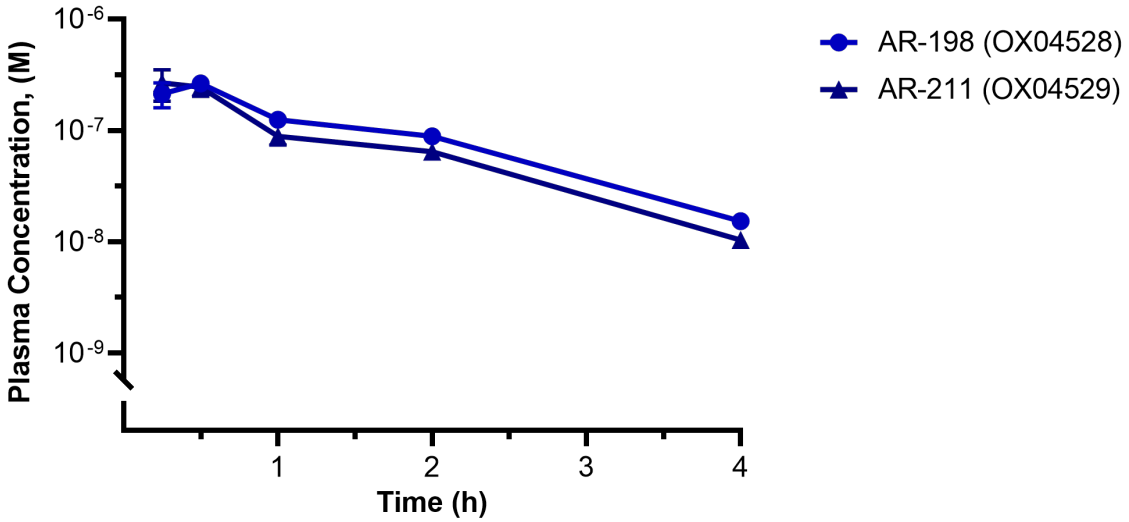

Figure 16: Murine pharmacokinetics of AR-198 and AR-211. Total plasma concentrations of AR-198 and AR-211 following oral dosing (10 mg/kg) of male C57BL/6J mice, experiments performed by Wuxi AppTec Ltd (Hong Kong). Points represent mean ± SEM, $n = 3$.

Table IX: Murine pharmacokinetic parameters of AR-198 and AR-211.

Cmpd	Structure	PO (10 mg/kg)*						
		C_{max} (ng/mL) ±*SD*	T_{max} (h) ±*SD*	$t_{1/2}$ (h) ±*SD*	C_{max} (nM)	C_{4h} (nM)	$AUC_{0\text{-}inf}$ (ng.h/mL) ±*SD*	$MRT_{0\text{-}inf}$ (h) ±*SD*
68 AR-198 (OX04528)	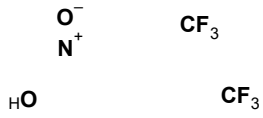	102 *±24*	0.417 *±0.14*	0.959 *±0.04*	280	15	142 *±14*	1.52 *±0.19*
69 AR-211 OX04529	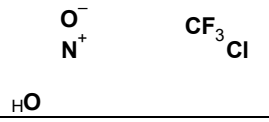	102 *±42*	0.417 *±0.14*	0.888 *±0.09*	310	10	106 *±16*	1.35 *±0.22*

*Male C57/BL6J mice. Adapted from Wang et al. (2023a), experiments performed by Wuxi AppTec Ltd (Hong Kong). AUC, area under curve; C_{max}, peak drug concentration; MRT, mean residence time; PO, *per os* oral administration; T_{max}, time of peak drug concentration.

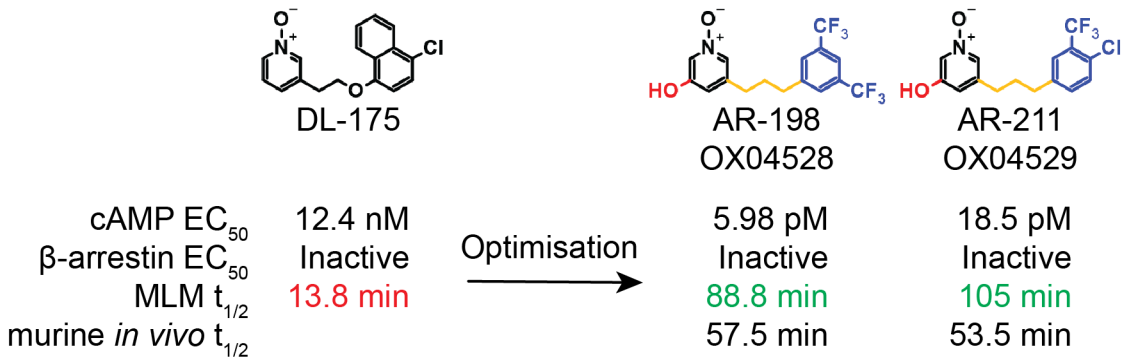

Figure 17: Summary of bioactivity data during optimisation of DL-175. Chemical structures and biological summary data following the optimisation of DL-175. AR-198 and AR-211 show enhanced potency against hGPR84, do not recruit β-arrestin-2, are metabolically stable, and have favourable murine *in vivo* PK half-lives. Adapted from Wang et al. (2023a).

2.2.4. Cell Line Development and Species Selectivity

Previous work in this laboratory has described the effects of 6-OAU and DL-175 on commercially available human GPR84 CHO cell lines, primary human monocytes and murine BMDMs, and the human U937 cell-line (Lucy et al., 2019). There is a particular need to assess possible differences of these agonists in head-to-head assays on mouse and human GPR84 given the prevalence of mice as a preclinical model.

Three clones expressing different levels of human and mouse GPR84 were isolated. One of these clones expressed high levels of the human protein, while two separate clones each expressed low levels of the human and mouse orthologues of GPR84 (Figure 18). Protein resolution by sodium dodecyl sulfate–polyacrylamide gel electrophoresis (SDS-PAGE) using cell lysates from each clone showed a markedly different HA-tag reactivity by Western Blot. The CHO-HA-hGPR84 #7F12 clone showed a strong but diffuse band, whereas only weak bands were seen in the CHO-HA-hGPR84 #3E11 and CHO-HA-mGPR84 #18E7 clones. No detection was observed in the commercial CHO-hGPR84 (DiscoverX) and CHO-K1 parental cell lines, both of which lack the HA-tag epitope (Figure 18 A). To ensure these bands were specific, the high expressing clone was then probed with an alternative α-HA primary antibody which demonstrated expression of GPR84 with two distinct bands between 55 and 70 kDa, as well as a higher apparent molecular weight band near 120 kDa (Figure 18 B). Similar patterns were observed by Marsango et al. (2022) when expressing hGPR84-eYFP in HEK293 cells. One suggestion was that the smaller bands represented different post-translationally modified versions of the receptor, while the high molecular weight bands may have aggregated or dimeric forms.

To test whether these expression differences were reflected in the mRNA levels of the human clones and how these might relate to physiological levels of expression I tested and compared these results by real time quantitative RT-PCR. Commercially available primers spanning the two exons of *GPR84* were used to ensure specificity of the amplification in PMA-differentiated THP-1 macrophages. It became evident that the PMA treatment to differentiate THP-1 monocytes into macrophage-like cells could itself upregulate *GPR84* above levels in untreated THP-1 monocytes

(Figure 18 C). However, further polarisation from THP-1 M0 to M1 or M2 using LPS or IL-4 could then further increase or decrease *GPR84* expression respectively. Unstimulated U937 cells had similar *GPR84* expression levels compared to unstimulated THP-1 cells, which was elevated with LPS treatment (Figure 18 D). A separate primer pair spanning a region in the coding sequence of *GPR84* was then used to determine expression levels in the CHO-HA-hGPR84 clones (Figure 18 E). Evidently CHO-HA-hGPR84 #7F12 constitutively expresses high levels of *GPR84* relative to unstimulated THP-1 cells and far above those seen in THP-1-M1 or LPS-stimulated U937 cells. In the CHO-HA-hGPR84 #3E11 clone expression levels were over 11× lower than the high expressing clone and approximated those of the LPS-stimulated U937 cells and PMA-differentiated THP-1 cells.

I then sought to determine whether these higher expression and total protein levels corresponded to an increased surface expression of GPR84 in the high expressing CHO-HA-hGPR84 #7F12 clone. Based on results showing an increased level of surface-accessible HA-tag immunoreactivity by immunocytochemistry I confirmed that the high expressing human clone did indeed have higher surface expression levels than either of the low expressing clones. In fact, the low expressing clones did not show any specific staining and were indistinguishable from the CHO-hGPR84 (DiscoverX) no-epitope and CHO-K1 controls (Figure 18 F - J).

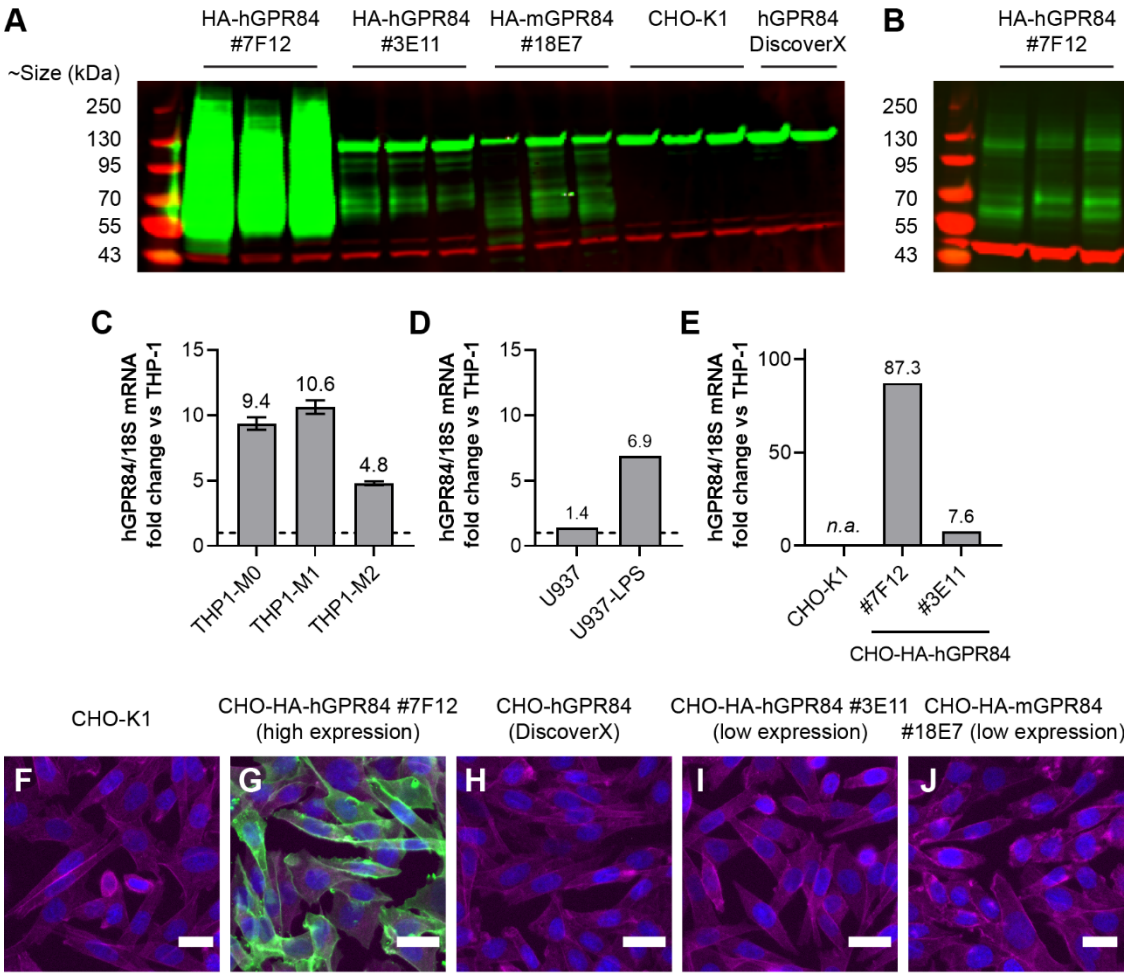

Figure 18: Receptor expression levels of human and mouse GPR84 cell lines. Total GPR84 expression in each cell line following protein resolution by SDS-PAGE and Western blotting against the HA-tag (*green*) using rabbit α-HA primary and ERK1/2 (*red*) (A), or rat α-HA primary and β-actin (*red*) (B). Three independent protein lysates were run on a single gel. GPR84 mRNA expression in PMA-differentiated THP-1 cells (C), U937 cells (D), and CHO-hGPR84 cell lines (E) determined by real time qRT-PCR. Bars represent mean ± SEM, $n = 3$ (C), or mean of duplicate conditions, $n = 1$ (D, E). (F - J) Surface GPR84 expression in each cell line following immunolabelling of the HA-tag (*green*), F-actin (*magenta*), and nuclei (*blue*) without cell membrane permeabilisation. Images acquired using a 20X 0.75 NA objective lens, scale bar = 25 µm. Adapted from Luscombe et al. (2023a).

I then tested the functional responses of these clones in assays measuring cAMP production. As would be expected, receptor expression levels were found to correlate with agonist potency. The rank order of potency began with the high expressing #7F12 cell line, followed by the commercial CHO-hGPR84 (DiscoverX) cell line, then the low expressing human #3E11 and mouse #18E7 cell lines (Figure 19 A - D). All cell lines had full efficacy responses at or below 1 µM of 6-OAU and DL-175. I then tested the specificity of these responses and demonstrated that the response to 1 µM agonist was absent in CHO-K1 parental cells (Figure 19 E), and could be blocked by pre-treatment

with pertussis toxin (PTX) or Antagonist 8 in all GPR84 expressing cell lines (Figure 19 E - I). In all three human GPR84 cell lines 6-OAU was equally as potent as DL-175. However, in the mouse GPR84 cell line 6-OAU was 6× less potent than DL-175 (Table X, unpaired t-test p = 0.01). Capric acid also highlights the potency shift between cell lines, as it achieved nanomolar EC_{50}'s in the high expressing cell line but high micromolar EC_{50}'s in the low expressing cell lines (Table X). Furthermore, neither 3-hydroxy capric acid, nor myristic acid caused full efficacy cAMP responses in the low expressing cell lines.

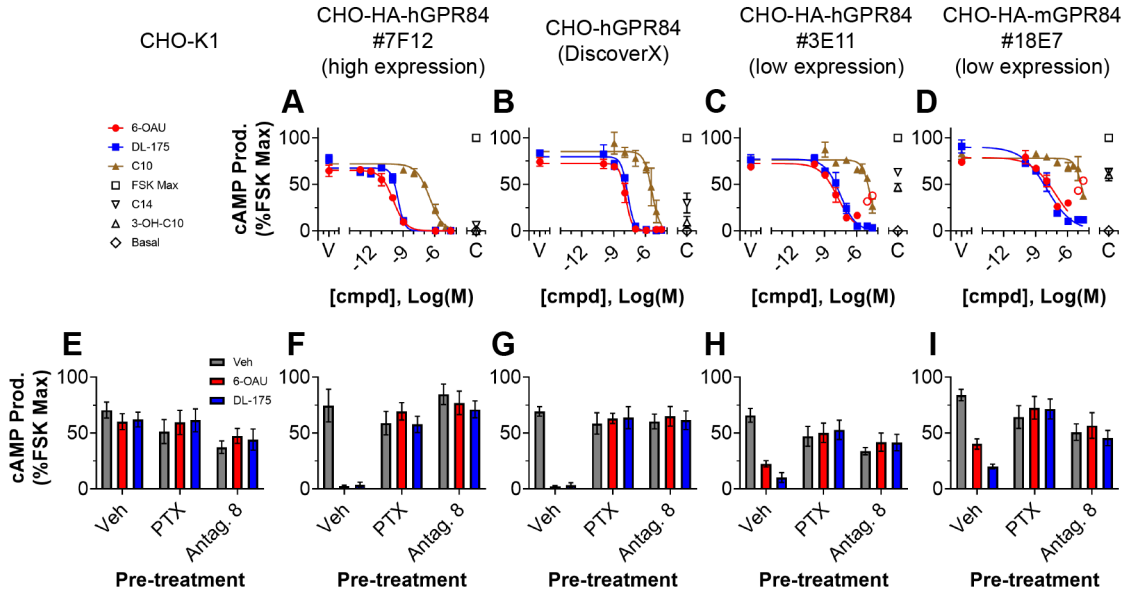

Figure 19: Functional characterisation of human and mouse GPR84 cell lines. The cAMP response in CHO-K1 (E), CHO-HA-hGPR74 #7F12 (A, F), CHO-hGPR84 (DiscoverX) (B, G), CHO-HA-hGPR84 #3E11 (C, H), and CHO-HA-mGPR84 #18E7 cells (D, I). (A-D) Agonist concentration-response curves of the inhibition of forskolin-stimulated cAMP production. Points represent mean ± SEM, *n* = 3-4, experiments performed in triplicate. (E-I) Responses to 1 µM agonist following pre-treatment with pertussis toxin (100 ng/mL) or Antagonist 8 (30 µM). Bars represent mean ± SEM, *n* = 3, each experiment performed in triplicate. Adapted from Luscombe et al. (2023a). FSK, forskolin; PTX, pertussis toxin.

Table X: Potency of GPR84 agonists in human and mouse GPR84 cell lines.

Compound	GPR84 cAMP Potency EC_{50} (nM) [pEC_{50} ± SEM]			
	Human #7F12 (high expression)	Human (DiscoverX)	Human #3E11 (low expression)	Mouse #18E7 (low expression)
6-OAU	0.120 [9.92 ± 0.15]	1.16 [8.94 ± 0.31]	15.3 [7.81 ± 0.25]	66.0 [7.18 ± 0.21]
DL-175	0.356 [9.45 ± 0.10]	1.98 [8.70 ± 0.16]	29.0 [7.54 ± 0.20]	11.0 [7.96 ± 0.21]
Capric acid	305 [6.52 ± 0.18]	3,595 [5.44 ± 0.39]	>10,000 [<5.00]	>10,000 [<5.00]

Reproduced with permission from Luscombe et al. (2023a).

Zebrafish represent another *in vivo* model used in biological research, and the protein sequence of zGPR84 bears a 50.37% similarity to hGPR84, with particular conservation in the transmembrane regions (Huang et al., 2014). I then also cloned zebrafish GPR84 due to its similarity to human GPR84 as compared to putative orthologues we had identified in invertebrate species including *Drosophila melanogaster* and *Caenorhabditis elegans*, but also based on previous research showing *zGpr84* is also upregulated by LPS (Huang et al., 2014). Here, I identified a functionally responsive zGPR84 clone using cAMP assays and tested a panel of agonists on human and zebrafish GPR84 in the same assay plate. As expected the orthosteric agonists 6-OAU and DL-175 as well as the allosteric agonist DIM could activate hGPR84 with nearly full efficacy (Figure 20 A). Zebrafish GPR84 responded to 6-OAU with the same potency (zGPR84 EC_{50} = 18.2 nM vs hGPR84 EC_{50} = 3.46 nM), DL-175 with a higher potency (zGPR84 EC_{50} = 0.541 nM vs hGPR84 EC_{50} = 5.41 nM), but did not respond to DIM. The agonists LY237, capric acid, and embelin maintained activity at zGPR84. Capric acid was still a low potency agonist (zGPR84 EC_{50} = 7.24 μM) (Figure 20 B). Given that capric acid retained activity at zGPR84 I then tested a panel of MCFAs and hydroxylated MCFAs (Figure 20 C) for activity. Hydroxylated MCFAs showed the same altered chain length specificity as hGPR84 in that the most potent compounds are of carbon length 10, 11, and shared between 11 and 12 for saturated, 2-hydroxy, and 3-hydroxy MCFAs respectively (Figure 20 D).

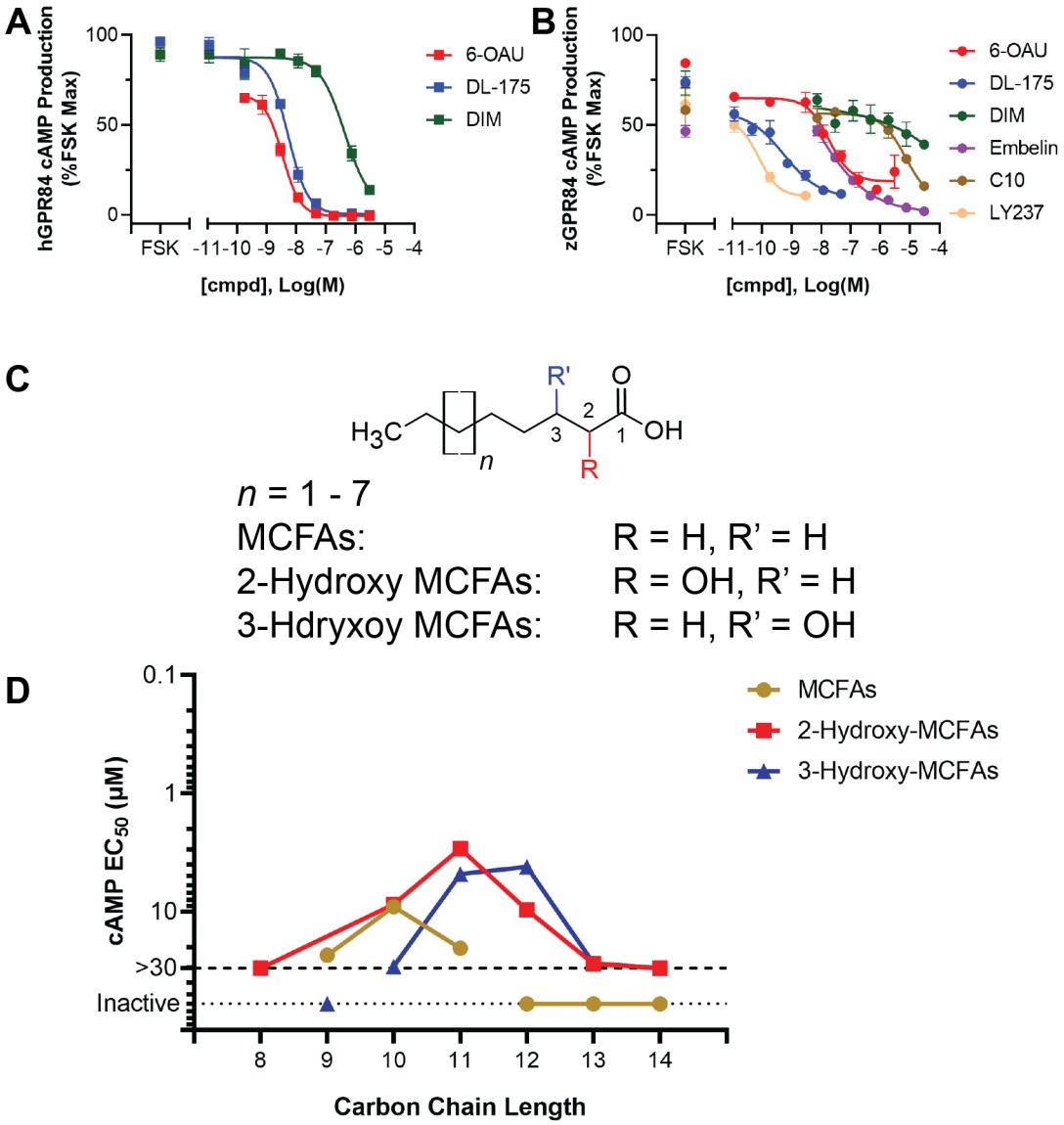

Figure 20: Most agonists maintain activity at zebrafish GPR84. (A, B) Agonist concentration-response curves for the inhibition of forskolin-stimulated cAMP production in CHO-hGPR84 (DiscoverX) cells (A) and CHO-HA-zGPR84 cells (B). Points represent mean ± SEM of triplicate, $n = 1$. (C) Chemical structures of MCFAs synthesised in-house for testing. (D) Zebrafish GPR84 EC_{50} values derived from concentration-response curves of test compounds for inhibition of forskolin-stimulated cAMP production in CHO-HA-zGPR84 cells. Points represent mean of 12-point curves performed in triplicate, $n = 1$. FSK, forskolin; MCFA, medium-chain fatty acid.

2.3. Discussion

2.3.1. Optimisation of the cAMP Assay for Screening

Assays for cAMP production are a functional readout for receptor activation and signalling via the G-protein pathway. These assays feature a native coupling system between receptor and G-protein, and not for example a transfected non-native chimeric G-protein. Although the receptor

overexpression would be considered non-physiological, this alters the observed potency of an agonist but maintains the relative potency ranking, and could therefore be considered an advantage in that we could determine EC_{50} values for low potency compounds that would otherwise be lost on low expressing or native cell lines. The antibody-based detection system is specific and sensitive, has a high dynamic range, and a good signal to background ratio based on the chemiluminescent readout. The ability to calculate absolute concentrations of cAMP is an advantage, however, as the resulting potency values do not change from the RLU measurements, and I opt to avoid this step during more extensive screening campaigns to minimise data handling and maximise reagent efficiency.

The assay in this format has been shown to be suitable for investigating SAR in a more high-throughput fashion. For screening campaigns the following controls will be used: forskolin max (100 μM) in order to ensure the 25 μM forskolin achieves roughly an EC_{80} as well as the potential to normalise the plate responses, capric acid max (100 μM) in order to determine the maximum receptor activation and potentially normalise responses to 100% efficacy, basal (no forskolin) in order to ensure the basal cAMP production is consistent between experiments, and forskolin EC_{80} (25 μM) in the absence of any test compounds from which to measure GPR84-mediated inhibition. As the readout is luminescence based and test compounds are highly unlikely to be luminescent, compound alone controls will not be included. However, the major limitation of this detection system is that it does not provide kinetic data and only a snapshot of activity at 30 minutes is measured.

2.3.2. Hydroxylated MCFAs

We have undertaken the most systematic analysis of 2- and 3-hydroxylated MCFAs to date, including the chiral resolution of the 3-hydroxy enantiomers. Tolerance of the alkyl chain for activity at GPR84 was in agreement with previous literature showing that capric acid was the most potent saturated MCFA (Wang et al., 2006). Hydroxylation at the 2- or 3- position generally resulted in an improved potency but also affected the chain length specificity of the agonist, with 2-hydroxy undecanoic acid (2-OH-C11), 3-hydroxy undecanoic acid (3-OH-C11) and 3-hydroxy lauric acid (3-OH-C12) being the most potent hydroxylated MCFAs. Taken together, this indicates a specificity based not only on the total carbon chain length of the MCFA, but the length from the nearest hydroxyl

group. The recent crystal structure of hGPR84 in complex with 3-hydroxy lauric acid showed a restricted pocket which tolerated its nonane tail and the nonane tail of and LY237 (Liu et al., 2023). Our data are in agreement with this observation in that, from the nearest hydroxyl group, capric acid, 2-hydroxy undecanoic acid, 3-hydroxy undecanoic acid, and 3-hydroxy lauric acid share a nonane or octane tail which are known to be well accommodated in the binding site of GPR84.

With submicromolar potencies these hydroxylated MCFAs may be better candidates to activate GPR84 *in vivo*. For example, 3-hydroxy capric acid, 3-hydroxy lauric acid, and 3-hydroxy myristic acid all have EC_{50} values below that of plasma levels that can be found in humans with defects in mitochondrial fatty acid β-oxidation (Costa et al., 1998). This is also true for capric acid, but cannot be determined for lauric acid or myristic acid which have EC_{50} values >10 μM. Milks, cheeses, and suet are known to contain 2- and 3-hydroxy MCFAs (Jenske and Vetter, 2009). Though under typical conditions human plasma concentrations of 3-hydroxy capric acid is below 1 μM, or near 3 μM with MCT supplementation (Jones and Bennett, 2011), it is still unlikely that circulating levels are high enough to activate GPR84. If the hydroxylated MCFAs were of bacterial origin, the local concentrations of these metabolites could theoretically be quite high, and 3-hydroxy capric acid, 3-hydroxy lauric acid, and 3-hydroxy myristic acid have recently been demonstrated to be highly enriched in a stationary phase of *E. coli* (Peters et al., 2022).

Chiral resolution of the 3-hydroxylated MCFAs showed enantioselectivity, but not for all chain lengths, and in two cases the (*R*) configuration was preferred and in one case the (*S*) configuration was preferred. The most striking difference was seen with a drop in potency of (*S*)-3-hydroxy capric acid, where the (*R*) enantiomer retained activity comparable to the racemic mixture. This could indicate a chain-length specific enantiomeric preference of the receptor for (*R*)-3-hydroxy capric acid. However, as both microbial and dietary 3-hydroxy fatty acids are found in the (*R*) configuration (Jenske and Vetter, 2008, Rietschel, 1976), and the (*S*)-3-hydroxy fatty acid products from β-oxidation are rapidly epimerised (Jin et al., 1992), it does not help to differentiate the possible origin of (*R*)-3-hydroxy capric acid for GPR84. Clearly, there is still a need to identify local concentrations of MCFAs and their hydroxylated forms in relevant tissues, and resolution of these

lipids, including the 2-hydroxylated MCFAs, may still help to identify possible sources of GPR84 agonists. These hydroxylated MCFAs, particularly 2-OH-C11, 3-OH-C10, and 3-OH-C12, may make useful tool compounds due to their enhanced potency compared to capric acid. As circulating concentrations of these species are still far lower than their EC_{50} values we did not test these agonists for selectivity against other GPCRs to characterise their utility as tool compounds *in vitro*.

2.3.3. Screening and Optimisation of DL-175

Small molecule probes are important tools for investigating biological systems in health and disease and open research avenues to help bridge basic with translational sciences (Schreiber et al., 2015). We have described herein the screening strategy and chemical optimisation of DL-175 resulting in the development of highly potent, biased, and orally bioavailable tool compounds AR-198 and AR-211. The effect of biased signalling on the function of innate immune cells is still poorly characterised, with only a few reports describing the use of DL-175 alongside 6-OAU to date. These new tools are also suitable for use in murine *in vivo* models, extending the possible observations on immune cell function to tissue level studies. So far, the effect of biased agonists of GPR84 *in vivo* remains unexplored. However, there is still a need for carefully controlled experiments as the selectivity profile of these two compounds against the wider range of GPCRs was not determined.

DL-175 has been pharmacologically demonstrated to occupy an orthosteric binding site, based on competition with ZQ-16 in functional assays, positive allosteric modulation by PSB-16671, and competitive antagonism by the orthosteric agonist Antagonist 1 (Jenkins et al., 2021, Marsango et al., 2022). Curiously however, the mutation of R172 to an Alanine in GPR84, which usually abolishes activity of orthosteric agonists, did not affect the activity of DL-175 in GTPγS assays (Marsango et al., 2022). Docking experiments based on the AlphaFold template suggested DL-175 sits deeper in the transmembrane bundle and does not contact R172 (Marsango et al., 2022). The introduction of a hydroxyl group to the pyridine-*N*-oxide of DL-175 during this optimisation process may have allowed for new hydrogen bonds with R172, potentially explaining the enhanced potency (Wang et al., 2023a). The impact of these binding modes on bias and efficacy in both signalling assays and immune cell function warrants further investigation.

2.3.4. Cell Line Development and Species Selectivity

The GPR84 cell lines afford an opportunity to study receptor pharmacology under controlled conditions. I identified two stable human GPR84 cell lines with over an 11× difference in mRNA expression despite similar transfection strategies. As the expression vectors contain the same promoter, and clones were grown out for 4+ weeks, these differences might instead reflect integration into more or less transcriptionally active genomic sites or different transgene copy numbers. Experiments quantifying the *GPR84* mRNA point to supraphysiological levels of expression in the high expressing cell line, and more physiological levels in the low expressing cell line.

The MCFA capric acid has previously been shown to be active at both human and mouse GPR84, which share 85% amino acid identity (Marsango et al., 2022a; Wang et al., 2006). We have shown under standardised assay conditions that both 6-OAU and DL-175 elicit specific low nanomolar cAMP responses at both human and mouse GPR84, supporting their use as balanced and biased agonists in murine models. These results also suggest that the putative agonists capric acid and 3-hydroxy capric acid will only elicit full efficacy responses at or below 30 μM in systems of high receptor expression. Whether these high levels of expression are achieved *in vivo* remains to be demonstrated. Nonetheless, evaluating ligands in systems with varying expression levels of their cognate receptor is important for a more complete pharmacological characterisation (Kenakin, 2007, Moran et al., 2018). Efficacy differences between 6-OAU and DL-175 were not observed, but it is worth noting that due to the ceiling of G_i-mediated inhibition of forskolin-stimulated cAMP production it is unlikely to be seen with high potency agonists.

Zebrafish GPR84 was found to respond to the orthosteric human GPR84 agonists with similar overall potency compared to human GPR84 despite a protein similarity of approximately only 50%. The allosteric agonist DIM lost activity at zGPR84, and considering the differences in protein sequence could likely have been due to a lack of a homologous binding site region. The MCFAs retained activity at zGPR84 with an overall lower potency, and notably, retained the chain length specificity we observed earlier in studies on the human receptor. Previous research has shown

that *zGpr84* is expressed in zebrafish liver, heart, and intestines, and expression is regulated during embryogenesis, by LPS, and by fasting state (Huang et al., 2014). Furthermore, RAW264.7 cells transfected with zGPR84 produce *Il-12* in response to lauric acid (Huang et al., 2014) and has been suggested to enhance phagocytosis of *E. coli* and *S. aureus* (Wang et al., 2019). However, these reports did not test for agonist potency at zGPR84. We have shown here that MCFAs in general retain activity at zGPR84, but that in our cell line lauric acid was in fact inactive. Further research using zebrafish as an *in vivo* model system would benefit from the use of more potent zGPR84 agonists such as 6-OAU or DL-175. However, the overall retention of activity of the MCFAs and upregulation of zGPR84 by LPS does pose an interesting question about the origin of MCFAs encountered by zebrafish and what concentrations they might achieve *in vivo*.

2.4. Conclusions

New tools pave the research pathways of many scientific avenues, with the medical sciences and drug discovery areas being no exception. Therefore, in pursuit of Thesis Aim 1, we sought to develop chemical and biological tools for use in studying GPR84. By optimising the cAMP assay for use in a more high-throughput format it made for the efficient determination of agonist potency against hGPR84, driving SAR campaigns for both MCFAs and synthetic agonists. Hydroxylated forms of MCFAs were found to be more potent than their non-hydroxylated counterparts and could therefore be more physiologically relevant. Working with collaborators in the department of chemistry we also developed AR-198 and AR-211, two highly potent and metabolically stable analogues of DL-175 suitable for use as *in vivo* tools. These have numerous applications and will undoubtedly find use in the field for studying the effects of biased agonism *in vitro* and *in vivo*. Finally, I developed several transgenic CHO cell lines suitable for use as *in vitro* biological tools. The human, mouse, and zebrafish GPR84 cell lines were used to compare the species selectivity of commonly used GPR84 agonists. The hGPR84 clones of varying receptor expression can also find use given the more physiological expression level of the low expressing clone #3E11, and the immunoreactivity and receptor localisation advantage of the high expressing #7F12 clone.

Chapter Three.

THE KINETICS OF BIASED AGONISTS

3.1. Introduction

3.1.1. Label-Free Impedance Sensing

Previous studies have identified the structurally different GPR84 selective agonists 6-OAU and DL-175. While 6-OAU is a balanced agonist able to activate the G_i as well as β-arrestin pathways, DL-175 is a G-protein biased agonist that is unable to recruit β-arrestins (Lucy et al., 2019). When comparing 6-OAU and DL-175 in a human-derived U937 macrophage-like cell line it was evident that 6-OAU induces both chemotaxis and phagocytosis, while DL-175 maintains phagocytosis without any chemotactic effect (Lucy et al., 2019). These experiments suggest that GPR84 activation can be as pharmacologically tuneable as other immune cell receptors such as those for host defence (e.g. complement component and formyl peptide receptors), danger signalling (e.g. chemokine and purinergic receptors), and quorum sensing (e.g. aryl hydrocarbon and bitter taste receptors) (Dahlgren et al., 2016, Gaida et al., 2016, Greaves and Schall, 2000, McDonald et al., 2010, Moura-Alves et al., 2019).

Previous work in this laboratory has demonstrated the usefulness of impedance sensing as a label-free technique that is able to discriminate between 6-OAU and DL-175 (Lucy et al., 2019). In this assay, cells are seeded into wells containing a microarray of electrodes, which introduces an electrical resistance (measured as cell index) that increases upon cell attachment and proliferation (Atienza et al., 2005). In BMDMs and human U937 cells the impedance response to 1 μM DL-175 is more sustained than that for 6-OAU (Lucy et al., 2019). Therefore, impedance sensing is a kinetic and label-free technique that was able to discriminate between the molecular action of 6-OAU and DL-175. This is key, because at 1 μM the agonists would be expected to elicit identical responses in the cAMP and β-arrestin-2 assays; a concentration at which both agonists cause maximal inhibition of forskolin-stimulated cAMP production, and neither agonist actually recruits β-arrestin-2 due to

the low potency of 6-OAU and inactivity of DL-175 (Lucy et al., 2019). Therefore, the exact mechanism by which the agonists could elicit differential responses in the chemotaxis of U937 cells at 1 μM is unexplained. I therefore set out to identify further differences between 6-OAU and DL-175 using the xCELLigence cell electrical impedance (CEI) assay.

3.1.2. ERK & Akt Phosphorylation

GPCRs regulate the activity of other signalling proteins including ion channels, kinases, and transcription factors. GPR84 in particular has been linked to effector proteins such as phospholipase C, PI3K, Akt, ERK1/2, JNK, and p38 (Gao et al., 2020, Peters et al., 2022, Meng et al., 2017, Park et al., 2018, Recio et al., 2018). Akt and ERK1/2 are two transiently activated downstream kinases linked to GPR84 and prominent pharmacological readouts for the detection of alternative Gβɣ. Akt is a serine/threonine kinase associated with cellular proliferation, apoptosis, and surivival (New et al., 2007). It is also an important kinase in the mechanism of chemotaxis. Following receptor activation and dissociation of the heterotrimeric G-protein, free Gβɣ activates PI3K, which converts the membrane phospholipid PIP_2 into PIP_3, and recruits Akt which then influences actin remodelling (Jin et al., 2008). The MAPK cascade results in the activation of various nuclear and cytoplasmic proteins, and were linked to GPCRs through the arrestins and initially thought of as arrestin-dependent functions (Gurevich and Gurevich, 2019). It is now understood that GPCRs can activate ERK1/2 with varying levels of G-protein and β-arrestin dependency (Gurevich and Gurevich, 2019).

LPS-treated BMDMs stimulated with 6-OAU were shown to result in the phosphorylation of both ERK1/2 and Akt, but not in *Gpr84*$^{-/-}$ BMDMs (Recio et al., 2018). In IFN-ɣ-treated human macrophages, embelin was shown to phosphorylate ERK1/2 and Akt in a PTX-sensitive manner (Gaidarov et al., 2018). The Akt response was sensitive to inhibition by wortmannin, a PI3K inhibitor (Gaidarov et al., 2018). Similar phosphorylation was seen of ERK1/2 and Akt in THP-1-M1 macrophages stimulated with capric acid, 3-hydroxy capric acid, and 6-OAU (Peters et al., 2022). With the phosphorylation of both Akt and ERK1/2 being linked to various important cellular processes and already being well characterised in macrophages I then tested the agonists 6-OAU and DL-175 for differences in these responses in both the high and low expressing recombinant cell lines.

3.1.3. Receptor Internalisation

Receptor internalisation is a key process by which cells lose sensitivity to an external stimulus. Following receptor activation, β-arrestins bind to endocytic proteins and thereby link receptors to internalisation pathways (Shenoy and Lefkowitz, 2003). Still, the internalisation of a receptor by endocytosis does not necessarily terminate its signalling and does not prevent further signal initiation from the receptor (Eichel and von Zastrow, 2018). The relationship between receptor endocytosis and signalling is therefore bi-directional. Endosomal redistribution alters the environment of the receptor, segregating it from effector proteins localised at the plasma membrane such as phospholipase Cɣ, while also placing them in 'signalosomes' which appear more likely to include ERK1/2 and β-arrestins (Sorkin and von Zastrow, 2009). Receptor signalling following internalisation can be influenced by agonist bias too. In one extreme example of persistent signalling, the immune cell receptor $S1P_1$ has been shown to continue $G\alpha_i$ signalling for hours despite internalisation when treated with FTY720 but not S1P (Mullershausen et al., 2009). As expected cells had a reduced ability to elicit a Ca^{2+} response following internalisation by FTY720. Crucially, the internalisation and persistent signalling of $S1P_1$ was shown to depend on the alkyl tail length of FTY720, demonstrating the influence of chemical structure on receptor internalisation (Mullershausen et al., 2009).

To measure receptor internalisation I conducted assays measuring reductions in surface receptor expression upon agonist treatment. First, CHO-HA-hGPR84 #7F12 high expressing cells were incubated with agonist to cause internalisation, then fixed and stained for surface-accessible HA-tag without cell membrane permeabilisation. Differences in surface receptor were quantified by image analysis and the effect of agonists compared to vehicle. This measurement includes the detection of all HA-tagged receptor on the surface, including newly synthesised or forward trafficked receptor populations, and described as nett surface receptor.

3.1.4. Chapter Rationale and Experimental Aim

The aim of this chapter is to investigate the differential cellular responses to GPR84 agonists 6-OAU and DL-175 by quantifying their effect on cell morphology and adhesion, kinase phosphorylation, and receptor internalisation.

3.2. Results

3.2.1. Label-Free Impedance Sensing

In order to determine if the distinct impedance traces of 6-OAU and DL-175 in primary cells could be recapitulated in CHO cells we tested the newly developed CHO-GPR84 cell lines in CEI assays (Figure 21 A, B). The BMDM response to DL-175 was characterised by a delayed decay in signal compared to 6-OAU (Figure 21 C). This could be recapitulated in both human and mouse cell lines with low receptor expression (Figure 21 F, G). Conversely, the high expressing and commercial hGPR84 cell lines exhibited a constitutively elevated signal in which 6-OAU and DL-175 had identical responses (Figure 21 D, E). The 6-OAU signal in the high expressing cell line remained elevated to 60 minutes, in the commercial cell line it had reached baseline by 30 minutes, and in the low expressing cell lines it had decayed by 15 minutes, paralleling the decay of the BMDM response at 20 minutes. Furthermore, pre-incubation with the GRK2/3 inhibitor compound 101 (Lowe et al., 2015) augmented the positive impedance response elicited by 6-OAU in BMDMs (Figure 21 I) and low expressing cell lines (Figure 21 L, M), but not the high expressing or commercial cell lines (Figure 21 J, K). Responses to 6-OAU and DL-175 have previously been shown to be absent in GPR84 KO BMDMs (Lucy et al., 2019), and here lacked any signal in CHO-K1 parental cells (Figure 21 H, N).

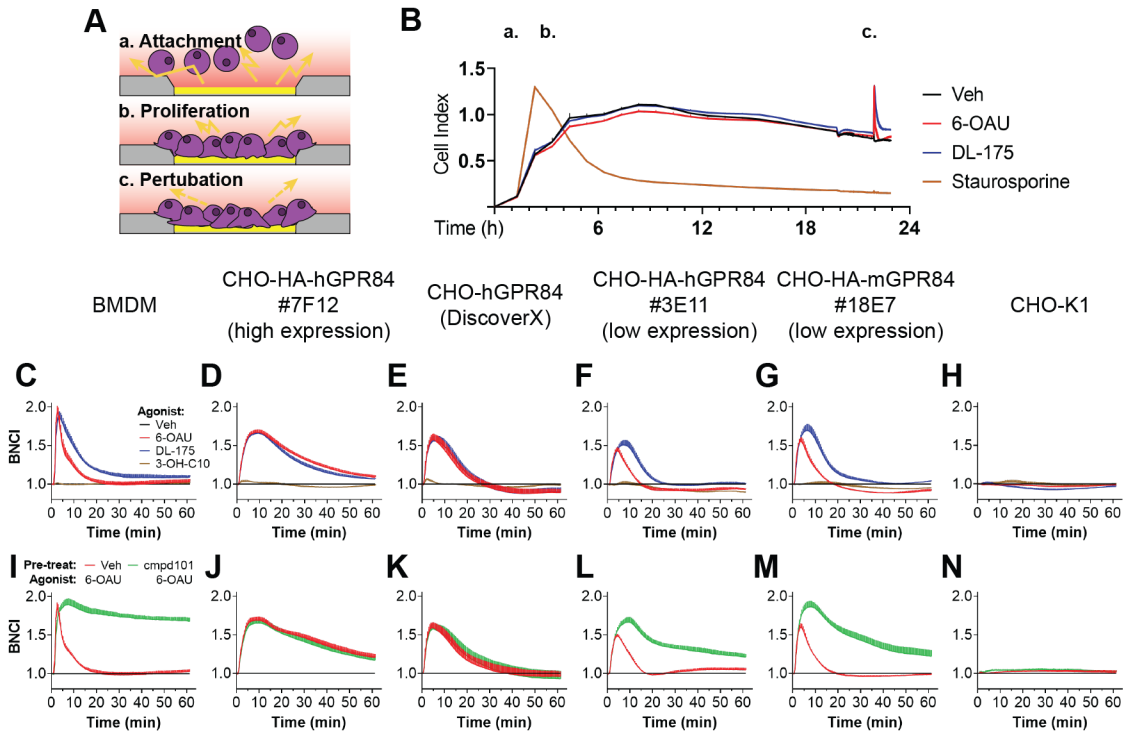

Figure 21: Impedance phenotypes of macrophages and GPR84 cell lines. GPR84 agonists 6-OAU and DL-175 elicit distinct impedance phenotypes in BMDMs and heterologous CHO expression systems. (A) Cells are seeded into 96-well xCELLigence E-plates containing a microarray of gold electrodes. (B) Example time course data showing the impedance response of BMDMs as they attach and proliferate. Staurosporine (600 nM) was added 1 h after cell seeding to demonstrate the effect of cytotoxic pressure resulting in cell death and detachment. Cells were plated 22 h prior to stimulation with 1 µM 6-OAU or DL-175 (C - H), or pre-treated for 2 h with 30 µM cmpd101 or vehicle (DMSO) followed by stimulation with 1 µM 6-OAU (I - N). Cell index values were normalised to baseline conditions (Veh, C - H; Veh-Veh, I - N). Lines depict mean ± SEM, *n* = 3, experiments performed in duplicate. Adapted from Luscombe et al. (2023a). BMDM, bone marrow-derived macrophage; BNCI, baseline-normalised cell index.

Results using agonists at 1 µM indicate that the responses in murine BMDMs and human U937 cells (Lucy et al., 2019) were translatable to CHO cells and do not differ between human and mouse orthologues. Therefore, we sought to characterise these ligands more thoroughly using kinetic assays in the CHO-HA-hGPR84 #3E11 low expressing cell line. Treatment with 6-OAU and DL-175 caused concentration-dependent increases in the maximum signal of the initial baseline normalised cell index BNCI peak (Figure 22 A, B). The distinctly prolonged phenotype of DL-175 was consistent across the concentrations tested, even when comparing it to concentrations of 6-OAU that resulted in a similar maximum peak. CRCs generated using BNCI peak maxima showed both ligands elicited similar low nanomolar EC_{50}'s (Figure 22 C). The response of 6-OAU, EC_{50} = 15.2

nM (pEC_{50} = 7.82 ± 0.13), and DL-175, EC_{50} = 83.5 nM (pEC_{50} = 7.08 ± 0.20) were similar to their cAMP potencies in the same cell line (15.4 nM and 29.0 nM) and potencies previously determined in murine BMDMs (129 nM and 50.3 nM) (Lucy et al., 2019). The peak signal elicited by DL-175, E_{max} = 1.82, was found to be 1.6-fold higher than 6-OAU, E_{max} = 1.15. The specificity of each response was demonstrated by pre-treatment and blockade of effect using Antagonist 8 and pertussis toxin (Figure 22 D).

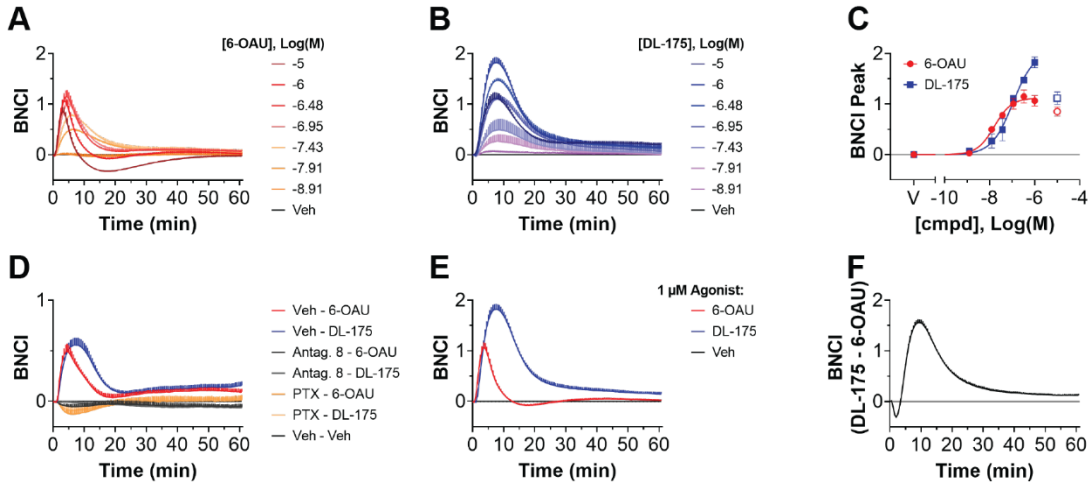

Figure 22: Differences between the impedance responses of 6-OAU and DL-175. CHO-HA-hGPR84 #3E11 low expressing cells were seeded 20 - 22 h prior to stimulation with varying concentrations of 6-OAU (A) or DL-175 (B). (C) Peak BNCI values from A and B were plotted as concentration-response curves. (D) Responses to 1 µM 6-OAU or DL-175 following 2 h pre-incubations with Antagonist 8, pertussis toxin, or vehicle. (E) comparison of the 1 µM responses from A and B. (F) Differences between the 1 µM impedance responses in E, which were calculated by subtracting the 6-OAU response from the DL-175 response. Lines depict mean ± SEM, *n* = 3, experiments performed in duplicate. Adapted from Luscombe et al. (2023a). BNCI, baseline-normalised cell index.

Table XI: GPR84 impedance responses to 1 µM 6-OAU and DL-175.

Descriptor	6-OAU	DL-175	Significance
AUC (min × BNCI)	6.8 ± 0.6	32 ± 1	****
Peak time (min)	3.528 ± 0.006	7.5 ± 0.3	***
Max slope, Ascending (BNCI / min)	0.56 ± 0.05	0.55 ± 0.05	ns
time of max slope ascending (min)	1.747 ± 0.006	2.4 ± 0.2	*
Max slope, Descending (BNCI / min)	-0.24 ± 0.02	-0.17 ± 0.04	ns
Time of max slope descending (min)	5.29 ± 0.01	12.7 ± 0.3	****

Unpaired t-test P-values: ≤0.0001 (****), ≤0.001 (***), ≤0.01 (**), ≤0.05 (*), >0.05, *ns*. All units given as mean ± SEM, *n* = 3. AUC, area under curve; BNCI, baseline normalised cell index. Reproduced with permission from Luscombe et al. (2023a).

Comparison of the responses elicited by 1 μM agonist highlights the differences between DL-175 and 6-OAU in terms of the max signal and the sustained response of DL-175 (Figure 22 E). We further analysed these traces and found that the gradient of the slopes of the ascending and descending phases were almost identical (Table XI). Both ligands caused rapid increases in the first three minutes. DL-175 then exhibited a delay in the impedance peak time (7.5 min), which occurred 4 minutes after the peak of 6-OAU (3.5 min). This delay was concomitant with delays in the time of the max slope of the ascending and descending phases, as well as a greater area under curve (Table XI). In addition to differences at 1 μM, these delays were also present at all other concentrations tested between 10 nM and 10 μM. To highlight these kinetic differences in impedance responses I subtracted the 6-OAU response from the DL-175 response (Figure 22 F). It is evident that the agonists exhibited similar responses within 3.5 minutes of addition, before rapidly diverging such that they were most different near the 10 minute time point. The signals then converged and continued to signal at comparable levels from approximately 30 minutes onwards. Just as high expression systems might mask subtle differences between agonists, long time points might miss key times in which the DL-175 and 6-OAU G-protein-mediated responses differ, highlighting the importance of kinetic readouts in assays for signalling bias.

3.2.2. ERK & Akt Phosphorylation

Due to the time-dependent distinction between 6-OAU and DL-175 in the impedance assays we sought to utilise time courses to measure the activation of two transiently activated downstream kinases linked to GPR84 activation (Peters et al., 2022; Recio et al., 2018). We compared the agonist mediated phosphorylation of ERK and Akt in the high expressing and low expressing cell lines by separating proteins by SDS-PAGE and simultaneously probing for total- and phospho-protein. The same cell lysates were used to probe for ERK and Akt. Following agonist incubations for various time points we found that both 6-OAU and DL-175 caused transient responses.

In the high expressing human GPR84 #7F12 cell line both agonists caused similar peaks in Akt phosphorylation at 10 minutes (Figure 23 A, C). In contrast, the low expressing #3E11 cell line responded to 6-OAU with a peak in Akt activation at 5 minutes, compared to the delayed and

suppressed peak of DL-175 occurring at 10 minutes (Figure 23 B, D). In the case of GPR84-mediated ERK activation both 6-OAU and DL-175 caused similar responses with peaks at or near 5 minutes in both the high and low expressing human GPR84 cell lines (Figure 23 E - H). The ERK and Akt responses were prolonged in the high expressing human GPR84 cell line when compared to the low expressing cell line.

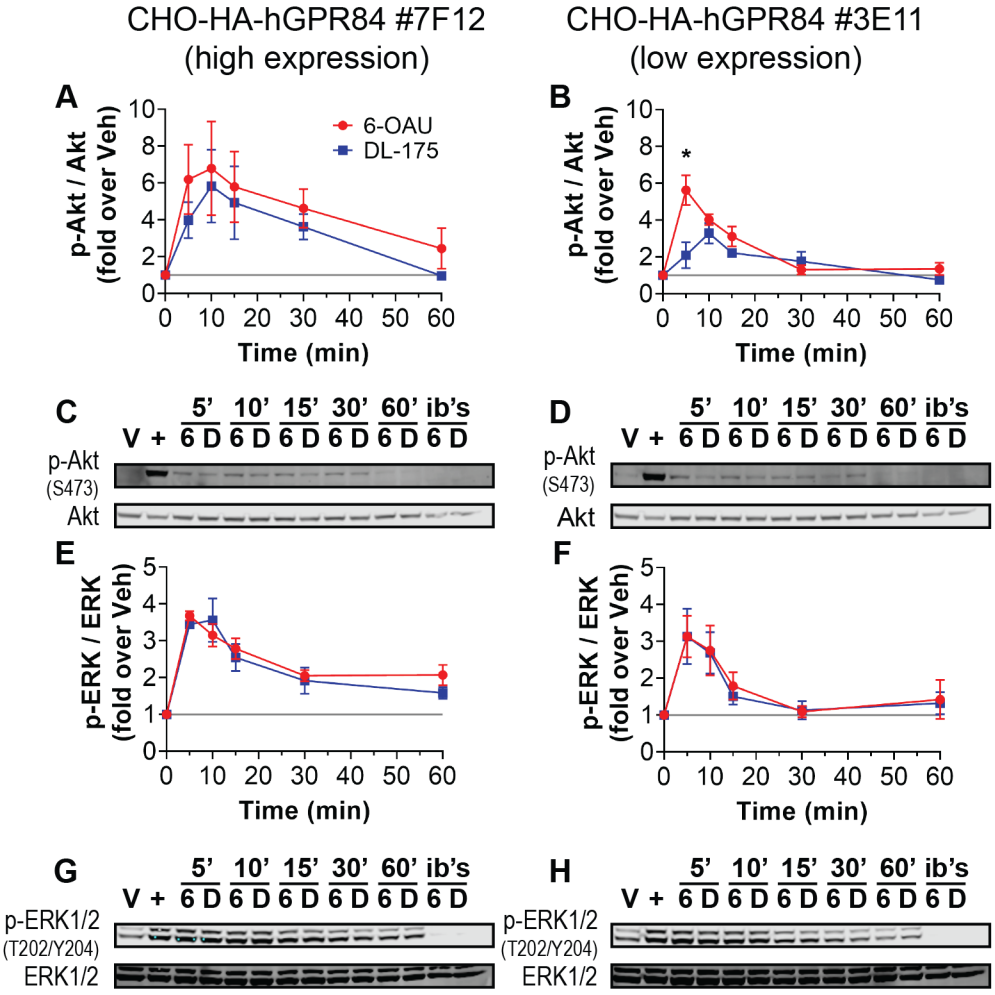

Figure 23: Time course of GPR84-mediated ERK and Akt activation. CHO-HA-hGPR84 #7F12 high expressing cells (A, C, E, G) or CHO-HA-hGPR84 #3E11 low expressing cells (B, D, F, H) were stimulated with 6-OAU or DL-175 (1 µM) for 5 - 60 min before cell lysis and protein detection by Western blot. (A, B, E, F) Phosphorylated protein was normalised to total protein then expressed as fold-change over vehicle (DMSO) at 10 min. Points represent mean ± SEM, $n = 3$. Unpaired t-test between 6-OAU and DL-175, $P \leq 0.05$ (*). (C, D G, H) Representative Western blots shown by separating the 700 nm and 800 nm near-infrared channels for clarity. V, vehicle; +, positive control (Calcyulin A and FBS); ib's, inhibitors (MK-2206 and U0126); 6, 6-OAU; D, DL-175. Adapted from Luscombe et al. (2023a).

3.2.3. Receptor Internalisation

Having established that DL-175 exhibits signalling bias through multiple pathways, I then went to test whether this was associated with differences in the subcellular localisation of the receptor. Assays for surface receptor expression were conducted by quantifying reductions in surface-accessible HA-tag on high expressing HA-hGPR84 cells. Both 6-OAU and DL-175 caused reductions in plasma membrane receptor over time in a concentration-dependent manner (Figure 24 A - C). The reduction was more pronounced upon treatment with 6-OAU than DL-175. Treatment with 1 μM 6-OAU achieved a significantly lower plateau than DL-175, but did not achieve this lower plateau faster than DL-175 (Fig. 24 D, Table XII). The slight differences in one-phase decay half-lives and rate constants indicate that treatment with 1 μM 6-OAU reaches a steady state of 70% surface receptor in approximately 30 minutes (4 half-lives), compared to DL-175 which takes a longer time (>50 minutes) to reach the level of 89% surface receptor compared to vehicle. The marked differences between agonists were plotted by subtracting 6-OAU from DL-175, which underscores the way in which 6-OAU rapidly ($t_{1/2}$ = 5 minutes) achieved and sustained greater reductions in nett surface receptor than DL-175 (Figure 24 E).

DL-175 fails to cause equivalent reductions in nett surface receptor as 6-OAU, even when incubated for long periods at higher concentrations. The concentration response-curves at 1 h, modelled using 3-parameter fitting, highlight the greater efficacy and potency of 6-OAU (Figure 25 J, Table XII). Reductions in surface receptor were not observed with other GPR84 agonists capric acid and 3-hydroxy capric acid. No reductions were seen with Antagonist 8 (GPR84 antagonist), myristic acid (non-efficacious MCFA), and DL-222 (inactive analogue of DL-175) (Lucy et al., 2019) when compared to either vehicle (DMSO) or no vehicle (buffer only) (Figure 25 A – I, K). Finally, pre-treatment with Antagonist 8 was able to abrogate these reductions in nett surface receptor (Figure 25 L).

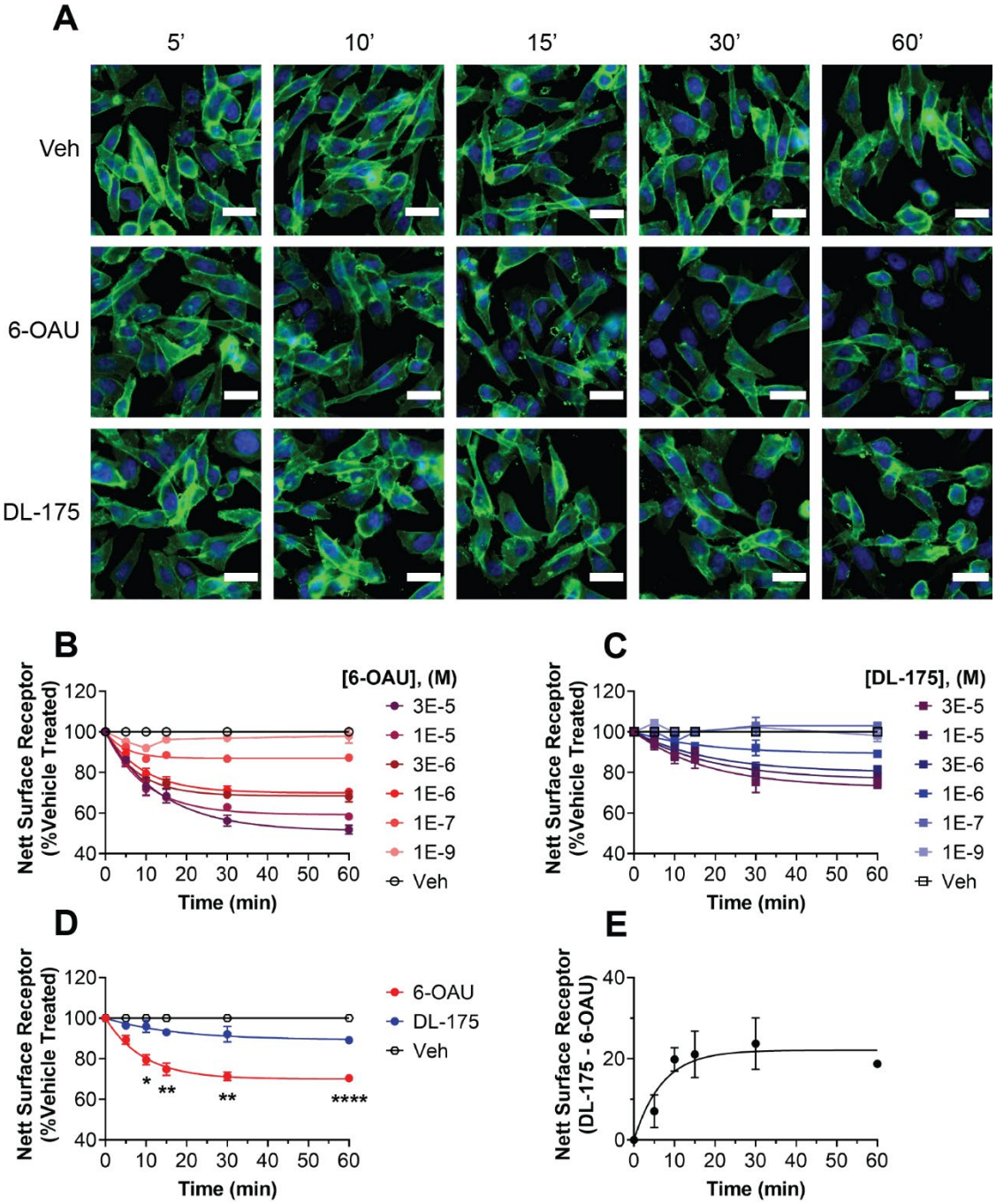

Figure 24: Agonist-induced internalisation of GPR84. (A) CHO-HA-hGPR84 #7F12 high expressing cells were stimulated with 6-OAU or DL-175 (1 µM) for 5 - 60 min before fixation without membrane permeabilisation, then stained for the HA-tag (*green*) and nuclei (*blue*). Images acquired using a 20X 0.75 NA objective lens, scale bar = 25 µm. Quantification of the green channel fluorescence intensity in segmented cell masks show reductions in nett surface receptor following treatment with varying concentrations of 6-OAU (B) or DL-175 (C). (D) Comparison of the reductions in nett surface receptor using 1 µM agonist from B and C. (E) Differences between the 1 µM responses in D, which were calculated by subtracting the 6-OAU response from the DL-175 response. Points represent mean ± SEM, $n = 3$, experiments performed in triplicate. Unpaired t-test between 6-OAU and DL-175 P-values: ≤0.0001 (****), ≤0.001 (***), ≤0.01 (**), ≤0.05 (*), >0.05, *ns*. Adapted from Luscombe et al. (2023a).

Table XII: GPR84 internalisation responses of 6-OAU and DL-175.

Data Set	Descriptor	6-OAU	DL-175	Significance
1 µM agonist (Figure 24 D)	Plateau (Nett Surface Receptor, %Veh treated)	70 ± 1	89 ± 1	***
1 µM agonist (Figure 24 D)	K (min^{-1})	0.11 ± 0.02	0.06 ± 0.02	*ns*
1 µM agonist (Figure 24 D)	$t_{1/2}$ (min)	7 ± 1	13 ± 4	*ns*
CRC (Figure 25 J)	E_{max} (%Internalised)	45 ± 1	27 ± 2	**
CRC (Figure 25 J)	pEC_{50}	6.1 ± 0.1	5.73 ± 0.08	*

Unpaired t-test P-values: ≤0.0001 (****), ≤0.001 (***), ≤0.01 (**), ≤0.05 (*), >0.05, *ns*. All units given as mean ± SEM, *n* = 3. CRC, concentration-response curve. Reproduced with permission from Luscombe et al. (2023a).

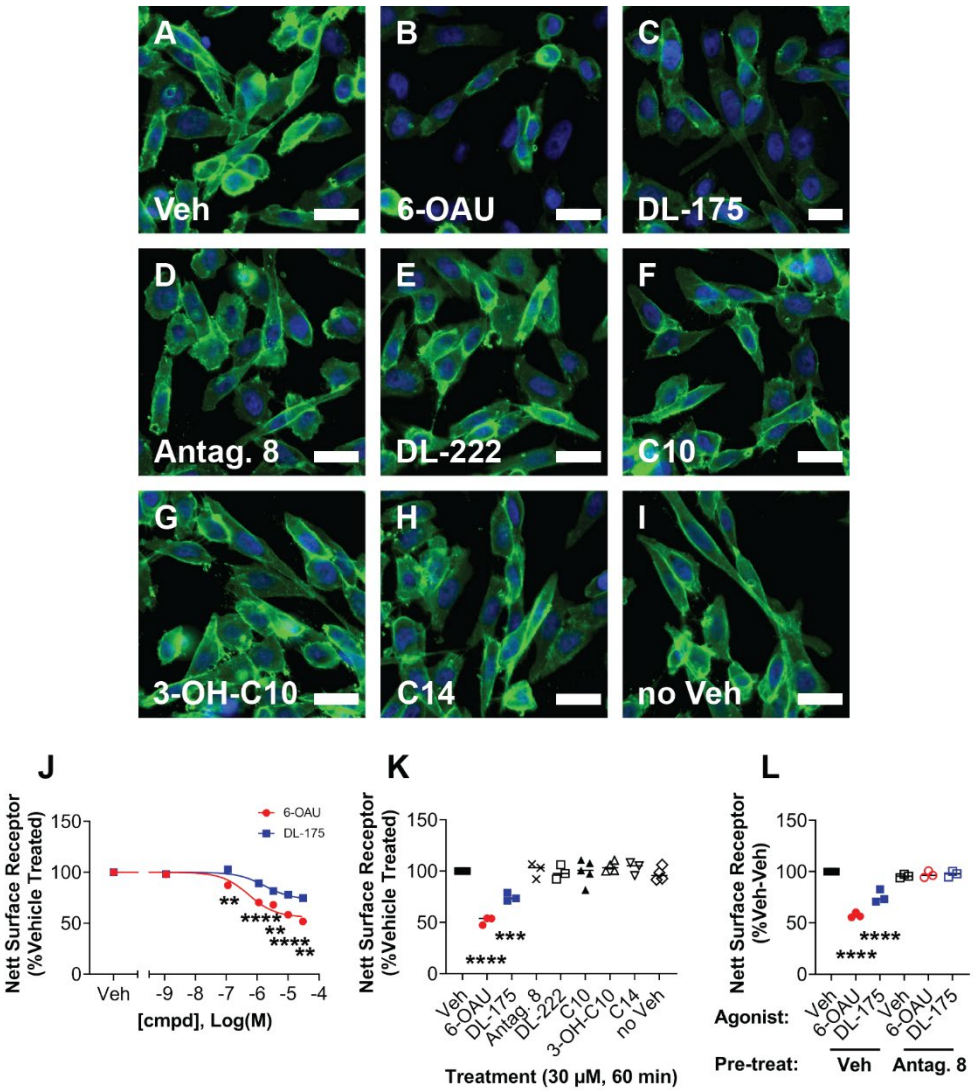

Figure 25: Specificity of the agonist-induced internalisation of GPR84. (A - I) CHO-HA-hGPR84 #7F12 high expressing cells were stimulated with various compounds (30 µM) for 60 min before fixation without permeabilising the cell membranes, then stained for the HA-tag (*green*) and nuclei (*blue*). Images acquired using a 20X 0.75 NA objective lens, scale bar = 25 µm. (J)

Quantification of the green channel fluorescence intensity in segmented cell masks show concentration-dependent reductions in nett surface receptor following treatment with 6-OAU and DL-175. Unpaired t-test conducted between 6-OAU and DL-175. (K) Reductions in nett surface receptor following 60 min treatment with 30 µM compound, (L) or with 2 h pre-treatment using 30 µM Antagonist 8 or Veh. One-way ANOVA conducted with multiple comparisons (Dunnett) against Veh (K) or Veh-Veh (L). Points represent mean ± SEM, n = 3, each experiment performed in triplicate. P-values: ≤0.0001 (****), ≤0.001 (***), ≤0.01 (**), ≤0.05 (*), >0.05, *ns*. Adapted from Luscombe et al. (2023a).

3.3. Discussion

3.3.1. Label-Free Impedance Sensing

Endogenous levels of GPCR expression levels can still cause cellular responses that can be robustly detected and quantified by label-free techniques. Leung et al., (2005) observed that the impedance signal from CHO cells overexpressing dopamine and muscarinic GPCRs were not higher than those from endogenously expressed serotonin, calcitonin, or prostaglandin receptors. Here, I have extended this observation by showing that the signal magnitude is not different between high and low expression levels of the same receptor in recombinant cell lines. When considering the phenotype of the CEI signals over time, however, there were clear differences between CHO cell lines bearing different GPR84 expression levels. The high expressing cell line exhibited a sustained signal, suggesting there was a substantial receptor reserve as cells treated with 6-OAU, DL-175, and 6-OAU with cmpd101 reach and maintain a maximum system efficacy. The maintenance of this signal elevation corresponds to the rank ordered cAMP potency: CHO-HA-hGPR84 #7F12 (high expression) > CHO-hGPR84 (DiscoverX) > CHO-HA-hGPR84 #3E11 (low expression), which supports the observation that G-protein-dependent effects are the primary influencers of the magnitude of the CEI response (Doijen et al., 2017). My hypothesis is that the higher receptor expression system has a sustained signalling via saturation of receptor-effector coupling, and the lower receptor expression alters this stoichiometry and allows for the measurement of higher fidelity CEI responses. My observation that the low expressing cell lines phenocopy BMDMs is consistent with a low receptor reserve and more physiological receptor-effector coupling. One consequence of this prediction would be that the overexpression of effector proteins, such as promiscuous G-proteins or fusion constructs, would negatively impact the fidelity of label-free responses.

My data show that the 6-OAU and DL-175 impedance responses have significant differences in peak and decay time but not in curve shape or direction. In contrast, β-adrenergic receptor ligands can be discretely classified by impedance phenotype at the β_2-adrenergic receptor (Stallaert et al., 2012), as can synthetic and endogenous cannabinoids acting at the CB_2 receptor (Hillger et al., 2017). The huge repertoire of GPCR-mediated impedance responses were reviewed extensively by Doijen et al., (2019) revealing a large diversity in the kinetics, direction, and magnitude of CEI responses which were sometimes bi- or multi-phasic. In light of the large diversity of possible impedance responses, our data suggests that 6-OAU and DL-175 affect similar downstream targets, but do so with different kinetics. A similar observation was made by Peters et al., (2022) who have shown, using an analogous optical label-free technology, that capric acid elicits a more sustained response than 3-hydroxy capric acid at GPR84. Experiments to determine the impedance responses of a broader range of ligands acting at GPR84 could help to correlate phases of the CEI response with a defined molecular activity.

It is an emerging consensus that G_i-coupled GPCRs cause positive impedance signals (Doijen et al., 2019). GPCR-β-arrestin signalling, on the other hand, appears to be more likely to alter the kinetics of the impedance response or cause more subtle changes in the trace without altering the primary peak responses (Doijen et al., 2017, Kammermann et al., 2011, Watts et al., 2012). My results support these findings by showing that the distinct phenotype of the G-protein biased agonist DL-175 was governed largely by kinetics, and the EC_{50}'s derived from impedance maxima correlated well with the cAMP EC_{50}'s. The prolonged impedance phenotype of DL-175 was observed at concentrations ranging from 10 nM up to 10 μM, indicative of some signalling bias at concentrations below 1 μM. At the concentration of 1 μM neither 6-OAU or DL-175 recruit β-arrestin-2 in the recombinant assay, an assay utilising a cell line which overexpresses both tagged-receptor and tagged-β-arrestin-2 and, if anything, would be expected to overestimate agonist potency. Yet, we have observed phenotypic impedance differences at 1 μM as well as at low nanomolar concentrations. We hypothesise that this could be due to differences in recruitment of the GRK2/3 kinases, which are negative regulators of G_i-pathway signalling and known to phosphorylate GPR84

(Marsango et al., 2022). The phosphorylation of GPR84 and inhibition of G_i-pathway signalling could be responsible for the kinetic differences in the impedance trace without necessarily leading to the recruitment of β-arrestin which only occurs at higher concentrations.

3.3.2. ERK & Akt Phosphorylation

Our results have revealed a bias of DL-175, which promotes equivalent ERK activation as 6-OAU but has a diminished ability to activate Akt. This outcome was dependent on both time and receptor expression, as it was only observed in the low expressing cell line and only at the 5 minute time point. Additionally, this bias was evident with agonists at 1 μM, below the concentration of detectable β-arrestin signalling with these agonists (Lucy et al., 2019). It has recently been shown that GPR84 signalling via $G\alpha_{15}$ results in ERK activation and ROS production in macrophages while Akt is driven by $G\alpha_i$ (Peters et al., 2022). This delineation of ERK versus Akt signalling provides a conceivable rationale that this bias exists at the level of G-protein coupling. While our studies have utilised a low expressing CHO-HA-hGPR84 cell line, we expect this effect to translate to other primary cells. At the same concentration of 1 μM, 6-OAU has been shown to activate Akt in BMDMs in a time course that mirrors our low expressing cell line; a peak at 5-10 minutes which has decayed by 30 minutes (Recio et al., 2018). ERK phosphorylation in BMDMs has a similar peak at 10 minutes, but appears to display a second peak at 60 minutes which we did not see in CHO cells (Recio et al., 2018). Other agonists have been used to show that GPR84 agonists activate ERK and Akt in human macrophages and THP-1-M1 macrophages (Gaidarov et al., 2018, Peters et al., 2022).

3.3.3. Receptor Internalisation

The pathways resulting in receptor internalisation dictate changes in surface expression over time, which result in an altered cell responsiveness to extracellular ligands. Due to the major influence assay time points have on signalling bias (Klein Herenbrink et al., 2016, Oyagawa et al., 2018), and given the known challenges when comparing agonist-induced internalisation at any single time point (Zhu et al., 2019), we tested for receptor internalisation at multiple time points and agonist concentrations within 60 minutes. To date, observations of GPR84 internalisation following treatment with 6-OAU, ZQ-16, and embelin have been primarily qualitative (Gaidarov et al., 2018,

Marsango et al., 2022, Suzuki et al., 2013, Zhang et al., 2016). By quantifying reductions in surface GPR84 we have demonstrated that 6-OAU promotes greater internalisation than DL-175. Treatment with 1 μM agonist shows that 6-OAU internalisation rapidly diverges from DL-175 within 10 minutes. The MCFAs capric acid and 3-hydroxy capric acid, which were tested at 100× their cAMP EC_{50}'s, did not result in significant internalisation, which is in line with previous reports that surface receptor expression was increased in CHO cells and unchanged in HEK cells following treatment with 100 μM capric acid and 3-hydroxy capric acid (Peters et al., 2020).

GPCR internalisation is canonically linked to the phosphorylation of the C-terminal tail and/or intracellular loops and the subsequent recruitment of β-arrestin. These changes to the intracellular core of the receptor act in concert to both arrest G-protein signalling and initiate new molecular pathways (Choi et al., 2018). In line with this sequence of events, it has been shown that activation with DL-175 fails to phosphorylate two key threonine resides in the third intracellular loop of GPR84 that are required for agonist-induced internalisation (Marsango et al., 2022). Furthermore, we and others have reported the low potency of 6-OAU and lack of efficacy of DL-175 in β-arrestin recruitment assays (Fredriksson et al., 2022, Marsango et al., 2022, Mårtensson et al., 2021). By quantifying cell surface receptor over time, we show that GPR84 undergoes robust agonist-induced internalisation at concentrations of agonist (e.g. 1 μM 6-OAU) that do not show detectable β-arrestin recruitment, suggesting that GPR84 might be internalised in a β-arrestin-independent manner. This was also suggested by a previous observation that inhibition of the β-arrestin/AP-2 endocytic complex has no effect on the surface expression of GPR84 in CHO cells (Peters et al., 2020). Other G_i-coupled immune cell GPCRs are known to internalise in a β-arrestin-independent manner, such as FPR2 (Sundqvist et al., 2020). However, many questions remain unanswered regarding the mechanism of GPR84 internalisation and its effect on other signalling pathways.

3.4. Conclusions

An important hurdle towards unlocking the potential therapeutic value of GPR84 is a deeper understanding of which intracellular signalling pathways it engages and the time course that it follows. Therefore, to investigate Thesis Aim 2, I have developed heterologous cell lines with low

GPR84 expression levels that phenocopy the response of primary cells in a label-free CEI sensing system that measures cell morphology and adhesion and then applied these tools to study the signalling differences of two agonists previously described to differentially influence chemotaxis. DL-175 has been shown to lack the GRK2/3-mediated phosphorylation of GPR84 (Marsango et al., 2022), lack recruitment of the canonical GPCR desensitising protein β-arrestin (Lucy et al., 2019), and is now identified as having an impaired ability to internalise GPR84 as well as a suppressed downstream activation of Akt. These signalling differences were found to be transient, as DL-175 exhibited delays in both its impedance response and activation of Akt compared to 6-OAU. Importantly, these subtle differences in signalling kinetics could be masked by both long time points and high receptor expression. These findings support the use of label-free assays in differentiating the effects of agonists on both recombinant and primary cells, and underscores the importance of both receptor number and time points when evaluating the signalling of newly developed agonists.

Chapter Four.

THE EFFECTS OF BIAS ON RECEPTOR REGULATION

4.1. Introduction

4.1.1. Development and Characterisation of a Screening Library

During the extensive SAR campaign to develop AR-198 and AR-211 as described by Wang et al. (2023a) we also discovered compounds that were able to recruit β-arrestin-2. These included agonists possessing picomolar cAMP potency values such as PW-290 and PW-303. Due to the more extensive pharmacological characterisation of 6-OAU and DL-175, the initial pair of balanced and biased agonists, our collaborators in the department of chemistry also synthesised head/tail swaps of 6-OAU and DL-175, resulting in PW-209 with the uracil head group of 6-OAU and the ether-linked chloro-napthyl tail group of DL-175, as well as PW-210 with the pyridine-*N*-oxide head of DL-175 and alkyl tail of 6-OAU. Numerous other projects resulted in ligands with various levels of activity at GPR84 and unique structures. For example, PW-412 was synthesised as a photoaffinity probe and contained a photoactivatable diazirine functional group as well as an acetylene click handle for further chemical ligation. PW-462 was synthesised with an adamantane group in the alkyl tail to test the tolerance of the binding site to large non-conjugated cyclic structures. Finally, MY-128 was the result of testing the binding site for tolerance to a tricyclic fluorine group that could then be progressed to fluorescent groups such as BODIPY or anthracene.

These compounds featured alongside others that were immediately available to me as a researcher in a database of structures and activity. Not all compounds were developed in-house, as standard agonists such as 6-OAU and MCFAs were in the database. To pursue further biology my aim was to test a diverse set of compounds side-by-side in further functional assays in order to better characterise the relationship between structure and activity while also sampling a wider range of the chemical space than simply choosing biased and non-biased agonists. With 268 compounds having

been tested for activity at hGPR84 being too burdensome, I therefore had to select a subset of these compounds to progress into desensitisation, internalisation, and other assays.

4.1.2. Receptor Desensitisation

GPCR signalling can be activated by agonists but needs to be turned off in order to preserve any meaningful signalling texture throughout the body. Many of the functions of GPCRs rely on receptor desensitisation, recycling, and degradation during their natural receptor life-cycle in their role in physiology. Chemotaxis, for example, relies on an extremely finely tuned response to chemoattractant gradients at the leading edge of the cell. Here, receptors are activated and directional movement is maintained by the tightly regulated and spatially controlled desensitisation of receptors (DeFea, 2007). Furthermore, GRK2 desensitisation plays a crucial role in neutrophil swarming behaviour by desensitising chemoattractant receptors, arresting migration to allow for the optimal phagocytosis and containment of bacteria while also preventing an uncontrolled aggregation of neutrophils at a site of infection (Kienle et al., 2021). Olfaction and gustation are two other processes driven by a large family of GPCRs, and the adaptation and sensitisation to odours is regulated by downstream kinases including GRKs and arrestin-mediated endocytosis (Mashukova et al., 2006). The vision system is driven by light-activated rhodopsin receptors which are in an extremely high density on photoreceptor cells, providing sensitivity to even single photons (Shi et al., 2005, Gurevich and Gurevich, 2019). This is a high gain system where activated rhodopsin recruits GRKs which then trans-phosphorylate nearby inactive receptors, resulting in a photobleaching effect. Dark adaptation is then able to fully restore visual sensitivity when receptors are dephosphorylated (Shi et al., 2005). The importance of desensitisation in the visual system is underscored by the existence of two arrestin subtypes, arrestin-1 and arrestin-4 which are visually specialised, leaving arrestin-2 (β-arrestin-1) and arrestin-3 (β-arrestin-2) for all other GPCRs (Gurevich and Gurevich, 2019).

The phosphorylation of the intracellular face of a receptor alters its relative affinity for other proteins, resulting in desensitisation of G-protein signalling and the promotion of arrestin signalling (Duan et al., 2023). The binding of arrestins further acts to arrest G-protein signalling (Gurevich and Gurevich, 2019). Recent structural studies have revealed that GRK2 not only binds to the same

region on the GPCR as the G-protein but can also simultaneously bind to the G-protein itself (Duan et al., 2023, Tesmer et al., 2005). The importance of desensitisation in drug design in particular can be highlighted by the use of $S1P_1$-desensitising agonists for the treatment of multiple sclerosis, while agonists causing persistent $S1P_1$ signalling are sought after instead for their endothelial protective properties (Grailhe et al., 2020).

Agonist-induced phosphorylation of GPR84 has been shown to occur at two key threonine residues in ICL3, T263 and T264, which are also responsible in large part for the affinity and subsequent interaction with β-arrestin-1 and β-arrestin-2 (Marsango et al., 2022). Functional studies using the GRK2/3 inhibitor also support the physiological involvement of these kinases in GPR84 desensitisation. The label-free impedance response of BMDMs stimulated with DL-175 is more prolonged than the response to 6-OAU, and interestingly, pre-treatment with cmpd101 results in a 6-OAU response that mirrors DL-175 alone (Lucy et al., 2019). In neutrophils, the ROS response of ZQ-16 was also prolonged by treatment with cmpd101, whereas the response of DL-175 was not affected (Fredriksson et al., 2022). Taken together these studies suggest GRK2/3 is likely the primary mechanism of desensitisation of GPR84 in macrophages and neutrophils.

In order to measure receptor desensitisation I have opted to use the CEI sensing xCELLigence system which has previously been shown to detect specific and measurable changes in GPR84 activation in the transgenic CHO-HA-hGPR84 #3E11 cell line in a way that phenocopies BMDMs (Luscombe et al., 2023a). The advantages of this format is that the cells are robust and grown in full growth media, the assay is sensitive and high-throughput, and the readout is label-free, temporally resolved, and therefore captures a variety of downstream signals. The disadvantages are that the precise signalling pathway is unknown, and the high cost of gold electrode coated E-plates. With these in consideration, I aimed to test the screening set for the potency with which they could inhibit stimulation with ZQ-16 at short time-frames.

4.1.3. Receptor Internalisation

Receptor phosphorylation alters its affinity for downstream effectors, including G-proteins and arrestins, and while arrestins do indeed ‘arrest’ further G-protein signalling, they are now

appreciated more as scaffolding proteins from which further signalling is initiated (Gurevich and Gurevich, 2019). The phosphorylation patterns can differ too, with multiple GRK subtypes, protein kinase A, and protein kinase C all known to contribute to homo- and heterologous desensitisation (Rajagopal and Shenoy, 2018). Distinct phosphorylation patterns can also differentially influence the conformation of arrestins and their downstream responses (Nobles et al., 2011). Desensitisation occurs on the minute timescale, and subsequent downregulation of receptor then causes long-term desensitisation, occurring on the hour timescale (Rajagopal and Shenoy, 2018). These are the mechanisms underlying tachyphylaxis, the reduction of effect observed with long or repeated stimulation of a pharmacological agent and clinically important phenomenon. Internalised receptors can then be trafficked back to the surface to re-sensitise a cell or trafficked to endo-lysosomes and degraded to result in even longer desensitisation (Rajagopal and Shenoy, 2018).

In light of my previous discussion on how agonist-induced desensitisation and internalisation serve important biological functions by inhibiting receptor signalling and preventing over-stimulation, and the findings that GPR84 desensitisation on the minute timescale correlated well with cAMP potency, I will now present some rationale for why GPR84 internalisation may not necessarily follow this correlation. GPCRs are pleiotropic signalling proteins that adopt conformational states in ways that promote some effects and not others (Kenakin, 2003). Evidence was given herein for the existence of highly biased GPR84 agonists that cause selective signalling via one of two transducer proteins, and also that the receptor appears to exhibit some level of system bias towards the G-protein pathway. That receptor occupancy results in receptor activation, G-protein signalling, desensitisation, phosphorylation, and internalisation is, however, not necessarily the case. The concept of 'collateral efficacy' points to a more discontinuous mechanism (Kenakin, 2005). In contrast to 'linear efficacy' agonists can induce some of these receptor functions without affecting others beyond the pathway biases of G-proteins and β-arrestins (Kenakin, 2005). The two endogenous chemokines CCL19 and CCL21 cause G-protein activation and calcium mobilisation at CCR7 with equal potency, but only CCL19 causes desensitisation by phosphorylation and recruitment of β-arrestin, and furthermore shows a higher degree of β-arrestin-dependent ERK1/2

phosphorylation (Kohout et al., 2004). There are also monoclonal antibodies that can bind to the HIV co-receptor CCR5 and cause downregulation but not activation, resulting in a long-lasting downregulation of receptor as a protective mechanism (Kenakin, 2003, Pastori et al., 2006). Likewise, the amino truncated peptide antagonist RANTES(9-68) can prevent HIV infection by downregulating CCR5, but does not activate G_i-proteins or elicit a Ca^{2+} response (Amara et al., 1997).

As the biased GPR84 agonist DL-175 is known to lack receptor phosphorylation, recruitment of β-arrestin-2, and internalisation, I sought to test for changes in cell surface expression following treatment with the wider screening set of agonists. To achieve this, I will use time course data of receptor internalisation as previous results showed a rapid but time-dependent difference between internalisation of 6-OAU and DL-175.

4.1.4. Chapter Rationale and Experimental Aim

The aim of this chapter is to assess the influence of biased signalling on the regulation of GPR84 by developing a chemically and biologically diverse set of agonists to study receptor desensitisation and internalisation and then testing these compounds for effects on macrophages.

4.2. Results

4.2.1. Development and Characterisation of a Screening Library

The initial in-house library contained 268 compounds, featuring synthetic agonists, MCFAs, lipid-mimetics, antagonists / NAMs, and DIM derivatives (Figure 26). First, I flattened the structures into 2D representations in order to apply binary descriptors to each compound, then merged duplicate structures from batches and scale-ups as well as enantiomers. I then set an activity threshold in order to filter out any low potency compounds with a cAMP $EC_{50} > 1$ μM. This step therefore also filtered out antagonists, NAMs, DIM, and many low potency MCFAs. Then, in order to select a chemically diverse set of compounds in an unbiased manner I utilised the 'Select Diverse Compounds' function

in DataWarrior using the FragFP structure descriptor, a fingerprint of the agonist based on substructure fragments (Sander et al., 2015). Here, the first compound is the most different to the other 90 in the set. The second is the most different from the first, and the third is the most different from compounds 1 and 2. Interestingly, DL-175 was the first most diverse compound, supporting its unique structure from the initial hit being dissimilar to 6-OAU. It is worth noting that I further filtered the diversity selection based on availability and purity. The third most diverse compound was then found to be 6-OAU, further supporting this pair of agonists as chemically dissimilar. In total, 15 compounds were chosen in the diversity set. To compare and contrast this chemical diversity with known biological activity, I also chose 8 compounds representing different levels of G-protein bias for the activity set. DL-175 and 6-OAU were in both sets. Together, these sets constituted the screening set for use in further biological assays (Figure 27).

The 90 sub-micromolar compounds can be divided into the broad ligand classes of naturally occurring MCFAs, lipid-mimetics which have a polar head group and alkyl tail, and synthetic agonists which have other modifications and no alkyl tail. The molecular weight of synthetic agonists were found to be higher than the lipid mimetics and MCFAs, while the cLogP was higher in lipid mimetics than synthetic agonists (Figure 28 A, B). I then analysed the chemical properties of the screening set and compared it to the original library of 90 sub-micromolar compounds to test whether they were skewed in any of their 1D chemical properties. In fact, both sets were found to bear similar average molecular weights and cLogP values as the full 90 compound library. The diversity set had a larger range of hydrogen bond donors (HBD) and cLogP values than the activity set, but a smaller range of molecular weight (Figure 28 C - F).

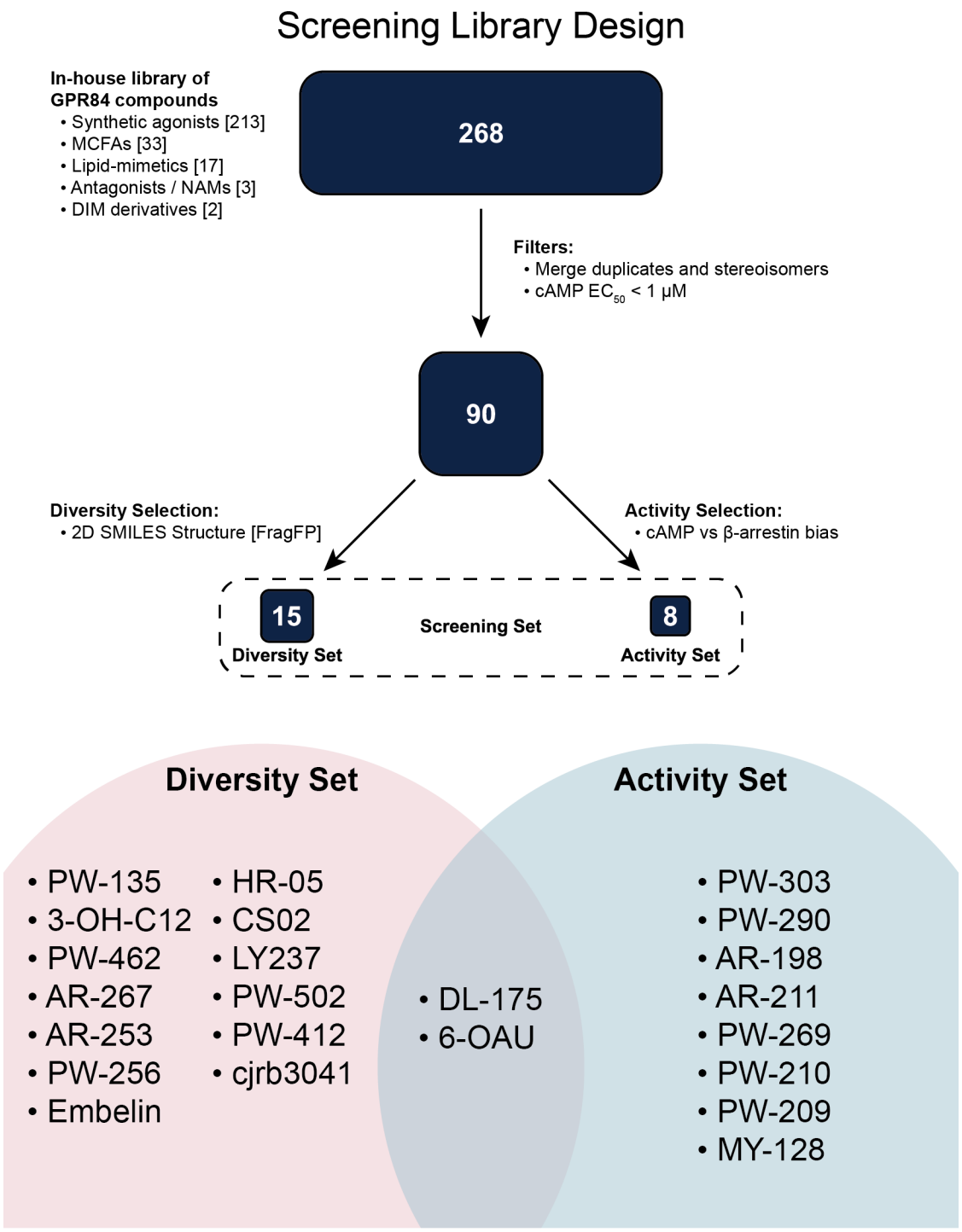

Figure 26: Library design of chemically and biologically diverse agonists. An in-house library of GPR84 ligands with cAMP activity data contained 268 compounds from various ligand classes. Activity and substructure filters resulted in a chemically diverse set of ligands referred to as the diversity set, while compounds possessing varying levels of cAMP vs β-arrestin bias were selected and referred to as the activity set. These two sets together form the screening set for use in further biological assays. Chemical database and filtering steps were managed using OSIRIS DataWarrior v05.05.00 (Sander et al., 2015).

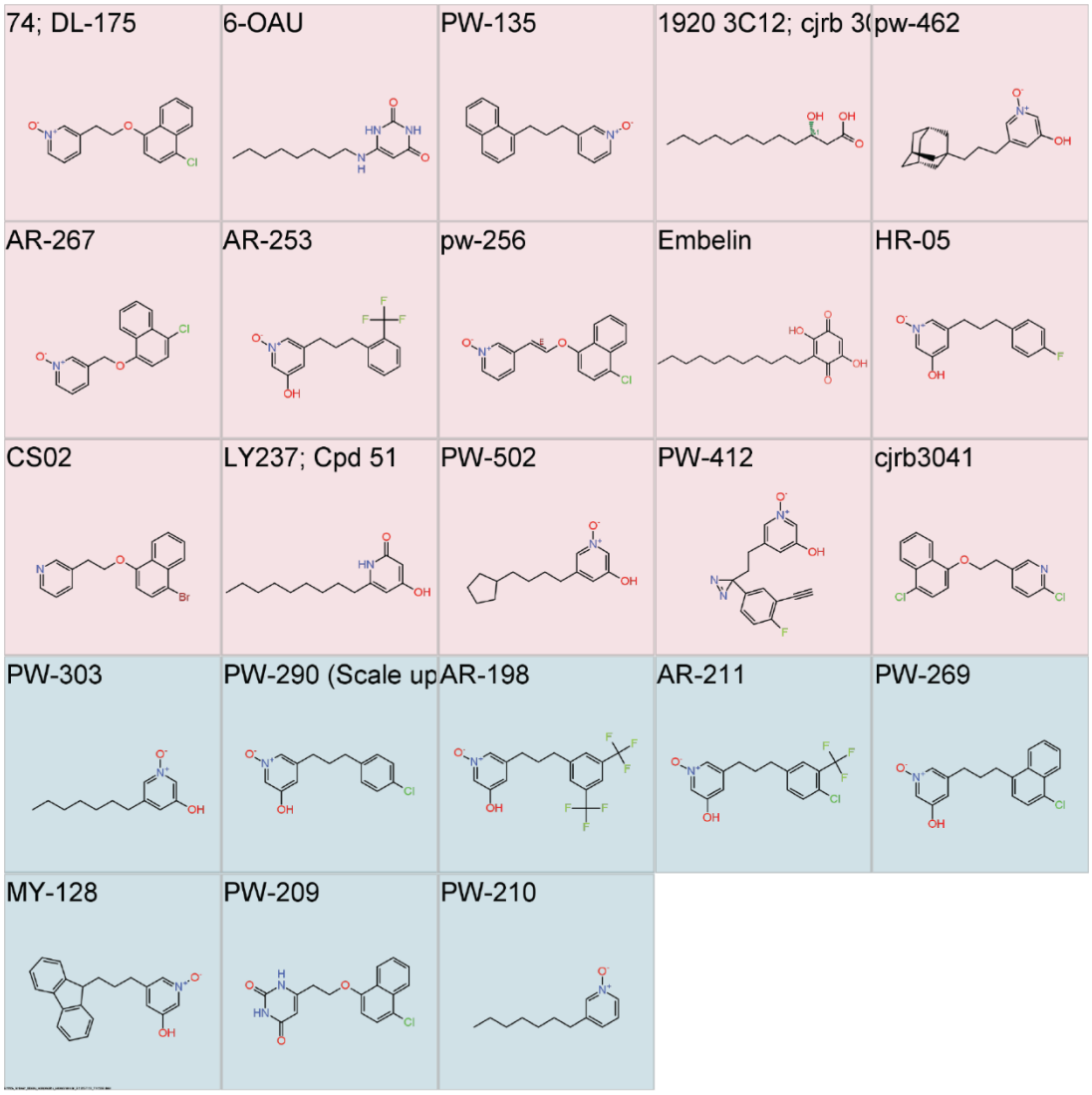

Figure 27: Chemical structures of the screening set. Diversity picks (*pink*) and activity picks (*blue*) made during the design of the screening set. Diversity picks are ordered left-to-right based on level of chemical diversity against the rest of the 90 compounds in the sub-micromolar agonist library.

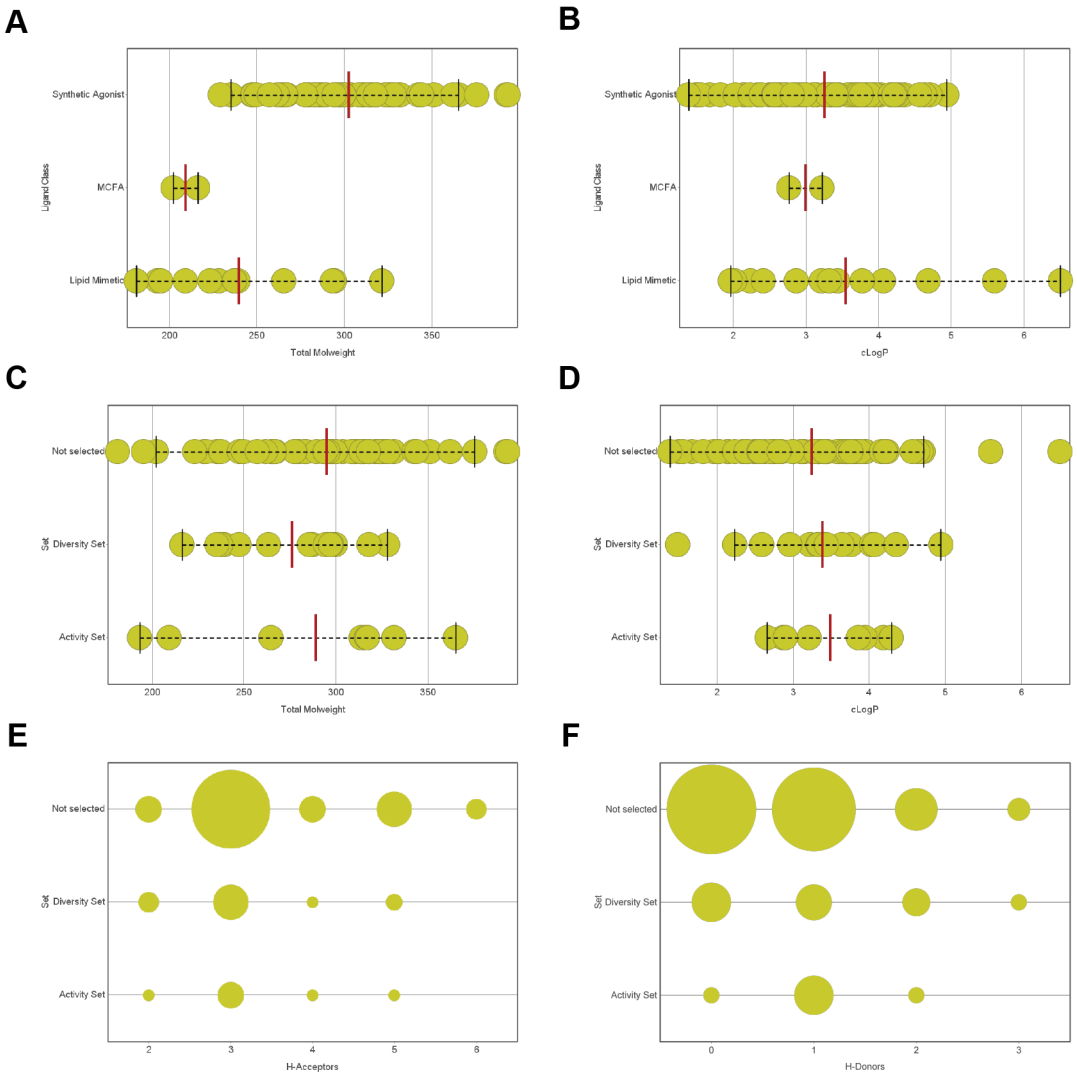

Figure 28: Library compound distribution according to four property ranges. (A) Molecular weight of the 90 sub-micromolar compounds by ligand class. (B) cLogP of the 90 sub-micromolar compounds by ligand class. The distribution of molecular weight (C), cLogP (D), and number of hydrogen bond acceptors (E) and donors (F) between the selected compounds in the diversity set, activity set, and compounds not selected for further investigation. Dots represent individual compounds with mean ± range in whiskers (A - D), and bubble plot sizes represent number of compounds (E, F).

Table XIII: Potencies of the screening set in cAMP and β-arrestin assays.

		cAMP		β-arrestin		β-arrestin / cAMP EC_{50}
Cmpd	Cmpd No	pEC_{50}±SEM, *n*	EC_{50} (M)	pEC_{50}±SEM, *n*	EC_{50} (M)	
PW-210	**1**	7.33±0.22, *4*	4.64E-08	4.03±0.15, *5*	9.15E-05	1,973
Embelin	**2**	7.52±0.32, *3*	2.99E-08	4.2±0.3, *4*	6.28E-05	2,102
PW-303	**3**	11.8±0.39, *6*	1.58E-12	8.26±0.22, *7*	5.49E-09	3,463
6-OAU	**4**	8.57±0.18, *12*	2.65E-09	5.02±0.05, *8*	9.36E-06	3,532
PW-290	**5**	10.85±0.11, *4*	1.40E-11	7.18±0.25, *5*	6.58E-08	4,714
PW-502	**6**	11.91±0.23, *5*	1.21E-12	7.56±0.56, *4*	2.72E-08	22,503
LY237	**7**	11.24±0.03, *3*	5.71E-12	6.78±0.44, *3*	1.63E-07	28,466
PW-462	**8**	9.93±0.12, *3*	1.16E-10	5.46±0.17, *6*	3.44E-06	29,557
HR-05	**9**	11.35±0.18, *3*	4.47E-12	6.32±0.29, *5*	4.78E-07	107,053
AR-253	**10**	9.47±0.49, *5*	3.34E-10	4.25±0.23, *2*	5.51E-05	165,120
PW-412	**11**	10.23±0.32, *2*	5.87E-11	4.76±0.7, *2*	1.74E-05	295,461
3-OH-C12	**12**	6.26±0.19, *4*	5.49E-07	n.d., *5*	> 8.00E-5	> 145
AR-267	**13**	6.3±0.07, *3*	4.97E-07	n.d., *2*	> 8.00E-5	> 160
CS02	**14**	6.45±0.19, *2*	3.47E-07	n.d., *2*	> 8.00E-5	> 230
PW-135	**15**	6.58±0.04, *3*	2.57E-07	n.d., *3*	> 8.00E-5	> 310
cjrb3041	**16**	6.92±0.51, *2*	1.18E-07	n.d., *5*	> 8.00E-5	> 678
DL-175	**17**	7.92±0.07, *33*	1.18E-08	n.d., *14*	> 8.00E-5	> 6,802
PW-209	**18**	8.02±0.21, *3*	9.40E-09	n.d., *5*	> 8.00E-5	> 8,506
PW-256	**19**	8.25±0.12, *2*	5.53E-09	n.d., *1*	> 8.00E-5	> 14,474
AR-211	**20**	10.8±0.13, *7*	1.57E-11	n.d., *3*	> 8.00E-5	> 5,080,975
MY-128	**21**	10.96±0.49, *2*	1.08E-11	n.d., *1*	> 8.00E-5	> 7,380,571
AR-198	**22**	11.17±0.1, *5*	6.73E-12	n.d., *3*	> 8.00E-5	> 11,887,485
PW-269	**23**	11.38±0.14, *6*	4.09E-12	n.d., *1*	> 8.00E-5	> 19,562,453

The initial filtering step for cAMP activity and the selection of the activity set were carried out based on preliminary cAMP and β-arrestin data. Then, in collaboration with the chemistry team, we completed multiple biological replicates for both assays on the screening set (Table XIII). EC_{50} values for the cAMP assay ranged from 549 nM to 1.21 pM. EC_{50} values for the β-arrestin-2 recruitment assay ranged from inactive to between 91.5 μM (a modelled EC_{50}) and 5.49 nM. I then calculated the G-protein bias by dividing the β-arrestin EC_{50} by the cAMP EC_{50}, yielding a number indicative of the level of G-protein bias. The compounds were rank ordered based on their level of bias and numbered 1 through to 23. This rank ordering is to give a snapshot of the bias level but is by no means a perfect descriptor, as one consequence of this calculation is the bias is influenced heavily by cAMP potency. PW-210 is reported as the most balanced agonist, which is true although this is mostly driven by a lower cAMP potency balancing the low β-arrestin potency. Likewise, bias levels for compounds with no detectable recruitment at 80 μM were summarised as 'greater-than' a certain value, leaving low potency compounds like 3-OH-C12 in the 'biased' category and ranked compound number 12 despite only having a bias level of "> 145", leaving open the possibility that it is in fact the most balanced agonist in the set. However, one of the primary goals of this ranking for follow-up assays is to determine the expected level of bias at screening concentrations of 10 μM (10 × EC_{50} cutoff). At 10 μM compounds 1 - 9 would be expected near-maximum recruitment of β-arrestin, whereas the compounds numbered 10 - 23 would be expected low or negligible recruitment of β-arrestin.

In order to view structural similarities and differences between agonists with activity in the β-arrestin assay, the pEC_{50} values of compounds in each assay were plotted by ligand class. The lipid-mimetics and synthetic agonists had similar ranges of cAMP activities (Figure 29 A). The lipid-mimetics did not contain compounds inactive in the β-arrestin-2 assay (Figure 29 B). To explore this further I applied substructure filters to the screening set. Firstly, I viewed compounds containing the 3-hydroxypyridine-*N*-oxide substructure and rank ordered these compounds by β-arrestin-2 pEC_{50}, revealing a tendency for the larger molecular weight alkyl tails to have lower β-arrestin-2 recruitment

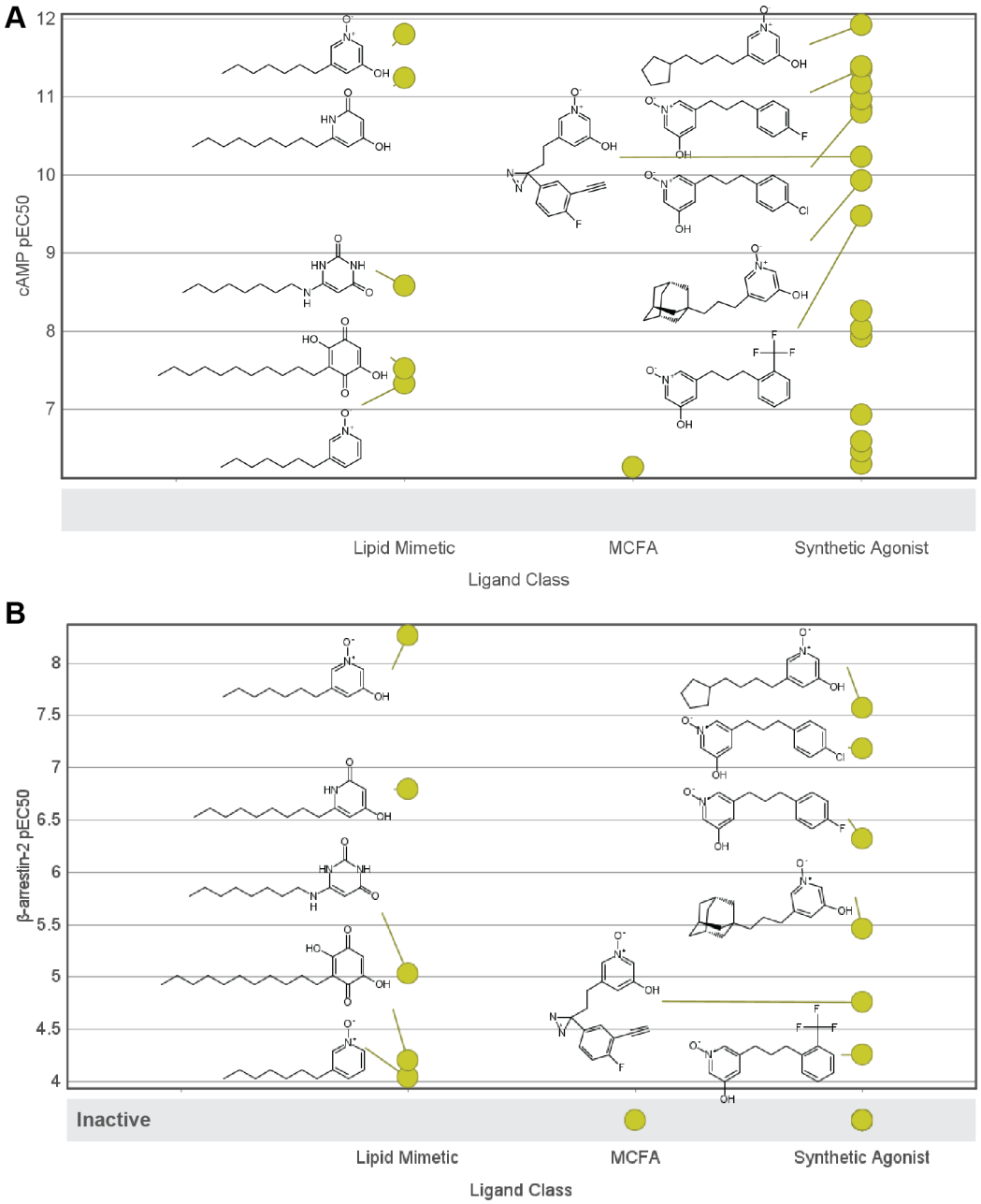

Figure 29: Potencies of compounds in the GPR84 screening set by ligand class. Potency by compound in cAMP (A) and β-arrestin-2 (B) assays sorted by ligand class. Dots represent mean pEC_{50} values of each compound as per Table XIII, with chemical structures shown for compounds with activity in the β-arrestin-2 assay.

and higher bias (Figure 30 A). In particular, the compounds PW-303 with an octane alkyl tail and PW-269 with the well characterised naphthalene group were starkly contrasted in their activities. I then filtered the screening set according to the tail group substructure, searching for compounds containing either napthelene (*red*) or octane groups (*green*) and then plotted these side-by-side in a graph with cAMP pEC_{50} (abscissa) and β-arrestin-2 pEC_{50} (ordinate) (Figure 30 B). All compounds

containing the naphthalene substructure were inactive in the β-arrestin-2 assay and therefore biased, whereas octane containing compounds had ranges of activity in both assays. Taken together these data suggest that the structure of the tail region is highly influential to the recruitment of β-arrestin-2 and therefore the level of bias of a compound.

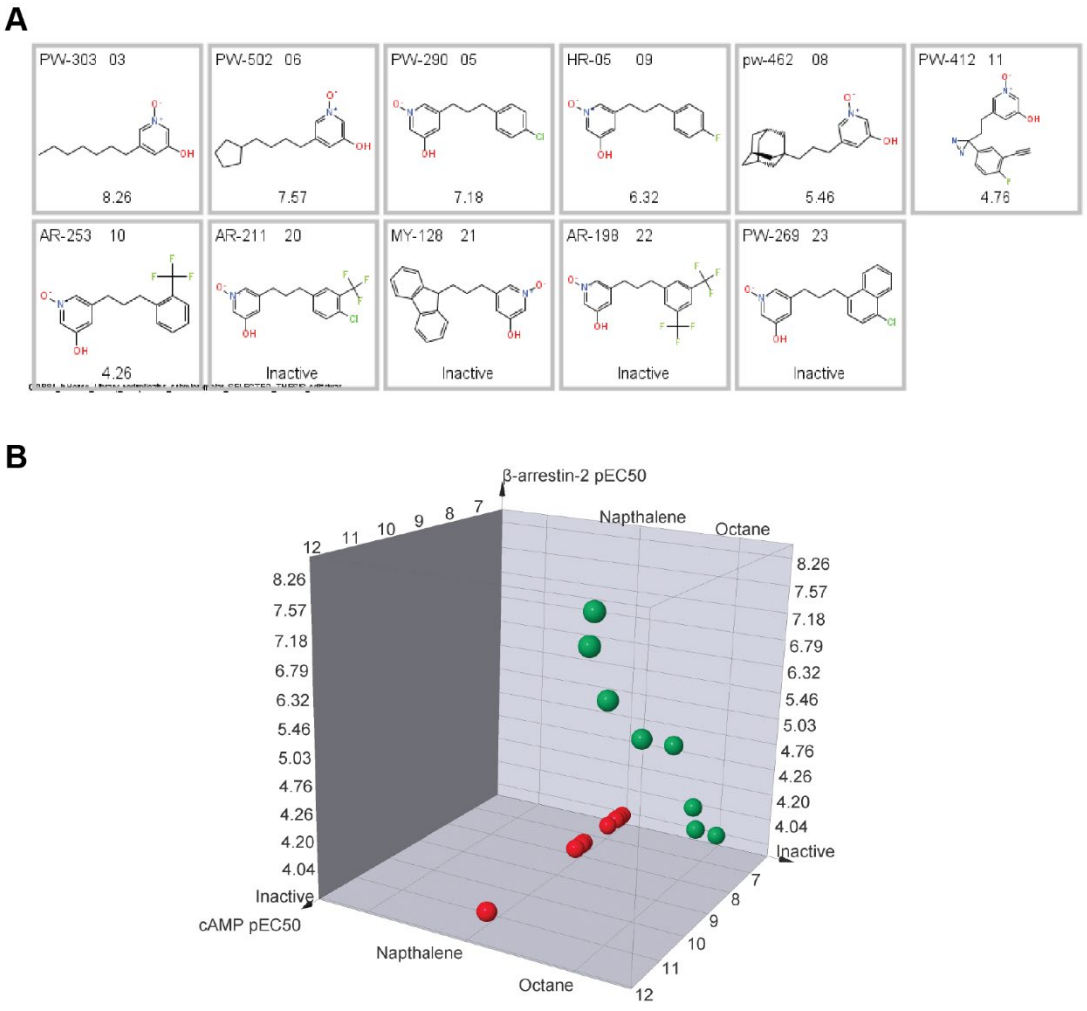

Figure 30: Potencies of compounds in the screening set by substructure. Potencies of compounds in the GPR84 screening set by substructure. (A) Compounds containing the 3-hydroxypyridine-*N*-oxide motif were ordered by β-arrestin-2 pEC_{50}. Compound name, number, and structure are shown and ordered by β-arrestin-2 pEC_{50} below the structure. (B) Compounds meeting a substructure search for naphthalene (*red*) or octane (*green*) were plotted against cAMP pEC_{50} and β-arrestin-2 pEC_{50}. Values and points represent mean pEC_{50} values of each compound as per Table XIII.

4.2.2. Receptor Desensitisation

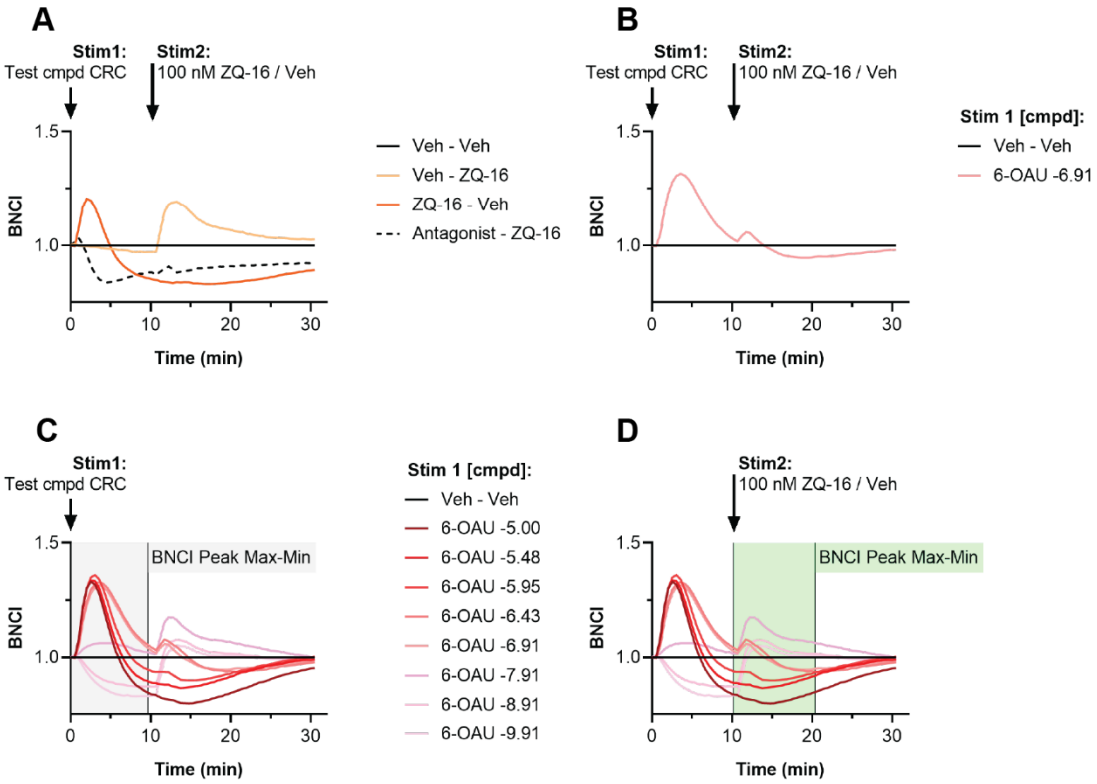

Figure 31: Format of impedance-based desensitisation assays. CHO-HA-hGPR84 #3E11 cells were seeded into 96-well xCELLigence E-plates 22 h prior to two stimulations, the first (stim1) with controls (A) or test agonist (B), followed by a second challenge (stim2) using ZQ-16 (100 nM). The BNCI peak maxima were measured in the shaded regions following the agonist additions in stim1 (C, *grey*) and the desensitised response to ZQ-16 in stim2 (D, *green*). Cell index values were normalised to baseline (Veh-Veh). BNCI, baseline normalised cell index; CRC, concentration-response curve.

The desensitisation assay utilised the xCELLigence RTCA SP system to measure changes in CEI using a two stimulation no-wash paradigm. CHO-HA-hGPR84 #3E11 cells were stimulated with test compound 10 minutes before a second stimulation with ZQ-16, a high potency agonist not contained within the screening set. If no agonist is present in the first stimulation, a maximum effect is observed during the second stimulation (Veh – ZQ-16) (Figure 31 A). If agonist is applied during the first stimulation then a reduced maximum BNCI to ZQ-16 was observed (Figure 31 B). This effect is concentration-dependent, and when a CRC of agonist is applied in the first stimulation then a concentration-dependent decrease in the second stimulation to ZQ-16 is observed. In order to quantify this, I calculated the Max-Min BNCI values in the respective regions of the first stimulation using the screening set (Figure 31 C) and then the Max-Min BNCI values in the second stimulation

(Figure 31 D). I then plotted these as a function of the CRC, yielding a pEC_{50} value for the first stimulation, and pIC_{50} value for the second stimulation.

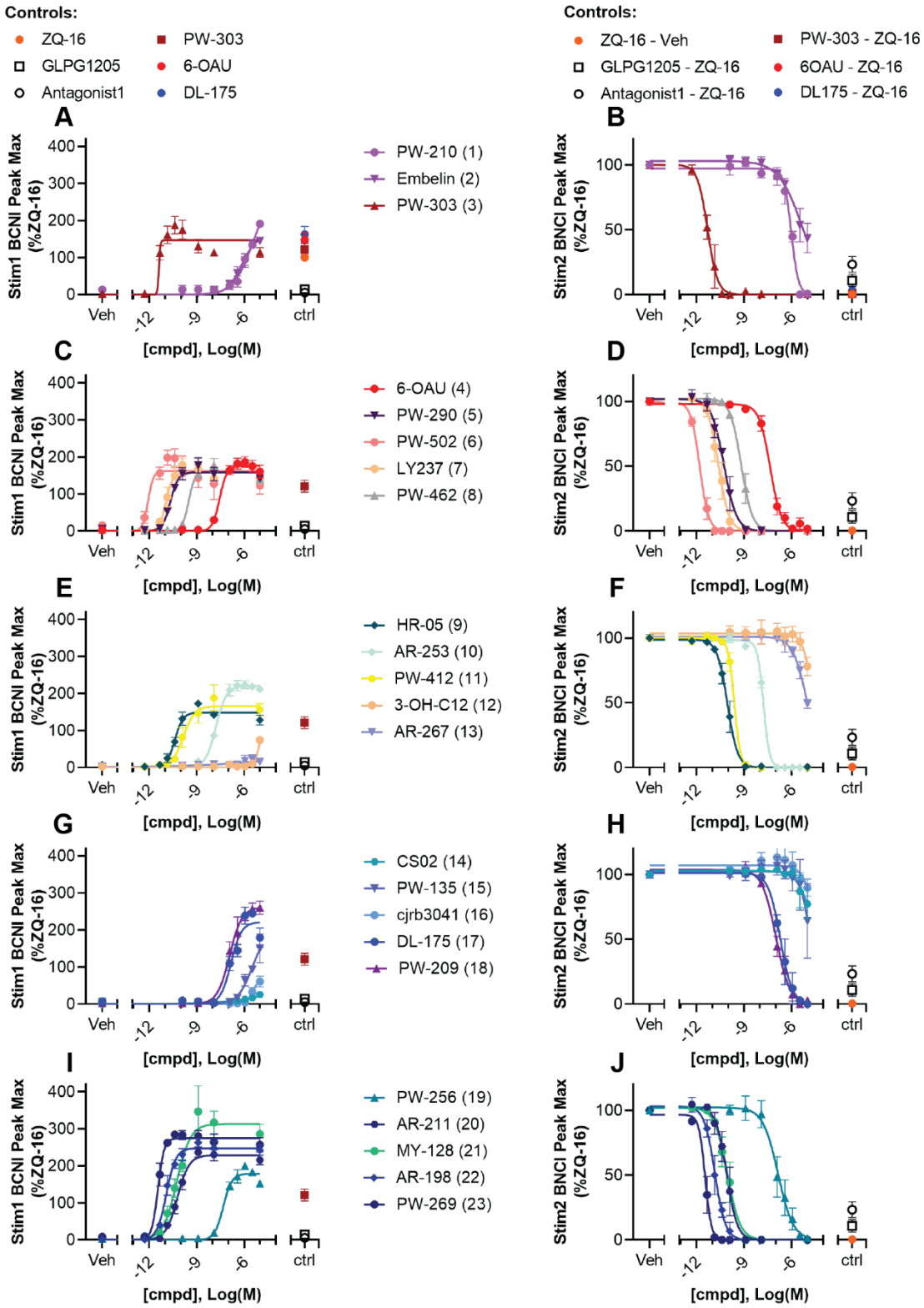

Figure 32: Cell electrical impedance assays for desensitisation. CHO-HA-hGPR84 #3E11 cells were seeded into 96-well xCELLigence E-plates 22 h prior to stimulation, with BNCI peak maxima being recorded for the first stimulation (stim1), and second stimulation (stim2). Agonist CRCs elicit a primary response during

stim1 (A, C, E, G, I) which were normalised to the response of ZQ-16. Cells were then challenged again with a second stimulation using 100 nM ZQ-16 to measure desensitisation (B, D, F, H, J), and normalised to the vehicle pre-treatment condition (Veh – ZQ-16). Points represent mean ± SEM, *n* = 3. BNCI, baseline normalised cell index.

There was a strong correlation between pIC_{50} and pEC_{50} values, showing that a greater potency with which a compound causes an impedance response was correlated to the potency with which it could inhibit the subsequent ZQ-16 induced impedance response (Figure 32). All compounds either caused or had CRCs consistent with full inhibition of the ZQ-16 response, showing a similar efficacy as the antagonist blockade with either GLPG1205 or Antagonist 1 (Figure 32). As the magnitude of positive impedance responses are primarily influenced by G_i activity (Doijen et al., 2019), I then tested the correlation of desensitisation to cAMP. The desensitisation pIC_{50} and cAMP pEC_{50} values were also found to be strongly correlated (Pearson r = 0.987, p < 0.0001) (Figure 33 A). For the compounds that were active in the β-arrestin assay, a less strong correlation was found (Pearson r = 0.879, p = 0.0004) (Figure 33 B). Compounds caused desensitisation with a lower potency than cAMP production and higher potency than β-arrestin recruitment. The rank order of compounds based on the desensitisation pIC_{50} shows that the 'balanced' compounds 1 – 9 do not cluster together, suggesting the bias level is not a major determinant of the desensitisation of the ZQ-16 impedance response (Figure 34).

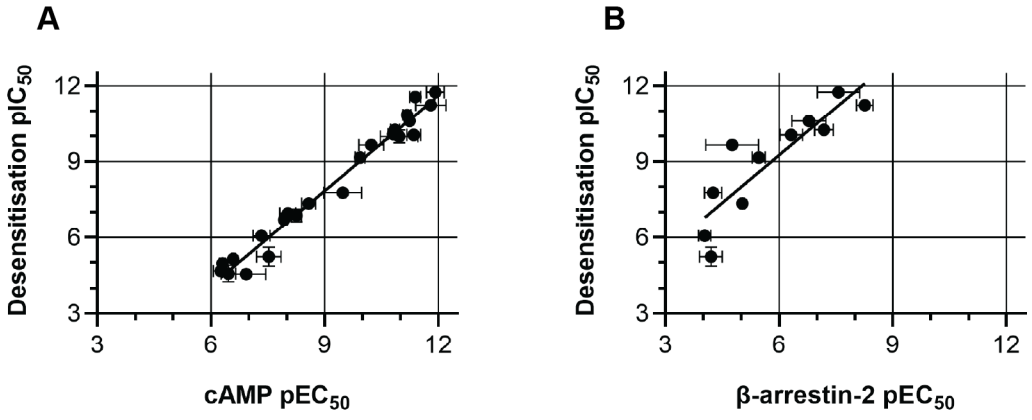

Figure 33: Desensitisation correlates with cAMP and β-arrestin potency. The impedance assay desensitisation pIC_{50} of each compound in the screening set was plotted against cAMP pEC_{50} (A) or against β-arrestin-2 pEC_{50} for β-arrestin active compounds only. Points represent mean ± SEM, *n* = 3 (desensitisation), *n* = 2 – 33 (cAMP), or *n* = 2 – 18 (β-arrestin). Simple linear regression line goodness of fit $r^2 = 0.963$ (A), $r^2 = 0.762$ (B).

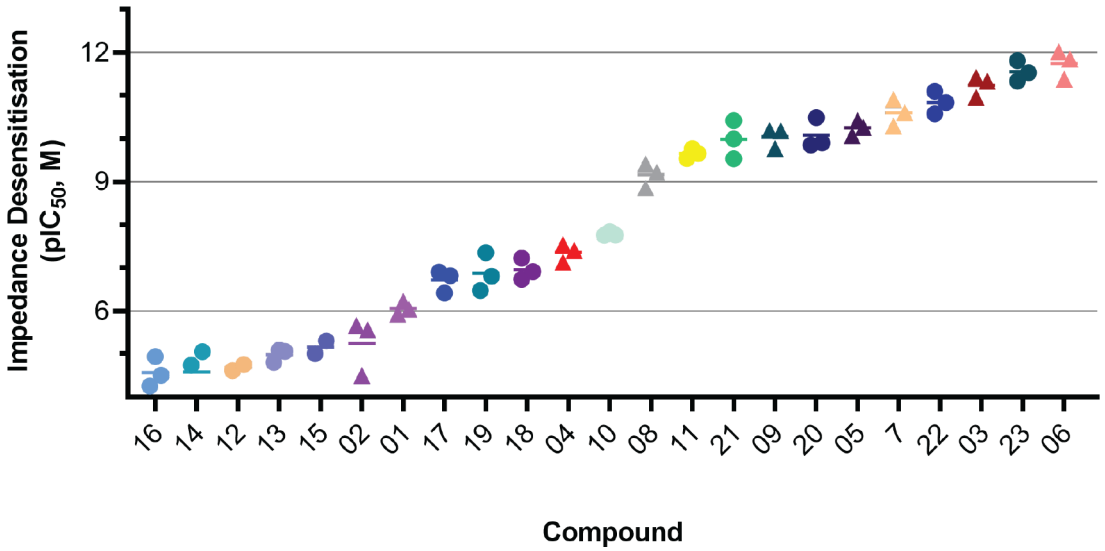

Figure 34: Relationship of bias to the desensitisation potency of the screening set. GPR84 desensitisation following stimulation with the screening set of balanced agonists (▲) and biased agonists (●). CHO-HA-hGPR84 #3E11 cells were stimulated with various concentrations of agonist before a second challenge with 100 nM ZQ-16. The desensitisation of cells to ZQ-16 was rank-ordered by compound pIC_{50}, with more potent desensitisation yielding higher pIC_{50} values. Points represent mean of each experiment, $n = 3$.

4.2.3. Receptor Internalisation

In these experiments on the screening set I measured receptor internalisation by quantifying reductions in nett surface receptor following incubation with agonist for 1, 4, and 16 h as compared to vehicle. The fixation and immunolabelling of cells without permeabilisation of the cell membrane allowed for the quantification of receptor remaining on the surface following agonist stimulation, but still labels newly synthesised and recycled receptors. Following preliminary experiments the high potency balanced agonist PW-303 was chosen as a control for maximum internalisation, where incubation at 30 µM showed a peak at 4 h to achieve a value of 44% of vehicle nett surface receptor (Figure 35 A). Incubation with GPR84 antagonists Antagonist 1 and GLPG1205 did not result in decreased surface receptor (Figure 35 B). Agonists were tested at 10 µM, reasoning that this was 10× the 1 µM cAMP EC_{50} cut-off for all compounds. Consistently across the agonist screening set there was a decrease in surface receptor between the 1 h and 4 h time points, and for most compounds this remained stable until the 16 h time point, suggesting some equilibrium of internalisation and recycling (Figure 35 C - F). Some of the low potency biased agonists did not cause significant levels

of internalisation (Figure 35 E). Some of the biased agonists which caused lower degrees of internalisation such as compounds 19 - 23 peaked at values of nett surface receptor of ~65% by 4 h and then returned to vehicle by 16 h, revealing an altered time course of receptor trafficking (Figure 35 F).

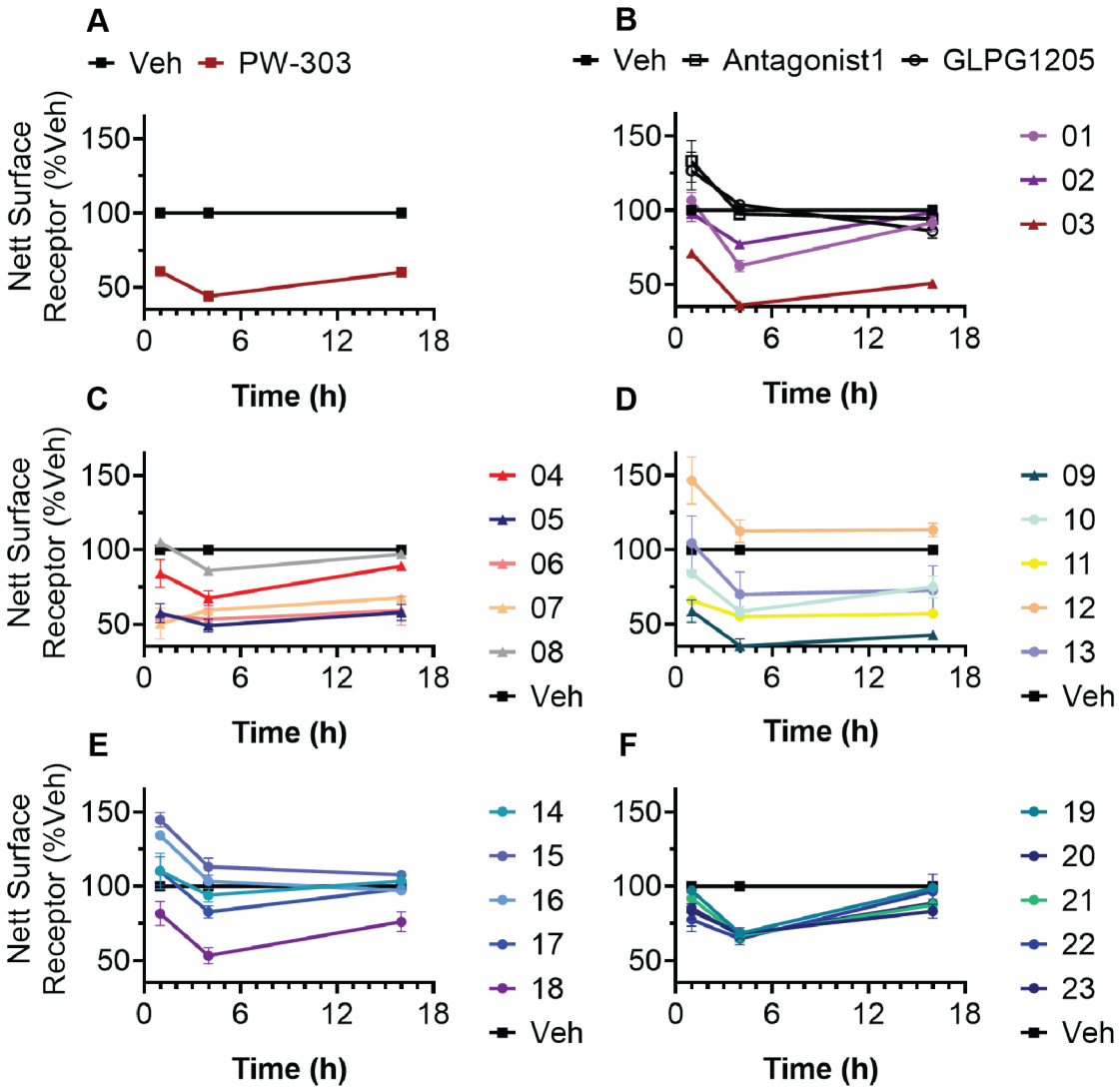

Figure 35: Time course of receptor internalisation induced by the screening set. (A - F) CHO-HA-hGPR84 #7F12 cells were stimulated with balanced agonists (▲) and biased agonists (●) (10 µM), vehicle (DMSO), or controls (30 µM PW-303, 10 µM Antagonist 1, 10 µM GLPG1205) for 1, 4, or 16 h before fixation, staining, and quantification of surface accessible HA-tag. Reductions in nett surface receptor were normalised to vehicle and plotted over time. Points represent mean ± SEM, *n* = 3, experiments performed in triplicate.

To distil the remaining surface receptor down to a single number for each compound while maintaining some representation of the time-course effect, I then did an area under curve (AUC) analysis on each compound from 0 – 16 h. This analysis yielded a number which was still expressed

as percent vehicle effect. Plotting the AUC values against the other signalling assays showed that internalisation of GPR84 by the screening set was less well correlated with potencies derived from the cAMP (Pearson r = -0.743, p < 0.0001), β-arrestin (Pearson r = -0.681, p = 0.0209), and desensitisation assays (Pearson r = -0.721, p = 0.0001) (Figure 36). As only β-arrestin compounds were plotted in the comparison to β-arrestin-2 pEC_{50} it stands that this is a likely an overestimation of the correlation.

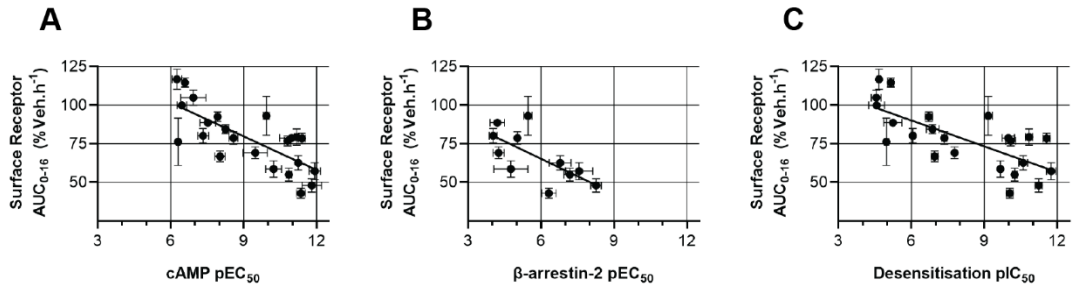

Figure 36: Internalisation poorly correlates with cAMP, β-arrestin, and desensitisation. The nett surface receptor remaining after agonist (10 μM) stimulation of each compound in the screening set was plotted against cAMP pEC_{50} (A), β-arrestin-2 pEC_{50} for β-arrestin active compounds only (B), or desensitisation pIC_{50} (C). Points represent mean ± SEM, *n* = 3 (internalisation), *n* = 2 – 33 (cAMP), *n* = 2 – 18 (β-arrestin), *n* = 3 (desensitisation). Simple linear regression line goodness of fit $r^2 = 0.470$ (A), $r^2 = 0.372$ (B), $r^2 = 0.442$ (C).

When replicates were rank ordered from lowest to highest level of internalisation there was a clear spectrum of activity in the screening set (Figure 37). Balanced agonists were overrepresented as efficacious internalising compounds. The top 5 internalising compounds were HR-05 (9), PW-303 (3), PW-290 (5), PW-502 (6), and PW-412 (11), all of which are highly potent agonists containing the 3-hydroxypyridine-*N*-oxide head group and the first four of which were tested at between 21× and >1,800× their β-arrestin-2 pEC_{50}, and PW-412 at approximately 1× β-arrestin-2 EC_{50}. The most potent balanced agonist was PW-462 (8), which caused very little internalisation despite being an extremely potent sub-nanomolar agonist tested at ~3× its β-arrestin-2 pEC_{50}. Highly biased agonists, possessing picomolar cAMP potencies and bias levels of > 5,000,000 (compounds 20 – 23) were not in the top 10, and were actually clustered near the middle of the rank-ordered graph, achieving approximately 50% of the effect size of the PW-303 control.

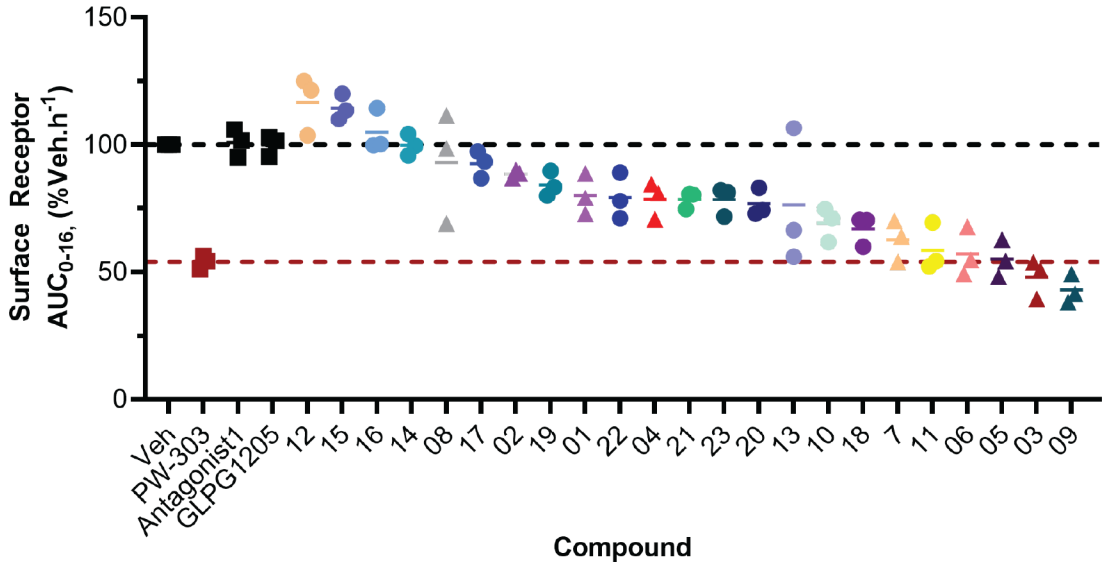

Figure 37: Relationship of bias to the internalisation time course of the screening set. Area under the curve analysis of agonist-induced receptor internalisation following stimulation with the screening set of balanced agonists (▲) and biased agonists (●). CHO-HA-hGPR84 #7F12 cells were stimulated with agonist (10 µM), vehicle (DMSO), or controls (30 µM PW-303, 10 µM Antagonist 1, 10 µM GLPG1205) for 1, 4, or 16 h before fixation, staining, and quantification of surface accessible HA-tag. Area under the curve for each test compound was then calculated and normalised to vehicle, with more internalisation yielding lower surface receptor percentages. Points represent mean of each experiment, n = 3, with compound line showing the mean of the pooled replicates. Average of vehicle (*black*) and PW-303 (*red*) controls shown as horizontal dashed lines.

To gain deeper insights into the relationship between internalisation and desensitisation by compound, I then plotted these responses on the same graph as the percent internalised (100 - % remaining surface receptor) and desensitisation pIC_{50} in order to show higher responses in each assay as higher numbers on the axes (Figure 38). In this representation the distance between data points represents a deviation away from the prediction that desensitisation leads to internalisation. The highly biased agonists 20 – 23 are all potent desensitisers but lack concomitant internalisation. Two other compounds stand out; AR-267 (13) causes a higher degree of internalisation than expected given its low potency of desensitisation, and PW-462 (8) is a potent desensitiser but causes little internalisation. These data confirm that the disconnect between desensitisation and internalisation of GPR84 is dependent on the agonist and agonist structure.

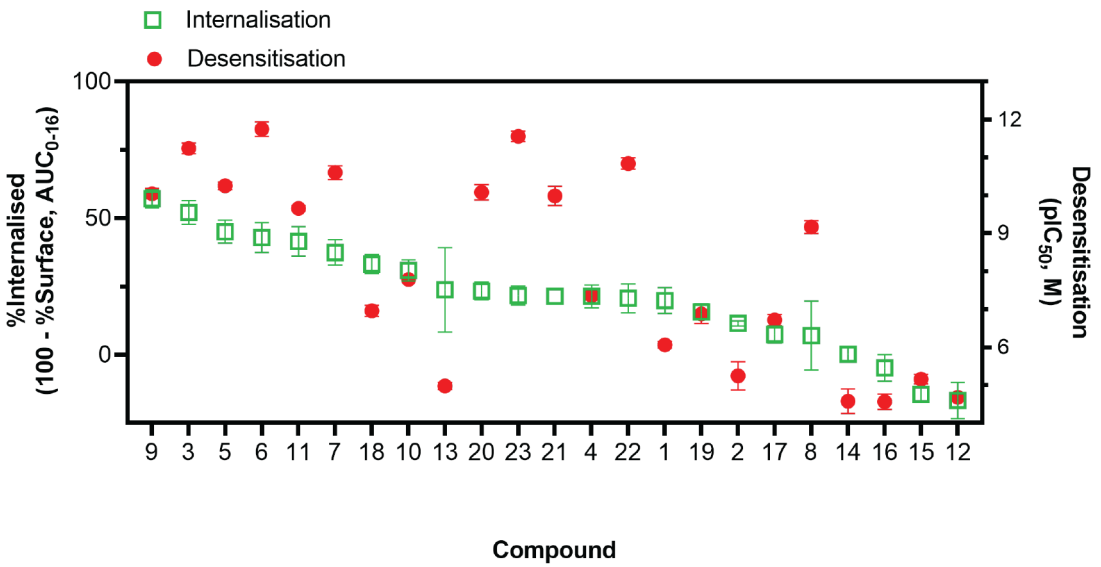

Figure 38: Relationship between internalisation and desensitisation. Compounds in the screening set were rank ordered on their ability to cause internalisation as measured by reductions in nett surface receptor by immunocytochemistry (*green open squares*), with higher internalisation yielding higher percentages on the left y-axis. The potency with which each compound was able to desensitise the cellular impedance response to a second challenge with ZQ-16 was then plotted (*red circles*) with more potent desensitisation bearing higher pIC_{50} values on the right y-axis. Compounds are numbered 1 - 23 as previously described based on their cAMP vs β-arrestin-2 bias. Points represent mean ± SEM, $n = 3$.

4.3. Discussion

4.3.1. Development and Characterisation of a Screening Library

The chemistry dictating what makes some structures desirable and others undesirable in a therapeutic sense has been studied since the early days of drug discovery. Following an analysis of Pfizer's drug databases, Lipinski published a landmark 'rule-of-five' paper describing the tendency of orally bioavailable drugs to be relatively small and lipophilic molecules (Lipinski et al., 1997). Although a contentious metric, it is worth noting all compounds adhere to this rule of five. The process of optimising a lead compound into a drug typically involves adding more complexity by way of molecular weight, number of rings, and number of rotatable bonds (Oprea et al., 2001). Lead-like compounds are therefore typically smaller and less functionalised than drug-like compounds (Oprea et al., 2001). Overall, our results show that all ligand classes and screening sets of ligands in the 90 sub-micromolar agonist set fall in the lead-like space in terms of molecular weight. In contrast, all ligand classes and screening sets of ligands are relatively hydrophilic, with cLogP values above 3, and fall above that of expected values for drug-like molecules. HBA and HBD are also closer to

the lead-like space for all screening sets. Taken together these four descriptors can be rationalised for GPR84 given it responds to lipids and lipid-like agonists and has a sterically restricted orthosteric binding site with both a buried hydrophobic portion and a hydrophilic site (Liu et al., 2023, Zhang et al., 2023). Overall, the aim of selecting a diverse set of agonists was to better sample the chemical space of GPR84 agonists. These descriptors give some small insight that the diversity set has a smaller range of molecular weight than the activity set, an equal range of hydrogen bond acceptor (HBA), and a larger range of cLogP and HBD values, suggesting that it does indeed capture some areas not represented by choosing high potency agonists.

The cAMP and β-arrestin data show a large range in potencies for hGPR84, and excitingly, a large range of bias. This will assist with teasing apart the impact of bias on other processes. The six most potent compounds by cAMP possessed picomolar EC_{50} values and all featured *meta*-substituted hydroxyl groups to the alkyl tail. Interestingly these six compounds had varying levels of bias, PW-502 (6), PW-303 (3), PW-269 (23), HR-05 (9), LY237 (7), and AR-198 (22), suggesting that the potency boost from the 3-position hydroxyl group identified during the optimisation of DL-175 does not influence the β-arrestin activity. The hypothesis of Wang et al. (2023a) was that his hydroxyl group on AR-198 and AR-211 acted as a HBD similar to the dihydroxypyridine of LY237, so it would be reasonable to rationalise this is the case for all of the 3-hydroxypyridine-*N*-oxides of PW-502, PW-303, and PW-269. In fact, without exception, the 12 most potent compounds and only sub-nanomolar compounds in the screening set feature this 3-hydroxypyridine-*N*-oxide or the 2,4-dihydroxypyridine tautomer of LY237. We also previously speculated that this functional group conferred an altered binding mode by making contact with R172 in the ECL2, which would explain an enhanced affinity by way of decreased k_{off} at GPR84. These top 12 potent compounds also exhibit the full range of β-arrestin activity, suggesting again that this functional group does not influence β-arrestin signalling. A few lines of evidence suggest the tail region is more likely to influence the signalling bias; firstly all of the lipid-mimetics with alkyl tails are active in the β-arrestin assay, secondly the higher molecular weight tail regions associated with a 3-hydroxypyridine-*N*-oxide motif have lower activity in the β-arrestin assay, thirdly all naphthalene-containing substructures are

inactive in the β-arrestin assay, and finally the pair-wise comparisons between 6-OAU (4) and DL-175 (17), and PW-210 (1) and PW-209 (18) show that the octane or naphthalene tail regions influence bias irrespective of the uracil or pyridine-*N*-oxide head group. These data strongly suggest a role for molecular weight and aromatic groups to influence bias and warrants further investigation. Results on the two primary assays for cAMP and β-arrestin showed promise with regard to having selected both a chemically and biologically diverse set of agonists. It then became of interest what other receptor signalling pathways this screening set of agonists might differentially influence.

4.3.2. Receptor Desensitisation

The specificity of the desensitisation response was demonstrated by controls showing blockade of the ZQ-16 induced impedance response using both an allosteric GPR84 antagonist, GLPG1205, and orthosteric antagonist, Antagonist 1 (Jenkins et al., 2021, Labéguère et al., 2020). The correlation between the stimulation and inhibition potencies indicate that, at least in the case of the impedance response, activation and desensitisation are tightly coupled. When measuring desensitisation of the lipid-sensing immune-expressed receptor $S1P_1$, Grailhe et al. (2020) tested the ability of multiple agonists to inhibit an impedance response to S1P following a 1 h agonist stimulation and 5.5 h agonist washout. Even with long incubation times and a 5.5 h washout, the authors noted markedly different activation-to-desensitisation (IC_{50} / EC_{50}) between agonists. The G-protein biased agonist SAR247799 had an IC_{50} / EC_{50} value of 114, which was almost 700× the ratio of the more balanced agonist Siponimod (Grailhe et al., 2020). Comparison of GPR84 desensitisation to the $S1P_1$ receptor may not be appropriate for two major reasons; first, the potentially different signalling mechanism as $S1P_1$ has previously been shown to exhibit hours-long persistent signalling by internalised receptors (Mullershausen et al., 2009), and secondly that the $S1P_1$-desensitising drugs such as Fingolimod (FTY720) are phosphorylated *in vivo* and mimic S1P, but unlike S1P are not substrates for degradation by S1P-lyases *in vivo* and therefore bypass a physiological mechanism for removal of receptor stimulation (Bandhuvula et al., 2005). Our results align more with those from Deng et al. (2011) who used an optical label-free desensitisation screen to find compounds causing both a positive response while also inhibiting a second stimulation with

the GPR35 agonist zaprinast 1 h later. Follow-up studies on 18 compounds showed that they all dose-dependently desensitised the cells to zaprinast with a rank order of IC_{50} values correlating to those of their EC_{50} values (Deng et al., 2011).

G_i-coupled GPCR activation has been shown to typically result in positive impedance responses (Doijen et al., 2019), and comparison of biased agonists on the impedance responses of HCA_2 and CXCR3 showed that β-arrestin recruitment is more likely to influence the kinetics of the impedance response (Kammermann et al., 2011, Watts et al., 2012). By measuring the peak BNCI response it is likely that I have captured signalling more representative of the G-protein pathway, with evidence for this provided by a strong correlation of desensitisation potency by cAMP potency. In summary I was able to test the ability of the screening set to desensitise the impedance response to ZQ-16, but as this was so tightly correlated to cAMP potency there was no correlation to the level of bias of a compound. Correlating desensitisation with some measure of agonist efficacy would be of interest, given previous results on the β_2-AR supporting the idea that equipotent cAMP agonists with different efficacies result in different levels of desensitisation (Charlton, 2009). Although initially counter-intuitive, high efficacy agonists would be expected to cause lower degrees of desensitisation than potency-matched low efficacy agonists. This is because the high efficacy agonists would require a lower receptor occupancy to achieve maximal effect, thereby leaving more 'spare receptors' un-stimulated and not desensitised (Charlton, 2009). One consequence of this effect too is how dependent the desensitisation effect is on the agonist used as the second stimulus. As low efficacy agonists require more receptors to cause a full response, they are more sensitive to desensitisation (Charlton, 2009). Therefore, it may be of future use to not only characterise the efficacy of my screening set, but also the agonist used to measure desensitisation, and perhaps, re-screen the set using a low efficacy agonist.

4.3.3. Receptor Internalisation

The time course of reductions in nett surface receptor is a surrogate measurement to determine the level of internalisation introduced by an agonist. CHO-HA-hGPR84 #7F12 high expressing cells are first exposed to agonist for 1, 4, or 16 h, then fixed and stained without

permeabilising the membranes. This method detects the nett surface receptor remaining following agonist incubation, and therefore includes the labelling of receptors which have been internalised and then recycled to the surface and hence why we do not achieve reductions to 0. However, variations of this protocol exist which could allow for further discrimination between agonists. For example, labelling cells with primary antibody, then washing and incubating with agonist to induce internalisation, and then labelling with secondary in non-permeabilising conditions, results in the labelling of receptor remaining on the surface and not newly surface-trafficked receptor (Finlay et al., 2016). It is also then possible to permeabilise the cells, apply a second secondary antibody, and label the intracellular receptors that had been internalised (Finlay et al., 2016). The fate of the internalised receptors could also be investigated by co-localisation with lysosomal markers.

Here, I opted for time course data for simplicity and throughput. The potency of an agonists internalisation response could be achieved, but there are issues with analysing the data using standard equilibrium models of concentration and response (Zhu et al., 2019). The importance of the kinetic context on the perceived agonist bias was highlighted by Klein Herenbrink et al. (2016) in terms of downstream signalling pathways, which was extended by Zhu et al. (2019) to show that the potency of CB_1 agonists with regard to reductions in nett surface receptor were highly dependent on the time point, and that no single time point could be used to fairly compare agonists. To remedy this the authors proposed two models for measuring the potency of internalisation. I could not make the assumption that GPR84 synthesis rate is negligible as required for the quasi-steady state model, and the number of data points required for the calculations using the model-free method would be too burdensome for the entire screening set (Zhu et al., 2019). Instead, I opt to measure a time course of internalisation at a single concentration of each test agonist. In fact, as the goal was to discriminate compounds by activity, it is possibly advantageous to incorporate other metrics to describe agonists.

These data suggested that some agonists may increase surface expression, but the effect size was small and there were no control compounds to conclude this, as neither the orthosteric or allosteric antagonists caused upregulation. By stabilising the receptor in an inactive state some antagonists or inverse agonists are known to prevent constitutive internalisation of the receptor and

thereby upregulate surface expression (Grimsey et al., 2011). Other mechanisms, such as pharmacological chaperoning of GPCRs have been described (Petäjä-Repo et al., 2002). It is possible that the existing pool of surface expressed receptor, here found to be at least above 35% at all times, could prevent the detection of smaller differences in surface expression, though it is clear that no compounds caused large increases in surface expression.

These results showed that most agonists caused some degree of internalisation and that this was dependent on agonist structure but not strongly related to cAMP potency, β-arrestin, or desensitisation potency. Despite this, there was some link between bias level and internalisation, as the highly biased agonists failed to cause high levels of internalisation, and balanced agonists appeared to be overrepresented as high internalisers. One explanation is that the single-point concentration of internalisation data is correlated to β-arrestin activity at 10 μM, but not potency. Four of the top five internalising compounds, HR-05 (9), PW-303 (3), PW-290 (5), and PW-502 (6), were all also in the top five most potent agonists by β-arrestin, and also the only agonists being tested at >10× their β-arrestin-2 pEC_{50}. In a similar thread to the analysis of desensitisation activity, a potential correlate to measure going forward would be one of β-arrestin-2 efficacy, as opposed to potency. In summary, internalisation caused by the screening set was measured and found to be uncorrelated to the potency values of the other three metrics, but some evidence for a relationship to the level of bias and actual level of β-arrestin-2 recruitment was found.

Through the mechanisms of desensitisation and internalisation, an agonist as measured by second messenger assays may actually behave as an antagonist in physiological settings. The cAMP assay captures second messenger production at a 30-minute time point, and the β-arrestin-2 recruitment assay measures recruitment over 90 minutes. It is possible that at longer time points the mechanisms of tachyphylaxis, including desensitisation of downstream signalling components, could impact an agonists effectiveness or efficacy at GPR84 with regards to other functions. There is even precedent that potent agonists of the $S1P_1$ receptor result in the ubiquitination and proteasomal degradation of the receptor, resulting in a loss of effect (Cartier and Hla, 2019). These compounds are known as ‘functional antagonists’ due to the reality of their mechanism *in vivo*

causing extreme long-term downregulation of the receptor (Brinkmann et al., 2010). Indeed, this is an important factor for the clinical efficacy of $S1P_1$ agonists in treating multiple sclerosis by preventing the egress of autoreactive lymphocytes and the destruction of the myelin sheath (Cartier and Hla, 2019). Our studies do not suggest the presence of functional antagonists in the screening set because in almost all cases the nett surface receptor pool peaked at 4 h and recovered by 16 h. However, this does not rule out the possibility that the surface expressed receptor population is less functional. Further studies to measure desensitisation at 16 h would be a useful test for actual cell sensitivity.

4.4. Conclusions and Future Directions

Desensitisation and internalisation are two of the mechanisms underlying tachyphylaxis. The loss of cellular responsiveness to drug stimulation over time is an important factor in the clinic for both long-term drug treatment and tolerance, exemplified by the highly undesirable tolerance to opioids for pain relief, or the highly desirable prolonged bronchodilation with asthma medications (Kelly et al., 2008). In the complete characterisation of agonists at the immune-expressed inflammatory receptor GPR84, it was therefore of primary importance to determine their effect on receptor regulation. By testing a panel of structurally and biologically diverse agonists on assays for second messengers, β-arrestin bias, short-term desensitisation, and longer-term downregulation I can conclude there are agonist-selective effects on all readouts. A brief analysis of structural relationships suggest the importance of the tail region of the DL-175 scaffold for signalling bias. Short-term desensitisation did not correlate with bias level. Some correlation between bias and internalisation was found. Therefore, the bias level does not accurately describe an agonists ability to desensitise or internalise GPR84, consistent with the view of a pluridimensionality to ligand efficacy.

In this chapter I have assessed the influence of G-protein signalling bias on the regulation of GPR84 using a panel of structurally novel GPR84 agonists. However, in consideration of Thesis Aim 3, the influence of these biased agonists on macrophage function was not determined. The molecular pharmacology of GPR84 has proven complex and future work is needed at both the molecular level and at the physiological level. At the molecular level, measurements of receptor

phosphorylation or GRK recruitment would be valuable additions to this data set. At the physiological level, the influence of bias on macrophage ROS production, phagocytosis, cytokine secretion, and chemotaxis may reveal further correlations between agonist structure, activity, and function.

Chapter Five.

CONCLUSIONS

GPR84 research began when its structure was predicted and cDNA cloned from immune cells in 2001. Little was initially known and there was a scarcity of information regarding the function of GPR84 in humans and other species. Significant advancements have been made in the intervening 23 years; expression profiling in human and mouse, characterisation in model vertebrate species, the development of genetic knockout mice, the discovery of potent surrogate agonists and development of multiple radioligands, clinical trials on potent antagonists and NAMs, and very recently, cryo-EM structures of GPR84. Despite these advancements and the clinical interest in this receptor it remains an orphan. Capric acid was the first agonist to be proposed as a potential endogenous agonist. However, the immune-expression profile, regulation by inflammatory mediators, and pro-inflammatory effects of GPR84 do not support a role in dietary sensing of MCFAs. Likewise, the low circulating concentrations, low affinity, low potency, low efficacy, low selectivity, and low spatiotemporal overlap of capric acid with GPR84 does not support this conclusion.

Activation of GPR84 on innate immune cells by synthetic agonists has been linked to the secretion and mobilisation of inflammatory mediators, chemotaxis and migration, and bacterial adhesion and phagocytosis. Various allosteric modulators and biased agonists exist, including the G-protein biased agonist DL-175 which was reported and available commercially starting in 2019. In a review of the cAMP, β-arrestin-2, and GTPγS potencies of agonists at hGPR84 it appeared that this receptor is poorly coupled to the β-arrestin pathway. Beyond the system bias, very highly G-protein biased agonists do exist. Yet, very few studies have directly compared biased and non-biased agonists for function in innate immune cells. So few, in fact, that hardly any definitive conclusions can be drawn outside of any particular cell type. This is likely a consequence in part from the clinical interest which has understandably focussed on receptor antagonism. However, the best strategy to

exploit GPR84 therapeutically remains unknown. The advent of biased signalling has revolutionised the field of GPCR pharmacology and postulates that by selectively activating some receptor functions and not others you can define the outcomes of receptor signalling more carefully. Perhaps biased signalling at GPR84 will allow for the selective modulation of some of its inflammatory functions and not others. To explore this potential and the role of orphan receptor GPR84 in macrophage biology and inflammation it would first be necessary to understand the precise mechanisms behind the chemical control of receptor biology. To achieve this, I set out three thesis aims. In brief, these were to develop chemical and biological tools to study receptor function in Chapter Two, to investigate signalling differences between 6-OAU and DL-175 in Chapter Three, and to assess the influence of bias on receptor regulation and their effects on macrophages in Chapter Four.

Chemical probes are an essential part of the pharmacologist's toolkit with which to construct foundations of biological activity at the molecular level. In Chapter Two I detailed a collaboration with medicinal chemists to construct a detailed SAR of a series of biased agonists at GPR84 during the optimisation of DL-175. An alteration to the head group of DL-175 resulted in a 3-log cAMP potency boost while maintaining bias away from β-arrestin-2 recruitment. Modifications to both the linker and tail regions of DL-175 led to an improvement in metabolic stability in both MLM and in mouse PK studies. These optimisations resulted in the development of two novel probes suitable for use *in vivo*, AR-198 (OX04528) and AR-211 (OX04529). We also systematically tested MCFAs for cAMP potency, and showed that the chain-length specificity of GPR84 for medium-chain fatty acids can be altered with hydroxylation at the 2- or 3- positions, with the most potent hydroxylated MCFAs being 2-OH-C11, and 3-OH-C11 and 3-OH-C12. As sub-micromolar agonists, these MCFAs not only represent better probes to study GPR84 signalling than capric acid but may also be more physiologically relevant if local concentrations of each species can be identified in health and disease. Finally, I also developed transgenic CHO cell lines expressing human, murine, and zebrafish orthologues of GPR84 and demonstrated that most agonists retain activity at each species, encouraging the use of potent tool compounds such as 6-OAU and DL-175 when using model

species. These chemical and biological tools can be used to investigate GPR84 and potentially uncover broader truths about the pharmacology of the receptor, test therapeutic hypotheses, and inform the development of other novel compounds.

The phenomenon of signalling bias at GPCRs has ushered in a new era of functional drug screening with the goal of optimising drug candidates for therapeutic efficacy by promoting or diminishing effects associated with downstream pathways. In Chapter Three I characterised the signalling differences of GPR84 resulting from stimulation with 6-OAU and the G-protein biased agonist DL-175. The prolonged label-free CEI response of BMDMs to DL-175 was found to be receptor-mediated and could be recapitulated in heterologous cell lines. DL-175 caused similar levels of ERK phosphorylation as 6-OAU, but had slightly lower levels of Akt phosphorylation. Internalisation assays revealed DL-175 lacked significant internalisation compared to 6-OAU, even when incubated at higher concentrations or for longer periods of time. To tease these differences apart, I employed transgenic CHO expressing cell lines, and found that the differences in impedance sensing and Akt phosphorylation only manifested in the low expressing cell lines. Furthermore, the differences were transient, with agonist differences manifesting at time points between 5 and 10 minutes. These two agonists have previously been shown to differentially influence immune cell function, and my experiments identified molecular differences between biased and non-biased agonists. Well characterised cell lines with defined levels of GPR84 expression open new ways in which to evaluate newly developed agonists by highlighting the importance of receptor reserve, time points, and the utility of label-free assays.

Agonists possess many efficacies that can be captured by using surrogate assays to measure multiple distinct receptor functions. In Chapter Four I developed a small but chemically and biologically diverse screening set to test for relationships between structure, bias, desensitisation, and internalisation. Label-free impedance based desensitisation assays measuring the loss of GPR84 responsiveness to ZQ-16 at 10 minutes showed a strong correlation between desensitisation potency and cAMP potency, but not the level of bias of an agonist. Internalisation assays measuring the reduction in surface-accessible receptor following a time course over 16 h showed a poor correlation

with cAMP potency, β-arrestin potency, and desensitisation potency, but some relationship to the level of bias was observed. In particular, I identified compounds which exhibited desensitisation of GPR84 with minimal internalisation, and vice versa. These properties are important because they allow us to understand how an agonist influences regulation of a receptor *in vitro* and therefore relates to function *in vivo*. The examination of the various efficacies that GPR84 exhibits is important for drug design and could be used to stratify compounds for further development.

In conclusion, by developing chemical and biological tools suitable for studying GPR84, then applying those tools to dissect differences between the agonists 6-OAU and DL-175, and finally assessing the influence of bias on receptor regulation, I have made significant progress on the aims set out in Chapter One. The outstanding work in Thesis Aim 3 is to characterise the functional effects of the screening set on macrophages. Few reports directly compare biased agonists in innate immune cells, and with the molecular characterisation of the screening set, further correlations to immune cell function would be of significant interest. The work described herein has helped to understand the molecular pharmacology of GPR84, opens new ways to test for therapeutic effects, and describes the efficacies of various agonists. These findings could help to develop compounds with therapeutically desirable properties once further progress is made to identify which properties might be desirable in health and disease.

Chapter Six.

METHODS

6.1. Development of CHO-HA-GPR84 Monoclonal Cell Lines

Cloning and transfections were carried out as described previously by Luscombe et al. (2023a). Gene fragments containing *Homo sapiens* (NCBI Reference Sequence: NM_020370.3), *Mus musculus* (NCBI Reference Sequence: NM_030720.3, codon optimised), and *Danio rerio* (NCBI Reference Sequence: NM_001105697_1) (O'Leary et al., 2016) GPR84 coding sequences preceded by an N-terminal HA-tag in a Kozak setting and flanked by restriction enzyme sites for AflII and XbaI were designed using SnapGene® software (from Insightful Science; available at snapgene.com) and synthesised by Twist Biosciences (San Francisco, CA). Fragments were PCR amplified, electrophoresed, gel extracted, and then sequence verified by Source BioScience (Nottingham, UK). HA-GPR84 fragments were cloned into a pcDNA3.1+ mammalian expression vector by sticky end restriction enzyme cloning. *E. coli* DH5α cells were transformed and colonies possessing recombinant plasmids were screened for by restriction enzyme digests, followed by plasmid scale up and DNA sequence verification.

CHO-K1 cells were transfected with HA-GPR84-pcDNA3.1+ using the Amaxa® Nucleofector™ 2b device (Lonza AAB-1001) and Cell Line Nucleofector® Kit T (Lonza VVCA-1002, as per the manufacturer's protocol) before selection pressure was applied using G418 (600 µg/mL; Thermo 10131027) for 10-14 days. Polyclonal cells were sorted by limiting dilution into 96-well plates and left to grow for 10-14 days. During outgrowth, clones were tested for responses to 6-OAU (10 µM) in a single point cAMP assay. Hits were later confirmed by response to three concentrations of 6-OAU, followed by side-by-side concentration-response curves and Western blots after 4 weeks of culture. Monoclonal CHO cell lines were selected based on their functional response to 6-OAU, positive α-HA-GPR84 antibody reactivity, and longevity in culture.

6.2. Cell Culture

Maintenance of CHO cell lines was carried out as described previously by Luscombe et al. (2023a). All CHO Cell lines were cultured and plated overnight in Ham's F12 (Thermo 21765029) supplemented with 10% fetal bovine serum (FBS; Sigma F4135), 19 mM HEPES (Sigma H0887), and 1% penicillin-streptomycin (Gibco 15140122). When propagating CHO-HA-GPR84 cell lines or CHO-hGPR84 (DiscoverX 95-0158C2) 600 µg/mL G418 (Thermo 10131027) was included. When propagating CHO-β-arrestin-2-hGPR84 (DiscoverX 93-0647C2) cells 300 µg/mL Hygromycin B was included in addition to G418 (Thermo 10687010).

Murine Bone Marrow Derived Macrophages were harvested and grown as described previously Recio et al. (2018). Bone marrow cells were prepared from the tibiae and femurs of C57BL/6 mice by flushing with PBS, then cultured for 7 days in DMEM supplemented with 10% FBS, 10% L929 cell-conditioned media (a source of M-CSF) (Englen et al., 1995), and 1% penicillin-streptomycin (Gibco 15140122). Isolated BMDMs were then frozen in FBS + 10% DMSO (Sigma D8418). For experiments, BMDMs were thawed and plated overnight with the inclusion of 100 ng/mL lipopolysaccharide (Merck L4391) to up-regulate GPR84 expression (Recio et al., 2018).

THP-1 (ATCC TIB 202) and U937 cells were cultured in RPMI (Thermo 11835063) supplemented with 10% FBS (Sigma F4135), 25 mM HEPES (Sigma H0887), and 1% penicillin-streptomycin (Gibco 15140122).

6.3. Assay for cAMP Production

Assays for cAMP production were performed as described previously by Luscombe et al. (2023a). CHO-hGPR84 (DiscoverX 95-0158C2) cells were used for screening of novel compounds unless otherwise described. Cells were plated at 15,000 cells / 20 µL / well in a white 384-well microplate (Greiner 781098) and incubated for 24 h at 37°C / 5% CO_2 before stimulation with forskolin (25 µM) and agonist for 30 min at 37°C. To test CHO-HA-GPR84 monoclones for sensitivity to PTX or antagonism the cells were pre-incubated for 24 h with pertussis toxin (100 ng/mL) or 30 min with Antagonist 8 (30 µM) at 37°C, then stimulated with forskolin (50 µM) and agonist for 30 min at 37°C. Drugs were dissolved in DMSO and prepared in PBS + 0.1% BSA. Cell

lysis and detection of cAMP was performed using the HitHunter® cAMP Assay for Small Molecules (DiscoverX 90-0075SM2 as per the manufacturer's instructions). Luminescence was measured 18-24 h after the final step on a PHERAstar® FS microplate reader (BMG Labtech). Data analysis and curve fitting were performed using GraphPad Prism (v9.5.0, Boston, MA).

6.4. Assay for β-arrestin-2 Recruitment

CHO-K1 cells stably expressing prolink tagged human GPR84 and enzyme acceptor tagged β-arrestin (DiscoverX 93-0647C2) were seeded in a white 384-well microplate (Greiner 781098) at 5,000 cells / 20 µL / well and incubated overnight at 37 °C / 5% CO2. Cells were then stimulated with agonist for 90 min. Drugs were dissolved in DMSO and prepared in PBS + 0.1% BSA + 0.125% Tween-80 to prevent compound aggregation at high concentrations (Lucy et al., 2019). Cell lysis and detection of β-arrestin was performed using the PathHunter® cAMP Assay for Small Molecules (DiscoverX 93-0001 as per the manufacturer's instructions). Luminescence was measured 1 h after the final step on a PHERAstar® FS microplate reader (BMG Labtech). Data analysis and curve fitting were performed using GraphPad Prism (v9.5.0, Boston, MA).

6.5. Assays for Selectivity Against FFA1, FFA4, and CB_2

Compounds progressed to selectivity were tested for Ca^{2+} mobilisation against select targets and were performed by Wuxi AppTec Ltd (Shanghai, China). In brief, CHO cells expressing human FFA1, FFA4, or CB_2 in a black 384-well microplate (Greiner 781090) were dye-loaded with Fluo-4 (Invitrogen F10471) in HBSS (Gibco 14025-076) + 20 mM HEPES for 50 min at 37°C / 5 % CO_2, then left for 10 minutes at RT. Cells were stimulated with agonist and the calcium response measured using a FLIPR (Molecular Devices). Data analysis and curve fitting were performed using GraphPad Prism (v9.5.0, Boston, MA).

6.6. Cytotoxicity Assay

CHO-K1 or CHO-hGPR84 (DiscoverX 95-0158C2) were plated at 15,000 cells / 20 µL / well in a white 384-well microplate (Greiner 781098) and incubated for 20 h at 37 °C / 5% CO2 in the presence of drug. Drugs were dissolved in DMSO and prepared in PBS + 0.1% BSA. Detection of cell viability was performed using the CytoTox 96® LDH Cytotoxicity Assay (Promega G1780).

The absorbance signal was measured at 490 nm in a SPECTROstar® Omega microplate reader. Data were first baseline subtracted to media-only conditions, then normalised to vehicle (0%) and maximum cell lysis (100%) determined by addition of Lysis Solution Triton X-100.

6.7. Assays for Metabolic Stability

Compound metabolic stability was measured by incubation with Mouse Liver Microsomes (MLM) and were performed by either Wuxi AppTec Ltd (Nanjing, China) or Cyprotex (Macclesfield, UK). In brief, compounds (1 µM) were incubated at 37 °C for 60 min in a protein fraction of mouse liver microsomes at 0.5 mg / mL in 100 mM potassium phosphate buffer. Samples were quenched following incubations for 5, 15, 30, 45, or 60 minute time points using acetonitrile, 200 ng/mL tolbutamide, and 200 ng/mL labetalol as an internal standard. Samples were shaken for 10 minutes before centrifugation and analysis by liquid chromatography with tandem mass spectrometry.

6.8. Murine Pharmacokinetic Studies

Compounds progressed to *in vivo* pharmacokinetic studies were tested in mice by Wuxi AppTec Ltd (Hong Kong) according to the local ethics review process. Male C57BL/6J mice (n = 3) were orally administered with 10 mg/kg of compound. Drugs were formulated at 1mg/mL in 30% propylene glycol, 10% chremophor EL, 20% solutol, 40% water. Blood was taken at pre-dose and at 0.25, 0.5, 1, 2, 4, 8 and 24 h after dosing. Plasma concentrations were determined by liquid chromatography-tandem mass spectrometry. The plasma concentrations were simulated by PO-Noncompartmental model 200 from the plasma concentrations obtained in the PK study using Phoenix WinNonlin 8.3.5 by Wuxi AppTec Ltd (Hong Kong).

6.9. Western Blotting

Western blotting was carried out as described previously by Luscombe et al. (2023a). Cells were seeded at 300,000 (GPR84 expression) or 500,000 (ERK and Akt assay) cells / 2 mL / well in a 6-well plate 48 h prior to harvesting. Cells were placed on ice to terminate the assay and gently washed twice with 3 mL of ice-cold PBS, before lysis with 50 µL 1.5×RIPA buffer with protease and phosphatase inhibitors. Lysates were rapidly scraped and frozen at -80°C. Clarified protein

concentrations were determined by Pierce™ BCA Protein Assay (Thermo 23225) before 25 µg / lane was resolved by SDS-PAGE under reducing conditions in 10% NuPAGE Bis-Tris gels (Thermo NP0302BOX). Proteins were transferred to a nitrocellulose membrane (Thermo LC2000), blocked with 5% non-fat dry milk in TBS for 1 h at room temperature, then probed overnight at 4°C with primary antibodies in TBST + 5% non-fat dry milk (Mouse α-p-Akt CST 4051, Rabbit α-Akt CST 9272, Rabbit α-p-ERK CST 9101, and Mouse α-ERK CST 9107 all at 1/1,000 for Akt/ERK, or 1/500 Rabbit α-HA CST 3724 with 1/1,000 Mouse α-ERK CST 9107, or 1/500 Rat α-HA Merck 11867423001 with 1/1,000 rabbit anti-β-actin CST 4967 for receptor expression). Secondary antibody in TBST + 5% non-fat dry milk (Goat α-Mouse DL680 Thermo 35519 and Goat α-Rabbit DL800 Thermo SA5-10036 at 1/10,000; or 1/5,000 Goat α-Rat DL800 Thermo SA5-10024, and 1/10,000 Goat α-Rabbit DL680 Thermo 35569) was applied for 1 h at room temperature before the membrane was dried and visualised on an Odyssey Sa Infrared Imaging System (LI-COR Biosciences) on the 700 nm and 800 nm channels simultaneously. Band signal intensity was quantified in ImageStudio Lite v5.2 (LI-COR Biosciences).

6.10. Assay for ERK and Akt Phosphorylation

To test for phosphorylation of ERK1/2 and Akt the cell plating, lysis, and protein detection by Western blotting were carried out as per the Western blotting protocol. Cells were serum starved for 18 - 24 h and pre-incubated with vehicle (2 h), or Akt inhibitor MK-2206 (10 µM, 24 h) and MEK inhibitor U0126 (10 µM, 2 h) as negative controls prior to stimulation with agonist. Agonists were prepared to 12×final concentration in serum-free media + 0.1% BSA and warmed to 37°C before addition at the appropriate time. Calyculin A (60 nM, 30 min) and FBS (10%, 10 min) were used as positive controls for ERK and Akt phosphorylation.

6.11. Real Time qRT-PCR

THP-1 cells were differentiated by exposure to 50 nM PMA (Selleckchem S7791) for 48 h and then polarised to either M1 with 100 ng/mL LPS, M2 with 20 ng/mL IL-4, or M0 (vehicle) for 24 h. U937 cells were stimulated with 1,000 ng/mL LPS for 3 h or remained unstimulated. CHO-HA-hGPR84 #3E11 cells were seeded overnight. All cell lines were grown to between 1 - 2 M cells

/ well in a 6-well plate prior to RNA extraction using the TRI reagent (Thermo 15596018) and Direct-zol RNA miniprep kit (Zymo Research R2052) as per the manufacturer's instructions. RNA was eluted using nuclease-free water (Thermo R0581) and concentration determined by NanoDrop ND-1000.

The Taqman RNA-to-Ct 1 step kit (Thermo 4392938) was used with the Taqman FAM Gene expression assay kit (Thermo 4453320) to determine gene expression. Two inventoried sets of Taqman primers targeting human *GPR84* were used; one set spanning multiple exons (Assay ID Hs00220561_m1) was used in THP-1 and U937 cells where *GPR84* is found in a genomic context, and one set spanning within the coding sequence only (Hs05001330_s1), which was used for the CHO-HA-hGPR84 clone expressing transgenic *GPR84*. Taqman primers against human *18S* (Assay ID Hs03003631_g1) were used as a housekeeping gene. One-step RT and PCR reactions were carried out using 100 ng of RNA template and PCR steps carried out on a StepOne Plus RT-PCR system (Applied Biosystems). Reactions were carried out in duplicate and average hGPR84 C_T values used to calculate ΔC_T against h18S. Expression was then normalised to levels in unstimulated THP-1 cells to calculate $\Delta\Delta C_T$. Relative fold gene expression was then presented as $2^{-\Delta\Delta CT}$. No template controls and no reverse transcriptase controls were used to ensure the amplification was specific.

6.12. Assay for Cell Electrical Impedance

Assays to test for impedance responses were carried out as described previously by Luscombe et al. (2023a). The xCELLigence Real-Time Cell Analysis (RTCA) SP instrument (Agilent) was used to measure CEIs (Solly et al., 2004) as per the manufacturer's protocol. Background impedance measurements were taken in each well of an RTCA E-Plate 96 PET (Agilent 300600910) using 50 µL of pre-warmed media. Cells were trypsinised and suspensions added at 40,000 cells / 100 µL / well for CHO cell lines, or 50,000 for BMDMs, equilibrated at room temperature for 30 min, then incubated for 20 - 22 h in media supplemented with 10% FBS. Drugs were dissolved in DMSO and prepared to 27×final concentration in serum-free media + 0.1% BSA before addition to the E-Plate. Antagonist 8 or vehicle (DMSO) was added 2 h prior to stimulation

with agonist. Pertussis toxin (dissolved in dH_2O) was pre-incubated for 24 h, and these conditions were controlled for with vehicle additions 2 h prior to stimulation. Impedance measurements were taken every 30 s for 1 h following inhibitor and agonist additions.

Cell Index (CI) measurements were exported and normalised to the time point immediately prior to drug addition. As all conditions were tested in duplicate, these were first averaged, then normalised to the vehicle-vehicle (baseline) condition, yielding baseline normalised cell index values (BNCI). Data analysis and curve fitting were performed using GraphPad Prism (v9.5.0, Boston, MA).

6.13. Assay for Impedance-Based Desensitisation

Desensitisation assays were based on the methods described in the protocol for CEI measurements using CHO-HA-hGPR84 #3E11 cells with altered drug additions. A two-stimulation paradigm was used whereby cells were first stimulated with test compound (stim1) and allowed to incubate for 10 minutes at 37°C / 5% CO_2, then a second stimulation with ZQ-16 or vehicle (DMSO) was applied and incubated for a further 20 minutes at 37°C / 5% CO_2. Drugs were dissolved in DMSO and prepared to 16×final concentration for stim1 and 17×final concentration for stim2 in serum-free media + 0.1% BSA. Cell Index measurements were exported and normalised to the time point immediately prior to stim1. Conditions were tested in singlicate and normalised to the vehicle-vehicle (baseline) condition, yielding baseline normalised cell index values. The maximum BNCI values achieved during the respective stimulation phase (stim1: 0 – 9.75 min, stim2: 10.26 – 20.45 min) were then calculated, and a Max-Min calculation performed to calculate the magnitude of difference from the minimum value just prior to the drug addition. Data analysis performed in Microsoft Excel 2016 (16.0.5422.1000) and plotted in GraphPad Prism (v9.5.0, Boston, MA).

6.14. Assay for Receptor Internalisation

Assays for receptor internalisation were performed as described previously by Luscombe et al. (2023a). Cells were plated at 12,000 cells / 20 µL / well in a black glass bottom 384-well microplate (Greiner 781892) coated with collagen I and incubated overnight. Drugs were dissolved in DMSO and prepared to 5×final concentration in assay media, then added to cells and incubated

for 5 - 60 min at 37°C / 5% CO_2. The plates were placed on ice for 2 min to halt further internalisation and washed with PBS ×4 using an AquaMax 2000 microplate washer (Molecular Devices). Cells were then fixed in 4% methanol-free formaldehyde for 20 min, washed with PBS ×4, and blocked for 45 min in PBS + 1% BSA. Without permeabilising cell membranes the cells were washed with PBS ×4, then incubated with 1/500 Rat α-HA 1° antibody (Merck 11867423001) for 2 h at room temperature. Cells were then washed in PBS ×8 and incubated with 1/500 Donkey α-Rat AF488 2° antibody (Thermo A-21208) and Hoechst 33342 (1 µg/mL) for 1 h at room temperature. Cells were then washed with PBS ×8 and stored at 4°C overnight. Experiments comparing surface expression between cell lines included 1× (~165 nM) Phalloidin AF555 (Thermo A34055) during the primary incubation step.

Images were captured using the EVOS M7000 (Invitrogen) using a 20× 0.75 NA objective lens. Each condition was assayed in triplicate, and in each replicate well 3 non-contiguous images were taken. An imageJ macro was then used to merge channels from each field of view into a single image stack. Image segmentation was performed on these multichannel images using the ZeroCostDL4Mic Cellpose 2D v1.15 notebook, a generalist method employing deep-learning to segment cell bodies and generate masks for each cell (Stringer et al., 2021, von Chamier et al., 2021). Default parameters were used with the cytoplasm2 model (Object_diameter=0, Flow_threshold=0.4, mask_threshold=0). A second ImageJ macro then used the ImageJ plugin ijp-LaRoMe from BioImaging And Optics Platform (https://github.com/BIOP) (Waisman et al., 2021) to convert labels created by Cellpose to regions of interest (ROIs) using the "Label image to ROIs" command and then batch process measurements within each ROI in each channel. This allowed for the rapid analysis of ~1,000 ROIs in each well. The mean GFP fluorescence intensity of each of the ~1,000 ROIs was first averaged, producing a single value per well. These values, correlating to the average surface receptor on cells, were averaged between technical replicates and then normalised to time-matched vehicle (DMSO) conditions.

One-phase decay slopes were fitted to the time-course data on 6-OAU and DL-175 in Chapter Three, which were also re-plotted as concentration-response curves using a three-parameter

curve fitting model in GraphPad Prism (v9.5.0, Boston, MA). Internalisation descriptors from the curve fits were conducted on each replicate before being pooled between biological replicates. Normalised values of nett surface receptor from independent biological replicates were pooled and presented in Prism. AUC analysis for the time course data for the screening set in Chapter Four was analysed in GraphPad Prism using with baseline Y = 0. The $AUC_{0\text{-}16}$ values were calculated on each biological replicate before being pooled for presentation.

6.15. Chemical Reagents

Purchased from Commercial Vendors:

6-OAU (Cayman Chemical 17687), DL-175 (Tocris 7082), embelin (Cayman Chemical 11838) capric acid (C10, Sigma C1875), myristic acid (C14, Sigma M2138), Antagonist 1 (MedChemExpress HY-139675), GLPG1205 (MedChemExpress HY-135303), forskolin (Cambridge Bioscience SM18-2), cmpd101 (Tocris 5642), MK-2206 (APExBio A3010), U0126 (Cell Guidance Systems SM106), calyculin A (ab141784), pertussis toxin (Tocris 3097), DMSO (Sigma D8418), Tween-80 (Sigma 8.22187), BSA (Sigma A7906), PBS (Thermo 14190094), Tris-buffered saline (Sigma T5941, T6066, S9888), Tween-20 (Sigma P1379), RIPA buffer (Millipore 20-188), protease and phosphatase inhibitors (Sigma 11836170001, P5726, P5726; CST 8553), non-fat dry skim milk powder (Sigma 70166), collagen I (Merck C3867), formaldehyde (Thermo 28906), Hoechst 33342 (ImmunoChemistry technologies 639).

Synthesised In-House:

Antagonist 8 (2-((1,4-Dioxan-2-yl)methoxy)-9-hydroxy-6,7-dihydro-4H-pyrimido[6,1-a]isoquinolin-4-one, CAS ID 1445846-30-9) was synthesised by collaborators as described previously by Recio et al. (2018).

DL-222 (2-(2-((4-chloronaphthalen-1-yl)oxy)ethyl)pyridine 1-oxide) was synthesised by collaborators as previously described by Lucy et al. (2019).

(*rac*)-3-hydroxy capric acid (3-OH-C10) was synthesised by collaborators as previously described by Luscombe et al. (2023a).

MCFAs and hydroxylated MCFAs described in Chapter Two were synthesised by collaborators in the Department of Chemistry, University of Oxford.

Analogues of DL-175 leading to the development of AR-198 (OX04528) and AR-211 (OX04529) were synthesised by collaborators as previously described by Wang et al. (2023a).

Compounds contained in the screening set described in Chapter Four that were not purchased commercially were synthesised by collaborators in the Department of Chemistry, University of Oxford.

6.16. Screening Library Design

Compound management and design of the screening set was performed using OSIRIS DataWarrior v05.05.00 (Sander et al., 2015). An initial database of in-house compounds was imported with name, SMILES strings, and preliminary data on cAMP and β-arrestin potencies. Structures were generated using the SMILES strings, the duplicates and stereoisomers were merged using the 'Merge Equivalent Rows' function, and compounds with cAMP EC_{50} > 1 μM separated. Diversity picks were made using the 'Select Diverse Compounds' function using the FragFP structure descriptor, a fingerprint of the agonist based on substructure fragments (Sander et al., 2015). The activity set of compounds were chosen based on their level of cAMP vs β-arrestin bias. Once the biological activities had been determined for final analysis the bioactivity data was updated in DataWarrior, and chemical properties and bioactivity data analysed using the built-in functions in DataWarrior.

BIBLIOGRAPHY

Abdel-Aziz, H., Schneider, M., Neuhuber, W., Meguid Kassem, A., Khailah, S., Müller, J., Gamal Eldeen, H., Khairy, A., M, T. K., Shcherbakova, A., Efferth, T. & Ulrich-Merzenich, G. 2016. GPR84 and TREM-1 Signaling Contribute to the Pathogenesis of Reflux Esophagitis. *Mol Med,* 21 (1)**,** 1011-1024. Doi: 10.2119/molmed.2015.00098

Aktar, R., Rondinelli, S. & Peiris, M. 2023. GPR84 in physiology-Many functions in many tissues. *Br J Pharmacol***,** 1-12. Doi: 10.1111/bph.16206

Alexander, S. P., Christopoulos, A., Davenport, A. P., Kelly, E., Mathie, A., Peters, J. A., Veale, E. L., Armstrong, J. F., Faccenda, E., Harding, S. D., Pawson, A. J., Southan, C., Davies, J. A., Abbracchio, M. P., Alexander, W., Al-Hosaini, K., Bäck, M., Barnes, N. M., Bathgate, R., Beaulieu, J. M., Bernstein, K. E., Bettler, B., Birdsall, N. J. M., Blaho, V., Boulay, F., Bousquet, C., Bräuner-Osborne, H., Burnstock, G., Caló, G., Castaño, J. P., Catt, K. J., Ceruti, S., Chazot, P., Chiang, N., Chini, B., Chun, J., Cianciulli, A., Civelli, O., Clapp, L. H., Couture, R., Csaba, Z., Dahlgren, C., Dent, G., Singh, K. D., Douglas, S. D., Dournaud, P., Eguchi, S., Escher, E., Filardo, E. J., Fong, T., Fumagalli, M., Gainetdinov, R. R., Gasparo, M., Gerard, C., Gershengorn, M., Gobeil, F., Goodfriend, T. L., Goudet, C., Gregory, K. J., Gundlach, A. L., Hamann, J., Hanson, J., Hauger, R. L., Hay, D. L., Heinemann, A., Hollenberg, M. D., Holliday, N. D., Horiuchi, M., Hoyer, D., Hunyady, L., Husain, A., Ap, I. J., Inagami, T., Jacobson, K. A., Jensen, R. T., Jockers, R., Jonnalagadda, D., Karnik, S., Kaupmann, K., Kemp, J., Kennedy, C., Kihara, Y., Kitazawa, T., Kozielewicz, P., Kreienkamp, H. J., Kukkonen, J. P., Langenhan, T., Leach, K., Lecca, D., Lee, J. D., Leeman, S. E., Leprince, J., Li, X. X., Williams, T. L., Lolait, S. J., Lupp, A., Macrae, R., Maguire, J., Mazella, J., Mcardle, C. A., et al. 2021. THE CONCISE GUIDE TO PHARMACOLOGY 2021/22: G protein-coupled receptors. *Br J Pharmacol,* 178 Suppl 1**,** S27-s156. Doi: 10.1111/bph.15538

Amara, A., Gall, S. L., Schwartz, O., Salamero, J., Montes, M., Loetscher, P., Baggiolini, M., Virelizier, J. L. & Arenzana-Seisdedos, F. 1997. HIV coreceptor downregulation as antiviral principle: SDF-1alpha-dependent internalization of the chemokine receptor CXCR4 contributes to inhibition of HIV replication. *J Exp Med,* 186 (1)**,** 139-46. Doi: 10.1084/jem.186.1.139

Amiri Moghaddam, J., Dávila-Céspedes, A., Kehraus, S., Crüsemann, M., Köse, M., Müller, C. E. & König, G. M. 2018. Cyclopropane-Containing Fatty Acids from the Marine Bacterium Labrenzia sp. 011 with Antimicrobial and GPR84 Activity. *Mar Drugs,* 16 (10)**,** 369. Doi: 10.3390/md16100369

Atienza, J. M., Zhu, J., Wang, X., Xu, X. & Abassi, Y. 2005. Dynamic monitoring of cell adhesion and spreading on microelectronic sensor arrays. *J Biomol Screen,* 10 (8)**,** 795-805. Doi: 10.1177/1087057105279635

Atwood, B. K., Lopez, J., Wager-Miller, J., Mackie, K. & Straiker, A. 2011. Expression of G protein-coupled receptors and related proteins in HEK293, AtT20, BV2, and N18 cell lines as revealed by microarray analysis. *BMC Genomics,* 12**,** 14. Doi: 10.1186/1471-2164-12-14

Audoy-Rémus, J., Bozoyan, L., Dumas, A., Filali, M., Lecours, C., Lacroix, S., Rivest, S., Tremblay, M. E. & Vallières, L. 2015. GPR84 deficiency reduces microgliosis, but accelerates dendritic degeneration and cognitive decline in a mouse model of Alzheimer's disease. *Brain Behav Immun,* 46**,** 112-20. Doi: 10.1016/j.bbi.2015.01.010

Bainton, R. J., Tsai, L. T., Schwabe, T., Desalvo, M., Gaul, U. & Heberlein, U. 2005. moody encodes two GPCRs that regulate cocaine behaviors and blood-brain barrier permeability in Drosophila. *Cell,* 123 (1)**,** 145-56. Doi: 10.1016/j.cell.2005.07.029

Bandhuvula, P., Tam, Y. Y., Oskouian, B. & Saba, J. D. 2005. The immune modulator FTY720 inhibits sphingosine-1-phosphate lyase activity. *J Biol Chem,* 280 (40)**,** 33697-700. Doi: 10.1074/jbc.C500294200

Bédard, A., Tremblay, P., Chernomoretz, A. & Vallières, L. 2007. Identification of genes preferentially expressed by microglia and upregulated during cuprizone-induced inflammation. *Glia,* 55 (8)**,** 777-89. Doi: 10.1002/glia.20477

Bellahcene, M., O'dowd, J. F., Wargent, E. T., Zaibi, M. S., Hislop, D. C., Ngala, R. A., Smith, D. M., Cawthorne, M. A., Stocker, C. J. & Arch, J. R. 2013. Male mice that lack the G-protein-coupled receptor GPR41 have low energy expenditure and increased body fat content. *Br J Nutr,* 109 (10)**,** 1755-64. Doi: 10.1017/s0007114512003923

Bouchard, C., Pagé, J., Bédard, A., Tremblay, P. & Vallières, L. 2007. G protein-coupled receptor 84, a microglia-associated protein expressed in neuroinflammatory conditions. *Glia,* 55 (8)**,** 790-800. Doi: 10.1002/glia.20506

Brinkmann, V., Billich, A., Baumruker, T., Heining, P., Schmouder, R., Francis, G., Aradhye, S. & Burtin, P. 2010. Fingolimod (FTY720): discovery and development of an oral drug to treat multiple sclerosis. *Nat Rev Drug Discov,* 9 (11)**,** 883-97. Doi: 10.1038/nrd3248

Briscoe, C. P., Tadayyon, M., Andrews, J. L., Benson, W. G., Chambers, J. K., Eilert, M. M., Ellis, C., Elshourbagy, N. A., Goetz, A. S., Minnick, D. T., Murdock, P. R., Sauls, H. R., Jr., Shabon, U., Spinage, L. D., Strum, J. C., Szekeres, P. G., Tan, K. B., Way, J. M., Ignar, D. M., Wilson, S. & Muir, A. I. 2003. The orphan G protein-coupled receptor GPR40 is activated by medium and long chain fatty acids. *J Biol Chem,* 278 (13)**,** 11303-11. Doi: 10.1074/jbc.M211495200

Calo, J., Comesaña, S., Alonso-Gómez, Á. L., Soengas, J. L. & Blanco, A. M. 2023. Fatty Acid Sensing in the Gastrointestinal Tract of Rainbow Trout: Different to Mammalian Model? *International Journal of Molecular Sciences,* 24 (5)**,** 4275.

Carnielli, V. P., Rossi, K., Badon, T., Gregori, B., Verlato, G., Orzali, A. & Zacchello, F. 1996. Medium-chain triacylglycerols in formulas for preterm infants: effect on plasma lipids, circulating concentrations of medium-chain fatty acids, and essential fatty acids. *Am J Clin Nutr,* 64 (2)**,** 152-8. Doi: 10.1093/ajcn/64.2.152

Cartier, A. & Hla, T. 2019. Sphingosine 1-phosphate: Lipid signaling in pathology and therapy. *Science,* 366 (6463)**,** eaar5551. Doi: 10.1126/science.aar5551

Cawston, E. E., Redmond, W. J., Breen, C. M., Grimsey, N. L., Connor, M. & Glass, M. 2013. Real-time characterization of cannabinoid receptor 1 (CB1) allosteric modulators reveals novel mechanism of action. *Br J Pharmacol,* 170 (4)**,** 893-907. Doi: 10.1111/bph.12329

Cha, S. B., Lee, W. J., Shin, M. K., Jung, M. H., Shin, S. W., Yoo, A. N., Kim, J. W. & Yoo, H. S. 2013. Early transcriptional responses of internalization defective Brucella abortus mutants in professional phagocytes, RAW 264.7. *BMC Genomics,* 14**,** 426. Doi: 10.1186/1471-2164-14-426

Chapman-Lopez, T. J. & Koh, Y. 2022. The Effects of Medium-Chain Triglyceride Oil Supplementation on Endurance Performance and Substrate Utilization in Healthy

Populations: A Systematic Review. *J Obes Metab Syndr,* 31 (3), 217-229. Doi: 10.7570/jomes22028

Charlton, S. J. 2009. Agonist efficacy and receptor desensitization: from partial truths to a fuller picture. *Br J Pharmacol,* 158 (1), 165-8. Doi: 10.1111/j.1476-5381.2009.00352.x

Chen, L. H., Zhang, Q., Xiao, Y. F., Fang, Y. C., Xie, X. & Nan, F. J. 2022. Phosphodiesters as GPR84 Antagonists for the Treatment of Ulcerative Colitis. *J Med Chem,* 65 (5), 3991-4006. Doi: 10.1021/acs.jmedchem.1c01813

Choi, M., Staus, D. P., Wingler, L. M., Ahn, S., Pani, B., Capel, W. D. & Lefkowitz, R. J. 2018. G protein-coupled receptor kinases (GRKs) orchestrate biased agonism at the β2-adrenergic receptor. *Sci Signal,* 11 (544), eaar7084. Doi: 10.1126/scisignal.aar7084

Christiansen, E., Watterson, K. R., Stocker, C. J., Sokol, E., Jenkins, L., Simon, K., Grundmann, M., Petersen, R. K., Wargent, E. T., Hudson, B. D., Kostenis, E., Ejsing, C. S., Cawthorne, M. A., Milligan, G. & Ulven, T. 2015. Activity of dietary fatty acids on FFA1 and FFA4 and characterisation of pinolenic acid as a dual FFA1/FFA4 agonist with potential effect against metabolic diseases. *Br J Nutr,* 113 (11), 1677-88. Doi: 10.1017/s000711451500118x

Colbran, L. L., Johnson, M. R., Mathieson, I. & Capra, J. A. 2021. Tracing the Evolution of Human Gene Regulation and Its Association with Shifts in Environment. *Genome Biology and Evolution,* 13 (11), evab237. Doi: 10.1093/gbe/evab237

Costa, C. G., Dorland, L., Holwerda, U., De Almeida, I. T., Poll-The, B. T., Jakobs, C. & Duran, M. 1998. Simultaneous analysis of plasma free fatty acids and their 3-hydroxy analogs in fatty acid beta-oxidation disorders. *Clin Chem,* 44 (3), 463-71.

Costanzo, A., Liu, D., Nowson, C., Duesing, K., Archer, N., Bowe, S. & Keast, R. 2019. A low-fat diet up-regulates expression of fatty acid taste receptor gene FFAR4 in fungiform papillae in humans: a co-twin randomised controlled trial. *Br J Nutr,* 122 (11), 1212-1220. Doi: 10.1017/s0007114519002368

Courchesne-Loyer, A., Lowry, C. M., St-Pierre, V., Vandenberghe, C., Fortier, M., Castellano, C. A., Wagner, J. R. & Cunnane, S. C. 2017. Emulsification Increases the Acute Ketogenic Effect and Bioavailability of Medium-Chain Triglycerides in Humans: Protein, Carbohydrate, and Fat Metabolism. *Curr Dev Nutr,* 1 (7), e000851. Doi: 10.3945/cdn.117.000851

Crotti, S., Agnoletto, E., Cancemi, G., Di Marco, V., Traldi, P., Pucciarelli, S., Nitti, D. & Agostini, M. 2016. Altered plasma levels of decanoic acid in colorectal cancer as a new diagnostic biomarker. *Anal Bioanal Chem,* 408 (23), 6321-8. Doi: 10.1007/s00216-016-9743-1

Dahlgren, C., Gabl, M., Holdfeldt, A., Winther, M. & Forsman, H. 2016. Basic characteristics of the neutrophil receptors that recognize formylated peptides, a danger-associated molecular pattern generated by bacteria and mitochondria. *Biochem Pharmacol,* 114, 22-39. Doi: 10.1016/j.bcp.2016.04.014

Defea, K. A. 2007. Stop that cell! Beta-arrestin-dependent chemotaxis: a tale of localized actin assembly and receptor desensitization. *Annu Rev Physiol,* 69, 535-60. Doi: 10.1146/annurev.physiol.69.022405.154804

Delany, J. P., Windhauser, M. M., Champagne, C. M. & Bray, G. A. 2000. Differential oxidation of individual dietary fatty acids in humans. *Am J Clin Nutr,* 72 (4), 905-11. Doi: 10.1093/ajcn/72.4.905

Deng, H., Hu, H., He, M., Hu, J., Niu, W., Ferrie, A. M. & Fang, Y. 2011. Discovery of 2-(4-Methylfuran-2(5H)-ylidene)malononitrile and Thieno[3,2-b]thiophene-2-carboxylic Acid Derivatives as G Protein-Coupled Receptor 35 (GPR35) Agonists. *Journal of Medicinal Chemistry,* 54 (20)**,** 7385-7396. Doi: 10.1021/jm200999f

Deroy, C., Rumianek, A. N., Wheeler, J. H. R., Nebuloni, F., Cook, P. R., Greaves, D. R. & Walsh, E. J. 2022. Assaying Macrophage Chemotaxis Using Fluid-Walled Microfluidics. *Advanced Materials Technologies,* 7 (9)**,** 2200279. Doi: 10.1002/admt.202200279

Dietrich, P. A., Yang, C., Leung, H. H., Lynch, J. R., Gonzales, E., Liu, B., Haber, M., Norris, M. D., Wang, J. & Wang, J. Y. 2014. GPR84 sustains aberrant β-catenin signaling in leukemic stem cells for maintenance of MLL leukemogenesis. *Blood,* 124 (22)**,** 3284-94. Doi: 10.1182/blood-2013-10-532523

Doijen, J., Van Loy, T., De Haes, W., Landuyt, B., Luyten, W., Schoofs, L. & Schols, D. 2017. Signaling properties of the human chemokine receptors CXCR4 and CXCR7 by cellular electric impedance measurements. *PLoS One,* 12 (9)**,** e0185354. Doi: 10.1371/journal.pone.0185354

Doijen, J., Van Loy, T., Landuyt, B., Luyten, W., Schols, D. & Schoofs, L. 2019. Advantages and shortcomings of cell-based electrical impedance measurements as a GPCR drug discovery tool. *Biosens Bioelectron,* 137**,** 33-44. Doi: 10.1016/j.bios.2019.04.041

Dranse, H. J., Kelly, M. E. & Hudson, B. D. 2013. Drugs or diet?--Developing novel therapeutic strategies targeting the free fatty acid family of GPCRs. *Br J Pharmacol,* 170 (4)**,** 696-711. Doi: 10.1111/bph.12327

Du Toit, E., Browne, L., Irving-Rodgers, H., Massa, H. M., Fozzard, N., Jennings, M. P. & Peak, I. R. 2018. Effect of GPR84 deletion on obesity and diabetes development in mice fed long chain or medium chain fatty acid rich diets. *Eur J Nutr,* 57 (5)**,** 1737-1746. Doi: 10.1007/s00394-017-1456-5

Duan, J., Liu, H., Zhao, F., Yuan, Q., Ji, Y., Cai, X., He, X., Li, X., Li, J., Wu, K., Gao, T., Zhu, S., Lin, S., Wang, M. W., Cheng, X., Yin, W., Jiang, Y., Yang, D. & Xu, H. E. 2023. GPCR activation and GRK2 assembly by a biased intracellular agonist. *Nature,* 620 (7974)**,** 676-681. Doi: 10.1038/s41586-023-06395-9

Eckhardt, M. 2023. Fatty Acid 2-Hydroxylase and 2-Hydroxylated Sphingolipids: Metabolism and Function in Health and Diseases. *Int J Mol Sci,* 24 (5)**,** 4908. Doi: 10.3390/ijms24054908

Eglen, R. M. 2002. Enzyme fragment complementation: a flexible high throughput screening assay technology. *Assay Drug Dev Technol,* 1 (1 Pt 1)**,** 97-104. Doi: 10.1089/154065802761001356

Eichel, K. & Von Zastrow, M. 2018. Subcellular Organization of GPCR Signaling. *Trends Pharmacol Sci,* 39 (2)**,** 200-208. Doi: 10.1016/j.tips.2017.11.009

Eiger, D. S., Boldizsar, N., Honeycutt, C. C., Gardner, J. & Rajagopal, S. 2021. Biased agonism at chemokine receptors. *Cell Signal,* 78**,** 109862. Doi: 10.1016/j.cellsig.2020.109862

Engelstoft, M. S., Park, W. M., Sakata, I., Kristensen, L. V., Husted, A. S., Osborne-Lawrence, S., Piper, P. K., Walker, A. K., Pedersen, M. H., Nøhr, M. K., Pan, J., Sinz, C. J., Carrington, P. E., Akiyama, T. E., Jones, R. M., Tang, C., Ahmed, K., Offermanns, S., Egerod, K. L., Zigman, J. M. & Schwartz, T. W. 2013. Seven transmembrane G protein-coupled receptor

repertoire of gastric ghrelin cells. *Mol Metab,* 2 (4)**,** 376-92. Doi: 10.1016/j.molmet.2013.08.006

Englen, M. D., Valdez, Y. E., Lehnert, N. M. & Lehnert, B. E. 1995. Granulocyte/macrophage colony-stimulating factor is expressed and secreted in cultures of murine L929 cells. *J Immunol Methods,* 184 (2)**,** 281-3. Doi: 10.1016/0022-1759(95)00136-x

Finlay, D. B., Joseph, W. R., Grimsey, N. L. & Glass, M. 2016. GPR18 undergoes a high degree of constitutive trafficking but is unresponsive to N-Arachidonoyl Glycine. *PeerJ,* 4**,** e1835. Doi: 10.7717/peerj.1835

Fisher, N. M., Seto, M., Lindsley, C. W. & Niswender, C. M. 2018. Metabotropic Glutamate Receptor 7: A New Therapeutic Target in Neurodevelopmental Disorders. *Front Mol Neurosci,* 11**,** 387. Doi: 10.3389/fnmol.2018.00387

Fredriksson, J., Holdfeldt, A., Mårtensson, J., Björkman, L., Møller, T. C., Müllers, E., Dahlgren, C., Sundqvist, M. & Forsman, H. 2022. GRK2 selectively attenuates the neutrophil NADPH-oxidase response triggered by β-arrestin recruiting GPR84 agonists. *Biochim Biophys Acta Mol Cell Res,* 1869 (7)**,** 119262. Doi: 10.1016/j.bbamcr.2022.119262

Fredriksson, R., Lagerström, M. C., Lundin, L. G. & Schiöth, H. B. 2003. The G-protein-coupled receptors in the human genome form five main families. Phylogenetic analysis, paralogon groups, and fingerprints. *Mol Pharmacol,* 63 (6)**,** 1256-72. Doi: 10.1124/mol.63.6.1256

Gagnon, L., Leduc, M., Thibodeau, J. F., Zhang, M. Z., Grouix, B., Sarra-Bournet, F., Gagnon, W., Hince, K., Tremblay, M., Geerts, L., Kennedy, C. R. J., Hébert, R. L., Gutsol, A., Holterman, C. E., Kamto, E., Gervais, L., Ouboudinar, J., Richard, J., Felton, A., Laverdure, A., Simard, J. C., Létourneau, S., Cloutier, M. P., Leblond, F. A., Abbott, S. D., Penney, C., Duceppe, J. S., Zacharie, B., Dupuis, J., Calderone, A., Nguyen, Q. T., Harris, R. C. & Laurin, P. 2018. A Newly Discovered Antifibrotic Pathway Regulated by Two Fatty Acid Receptors: GPR40 and GPR84. *Am J Pathol,* 188 (5)**,** 1132-1148. Doi: 10.1016/j.ajpath.2018.01.009

Gaida, M. M., Dapunt, U. & Hänsch, G. M. 2016. Sensing developing biofilms: the bitter receptor T2R38 on myeloid cells. *Pathog Dis,* 74 (3)**,** ftw004. Doi: 10.1093/femspd/ftw004

Gaidarov, I., Anthony, T., Gatlin, J., Chen, X., Mills, D., Solomon, M., Han, S., Semple, G. & Unett, D. J. 2018. Embelin and its derivatives unravel the signaling, proinflammatory and antiatherogenic properties of GPR84 receptor. *Pharmacol Res,* 131**,** 185-198. Doi: 10.1016/j.phrs.2018.02.021

Gamo, K., Kiryu-Seo, S., Konishi, H., Aoki, S., Matsushima, K., Wada, K. & Kiyama, H. 2008. G-protein-coupled receptor screen reveals a role for chemokine receptor CCR5 in suppressing microglial neurotoxicity. *J Neurosci,* 28 (46)**,** 11980-8. Doi: 10.1523/jneurosci.2920-08.2008

Gao, W. S., Qu, Y. J., Huai, J., Wei, H., Zhang, Y. & Yue, S. W. 2020. DOK3 is involved in microglial cell activation in neuropathic pain by interacting with GPR84. *Aging (Albany NY),* 13 (1)**,** 389-410. Doi: 10.18632/aging.202144

Goebel, M., Stengel, A., Lambrecht, N. W. & Sachs, G. 2011. Selective gene expression by rat gastric corpus epithelium. *Physiol Genomics,* 43 (5)**,** 237-54. Doi: 10.1152/physiolgenomics.00193.2010

González-Hernández, J. A., Bornstein, S. R., Ehrhart-Bornstein, M., Geschwend, J. E., Adler, G. & Scherbaum, W. A. 1994. Macrophages within the human adrenal gland. *Cell Tissue Res,* 278 (2)**,** 201-5. Doi: 10.1007/bf00414161

Grailhe, P., Boutarfa-Madec, A., Beauverger, P., Janiak, P. & Parkar, A. A. 2020. A label-free impedance assay in endothelial cells differentiates the activation and desensitization properties of clinical S1P1 agonists. *FEBS Open Bio,* 10 (10)**,** 2010-2020. Doi: 10.1002/2211-5463.12951

Greaves, D. R. & Schall, T. J. 2000. Chemokines and myeloid cell recruitment. *Microbes Infect,* 2 (3)**,** 331-6. Doi: 10.1016/s1286-4579(00)00293-8

Grimsey, N. L., Goodfellow, C. E., Dragunow, M. & Glass, M. 2011. Cannabinoid receptor 2 undergoes Rab5-mediated internalization and recycles via a Rab11-dependent pathway. *Biochim Biophys Acta,* 1813 (8)**,** 1554-60. Doi: 10.1016/j.bbamcr.2011.05.010

Groot-Kormelink, P. J., Fawcett, L., Wright, P. D., Gosling, M. & Kent, T. C. 2012. Quantitative GPCR and ion channel transcriptomics in primary alveolar macrophages and macrophage surrogates. *BMC Immunol,* 13**,** 57. Doi: 10.1186/1471-2172-13-57

Guo, L., Zhang, X., Zhou, D., Okunade, A. L. & Su, X. 2012. Stereospecificity of fatty acid 2-hydroxylase and differential functions of 2-hydroxy fatty acid enantiomers. *J Lipid Res,* 53 (7)**,** 1327-35. Doi: 10.1194/jlr.M025742

Gurevich, V. V. & Gurevich, E. V. 2019. GPCR Signaling Regulation: The Role of GRKs and Arrestins. *Front Pharmacol,* 10**,** 125. Doi: 10.3389/fphar.2019.00125

Haidukewych, D., Forsythe, W. I. & Sills, M. 1982. Monitoring octanoic and decanoic acids in plasma from children with intractable epilepsy treated with medium-chain triglyceride diet. *Clin Chem,* 28 (4 pt 1)**,** 642-5.

Hanson, M. A., Roth, C. B., Jo, E., Griffith, M. T., Scott, F. L., Reinhart, G., Desale, H., Clemons, B., Cahalan, S. M., Schuerer, S. C., Sanna, M. G., Han, G. W., Kuhn, P., Rosen, H. & Stevens, R. C. 2012. Crystal structure of a lipid G protein-coupled receptor. *Science,* 335 (6070)**,** 851-5. Doi: 10.1126/science.1215904

Hara, T., Kashihara, D., Ichimura, A., Kimura, I., Tsujimoto, G. & Hirasawa, A. 2014. Role of free fatty acid receptors in the regulation of energy metabolism. *Biochim Biophys Acta,* 1841 (9)**,** 1292-300. Doi: 10.1016/j.bbalip.2014.06.002

Hill, S. J., Williams, C. & May, L. T. 2010. Insights into GPCR pharmacology from the measurement of changes in intracellular cyclic AMP; advantages and pitfalls of differing methodologies. *Br J Pharmacol,* 161 (6)**,** 1266-75. Doi: 10.1111/j.1476-5381.2010.00779.x

Hillger, J. M., Le Roy, B., Wang, Z., Mulder-Krieger, T., Boomsma, D. I., Slagboom, P. E., Danen, E. H. J., Ap, I. J. & Heitman, L. H. 2017. Phenotypic screening of cannabinoid receptor 2 ligands shows different sensitivity to genotype. *Biochem Pharmacol,* 130**,** 60-70. Doi: 10.1016/j.bcp.2017.01.014

Hirasawa, A., Tsumaya, K., Awaji, T., Katsuma, S., Adachi, T., Yamada, M., Sugimoto, Y., Miyazaki, S. & Tsujimoto, G. 2005. Free fatty acids regulate gut incretin glucagon-like peptide-1 secretion through GPR120. *Nat Med,* 11 (1)**,** 90-4. Doi: 10.1038/nm1168

Hodson, L. & Fielding, B. A. 2010. Trafficking and partitioning of fatty acids: the transition from fasted to fed state. *Clinical Lipidology,* 5 (1)**,** 131-144. Doi: 10.2217/clp.09.72

Hohenhaus, D. M., Schaale, K., Le Cao, K. A., Seow, V., Iyer, A., Fairlie, D. P. & Sweet, M. J. 2013. An mRNA atlas of G protein-coupled receptor expression during primary human monocyte/macrophage differentiation and lipopolysaccharide-mediated activation identifies targetable candidate regulators of inflammation. *Immunobiology,* 218 (11)**,** 1345-53. Doi: 10.1016/j.imbio.2013.07.001

Houten, S. M. & Wanders, R. J. 2010. A general introduction to the biochemistry of mitochondrial fatty acid β-oxidation. *J Inherit Metab Dis,* 33 (5)**,** 469-77. Doi: 10.1007/s10545-010-9061-2

Howlett, A. C. 2002. The cannabinoid receptors. *Prostaglandins Other Lipid Mediat,* 68-69**,** 619-31. Doi: 10.1016/s0090-6980(02)00060-6

Huang, Q., Feng, D., Liu, K., Wang, P., Xiao, H., Wang, Y., Zhang, S. & Liu, Z. 2014. A medium-chain fatty acid receptor Gpr84 in zebrafish: Expression pattern and roles in immune regulation. *Developmental & Comparative Immunology,* 45 (2)**,** 252-258. Doi: 10.1016/j.dci.2014.03.017

Hume, D. A., Halpin, D., Charlton, H. & Gordon, S. 1984. The mononuclear phagocyte system of the mouse defined by immunohistochemical localization of antigen F4/80: macrophages of endocrine organs. *Proc Natl Acad Sci U S A,* 81 (13)**,** 4174-7. Doi: 10.1073/pnas.81.13.4174

Ichimura, A., Hirasawa, A., Hara, T. & Tsujimoto, G. 2009. Free fatty acid receptors act as nutrient sensors to regulate energy homeostasis. *Prostaglandins Other Lipid Mediat,* 89 (3-4)**,** 82-8. Doi: 10.1016/j.prostaglandins.2009.05.003

Ichimura, A., Hirasawa, A., Poulain-Godefroy, O., Bonnefond, A., Hara, T., Yengo, L., Kimura, I., Leloire, A., Liu, N., Iida, K., Choquet, H., Besnard, P., Lecoeur, C., Vivequin, S., Ayukawa, K., Takeuchi, M., Ozawa, K., Tauber, M., Maffeis, C., Morandi, A., Buzzetti, R., Elliott, P., Pouta, A., Jarvelin, M. R., Körner, A., Kiess, W., Pigeyre, M., Caiazzo, R., Van Hul, W., Van Gaal, L., Horber, F., Balkau, B., Lévy-Marchal, C., Rouskas, K., Kouvatsi, A., Hebebrand, J., Hinney, A., Scherag, A., Pattou, F., Meyre, D., Koshimizu, T. A., Wolowczuk, I., Tsujimoto, G. & Froguel, P. 2012. Dysfunction of lipid sensor GPR120 leads to obesity in both mouse and human. *Nature,* 483 (7389)**,** 350-4. Doi: 10.1038/nature10798

Iqbal, A. J., Regan-Komito, D., Christou, I., White, G. E., Mcneill, E., Kenyon, A., Taylor, L., Kapellos, T. S., Fisher, E. A., Channon, K. M. & Greaves, D. R. 2013. A real time chemotaxis assay unveils unique migratory profiles amongst different primary murine macrophages. *PLoS One,* 8 (3)**,** e58744. Doi: 10.1371/journal.pone.0058744

Israelsson, C., Bengtsson, H., Kylberg, A., Kullander, K., Lewén, A., Hillered, L. & Ebendal, T. 2008. Distinct cellular patterns of upregulated chemokine expression supporting a prominent inflammatory role in traumatic brain injury. *J Neurotrauma,* 25 (8)**,** 959-74. Doi: 10.1089/neu.2008.0562

Itoh, Y. & Hinuma, S. 2005. GPR40, a free fatty acid receptor on pancreatic beta cells, regulates insulin secretion. *Hepatol Res,* 33 (2)**,** 171-3. Doi: 10.1016/j.hepres.2005.09.028

Itoh, Y., Kawamata, Y., Harada, M., Kobayashi, M., Fujii, R., Fukusumi, S., Ogi, K., Hosoya, M., Tanaka, Y., Uejima, H., Tanaka, H., Maruyama, M., Satoh, R., Okubo, S., Kizawa, H., Komatsu, H., Matsumura, F., Noguchi, Y., Shinohara, T., Hinuma, S., Fujisawa, Y. & Fujino, M. 2003. Free fatty acids regulate insulin secretion from pancreatic beta cells through GPR40. *Nature,* 422 (6928)**,** 173-6. Doi: 10.1038/nature01478

Jenkins, L., Marsango, S., Mancini, S., Mahmud, Z. A., Morrison, A., Mcelroy, S. P., Bennett, K. A., Barnes, M., Tobin, A. B., Tikhonova, I. G. & Milligan, G. 2021. Discovery and Characterization of Novel Antagonists of the Proinflammatory Orphan Receptor GPR84. *ACS Pharmacol Transl Sci,* 4 (5)**,** 1598-1613. Doi: 10.1021/acsptsci.1c00151

Jenske, R. & Vetter, W. 2008. Enantioselective analysis of 2- and 3-hydroxy fatty acids in food samples. *J Agric Food Chem,* 56 (24)**,** 11578-83. Doi: 10.1021/jf802772a

Jenske, R. & Vetter, W. 2009. Concentrations of medium-chain 2- and 3-hydroxy fatty acids in foodstuffs. *Food Chemistry,* 114 (3)**,** 1122-1129. Doi: 10.1016/j.foodchem.2008.10.067

Jin, S. J., Hoppel, C. L. & Tserng, K. Y. 1992. Incomplete fatty acid oxidation. The production and epimerization of 3-hydroxy fatty acids. *J Biol Chem,* 267 (1)**,** 119-25.

Jin, T., Xu, X. & Hereld, D. 2008. Chemotaxis, chemokine receptors and human disease. *Cytokine,* 44 (1)**,** 1-8. Doi: 10.1016/j.cyto.2008.06.017

Jones, P. M. & Bennett, M. J. 2011. Clinical applications of 3-hydroxy fatty acid analysis by gas chromatography-mass spectrometry. *Biochim Biophys Acta,* 1811 (11)**,** 657-62. Doi: 10.1016/j.bbalip.2011.06.026

Joost, P. & Methner, A. 2002. Phylogenetic analysis of 277 human G-protein-coupled receptors as a tool for the prediction of orphan receptor ligands. *Genome Biol,* 3 (11)**,** Research0063. Doi: 10.1186/gb-2002-3-11-research0063

Jung, M., Shim, S., Im, Y. B., Park, W. B. & Yoo, H. S. 2018. Global gene-expression profiles of intracellular survival of the BruAb2_1031 gene mutated Brucella abortus in professional phagocytes, RAW 264.7 cells. *BMC Microbiol,* 18 (1)**,** 82. Doi: 10.1186/s12866-018-1223-7

Kalita, M., Park, J. H., Kuo, R. C., Hayee, S., Marsango, S., Straniero, V., Alam, I. S., Rivera-Rodriguez, A., Pandrala, M., Carlson, M. L., Reyes, S. T., Jackson, I. M., Suigo, L., Luo, A., Nagy, S. C., Valoti, E., Milligan, G., Habte, F., Shen, B. & James, M. L. 2023. PET Imaging of Innate Immune Activation Using (11)C Radiotracers Targeting GPR84. *JACS Au,* 3 (12)**,** 3297-3310. Doi: 10.1021/jacsau.3c00435

Kamber, R. A., Nishiga, Y., Morton, B., Banuelos, A. M., Barkal, A. A., Vences-Catalán, F., Gu, M., Fernandez, D., Seoane, J. A., Yao, D., Liu, K., Lin, S., Spees, K., Curtis, C., Jerby-Arnon, L., Weissman, I. L., Sage, J. & Bassik, M. C. 2021. Inter-cellular CRISPR screens reveal regulators of cancer cell phagocytosis. *Nature,* 597 (7877)**,** 549-554. Doi: 10.1038/s41586-021-03879-4

Kammermann, M., Denelavas, A., Imbach, A., Grether, U., Dehmlow, H., Apfel, C. M. & Hertel, C. 2011. Impedance measurement: a new method to detect ligand-biased receptor signaling. *Biochem Biophys Res Commun,* 412 (3)**,** 419-24. Doi: 10.1016/j.bbrc.2011.07.087

Kang, S. S., Kim, H. J., Jang, M. S., Moon, S., In Lee, S., Jeon, J. H., Baik, J. E., Park, O. J., Son, Y. M., Kim, G. R., Joo, D., Kim, H., Han, J. Y., Yun, C. H. & Han, S. H. 2012. Gene expression profile of human peripheral blood mononuclear cells induced by Staphylococcus aureus lipoteichoic acid. *Int Immunopharmacol,* 13 (4)**,** 454-60. Doi: 10.1016/j.intimp.2012.05.010

Karpe, F., Dickmann, J. R. & Frayn, K. N. 2011. Fatty acids, obesity, and insulin resistance: time for a reevaluation. *Diabetes,* 60 (10)**,** 2441-9. Doi: 10.2337/db11-0425

Kaspersen, M. H., Jenkins, L., Dunlop, J., Milligan, G. & Ulven, T. 2017. Succinct synthesis of saturated hydroxy fatty acids and in vitro evaluation of all hydroxylauric acids on FFA1, FFA4 and GPR84. *Medchemcomm,* 8 (6)**,** 1360-1365. Doi: 10.1039/c7md00130d

Kelly, E., Bailey, C. P. & Henderson, G. 2008. Agonist-selective mechanisms of GPCR desensitization. *Br J Pharmacol,* 153 Suppl 1 (Suppl 1)**,** S379-88. Doi: 10.1038/sj.bjp.0707604

Kenakin, T. 2003. Ligand-selective receptor conformations revisited: the promise and the problem. *Trends Pharmacol Sci,* 24 (7)**,** 346-54. Doi: 10.1016/s0165-6147(03)00167-6

Kenakin, T. 2005. New concepts in drug discovery: collateral efficacy and permissive antagonism. *Nat Rev Drug Discov,* 4 (11)**,** 919-27. Doi: 10.1038/nrd1875

Kenakin, T. 2007. Functional selectivity through protean and biased agonism: who steers the ship? *Mol Pharmacol,* 72 (6)**,** 1393-401. Doi: 10.1124/mol.107.040352

Khalil, N., Manganas, H., Ryerson, C. J., Shapera, S., Cantin, A. M., Hernandez, P., Turcotte, E. E., Parker, J. M., Moran, J. E., Albert, G. R., Sawtell, R., Hagerimana, A., Laurin, P., Gagnon, L., Cesari, F. & Kolb, M. 2019. Phase 2 clinical trial of PBI-4050 in patients with idiopathic pulmonary fibrosis. *Eur Respir J,* 53 (3)**,** 1800663. Doi: 10.1183/13993003.00663-2018

Kienle, K., Glaser, K. M., Eickhoff, S., Mihlan, M., Knöpper, K., Reátegui, E., Epple, M. W., Gunzer, M., Baumeister, R., Tarrant, T. K., Germain, R. N., Irimia, D., Kastenmüller, W. & Lämmermann, T. 2021. Neutrophils self-limit swarming to contain bacterial growth in vivo. *Science,* 372 (6548)**,** eabe7729. Doi: 10.1126/science.abe7729

Kim, D.-H., Park, J. C., Lee, Y. H., Hagiwara, A. & Lee, J.-S. 2021. Genome-wide identification of 216 G protein-coupled receptor (GPCR) genes from the marine water flea Diaphanosoma celebensis. *Comparative Biochemistry and Physiology Part D: Genomics and Proteomics,* 40**,** 100922. Doi: 10.1016/j.cbd.2021.100922

Kim, K. A., Gu, W., Lee, I. A., Joh, E. H. & Kim, D. H. 2012. High fat diet-induced gut microbiota exacerbates inflammation and obesity in mice via the TLR4 signaling pathway. *PLoS One,* 7 (10)**,** e47713. Doi: 10.1371/journal.pone.0047713

Kimura, I., Ichimura, A., Ohue-Kitano, R. & Igarashi, M. 2020. Free Fatty Acid Receptors in Health and Disease. *Physiol Rev,* 100 (1)**,** 171-210. Doi: 10.1152/physrev.00041.2018

Kimura, M., Yoon, H. R., Wasant, P., Takahashi, Y. & Yamaguchi, S. 2002. A sensitive and simplified method to analyze free fatty acids in children with mitochondrial beta oxidation disorders using gas chromatography/mass spectrometry and dried blood spots. *Clin Chim Acta,* 316 (1-2)**,** 117-21. Doi: 10.1016/s0009-8981(01)00741-0

Klein Herenbrink, C., Sykes, D. A., Donthamsetti, P., Canals, M., Coudrat, T., Shonberg, J., Scammells, P. J., Capuano, B., Sexton, P. M., Charlton, S. J., Javitch, J. A., Christopoulos, A. & Lane, J. R. 2016. The role of kinetic context in apparent biased agonism at GPCRs. *Nat Commun,* 7**,** 10842. Doi: 10.1038/ncomms10842

Kohout, T. A., Nicholas, S. L., Perry, S. J., Reinhart, G., Junger, S. & Struthers, R. S. 2004. Differential desensitization, receptor phosphorylation, beta-arrestin recruitment, and ERK1/2 activation by the two endogenous ligands for the CC chemokine receptor 7. *J Biol Chem,* 279 (22)**,** 23214-22. Doi: 10.1074/jbc.M402125200

Köse, M., Pillaiyar, T., Namasivayam, V., De Filippo, E., Sylvester, K., Ulven, T., Von Kügelgen, I. & Müller, C. E. 2020. An Agonist Radioligand for the Proinflammatory Lipid-Activated G Protein-Coupled Receptor GPR84 Providing Structural Insights. *J Med Chem,* 63 (5)**,** 2391-2410. Doi: 10.1021/acs.jmedchem.9b01339

Kunwar, P. S., Starz-Gaiano, M., Bainton, R. J., Heberlein, U. & Lehmann, R. 2003. Tre1, a G protein-coupled receptor, directs transepithelial migration of Drosophila germ cells. *PLoS Biol,* 1 (3)**,** E80. Doi: 10.1371/journal.pbio.0000080

Labarthe, F., Gélinas, R. & Des Rosiers, C. 2008. Medium-chain fatty acids as metabolic therapy in cardiac disease. *Cardiovasc Drugs Ther,* 22 (2)**,** 97-106. Doi: 10.1007/s10557-008-6084-0

Labéguère, F., Dupont, S., Alvey, L., Soulas, F., Newsome, G., Tirera, A., Quenehen, V., Mai, T. T. T., Deprez, P., Blanqué, R., Oste, L., Le Tallec, S., De Vos, S., Hagers, A., Vandevelde, A., Nelles, L., Vandervoort, N., Conrath, K., Christophe, T., Van Der Aar, E., Wakselman, E., Merciris, D., Cottereaux, C., Da Costa, C., Saniere, L., Clement-Lacroix, P., Jenkins, L., Milligan, G., Fletcher, S., Brys, R. & Gosmini, R. 2020. Discovery of 9-Cyclopropylethynyl-2-((S)-1-[1,4]dioxan-2-ylmethoxy)-6,7-dihydropyrimido[6,1-a]isoquinolin-4-one (GLPG1205), a Unique GPR84 Negative Allosteric Modulator Undergoing Evaluation in a Phase II Clinical Trial. *J Med Chem,* 63 (22)**,** 13526-13545. Doi: 10.1021/acs.jmedchem.0c00272

Lagerstedt, S. A., Hinrichs, D. R., Batt, S. M., Magera, M. J., Rinaldo, P. & Mcconnell, J. P. 2001. Quantitative determination of plasma c8-c26 total fatty acids for the biochemical diagnosis of nutritional and metabolic disorders. *Mol Genet Metab,* 73 (1)**,** 38-45. Doi: 10.1006/mgme.2001.3170

Lattin, J. E., Schroder, K., Su, A. I., Walker, J. R., Zhang, J., Wiltshire, T., Saijo, K., Glass, C. K., Hume, D. A., Kellie, S. & Sweet, M. J. 2008. Expression analysis of G Protein-Coupled Receptors in mouse macrophages. *Immunome Res,* 4**,** 5. Doi: 10.1186/1745-7580-4-5

Le Poul, E., Loison, C., Struyf, S., Springael, J. Y., Lannoy, V., Decobecq, M. E., Brezillon, S., Dupriez, V., Vassart, G., Van Damme, J., Parmentier, M. & Detheux, M. 2003. Functional characterization of human receptors for short chain fatty acids and their role in polymorphonuclear cell activation. *J Biol Chem,* 278 (28)**,** 25481-9. Doi: 10.1074/jbc.M301403200

Leung, G., Tang, H. R., Mcguinness, R., Verdonk, E., Michelotti, J. M. & Liu, V. F. 2005. Cellular Dielectric Spectroscopy: A Label-Free Technology for Drug Discovery. *JALA: Journal of the Association for Laboratory Automation,* 10 (4)**,** 258-269. Doi: 10.1016/j.jala.2005.06.002

Li, S. X., Wang, S. W., Chen, L. H., Zhang, Q., Lu, D., Chen, J., Fang, Y. C., Gu, M., Xie, X. & Nan, F. J. 2023a. Unsymmetrical Phosphodiesters as GPR84 Antagonists with High Blood Exposure for the Treatment of Lung Inflammation. *J Med Chem,* 66 (8)**,** 5820-5838. Doi: 10.1021/acs.jmedchem.3c00053

Li, Y., Song, W. J., Yi, S. K., Yu, H. X., Mo, H. L., Yao, M. X., Tao, Y. X. & Wang, L. X. 2023b. Molecular Cloning, Tissue Distribution, and Pharmacological Characterization of GPR84 in Grass Carp (Ctenopharyngodon Idella). *Animals (Basel),* 13 (19)**,** 3001. Doi: 10.3390/ani13193001

Lichtenstein, L., Mattijssen, F., De Wit, N. J., Georgiadi, A., Hooiveld, G. J., Van Der Meer, R., He, Y., Qi, L., Köster, A., Tamsma, J. T., Tan, N. S., Müller, M. & Kersten, S. 2010. Angptl4 protects against severe proinflammatory effects of saturated fat by inhibiting fatty acid

uptake into mesenteric lymph node macrophages. *Cell Metab,* 12 (6)**,** 580-92. Doi: 10.1016/j.cmet.2010.11.002

Lipinski, C. A., Lombardo, F., Dominy, B. W. & Feeney, P. J. 1997. Experimental and computational approaches to estimate solubility and permeability in drug discovery and development settings. *Advanced Drug Delivery Reviews,* 23 (1)**,** 3-25. Doi: 10.1016/S0169-409X(96)00423-1

Liu, D., Costanzo, A., Evans, M. D. M., Archer, N. S., Nowson, C., Duesing, K. & Keast, R. 2018. Expression of the candidate fat taste receptors in human fungiform papillae and the association with fat taste function. *Br J Nutr,* 120 (1)**,** 64-73. Doi: 10.1017/s0007114518001265

Liu, H., Zhang, Q., He, X., Jiang, M., Wang, S., Yan, X., Cheng, X., Liu, Y., Nan, F. J., Xu, H. E., Xie, X. & Yin, W. 2023. Structural insights into ligand recognition and activation of the medium-chain fatty acid-sensing receptor GPR84. *Nat Commun,* 14 (1)**,** 3271. Doi: 10.1038/s41467-023-38985-6

Liu, Y., Xu, H., Dahir, N., Calder, A., Lin, F. & Gilbertson, T. A. 2021. GPR84 Is Essential for the Taste of Medium Chain Saturated Fatty Acids. *J Neurosci,* 41 (24)**,** 5219-5228. Doi: 10.1523/jneurosci.2530-20.2021

Liu, Y., Zhang, Q., Chen, L. H., Yang, H., Lu, W., Xie, X. & Nan, F. J. 2016. Design and Synthesis of 2-Alkylpyrimidine-4,6-diol and 6-Alkylpyridine-2,4-diol as Potent GPR84 Agonists. *ACS Med Chem Lett,* 7 (6)**,** 579-83. Doi: 10.1021/acsmedchemlett.6b00025

Lotti, C., Rubert, J., Fava, F., Tuohy, K., Mattivi, F. & Vrhovsek, U. 2017. Development of a fast and cost-effective gas chromatography-mass spectrometry method for the quantification of short-chain and medium-chain fatty acids in human biofluids. *Anal Bioanal Chem,* 409 (23)**,** 5555-5567. Doi: 10.1007/s00216-017-0493-5

Lowe, J. D., Sanderson, H. S., Cooke, A. E., Ostovar, M., Tsisanova, E., Withey, S. L., Chavkin, C., Husbands, S. M., Kelly, E., Henderson, G. & Bailey, C. P. 2015. Role of G Protein-Coupled Receptor Kinases 2 and 3 in μ-Opioid Receptor Desensitization and Internalization. *Mol Pharmacol,* 88 (2)**,** 347-56. Doi: 10.1124/mol.115.098293

Lu, V. B., Gribble, F. M. & Reimann, F. 2018. Free Fatty Acid Receptors in Enteroendocrine Cells. *Endocrinology,* 159 (7)**,** 2826-2835. Doi: 10.1210/en.2018-00261

Lucy, D., Purvis, G. S. D., Zeboudj, L., Chatzopoulou, M., Recio, C., Bataille, C. J. R., Wynne, G. M., Greaves, D. R. & Russell, A. J. 2019. A Biased Agonist at Immunometabolic Receptor GPR84 Causes Distinct Functional Effects in Macrophages. *ACS Chem Biol,* 14 (9)**,** 2055-2064. Doi: 10.1021/acschembio.9b00533

Luscombe, V. B., Baena-López, L. A., Bataille, C. J. R., Russell, A. J. & Greaves, D. R. 2023a. Kinetic insights into agonist-dependent signalling bias at the pro-inflammatory G-protein coupled receptor GPR84. *Eur J Pharmacol,* 956**,** 175960. Doi: 10.1016/j.ejphar.2023.175960

Luscombe, V. B., Lucy, D., Bataille, C. J. R., Russell, A. J. & Greaves, D. R. 2020. 20 Years an Orphan: Is GPR84 a Plausible Medium-Chain Fatty Acid-Sensing Receptor? *DNA Cell Biol,* 39 (11)**,** 1926-1937. Doi: 10.1089/dna.2020.5846

Luscombe, V. B., Wang, P., Russell, A. J. & Greaves, D. R. 2023b. Biased agonists of GPR84 and insights into biological control. *British Journal of Pharmacology,* Accepted (n/a)**,** 1–15. Doi: doi.org/10.1111/bph.16310

Madeddu, S., Woods, T. A., Mukherjee, P., Sturdevant, D., Butchi, N. B. & Peterson, K. E. 2015. Identification of Glial Activation Markers by Comparison of Transcriptome Changes between Astrocytes and Microglia following Innate Immune Stimulation. *PLoS One,* 10 (7)**,** e0127336. Doi: 10.1371/journal.pone.0127336

Maglott, D., Ostell, J., Pruitt, K. D. & Tatusova, T. 2005. Entrez Gene: gene-centered information at NCBI. *Nucleic Acids Research,* 33 (suppl_1)**,** D54-D58. Doi: 10.1093/nar/gki031

Mahmud, Z. A., Jenkins, L., Ulven, T., Labéguère, F., Gosmini, R., De Vos, S., Hudson, B. D., Tikhonova, I. G. & Milligan, G. 2017. Three classes of ligands each bind to distinct sites on the orphan G protein-coupled receptor GPR84. *Sci Rep,* 7 (1)**,** 17953. Doi: 10.1038/s41598-017-18159-3

Mancini, S. J., Mahmud, Z. A., Jenkins, L., Bolognini, D., Newman, R., Barnes, M., Edye, M. E., Mcmahon, S. B., Tobin, A. B. & Milligan, G. 2019. On-target and off-target effects of novel orthosteric and allosteric activators of GPR84. *Sci Rep,* 9 (1)**,** 1861. Doi: 10.1038/s41598-019-38539-1

Marlo, J. E., Niswender, C. M., Days, E. L., Bridges, T. M., Xiang, Y., Rodriguez, A. L., Shirey, J. K., Brady, A. E., Nalywajko, T., Luo, Q., Austin, C. A., Williams, M. B., Kim, K., Williams, R., Orton, D., Brown, H. A., Lindsley, C. W., Weaver, C. D. & Conn, P. J. 2009. Discovery and characterization of novel allosteric potentiators of M1 muscarinic receptors reveals multiple modes of activity. *Mol Pharmacol,* 75 (3)**,** 577-88. Doi: 10.1124/mol.108.052886

Marsango, S., Ward, R. J., Jenkins, L., Butcher, A. J., Al Mahmud, Z., Dwomoh, L., Nagel, F., Schulz, S., Tikhonova, I. G., Tobin, A. B. & Milligan, G. 2022. Selective phosphorylation of threonine residues defines GPR84-arrestin interactions of biased ligands. *J Biol Chem,* 298 (5)**,** 101932. Doi: 10.1016/j.jbc.2022.101932

Mårtensson, J., Sundqvist, M., Manandhar, A., Ieremias, L., Zhang, L., Ulven, T., Xie, X., Björkman, L. & Forsman, H. 2021. The Two Formyl Peptide Receptors Differently Regulate GPR84-Mediated Neutrophil NADPH Oxidase Activity. *J Innate Immun,* 13 (4)**,** 242-256. Doi: 10.1159/000514887

Mashukova, A., Spehr, M., Hatt, H. & Neuhaus, E. M. 2006. Beta-arrestin2-mediated internalization of mammalian odorant receptors. *J Neurosci,* 26 (39)**,** 9902-12. Doi: 10.1523/jneurosci.2897-06.2006

Mcdonald, B., Pittman, K., Menezes, G. B., Hirota, S. A., Slaba, I., Waterhouse, C. C., Beck, P. L., Muruve, D. A. & Kubes, P. 2010. Intravascular danger signals guide neutrophils to sites of sterile inflammation. *Science,* 330 (6002)**,** 362-6. Doi: 10.1126/science.1195491

Meng, Y., Zhang, J., Zhang, F., Ai, W., Zhu, X., Shu, G., Wang, L., Gao, P., Xi, Q., Zhang, Y., Liang, X., Jiang, Q. & Wang, S. 2017. Lauric Acid Stimulates Mammary Gland Development of Pubertal Mice through Activation of GPR84 and PI3K/Akt Signaling Pathway. *J Agric Food Chem,* 65 (1)**,** 95-103. Doi: 10.1021/acs.jafc.6b04878

Mikkelsen, R. B., Arora, T., Trošt, K., Dmytriyeva, O., Jensen, S. K., Meijnikman, A. S., Olofsson, L. E., Lappa, D., Aydin, Ö., Nielsen, J., Gerdes, V., Moritz, T., Van De Laar, A., De Brauw, M., Nieuwdorp, M., Hjorth, S. A., Schwartz, T. W. & Bäckhed, F. 2022. Type 2 diabetes is

associated with increased circulating levels of 3-hydroxydecanoate activating GPR84 and neutrophil migration. *iScience,* 25 (12)**,** 105683. Doi: 10.1016/j.isci.2022.105683

Montgomery, M. K., Osborne, B., Brandon, A. E., O'reilly, L., Fiveash, C. E., Brown, S. H. J., Wilkins, B. P., Samsudeen, A., Yu, J., Devanapalli, B., Hertzog, A., Tolun, A. A., Kavanagh, T., Cooper, A. A., Mitchell, T. W., Biden, T. J., Smith, N. J., Cooney, G. J. & Turner, N. 2019. Regulation of mitochondrial metabolism in murine skeletal muscle by the medium-chain fatty acid receptor Gpr84. *Faseb j,* 33 (11)**,** 12264-12276. Doi: 10.1096/fj.201900234R

Moodaley, R., Smith, D. M., Tough, I. R., Schindler, M. & Cox, H. M. 2017. Agonism of free fatty acid receptors 1 and 4 generates peptide YY-mediated inhibitory responses in mouse colon. *Br J Pharmacol,* 174 (23)**,** 4508-4522. Doi: 10.1111/bph.14054

Moore-Morris, T., Varrault, A., Mangoni, M. E., Le Digarcher, A., Negre, V., Dantec, C., Journot, L., Nargeot, J. & Couette, B. 2009. Identification of potential pharmacological targets by analysis of the comprehensive G protein-coupled receptor repertoire in the four cardiac chambers. *Mol Pharmacol,* 75 (5)**,** 1108-16. Doi: 10.1124/mol.108.054155

Moran, S. P., Cho, H. P., Maksymetz, J., Remke, D. H., Hanson, R. M., Niswender, C. M., Lindsley, C. W., Rook, J. M. & Conn, P. J. 2018. PF-06827443 Displays Robust Allosteric Agonist and Positive Allosteric Modulator Activity in High Receptor Reserve and Native Systems. *ACS Chem Neurosci,* 9 (9)**,** 2218-2224. Doi: 10.1021/acschemneuro.8b00106

Moran, S. P., Xiang, Z., Doyle, C. A., Maksymetz, J., Lv, X., Faltin, S., Fisher, N. M., Niswender, C. M., Rook, J. M., Lindsley, C. W. & Conn, P. J. 2019. Biased M1 receptor-positive allosteric modulators reveal role of phospholipase D in M1-dependent rodent cortical plasticity. *Sci Signal,* 12 (610)**,** eaax2057. Doi: 10.1126/scisignal.aax2057

Mori, K., Naganuma, T. & Kihara, A. 2023. Role of 2-hydroxy acyl-CoA lyase HACL2 in odd-chain fatty acid production via α-oxidation in vivo. *Mol Biol Cell,* 34 (9)**,** ar85. Doi: 10.1091/mbc.E23-02-0042

Moura-Alves, P., Puyskens, A., Stinn, A., Klemm, M., Guhlich-Bornhof, U., Dorhoi, A., Furkert, J., Kreuchwig, A., Protze, J., Lozza, L., Pei, G., Saikali, P., Perdomo, C., Mollenkopf, H. J., Hurwitz, R., Kirschhoefer, F., Brenner-Weiss, G., Weiner, J., 3rd, Oschkinat, H., Kolbe, M., Krause, G. & Kaufmann, S. H. E. 2019. Host monitoring of quorum sensing during Pseudomonas aeruginosa infection. *Science,* 366 (6472)**,** eaaw1629. Doi: 10.1126/science.aaw1629

Mu, H. & Høy, C. E. 2004. The digestion of dietary triacylglycerols. *Prog Lipid Res,* 43 (2)**,** 105-33. Doi: 10.1016/s0163-7827(03)00050-x

Müller, M. M., Lehmann, R., Klassert, T. E., Reifenstein, S., Conrad, T., Moore, C., Kuhn, A., Behnert, A., Guthke, R., Driesch, D. & Slevogt, H. 2017. Global analysis of glycoproteins identifies markers of endotoxin tolerant monocytes and GPR84 as a modulator of TNFα expression. *Sci Rep,* 7 (1)**,** 838. Doi: 10.1038/s41598-017-00828-y

Mullershausen, F., Zecri, F., Cetin, C., Billich, A., Guerini, D. & Seuwen, K. 2009. Persistent signaling induced by FTY720-phosphate is mediated by internalized S1P1 receptors. *Nat Chem Biol,* 5 (6)**,** 428-34. Doi: 10.1038/nchembio.173

Muredda, L., Kępczyńska, M. A., Zaibi, M. S., Alomar, S. Y. & Trayhurn, P. 2018. IL-1β and TNFα inhibit GPR120 (FFAR4) and stimulate GPR84 (EX33) and GPR41 (FFAR3) fatty acid receptor expression in human adipocytes: implications for the anti-inflammatory action of

n-3 fatty acids. *Arch Physiol Biochem,* 124 (2), 97-108. Doi: 10.1080/13813455.2017.1364774

Nagasaki, H., Kondo, T., Fuchigami, M., Hashimoto, H., Sugimura, Y., Ozaki, N., Arima, H., Ota, A., Oiso, Y. & Hamada, Y. 2012. Inflammatory changes in adipose tissue enhance expression of GPR84, a medium-chain fatty acid receptor: TNFα enhances GPR84 expression in adipocytes. *FEBS Lett,* 586 (4), 368-72. Doi: 10.1016/j.febslet.2012.01.001

New, D. C., Wu, K., Kwok, A. W. & Wong, Y. H. 2007. G protein-coupled receptor-induced Akt activity in cellular proliferation and apoptosis. *Febs j,* 274 (23), 6025-36. Doi: 10.1111/j.1742-4658.2007.06116.x

Nguyen, Q. T., Nsaibia, M. J., Sirois, M. G., Calderone, A., Tardif, J. C., Fen Shi, Y., Ruiz, M., Daneault, C., Gagnon, L., Grouix, B., Laurin, P. & Dupuis, J. 2020. PBI-4050 reduces pulmonary hypertension, lung fibrosis, and right ventricular dysfunction in heart failure. *Cardiovasc Res,* 116 (1), 171-182. Doi: 10.1093/cvr/cvz034

Nicol, L. S., Dawes, J. M., La Russa, F., Didangelos, A., Clark, A. K., Gentry, C., Grist, J., Davies, J. B., Malcangio, M. & Mcmahon, S. B. 2015. The role of G-protein receptor 84 in experimental neuropathic pain. *J Neurosci,* 35 (23), 8959-69. Doi: 10.1523/jneurosci.3558-14.2015

Nikaido, Y., Koyama, Y., Yoshikawa, Y., Furuya, T. & Takeda, S. 2015. Mutation analysis and molecular modeling for the investigation of ligand-binding modes of GPR84. *J Biochem,* 157 (5), 311-20. Doi: 10.1093/jb/mvu075

Nobles, K. N., Xiao, K., Ahn, S., Shukla, A. K., Lam, C. M., Rajagopal, S., Strachan, R. T., Huang, T. Y., Bressler, E. A., Hara, M. R., Shenoy, S. K., Gygi, S. P. & Lefkowitz, R. J. 2011. Distinct phosphorylation sites on the β(2)-adrenergic receptor establish a barcode that encodes differential functions of β-arrestin. *Sci Signal,* 4 (185), ra51. Doi: 10.1126/scisignal.2001707

O'leary, N. A., Wright, M. W., Brister, J. R., Ciufo, S., Haddad, D., Mcveigh, R., Rajput, B., Robbertse, B., Smith-White, B., Ako-Adjei, D., Astashyn, A., Badretdin, A., Bao, Y., Blinkova, O., Brover, V., Chetvernin, V., Choi, J., Cox, E., Ermolaeva, O., Farrell, C. M., Goldfarb, T., Gupta, T., Haft, D., Hatcher, E., Hlavina, W., Joardar, V. S., Kodali, V. K., Li, W., Maglott, D., Masterson, P., Mcgarvey, K. M., Murphy, M. R., O'neill, K., Pujar, S., Rangwala, S. H., Rausch, D., Riddick, L. D., Schoch, C., Shkeda, A., Storz, S. S., Sun, H., Thibaud-Nissen, F., Tolstoy, I., Tully, R. E., Vatsan, A. R., Wallin, C., Webb, D., Wu, W., Landrum, M. J., Kimchi, A., Tatusova, T., Dicuccio, M., Kitts, P., Murphy, T. D. & Pruitt, K. D. 2016. Reference sequence (RefSeq) database at NCBI: current status, taxonomic expansion, and functional annotation. *Nucleic Acids Res,* 44 (D1), D733-45. Doi: 10.1093/nar/gkv1189

Offermanns, S. & Schwaninger, M. 2015. Nutritional or pharmacological activation of HCA(2) ameliorates neuroinflammation. *Trends Mol Med,* 21 (4), 245-55. Doi: 10.1016/j.molmed.2015.02.002

Oh, D. Y., Talukdar, S., Bae, E. J., Imamura, T., Morinaga, H., Fan, W., Li, P., Lu, W. J., Watkins, S. M. & Olefsky, J. M. 2010. GPR120 is an omega-3 fatty acid receptor mediating potent anti-inflammatory and insulin-sensitizing effects. *Cell,* 142 (5), 687-98. Doi: 10.1016/j.cell.2010.07.041

Ohue-Kitano, R., Nonaka, H., Nishida, A., Masujima, Y., Takahashi, D., Ikeda, T., Uwamizu, A., Tanaka, M., Kohjima, M., Igarashi, M., Katoh, H., Tanaka, T., Inoue, A., Suganami, T.,

Hase, K., Ogawa, Y., Aoki, J. & Kimura, I. 2023. Medium-chain fatty acids suppress lipotoxicity-induced hepatic fibrosis via the immunomodulating receptor GPR84. *JCI Insight,* 8 (2)**,** e165469. Doi: 10.1172/jci.insight.165469

Onkenhout, W., Venizelos, V., Van Der Poel, P. F., Van Den Heuvel, M. P. & Poorthuis, B. J. 1995. Identification and quantification of intermediates of unsaturated fatty acid metabolism in plasma of patients with fatty acid oxidation disorders. *Clin Chem,* 41 (10)**,** 1467-74.

Oprea, T. I., Bologa, C. G., Brunak, S., Campbell, A., Gan, G. N., Gaulton, A., Gomez, S. M., Guha, R., Hersey, A., Holmes, J., Jadhav, A., Jensen, L. J., Johnson, G. L., Karlson, A., Leach, A. R., Ma'ayan, A., Malovannaya, A., Mani, S., Mathias, S. L., Mcmanus, M. T., Meehan, T. F., Von Mering, C., Muthas, D., Nguyen, D.-T., Overington, J. P., Papadatos, G., Qin, J., Reich, C., Roth, B. L., Schürer, S. C., Simeonov, A., Sklar, L. A., Southall, N., Tomita, S., Tudose, I., Ursu, O., Vidović, D., Waller, A., Westergaard, D., Yang, J. J. & Zahoránszky-Köhalmi, G. 2018. Unexplored therapeutic opportunities in the human genome. *Nature Reviews Drug Discovery,* 17 (5)**,** 317-332. Doi: 10.1038/nrd.2018.14

Oprea, T. I., Davis, A. M., Teague, S. J. & Leeson, P. D. 2001. Is there a difference between leads and drugs? A historical perspective. *J Chem Inf Comput Sci,* 41 (5)**,** 1308-15. Doi: 10.1021/ci010366a

Ostlund-Lindqvist, A. M., Gustafson, S., Lindqvist, P., Witztum, J. L. & Little, J. A. 1983. Uptake and degradation of human chylomicrons by macrophages in culture. Role of lipoprotein lipase. *Arteriosclerosis,* 3 (5)**,** 433-40. Doi: 10.1161/01.atv.3.5.433

Oyagawa, C. R. M., De La Harpe, S. M., Saroz, Y., Glass, M., Vernall, A. J. & Grimsey, N. L. 2018. Cannabinoid Receptor 2 Signalling Bias Elicited by 2,4,6-Trisubstituted 1,3,5-Triazines. *Front Pharmacol,* 9**,** 1202. Doi: 10.3389/fphar.2018.01202

Pandey, S., Kumari, P., Baidya, M., Kise, R., Cao, Y., Dwivedi-Agnihotri, H., Banerjee, R., Li, X. X., Cui, C. S., Lee, J. D., Kawakami, K., Maharana, J., Ranjan, A., Chaturvedi, M., Jhingan, G. D., Laporte, S. A., Woodruff, T. M., Inoue, A. & Shukla, A. K. 2021. Intrinsic bias at non-canonical, β-arrestin-coupled seven transmembrane receptors. *Mol Cell,* 81 (22)**,** 4605-4621.e11. Doi: 10.1016/j.molcel.2021.09.007

Panth, N., Abbott, K. A., Dias, C. B., Wynne, K. & Garg, M. L. 2018. Differential effects of medium- and long-chain saturated fatty acids on blood lipid profile: a systematic review and meta-analysis. *Am J Clin Nutr,* 108 (4)**,** 675-687. Doi: 10.1093/ajcn/nqy167

Papamandjaris, A. A., Macdougall, D. E. & Jones, P. J. 1998. Medium chain fatty acid metabolism and energy expenditure: obesity treatment implications. *Life Sci,* 62 (14)**,** 1203-15. Doi: 10.1016/s0024-3205(97)01143-0

Park, J. W., Yoon, H. J., Kang, W. Y., Cho, S., Seong, S. J., Lee, H. W., Yoon, Y. R. & Kim, H. J. 2018. G protein-coupled receptor 84 controls osteoclastogenesis through inhibition of NF-κB and MAPK signaling pathways. *J Cell Physiol,* 233 (2)**,** 1481-1489. Doi: 10.1002/jcp.26035

Pastori, C., Weiser, B., Barassi, C., Uberti-Foppa, C., Ghezzi, S., Longhi, R., Calori, G., Burger, H., Kemal, K., Poli, G., Lazzarin, A. & Lopalco, L. 2006. Long-lasting CCR5 internalization by antibodies in a subset of long-term nonprogressors: a possible protective effect against disease progression. *Blood,* 107 (12)**,** 4825-33. Doi: 10.1182/blood-2005-06-2463

Peiris, M., Aktar, R., Raynel, S., Hao, Z., Mumphrey, M. B., Berthoud, H. R. & Blackshaw, L. A. 2018. Effects of Obesity and Gastric Bypass Surgery on Nutrient Sensors, Endocrine Cells,

and Mucosal Innervation of the Mouse Colon. *Nutrients,* 10 (10)**,** 1529. Doi: 10.3390/nu10101529

Peiris, M., Aktar, R., Reed, D., Cibert-Goton, V., Zdanaviciene, A., Halder, W., Robinow, A., Corke, S., Dogra, H., Knowles, C. H. & Blackshaw, A. 2022. Decoy bypass for appetite suppression in obese adults: role of synergistic nutrient sensing receptors GPR84 and FFAR4 on colonic endocrine cells. *Gut,* 71 (5)**,** 928-937. Doi: 10.1136/gutjnl-2020-323219

Perry, K. J., Johnson, V. R., Malloch, E. L., Fukui, L., Wever, J., Thomas, A. G., Hamilton, P. W. & Henry, J. J. 2010. The G-protein-coupled receptor, GPR84, is important for eye development in Xenopus laevis. *Developmental Dynamics,* 239 (11)**,** 3024-3037. Doi: 10.1002/dvdy.22446

Petäjä-Repo, U. E., Hogue, M., Bhalla, S., Laperrière, A., Morello, J. P. & Bouvier, M. 2002. Ligands act as pharmacological chaperones and increase the efficiency of delta opioid receptor maturation. *Embo j,* 21 (7)**,** 1628-37. Doi: 10.1093/emboj/21.7.1628

Peters, A., Rabe, P., Krumbholz, P., Kalwa, H., Kraft, R., Schöneberg, T. & Stäubert, C. 2020. Natural biased signaling of hydroxycarboxylic acid receptor 3 and G protein-coupled receptor 84. *Cell Commun Signal,* 18 (1)**,** 31. Doi: 10.1186/s12964-020-0516-2

Peters, A., Rabe, P., Liebing, A. D., Krumbholz, P., Nordström, A., Jäger, E., Kraft, R. & Stäubert, C. 2022. Hydroxycarboxylic acid receptor 3 and GPR84 - Two metabolite-sensing G protein-coupled receptors with opposing functions in innate immune cells. *Pharmacol Res,* 176**,** 106047. Doi: 10.1016/j.phrs.2021.106047

Pillaiyar, T., Köse, M., Namasivayam, V., Sylvester, K., Borges, G., Thimm, D., Von Kügelgen, I. & Müller, C. E. 2018. 6-(Ar)Alkylamino-Substituted Uracil Derivatives: Lipid Mimetics with Potent Activity at the Orphan G Protein-Coupled Receptor 84 (GPR84). *ACS Omega,* 3 (3)**,** 3365-3383. Doi: 10.1021/acsomega.7b02092

Pillaiyar, T., Köse, M., Sylvester, K., Weighardt, H., Thimm, D., Borges, G., Förster, I., Von Kügelgen, I. & Müller, C. E. 2017. Diindolylmethane Derivatives: Potent Agonists of the Immunostimulatory Orphan G Protein-Coupled Receptor GPR84. *J Med Chem,* 60 (9)**,** 3636-3655. Doi: 10.1021/acs.jmedchem.6b01593

Planell, N., Masamunt, M. C., Leal, R. F., Rodríguez, L., Esteller, M., Lozano, J. J., Ramírez, A., Ayrizono, M. L. S., Coy, C. S. R., Alfaro, I., Ordás, I., Visvanathan, S., Ricart, E., Guardiola, J., Panés, J. & Salas, A. 2017. Usefulness of Transcriptional Blood Biomarkers as a Non-invasive Surrogate Marker of Mucosal Healing and Endoscopic Response in Ulcerative Colitis. *J Crohns Colitis,* 11 (11)**,** 1335-1346. Doi: 10.1093/ecco-jcc/jjx091

Power, C. A., Church, D. J., Meyer, A., Alouani, S., Proudfoot, A. E., Clark-Lewis, I., Sozzani, S., Mantovani, A. & Wells, T. N. 1997. Cloning and characterization of a specific receptor for the novel CC chemokine MIP-3alpha from lung dendritic cells. *J Exp Med,* 186 (6)**,** 825-35. Doi: 10.1084/jem.186.6.825

Puengel, T., De Vos, S., Hundertmark, J., Kohlhepp, M., Guldiken, N., Pujuguet, P., Auberval, M., Marsais, F., Shoji, K. F., Saniere, L., Trautwein, C., Luedde, T., Strnad, P., Brys, R., Clément-Lacroix, P. & Tacke, F. 2020. The Medium-Chain Fatty Acid Receptor GPR84 Mediates Myeloid Cell Infiltration Promoting Steatohepatitis and Fibrosis. *J Clin Med,* 9 (4)**,** 1140. Doi: 10.3390/jcm9041140

Qin, G., Liu, S., Liu, J., Hu, H., Yang, L., Zhao, Q., Li, C., Zhang, B. & Zhang, Y. 2023. Overcoming resistance to immunotherapy by targeting GPR84 in myeloid-derived suppressor cells. *Signal Transduct Target Ther,* 8 (1)**,** 164. Doi: 10.1038/s41392-023-01388-6

Rajagopal, S. & Shenoy, S. K. 2018. GPCR desensitization: Acute and prolonged phases. *Cell Signal,* 41**,** 9-16. Doi: 10.1016/j.cellsig.2017.01.024

Recio, C., Lucy, D., Purvis, G. S. D., Iveson, P., Zeboudj, L., Iqbal, A. J., Lin, D., O'callaghan, C., Davison, L., Griesbach, E., Russell, A. J., Wynne, G. M., Dib, L., Monaco, C. & Greaves, D. R. 2018. Activation of the Immune-Metabolic Receptor GPR84 Enhances Inflammation and Phagocytosis in Macrophages. *Front Immunol,* 9**,** 1419. Doi: 10.3389/fimmu.2018.01419

Reyes, A. W. B., Kim, H., Huy, T. X. N., Vu, S. H., Nguyen, T. T., Kang, C. K., Min, W., Lee, H. J., Lee, J. H. & Kim, S. 2021. Immune-metabolic receptor GPR84 surrogate and endogenous agonists, 6-OAU and lauric acid, alter Brucella abortus 544 infection in both in vitro and in vivo systems. *Microb Pathog,* 158**,** 105079. Doi: 10.1016/j.micpath.2021.105079

Rietschel, E. T. 1976. Absolute configuration of 3-hydroxy fatty acids present in lipopolysaccharides from various bacterial groups. *Eur J Biochem,* 64 (2)**,** 423-8. Doi: 10.1111/j.1432-1033.1976.tb10318.x

Ritchie, R. H., Zerenturk, E. J., Prakoso, D. & Calkin, A. C. 2017. Lipid metabolism and its implications for type 1 diabetes-associated cardiomyopathy. *J Mol Endocrinol,* 58 (4)**,** R225-R240. Doi: 10.1530/jme-16-0249

Rocha, J. J., Jayaram, S. A., Stevens, T. J., Muschalik, N., Shah, R. D., Emran, S., Robles, C., Freeman, M. & Munro, S. 2023. Functional unknomics: Systematic screening of conserved genes of unknown function. *PLoS Biol,* 21 (8)**,** e3002222. Doi: 10.1371/journal.pbio.3002222

Rodriguez, M., Funke, S., Fink, M., Demmelmair, H., Turini, M., Crozier, G. & Koletzko, B. 2003. Plasma fatty acids and [13C]linoleic acid metabolism in preterm infants fed a formula with medium-chain triglycerides. *J Lipid Res,* 44 (1)**,** 41-8. Doi: 10.1194/jlr.m200218-jlr200

Rouillard, A. D., Gundersen, G. W., Fernandez, N. F., Wang, Z., Monteiro, C. D., Mcdermott, M. G. & Ma'ayan, A. 2016. The harmonizome: a collection of processed datasets gathered to serve and mine knowledge about genes and proteins. *Database,* 2016. Doi: 10.1093/database/baw100

Rumianek, A. N. & Greaves, D. R. 2020. How Have Leukocyte In Vitro Chemotaxis Assays Shaped Our Ideas about Macrophage Migration? *Biology (Basel),* 9 (12)**,** 439. Doi: 10.3390/biology9120439

Sam, Q. H., Ling, H., Yew, W. S., Tan, Z., Ravikumar, S., Chang, M. W. & Chai, L. Y. A. 2021. The Divergent Immunomodulatory Effects of Short Chain Fatty Acids and Medium Chain Fatty Acids. *Int J Mol Sci,* 22 (12)**,** 6453. Doi: 10.3390/ijms22126453

Sander, T., Freyss, J., Von Korff, M. & Rufener, C. 2015. DataWarrior: an open-source program for chemistry aware data visualization and analysis. *J Chem Inf Model,* 55 (2)**,** 460-73. Doi: 10.1021/ci500588j

Saniere, L., Marsais, F., Jagerschmidt, C., Meurisse, S., Cuzic, S., Shoji, K., Clement-Lacroix, P., Osselaer, N. V. & Vos, S. D. 2019. Characterization of GLPG1205 in Mouse Fibrosis Models: A Potent and Selective Antagonist of GPR84 for Treatment of Idiopathic

Pulmonary Fibrosis. *A19. LESS IDIOPATHIC: STRUCTURAL AND FUNCTIONAL ABNORMALITIES IN IPF*.

Sato, K., Ohno-Oishi, M., Yoshida, M., Sato, T., Aizawa, T., Sasaki, Y., Maekawa, S., Ishikawa, M., Omodaka, K., Kawano, C., Ohue-Kitano, R., Kimura, I. & Nakazawa, T. 2023. The GPR84 molecule is a mediator of a subpopulation of retinal microglia that promote TNF/IL-1α expression via the rho-ROCK pathway after optic nerve injury. *Glia,* 71 (11)**,** 2609-2622. Doi: 10.1002/glia.24442

Schreiber, S. L., Kotz, J. D., Li, M., Aubé, J., Austin, C. P., Reed, J. C., Rosen, H., White, E. L., Sklar, L. A., Lindsley, C. W., Alexander, B. R., Bittker, J. A., Clemons, P. A., De Souza, A., Foley, M. A., Palmer, M., Shamji, A. F., Wawer, M. J., Mcmanus, O., Wu, M., Zou, B., Yu, H., Golden, J. E., Schoenen, F. J., Simeonov, A., Jadhav, A., Jackson, M. R., Pinkerton, A. B., Chung, T. D., Griffin, P. R., Cravatt, B. F., Hodder, P. S., Roush, W. R., Roberts, E., Chung, D. H., Jonsson, C. B., Noah, J. W., Severson, W. E., Ananthan, S., Edwards, B., Oprea, T. I., Conn, P. J., Hopkins, C. R., Wood, M. R., Stauffer, S. R. & Emmitte, K. A. 2015. Advancing Biological Understanding and Therapeutics Discovery with Small-Molecule Probes. *Cell,* 161 (6)**,** 1252-65. Doi: 10.1016/j.cell.2015.05.023

Schulz, N., Himmelbauer, H., Rath, M., Van Weeghel, M., Houten, S., Kulik, W., Suhre, K., Scherneck, S., Vogel, H., Kluge, R., Wiedmer, P., Joost, H. G. & Schürmann, A. 2011. Role of medium- and short-chain L-3-hydroxyacyl-CoA dehydrogenase in the regulation of body weight and thermogenesis. *Endocrinology,* 152 (12)**,** 4641-51. Doi: 10.1210/en.2011-1547

Schulze, A. S., Kleinau, G., Krakowsky, R., Rochmann, D., Das, R., Worth, C. L., Krumbholz, P., Scheerer, P. & Stäubert, C. 2022. Evolutionary analyses reveal immune cell receptor GPR84 as a conserved receptor for bacteria-derived molecules. *iScience,* 25 (10)**,** 105087. Doi: 10.1016/j.isci.2022.105087

Sellegounder, D., Liu, Y., Wibisono, P., Chen, C. H., Leap, D. & Sun, J. 2019. Neuronal GPCR NPR-8 regulates C. elegans defense against pathogen infection. *Sci Adv,* 5 (11)**,** eaaw4717. Doi: 10.1126/sciadv.aaw4717

Shao, Z., Yin, J., Chapman, K., Grzemska, M., Clark, L., Wang, J. & Rosenbaum, D. M. 2016. High-resolution crystal structure of the human CB1 cannabinoid receptor. *Nature,* 540 (7634)**,** 602-606. Doi: 10.1038/nature20613

Sheils, T. K., Mathias, S. L., Kelleher, K. J., Siramshetty, V. B., Nguyen, D.-T., Bologa, C. G., Jensen, L. J., Vidović, D., Koleti, A., Schürer, S. C., Waller, A., Yang, J. J., Holmes, J., Bocci, G., Southall, N., Dharkar, P., Mathé, E., Simeonov, A. & Oprea, T. I. 2020. TCRD and Pharos 2021: mining the human proteome for disease biology. *Nucleic Acids Research,* 49 (D1)**,** D1334-D1346. Doi: 10.1093/nar/gkaa993

Shenoy, S. K. & Lefkowitz, R. J. 2003. Multifaceted roles of beta-arrestins in the regulation of seven-membrane-spanning receptor trafficking and signalling. *Biochem J,* 375 (Pt 3)**,** 503-15. Doi: 10.1042/bj20031076

Shi, G. W., Chen, J., Concepcion, F., Motamedchaboki, K., Marjoram, P., Langen, R. & Chen, J. 2005. Light causes phosphorylation of nonactivated visual pigments in intact mouse rod photoreceptor cells. *J Biol Chem,* 280 (50)**,** 41184-91. Doi: 10.1074/jbc.M506935200

Shrestha, R., Hui, S. P., Imai, H., Hashimoto, S., Uemura, N., Takeda, S., Fuda, H., Suzuki, A., Yamaguchi, S., Hirano, K. & Chiba, H. 2015. Plasma capric acid concentrations in healthy subjects determined by high-performance liquid chromatography. *Ann Clin Biochem,* 52 (Pt 5)**,** 588-96. Doi: 10.1177/0004563215569081

Sills, M. A., Forsythe, W. I. & Haidukewych, D. 1986. Role of octanoic and decanoic acids in the control of seizures. *Arch Dis Child,* 61 (12)**,** 1173-7. Doi: 10.1136/adc.61.12.1173

Smith, J. S., Lefkowitz, R. J. & Rajagopal, S. 2018. Biased signalling: from simple switches to allosteric microprocessors. *Nat Rev Drug Discov,* 17 (4)**,** 243-260. Doi: 10.1038/nrd.2017.229

Smith, N. J. 2012. Low affinity GPCRs for metabolic intermediates: challenges for pharmacologists. *Front Endocrinol (Lausanne),* 3**,** 1. Doi: 10.3389/fendo.2012.00001

Solly, K., Wang, X., Xu, X., Strulovici, B. & Zheng, W. 2004. Application of real-time cell electronic sensing (RT-CES) technology to cell-based assays. *Assay Drug Dev Technol,* 2 (4)**,** 363-72. Doi: 10.1089/adt.2004.2.363

Sorkin, A. & Von Zastrow, M. 2009. Endocytosis and signalling: intertwining molecular networks. *Nat Rev Mol Cell Biol,* 10 (9)**,** 609-22. Doi: 10.1038/nrm2748

Southern, C., Cook, J. M., Neetoo-Isseljee, Z., Taylor, D. L., Kettleborough, C. A., Merritt, A., Bassoni, D. L., Raab, W. J., Quinn, E., Wehrman, T. S., Davenport, A. P., Brown, A. J., Green, A., Wigglesworth, M. J. & Rees, S. 2013. Screening β-arrestin recruitment for the identification of natural ligands for orphan G-protein-coupled receptors. *J Biomol Screen,* 18 (5)**,** 599-609. Doi: 10.1177/1087057113475480

St-Pierre, V., Vandenberghe, C., Lowry, C. M., Fortier, M., Castellano, C. A., Wagner, R. & Cunnane, S. C. 2019. Plasma Ketone and Medium Chain Fatty Acid Response in Humans Consuming Different Medium Chain Triglycerides During a Metabolic Study Day. *Front Nutr,* 6**,** 46. Doi: 10.3389/fnut.2019.00046

Stallaert, W., Dorn, J. F., Van Der Westhuizen, E., Audet, M. & Bouvier, M. 2012. Impedance responses reveal β_2-adrenergic receptor signaling pluridimensionality and allow classification of ligands with distinct signaling profiles. *PLoS One,* 7 (1)**,** e29420. Doi: 10.1371/journal.pone.0029420

Stoddart, L. A., Smith, N. J. & Milligan, G. 2008. International Union of Pharmacology. LXXI. Free fatty acid receptors FFA1, -2, and -3: pharmacology and pathophysiological functions. *Pharmacol Rev,* 60 (4)**,** 405-17. Doi: 10.1124/pr.108.00802

Strambu, I. R., Seemayer, C. A., Fagard, L. M. A., Ford, P. A., Van Der Aa, T. a. K., De Haas-Amatsaleh, A. A., Modgill, V., Santermans, E., Sondag, E. N., Helmer, E. G., Maher, T. M., Costabel, U. & Cottin, V. 2023. GLPG1205 for idiopathic pulmonary fibrosis: a phase 2 randomised placebo-controlled trial. *Eur Respir J,* 61 (3)**,** 2201794. Doi: 10.1183/13993003.01794-2022

Stringer, C., Wang, T., Michaelos, M. & Pachitariu, M. 2021. Cellpose: a generalist algorithm for cellular segmentation. *Nat Methods,* 18 (1)**,** 100-106. Doi: 10.1038/s41592-020-01018-x

Suckow, A. T. & Briscoe, C. P. 2017. Key Questions for Translation of FFA Receptors: From Pharmacology to Medicines. *Handb Exp Pharmacol,* 236**,** 101-131. Doi: 10.1007/164_2016_45

Sundqvist, M., Christenson, K., Holdfeldt, A., Gabl, M., Mårtensson, J., Björkman, L., Dieckmann, R., Dahlgren, C. & Forsman, H. 2018. Similarities and differences between the responses induced in human phagocytes through activation of the medium chain fatty acid receptor GPR84 and the short chain fatty acid receptor FFA2R. *Biochim Biophys Acta Mol Cell Res,* 1865 (5)**,** 695-708. Doi: 10.1016/j.bbamcr.2018.02.008

Sundqvist, M., Holdfeldt, A., Wright, S. C., Møller, T. C., Siaw, E., Jennbacken, K., Franzyk, H., Bouvier, M., Dahlgren, C. & Forsman, H. 2020. Barbadin selectively modulates FPR2-mediated neutrophil functions independent of receptor endocytosis. *Biochim Biophys Acta Mol Cell Res,* 1867 (12)**,** 118849. Doi: 10.1016/j.bbamcr.2020.118849

Suzuki, M., Takaishi, S., Nagasaki, M., Onozawa, Y., Iino, I., Maeda, H., Komai, T. & Oda, T. 2013. Medium-chain fatty acid-sensing receptor, GPR84, is a proinflammatory receptor. *J Biol Chem,* 288 (15)**,** 10684-91. Doi: 10.1074/jbc.M112.420042

Swift, L. L., Hill, J. O., Peters, J. C. & Greene, H. L. 1990. Medium-chain fatty acids: evidence for incorporation into chylomicron triglycerides in humans. *Am J Clin Nutr,* 52 (5)**,** 834-6. Doi: 10.1093/ajcn/52.5.834

Symonds, E. L., Peiris, M., Page, A. J., Chia, B., Dogra, H., Masding, A., Galanakis, V., Atiba, M., Bulmer, D., Young, R. L. & Blackshaw, L. A. 2015. Mechanisms of activation of mouse and human enteroendocrine cells by nutrients. *Gut,* 64 (4)**,** 618-26. Doi: 10.1136/gutjnl-2014-306834

Tang, C., Ahmed, K., Gille, A., Lu, S., Gröne, H. J., Tunaru, S. & Offermanns, S. 2015. Loss of FFA2 and FFA3 increases insulin secretion and improves glucose tolerance in type 2 diabetes. *Nat Med,* 21 (2)**,** 173-7. Doi: 10.1038/nm.3779

Tejada-Martinez, D., Avelar, R. A., Lopes, I., Zhang, B., Novoa, G., De Magalhães, J. P. & Trizzino, M. 2022. Positive Selection and Enhancer Evolution Shaped Lifespan and Body Mass in Great Apes. *Mol Biol Evol,* 39 (2)**,** msab369. Doi: 10.1093/molbev/msab369

Tesmer, V. M., Kawano, T., Shankaranarayanan, A., Kozasa, T. & Tesmer, J. J. 2005. Snapshot of activated G proteins at the membrane: the Galphaq-GRK2-Gbetagamma complex. *Science,* 310 (5754)**,** 1686-90. Doi: 10.1126/science.1118890

Thomas, P. D., Ebert, D., Muruganujan, A., Mushayahama, T., Albou, L. P. & Mi, H. 2022. PANTHER: Making genome-scale phylogenetics accessible to all. *Protein Sci,* 31 (1)**,** 8-22. Doi: 10.1002/pro.4218

Trayhurn, P. & Denyer, G. 2012. Mining microarray datasets in nutrition: expression of the GPR120 (n-3 fatty acid receptor/sensor) gene is down-regulated in human adipocytes by macrophage secretions. *J Nutr Sci,* 1**,** e3. Doi: 10.1017/jns.2012.3

Ueno, H., Ito, R., Abe, S. I., Ookawara, M., Miyashita, H., Ogino, H., Miyamoto, Y., Yoshihara, T., Kobayashi, A., Tsujihata, Y., Takeuchi, K., Watanabe, M., Yamada, Y., Maekawa, T., Nishigaki, N. & Moritoh, Y. 2019. SCO-267, a GPR40 Full Agonist, Improves Glycemic and Body Weight Control in Rat Models of Diabetes and Obesity. *J Pharmacol Exp Ther,* 370 (2)**,** 172-181. Doi: 10.1124/jpet.118.255885

Ulven, T. & Christiansen, E. 2015. Dietary Fatty Acids and Their Potential for Controlling Metabolic Diseases Through Activation of FFA4/GPR120. *Annu Rev Nutr,* 35**,** 239-63. Doi: 10.1146/annurev-nutr-071714-034410

Vassilatis, D. K., Hohmann, J. G., Zeng, H., Li, F., Ranchalis, J. E., Mortrud, M. T., Brown, A., Rodriguez, S. S., Weller, J. R., Wright, A. C., Bergmann, J. E. & Gaitanaris, G. A. 2003. The G protein-coupled receptor repertoires of human and mouse. *Proc Natl Acad Sci U S A,* 100 (8)**,** 4903-8. Doi: 10.1073/pnas.0230374100

Velasco, C., Conde-Sieira, M., Comesaña, S., Chivite, M., Míguez, J. M. & Soengas, J. L. 2021. Role of the G protein-coupled receptors GPR84 and GPR119 in the central regulation of food intake in rainbow trout. *J Exp Biol,* 224 (13)**,** jeb242360. Doi: 10.1242/jeb.242360

Venkataraman, C. & Kuo, F. 2005. The G-protein coupled receptor, GPR84 regulates IL-4 production by T lymphocytes in response to CD3 crosslinking. *Immunol Lett,* 101 (2)**,** 144-53. Doi: 10.1016/j.imlet.2005.05.010

Vermeire, S., Reinisch, W., Wasko-Czopnik, D., Van Kaem, T., Desrivot, J., Vanhoutte, F. & Beetens, J. 2017. P610 Efficacy and safety of GLPG1205, a GPR84 antagonist, in ulcerative colitis: multi-centre proof-of-concept study. *Journal of Crohn's and Colitis,* 11 (suppl_1)**,** S390-S391. Doi: 10.1093/ecco-jcc/jjx002.734

Von Chamier, L., Laine, R. F., Jukkala, J., Spahn, C., Krentzel, D., Nehme, E., Lerche, M., Hernández-Pérez, S., Mattila, P. K., Karinou, E., Holden, S., Solak, A. C., Krull, A., Buchholz, T. O., Jones, M. L., Royer, L. A., Leterrier, C., Shechtman, Y., Jug, F., Heilemann, M., Jacquemet, G. & Henriques, R. 2021. Democratising deep learning for microscopy with ZeroCostDL4Mic. *Nat Commun,* 12 (1)**,** 2276. Doi: 10.1038/s41467-021-22518-0

Waisman, A., Norris, A. M., Elías Costa, M. & Kopinke, D. 2021. Automatic and unbiased segmentation and quantification of myofibers in skeletal muscle. *Sci Rep,* 11 (1)**,** 11793. Doi: 10.1038/s41598-021-91191-6

Wallace, T. C. 2019. Health Effects of Coconut Oil-A Narrative Review of Current Evidence. *J Am Coll Nutr,* 38 (2)**,** 97-107. Doi: 10.1080/07315724.2018.1497562

Wang, F., Ma, L., Ding, Y., He, L., Chang, M., Shan, Y., Siwko, S., Chen, G., Liu, Y., Jin, Y., Peng, X. & Luo, J. 2021. Fatty acid sensing GPCR (GPR84) signaling safeguards cartilage homeostasis and protects against osteoarthritis. *Pharmacol Res,* 164**,** 105406. Doi: 10.1016/j.phrs.2020.105406

Wang, J., Wu, X., Simonavicius, N., Tian, H. & Ling, L. 2006. Medium-chain fatty acids as ligands for orphan G protein-coupled receptor GPR84. *J Biol Chem,* 281 (45)**,** 34457-64. Doi: 10.1074/jbc.M608019200

Wang, M., Zhang, X., Zhang, S. & Liu, Z. 2019. Zebrafish fatty acids receptor Gpr84 enhances macrophage phagocytosis. *Fish Shellfish Immunol,* 84**,** 1098-1099. Doi: 10.1016/j.fsi.2018.11.023

Wang, P., Raja, A., Luscombe, V. B., Bataille, C. J. R., Lucy, D., Rogga, V. V., Greaves, D. R. & Russell, A. J. 2023a. Development of Highly Potent, G-Protein Pathway Biased, Selective, and Orally Bioavailable GPR84 Agonists. *Journal of Medicinal Chemistry*. Doi: 10.1021/acs.jmedchem.3c00951

Wang, Q., Wu, C., Li, P., Shao, S., Zhang, J., Zhu, M. & Yang, X. 2014. Molecular cloning and expression analysis of GPR84 and MPEG1 genes in porcine. *Acta Veterinaria et Zootechnica Sinica,* 45 (5)**,** 699-705.

Wang, S. W., Zhang, Q., Lu, D., Fang, Y. C., Yan, X. C., Chen, J., Xia, Z. K., Yuan, Q. T., Chen, L. H., Zhang, Y. M., Nan, F. J. & Xie, X. 2023b. GPR84 regulates pulmonary inflammation by modulating neutrophil functions. *Acta Pharmacol Sin,* 44 (8)**,** 1665-1675. Doi: 10.1038/s41401-023-01080-z

Watts, A. O., Scholten, D. J., Heitman, L. H., Vischer, H. F. & Leurs, R. 2012. Label-free impedance responses of endogenous and synthetic chemokine receptor CXCR3 agonists correlate with Gi-protein pathway activation. *Biochem Biophys Res Commun,* 419 (2)**,** 412-8. Doi: 10.1016/j.bbrc.2012.02.036

Wei, L., Tokizane, K., Konishi, H., Yu, H. R. & Kiyama, H. 2017. Agonists for G-protein-coupled receptor 84 (GPR84) alter cellular morphology and motility but do not induce pro-inflammatory responses in microglia. *J Neuroinflammation,* 14 (1)**,** 198. Doi: 10.1186/s12974-017-0970-y

Whittier, K. L., Boese, E. A., Gibson-Corley, K. N., Kirby, P. A., Darbro, B. W., Qian, Q., Ingram, W. J., Robertson, T., Remke, M., Taylor, M. D. & O'dorisio, M. S. 2013. G-protein coupled receptor expression patterns delineate medulloblastoma subgroups. *Acta Neuropathol Commun,* 1**,** 66. Doi: 10.1186/2051-5960-1-66

Widmayer, P., Kusumakshi, S., Hägele, F. A., Boehm, U. & Breer, H. 2017. Expression of the Fatty Acid Receptors GPR84 and GPR120 and Cytodifferentiation of Epithelial Cells in the Gastric Mucosa of Mouse Pups in the Course of Dietary Transition. *Front Physiol,* 8**,** 601. Doi: 10.3389/fphys.2017.00601

Wittenberger, T., Schaller, H. C. & Hellebrand, S. 2001. An expressed sequence tag (EST) data mining strategy succeeding in the discovery of new G-protein coupled receptors. *J Mol Biol,* 307 (3)**,** 799-813. Doi: 10.1006/jmbi.2001.4520

Yao, M. X., Yu, H. X., Mo, H. L., Zhang, Z. H., Song, Q. C., Liu, Q., Yang, Q. Y., Wang, L. X. & Li, Y. 2023. Structural and pharmacological characterization of a medium-chain fatty acid receptor GPR84 in common carp (Cyprinus carpio). *Dev Comp Immunol,* 153**,** 105126. Doi: 10.1016/j.dci.2023.105126

Yen, Y. C., Schafer, C. T., Gustavsson, M., Eberle, S. A., Dominik, P. K., Deneka, D., Zhang, P., Schall, T. J., Kossiakoff, A. A., Tesmer, J. J. G. & Handel, T. M. 2022. Structures of atypical chemokine receptor 3 reveal the basis for its promiscuity and signaling bias. *Sci Adv,* 8 (28)**,** eabn8063. Doi: 10.1126/sciadv.abn8063

Yin, C., Cheng, L., Pan, J., Chen, L., Xue, Q., Qin, J., Wang, S., Du, B., Liu, M., Zhang, Y., Jiang, W., Qian, M. & Ren, H. 2020. Regulatory role of Gpr84 in the switch of alveolar macrophages from CD11b(lo) to CD11b(hi) status during lung injury process. *Mucosal Immunol,* 13 (6)**,** 892-907. Doi: 10.1038/s41385-020-0321-7

Yosten, G. L., Harada, C. M., Haddock, C., Giancotti, L. A., Kolar, G. R., Patel, R., Guo, C., Chen, Z., Zhang, J., Doyle, T. M., Dickenson, A. H., Samson, W. K. & Salvemini, D. 2020. GPR160 de-orphanization reveals critical roles in neuropathic pain in rodents. *J Clin Invest,* 130 (5)**,** 2587-2592. Doi: 10.1172/jci133270

Yousefi, S., Cooper, P. R., Potter, S. L., Mueck, B. & Jarai, G. 2001. Cloning and expression analysis of a novel G-protein-coupled receptor selectively expressed on granulocytes. *J Leukoc Biol,* 69 (6)**,** 1045-52. Doi: 10.1189/jlb.69.6.1045

Yu, H.-X., Li, Y., Ezeorba, T., Mo, H.-L., Zhang, Z.-H., Yang, Q.-Y. & Wang, L.-X. 2022. Molecular characterization and functional exploration of GPR84 in Chinese Giant Salamander (Andrias davidianus). *Developmental & Comparative Immunology,* 137**,** 104526. Doi: 10.1016/j.dci.2022.104526

Zaibi, M. S., Kępczyńska, M. A., Harikumar, P., Alomar, S. Y. & Trayhurn, P. 2018. IL-33 stimulates expression of the GPR84 (EX33) fatty acid receptor gene and of cytokine and

chemokine genes in human adipocytes. *Cytokine,* 110**,** 189-193. Doi: 10.1016/j.cyto.2018.05.008

Zhang, L., Keung, W., Samokhvalov, V., Wang, W. & Lopaschuk, G. D. 2010. Role of fatty acid uptake and fatty acid beta-oxidation in mediating insulin resistance in heart and skeletal muscle. *Biochim Biophys Acta,* 1801 (1)**,** 1-22. Doi: 10.1016/j.bbalip.2009.09.014

Zhang, Q., Chen, L. H., Yang, H., Fang, Y. C., Wang, S. W., Wang, M., Yuan, Q. T., Wu, W., Zhang, Y. M., Liu, Z. J., Nan, F. J. & Xie, X. 2022. GPR84 signaling promotes intestinal mucosal inflammation via enhancing NLRP3 inflammasome activation in macrophages. *Acta Pharmacol Sin,* 43 (8)**,** 2042-2054. Doi: 10.1038/s41401-021-00825-y

Zhang, Q., Yang, H., Li, J. & Xie, X. 2016. Discovery and Characterization of a Novel Small-Molecule Agonist for Medium-Chain Free Fatty Acid Receptor G Protein-Coupled Receptor 84. *J Pharmacol Exp Ther,* 357 (2)**,** 337-44. Doi: 10.1124/jpet.116.232033

Zhang, X., Wang, Y., Supekar, S., Cao, X., Zhou, J., Dang, J., Chen, S., Jenkins, L., Marsango, S., Li, X., Liu, G., Milligan, G., Feng, M., Fan, H., Gong, W. & Zhang, C. 2023. Pro-phagocytic function and structural basis of GPR84 signaling. *Nat Commun,* 14 (1)**,** 5706. Doi: 10.1038/s41467-023-41201-0

Zhu, X., Finlay, D. B., Glass, M. & Duffull, S. B. 2019. Model-free and kinetic modelling approaches for characterising non-equilibrium pharmacological pathway activity: Internalisation of cannabinoid CB(1) receptors. *Br J Pharmacol,* 176 (14)**,** 2593-2607. Doi: 10.1111/bph.14684

Zidar, D. A., Violin, J. D., Whalen, E. J. & Lefkowitz, R. J. 2009. Selective engagement of G protein coupled receptor kinases (GRKs) encodes distinct functions of biased ligands. *Proc Natl Acad Sci U S A,* 106 (24)**,** 9649-54. Doi: 10.1073/pnas.0904361106